MCEER
MULTIDISCIPLINARY CENTER FOR EARTHQUAKE ENGINEERING RESEARCH
A National Center of Excellence in Advanced Technology Applications

ISSN 1520-295X

Experimental and Analytical Studies of Base Isolation Systems for Seismic Protection of Power Transformers

by

Nobuo Murota, Maria Q. Feng and Gee-Yu Liu
University of California, Irvine
Department of Civil and Environmental Engineering
Engineering Gateway 4139
Irvine, California 92697

Technical Report MCEER-05-0008

September 30, 2005

This research was conducted at the University of California, Irvine, Bridgestone Corporation and the National Center for Research on Earthquake Engineering, and was supported primarily by the Earthquake Engineering Research Centers Program of the National Science Foundation under award number EEC-9701471.

NOTICE

MCEER
MULTIDISCIPLINARY CENTER FOR EARTHQUAKE ENGINEERING RESEARCH
A National Center of Excellence in Advanced Technology Applications

---

Experimental and Analytical Studies of Base Isolation Systems for Seismic Protection of Power Transformers

by

Nobuo Murota[1], Maria Q. Feng[2] and Gee-Yu Liu[3]

Publication Date: September 30, 2005
Submittal Date: April 5, 2005

Technical Report MCEER-05-0008

Task Number 1.10b

NSF Master Contract Number EEC-9701471

1 Senior Engineer, Department of Seismic Isolation Engineering, Bridgestone Corporation, Japan
2 Professor, Department of Civil and Environmental Engineering, University of California, Irvine
3 Associate Research Fellow, National Center for Research on Earthquake Engineering, Taipei, Taiwan

MULTIDISCIPLINARY CENTER FOR EARTHQUAKE ENGINEERING RESEARCH
University at Buffalo, State University of New York
Red Jacket Quadrangle, Buffalo, NY 14261

Preface

The Multidisciplinary Center for Earthquake Engineering Research (MCEER) is a national center of excellence in advanced technology applications that is dedicated to the reduction of earthquake losses nationwide. Headquartered at the University at Buffalo, State University of New York, the Center was originally established by the National Science Foundation in 1986, as the National Center for Earthquake Engineering Research (NCEER).

Comprising a consortium of researchers from numerous disciplines and institutions throughout the United States, the Center's mission is to reduce earthquake losses through research and the application of advanced technologies that improve engineering, pre-earthquake planning and post-earthquake recovery strategies. Toward this end, the Center coordinates a nationwide program of multidisciplinary team research, education and outreach activities.

MCEER's research is conducted under the sponsorship of two major federal agencies: the National Science Foundation (NSF) and the Federal Highway Administration (FHWA), and the State of New York. Significant support is derived from the Federal Emergency Management Agency (FEMA), other state governments, academic institutions, foreign governments and private industry.

MCEER's NSF-sponsored research objectives are twofold: to increase resilience by developing seismic evaluation and rehabilitation strategies for the post-disaster facilities and systems (hospitals, electrical and water lifelines, and bridges and highways) that society expects to be operational following an earthquake; and to further enhance resilience by developing improved emergency management capabilities to ensure an effective response and recovery following the earthquake (see the figure below).

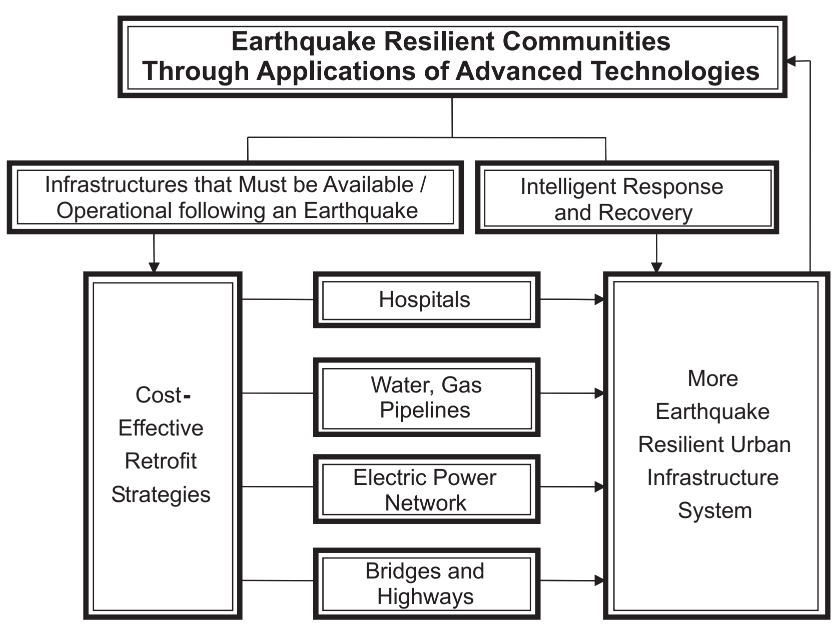

A cross-program activity focuses on the establishment of an effective experimental and analytical network to facilitate the exchange of information between researchers located in various institutions across the country. These are complemented by, and integrated with, other MCEER activities in education, outreach, technology transfer, and industry partnerships.

This report presents a comprehensive analysis of the use of base isolation technology for seismic protection of electric power transformers. The lightweight nature and base displacement constraints of power transformers require a different philosophy (from buildings and bridges) in designing a base isolation system. Two isolation systems were developed, one using sliding bearings combined with rubber bearings and the other using segmented high-damping rubber bearings. Tri-axial earthquake simulator testing was performed using a large-scale transformer model equipped with real bushings. Numerical simulation confirmed that the two isolation systems can perform differently under tri-axial ground motions, even when designed with the same force-displacement hysteresis. In conclusion, base isolation technology, when properly designed, was shown to be a highly effective method for seismic protection of power transformers.

ABSTRACT

This report presents a comprehensive study involving tri-axial earthquake simulator testing on seismic isolation of electric power transformers. The lightweight nature and base displacement constraints of power transformers require a different philosophy (from buildings and bridges) in designing a base isolation system. In this study, two isolation systems were developed, one using sliding bearings combined with rubber bearings and the other segmented high-damping rubber bearings. Tri-axial earthquake simulator testing was performed using a large-scale transformer model equipped with real bushings. Important observations were made on the seismic responses of the transformer and its bushing. In particular, the vertical component of the ground motion induced high-frequency response of the bushing when the transformer was isolated with the sliding isolation system. Numerical simulation confirmed that the two isolation systems, even designed with the same force-displacement hysteresis, can perform differently under tri-axial ground motions. This is because the vertical motion changes the friction forces in the sliding bearings that can excite high modes in the transformer-bushing system. Furthermore, the effect of the interaction with the bushing connecting cables on the seismic isolation performance was experimentally evaluated in this study. In conclusion, the base isolation technology, when properly designed, is a highly effective measure for seismic protection of power transformers.

ACKNOWLEDGEMENTS

This research was funded by the Multidisciplinary Center for Earthquake Engineering Research (MCEER). The earthquake simulator testing was carried out at the National Center for Research on Earthquake Engineering (NCREE) in Taiwan. I would like to express my greatest appreciation to the engineering staff in NCREE and Bridgestone Corporation for their generous cooperation.

Finally, I would like to thank Professor Masanobu Shinozuka and Professor Roberto Villaverde in University of California at Irvine, and Professor Chin-Hsiung Loh in National Taiwan University for their valuable advice and instructions.

TABLE OF CONTENTS

TABLE OF CONTENTS (Cont'd)

LIST OF ILLUSTRATIONS

LIST OF ILLUSTRATIONS (Cont'd)

LIST OF ILLUSTRATIONS (Cont'd)

LIST OF ILLUSTRATIONS (Cont'd)

LIST OF ILLUSTRATIONS (Cont'd)

LIST OF ILLUSTRATIONS (Cont'd)

LIST OF TABLES

LIST OF TABLES (Cont'd)

SECTION 1
INTRODUCTION

1.1 Background

Recent major earthquakes have significantly damaged many electrical power networks that are important to the delivery of electric power to tens of thousands of people in urban areas. Examples of these destructive earthquakes include: the 1994 Northridge earthquake in the United States, the 1995 Kobe (Hyogo-ken Nanbu) earthquake in Japan, the 1999 Izmit earthquake in Turkey, and the 1999 Chi-Chi earthquake in Taiwan. The seismic damage to electrical power facilities and their impacts are shown in Table 1-1, Figure 1-1, and Figure 1-2. While the duration of system disruption was relatively short to moderate (one day for Northridge; three days for Kobe; and two weeks for Chi-Chi), the estimated direct losses were reported to be in the hundreds of millions of dollars for each event. For example, the Los Angeles Department of Water and Power (LADWP) reported that following the Northridge earthquake, LADWP expended approximately $10.4 million to clean up debris, replace damaged equipment, and restore operations at its transmission-level facilities following the Northridge earthquake. In addition to the clean-up and repair costs, LADWP experienced revenue loss when the system went black following the earthquake. The net operational losses for LADWP's electrical system in a blackout condition average about $4.4 million per day. Furthermore, loss of power immediately after an earthquake can disrupt emergency response and recovery operations for the affected region. Thus power utilities are interested in ways to minimize, if not eliminate, earthquake damage and disruption to their systems (Shinozuka).

Since expensive substations are key facilities of electrical power networks, there needs to be a way to protect them from earthquakes. In fact, many of them are extremely vulnerable to seismic damage because they were designed to much lower seismic standards. Because transformers represent crucial substation equipment, the loss of their functionality can be devastating to the entire power system. For example, immediately following the 1994 Northridge and the 1995 Kobe earthquakes, many power transformers suffered severe damage and lost operation because of damage to the porcelain bushings, which are usually mounted on the top of the transformer (Shinozuka, 1995; Pansini 1998).

The power transformer is a device, without moving parts, which transfers electric power from one circuit to another by electromagnetic means. Typically, both the voltage and current undergo changes between the circuits. The size, shape, and installation of the transformer vary according to the voltage it handles, as shown in Figure 1-3. The basic components of a transformer are coils, an iron or steel core, a tank, oil, and bushings. The coils and the core are usually enclosed in the steel tank to protect it from vandalism and for safety purposes. The oil is usually placed in the tank to cover the coils and the core to provide cooling. Bushings take the terminals of the coils through the tank, insulating them from the tank, as shown in Figure 1-4. These typically consist of a conductor through an insulating collar, usually made of porcelain. For higher voltages, the porcelain cylinders may also be filled with oil or contain layers of insulation with metal foil inserted between them to equalize electric stresses among the layers.

Table 1-1 Major Damage in Substations during Kobe Earthquake

Equipment	Number of damage
Transformer	52
Disconnect switch	10
Condenser	4
Breaker	41
Lightning arrester	15

Some of the modes of failure in a transformer system during an earthquake include anchorage failure that can cause ripping of the transformer case and oil leakage and/or foundation failure causing rocking and tilting. An unanchored transformer sometimes causes an overturning of an entire transformer system during a severe earthquake. On the other hand, the tightly fixed

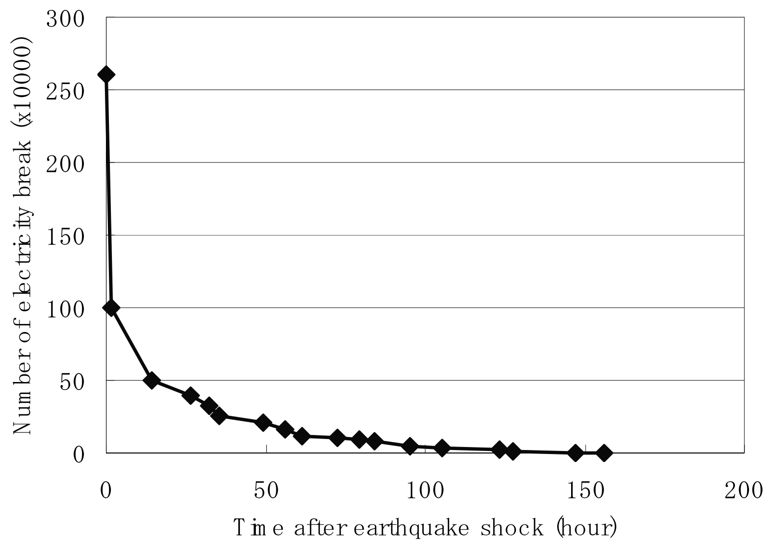

Figure 1-1 Number of Residence Experiencing Power Cuts after Kobe Earthquake

Broken arresters at the Itami Substation [An EQE Summary Report, 1995]

Damage to Transformer in Izmit Substation [EERI,1999]

Figure 1-2 Damages in Electrical Equipments in Substations

Figure 1-3 Transformers in Electric Substation

anchorage system may cause fatal damage in internal elements of the transformers by the high impact forces that are transmitted.

Another type of damage frequently occurs in a transformer system is the failure of porcelain bushings mounted on the transformer. The frequency usually varies from 3 to 15 (Hz) and may sometime cause large amplification in its response acceleration during earthquake. The failures on bushings include oil leakage from connection-interface of transformer and bushing or fracture of porcelain body. The porcelain is a brittle material and has almost no energy-absorbing capabilities, and the damage in the bushing will occur at the mounting-end of bushing by stress concentration, uplift of porcelain body, slip of gasket, caused by the inertia force as a results of high response acceleration during earthquake.

1.2 Conventional Seismic Design of Transformer

Since transformer bushings form an integral part of power transmission and distribution systems, their structural and electrical integrity are critical to maintaining power transmission. To mitigate the damage in transformer system and other electrical substation equipment, representatives from electrical utilities and equipment manufacturers, together with consulting engineers and members of the academic community jointly developed a new national standard, IEEE 693-1997. These requirements are expected to improve the seismic capability of substation equipment and provide the guidelines for seismic testing and qualification of bushings. In IEEE 693-1997, the bushings for 161-kV and larger must be qualified using earthquake simulator testing in which the input motion shall match the specified Required Response Spectrum shown in Figure 1-5. Three types of earthquake simulator testing are identified in IEEE 693-1997: 1) *time-history shake table test*; 2) *resonant frequency search*; and 3) *sine-beat testing*. Time history records of input motion for the *shake table test* shall match the specified response spectrum. In IEEE 693-1997, three seismic performance levels (PL) are specified -- High, Moderate, and Low. Each level is defined by response spectrum with 2, 5, and 10% damping. Corresponding peak ground acceleration of the spectrum of each levels are, 1.0g, 0.5g, and 0.25g for the horizontal direction, and 0.8g, 0.4g, and 0.2g for the vertical direction. However, IEEE 693-1997 also stated that because testing under the specified performance level is often impractical and not cost effective, it may be

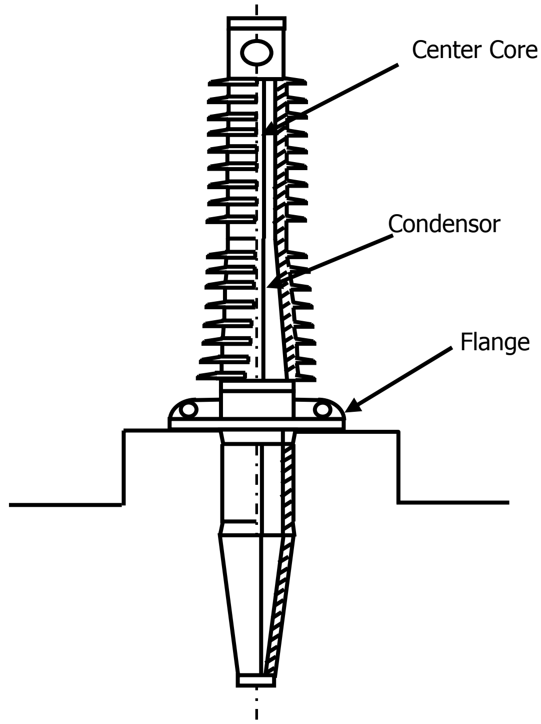

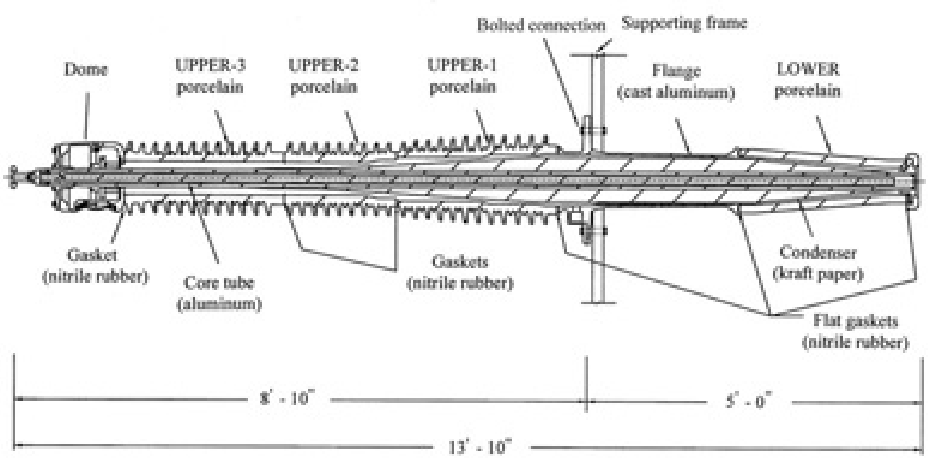

(Figure from Gilani Amir S. et al. (1999))

Figure 1-4 Porcelain Bushing

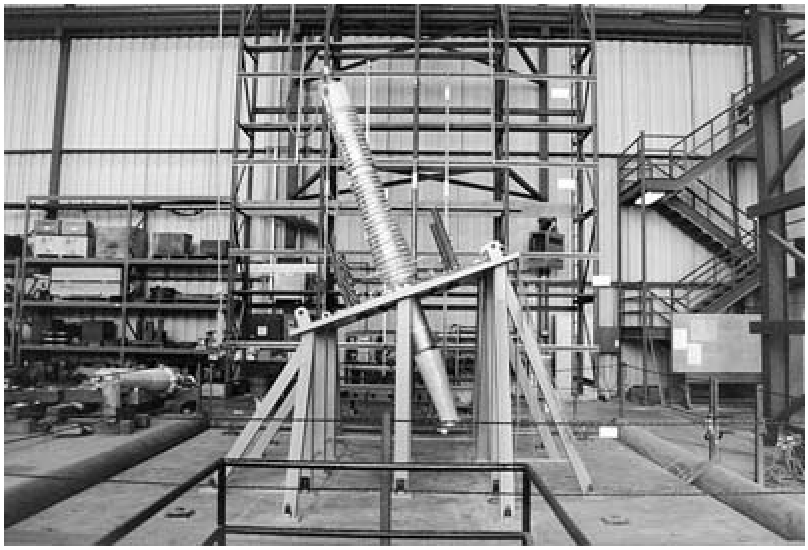

(Photo from [1-10])

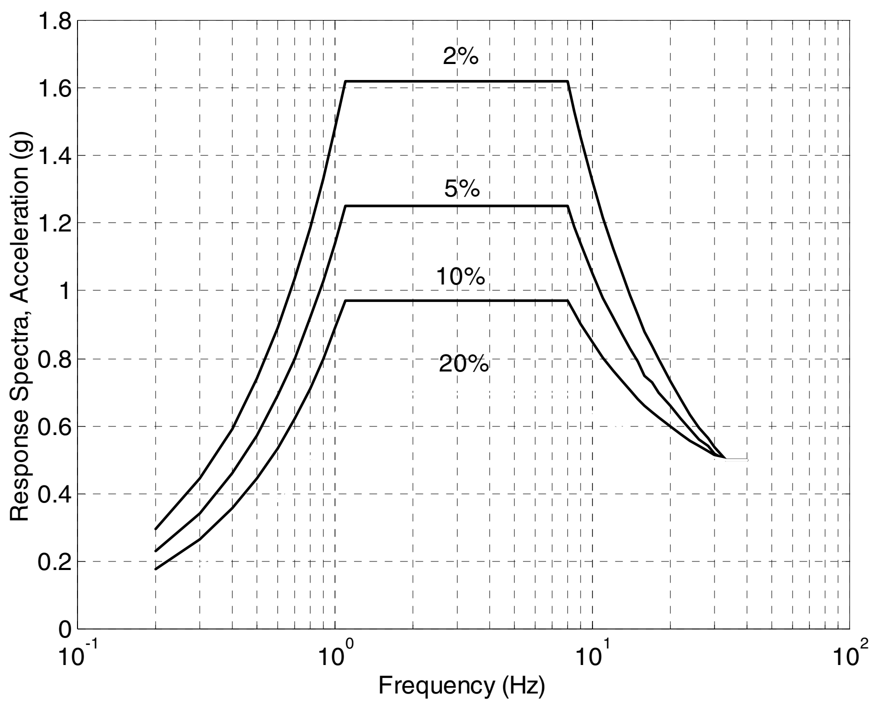

Figure 1-5 Qualification Test of Bushing and Spectra for Required Response Spectrum (IEEE 693-1997)

substituted by the shaking of one-half of PL. The test results shall be evaluated with a safety factor of two against the requirements of PL. The reduced response spectrum of 0.5 x PL is designated High-, and Moderate-Required Response Spectrum as shown in Figure 1-5.

In Japan, JEAG 5003 (1999) specified the required procedure to evaluate the seismic performance of transformer/bushing system. The specified seismic-level of the ground motion is 0.5g in horizontal and 0.3g in vertical direction. The required test for the bushing is a resonant sine wave shaking test. A shaking table test is optional, and the actual site-record shall be applied (compare to the artificial wave specified in IEEE 693). A comparison of the design requirements in IEEE 693-1997, JEAG 5003, and IEC68-3-3 (European code) is summarized in Table 1-2.

Table 1-2 Comparison of Standard for Seismic Evaluation of Facilities in Substation in Several Countries (JESC E0001 (1999))

		JEAG 5003 (1999)	**IEEE 693 (1997)**			**IEC 68-3-3 (1991)**					
Method		Tests or Analysis	Tests or Analysis			Tests					
Voltage class.		N/A	X			X					
Seismic-performance class.		N/A	X			X					
Design-level class.		N/A	X			General			Specific		
Frequency range		0.5 to 10 Hz; <0.5, >10Hz is tested by 0.5 or 10 Hz	1 to 33 Hz			1 to 35 Hz			1 to 35 Hz		
Seismic-intensity Class.		N/A	Low	Mid.	High	Low	Mid	High	Low	Mid.	High
Input level (g)	Hor.	0.3g, or 0.5g at pocket end		0.25	0.5	0.2	0.3	0.5	0.2	0.3	0.5
	Ver.	0.15g, or 0.5g at pocket end		0.2	0.4	0.1	0.15	0.25	0.1	0.15	0.25
Input point		Low end of frame or bushing-pocket	Low end of frame (equipment)			Low end of frame (equipment)			Low end of frame (equipment)		
Input direction		Uni-Axial. If required, Bi-Axial (x,z.).	Tri- or Bi-Axial *In Bi-Axial (x,z), intensity x $\sqrt{2}$			Uni-Axial :desired *Multi-Axial is not recommended			Uni- or Multi-Axial *In Bi-Axial (x,z), intensity x $\sqrt{2}$		
Input wave form	Sine	3 Resonance-sine waves	10 cycle/beat (only discont.-sw.)			Sine-Sweep Sine-Beat			Sine-Beat Continuous sine		
	Random	Actual e.q.record	Art-Wave matching RRS			Art-Wave matching RRS			Art-Wave matching RRS		
Dynamic analysis		Time history Modal analysis	R-spectrum anls. Modal analysis								

1.3 Past Studies on Seismic Protection of Transformer

Wilcoski (1997) conducted seismic qualification and fragility testing of a 500-kV transformer bushing by using the shaking table test to determine the dynamic characteristics of the bushing, to qualify the bushing to the IEEE 693-1997 spectrum anchored at 0.5g, and to define the capacity of bushings. A fundamental frequency of approximately 6 Hz and a damping ratio of between 2 to 3 % of critical were reported. During the fragility test, when the 2% IEEE 693-1997 response spectrum is matched with a PGA of 1.0g, the bushing leaked oil.

Villaverde (1999) conducted field-testing and analytical study of 230-kV and 500-kV bushings mounted on transformers. The objectives of the studies were to evaluate the dynamic characteristics of the transformer-bushing systems and to compute the amplification between the accelerations at the bushing flange and the ground as a result of the flexibility of the transformer tank and the turrets to which the bushings were attached. For the 230-kV bushings, a fundamental frequency of approximately 6Hz and a damping ratio of 2% of critical were reported. For the 500-kV bushings, a fundamental frequency of between 3 to 4 Hz and a damping ratio of between 2 and 4 % of critical were reported.

The seismic testing and evaluation of two 196-kV and three 550-kV bushings was carried out at the University of California at Berkeley (Gilani Amir, 1999). The objectives of the studies were to compute the dynamic properties of the bushings, to qualify the bushings to the IEEE 693-1997 required response spectrum, and to characterize the seismic performance of the bushings. For the 196-kV bushings, fundamental frequencies of between 14 and 16 Hz and damping ratios of between 2 to 4 % of critical were measured. For the 550-kV bushings, fundamental frequencies of approximately 8 Hz and damping ratio of between 3 to 4 % of critical were measured. None of the three 550-kV bushings met the IEEE 693-1997 requirements of the moderate-level qualification (target PGA equal to 1.0g). When subjected to severe shaking, all three bushings experienced oil leakage at the gasket connection and slip of the upper porcelain unit over the flange.

Bonacina (1995) and Serino (1995) performed several feasibility studies of base isolation for substation facilities by numerical simulation. Practical design examples of base isolation system for 170-kV gas-insulated substations were introduced. Two types of isolation systems were studied: 1) a high damping rubber bearing system (HRB) and 2) helical spring devices with viscous dampers (HS+VD) system. The designed isolation period of each system varied in the range of 1.5 to 2.0 seconds and 8% to 20% damping ratios. The response displacements were in the range of 17 to 19 centimeters. The effectiveness of the systems was demonstrated. Fujita (1984 and 1985) made experimental and analytical study on the base isolation of heavy weight equipment such as power transformers. This study mainly focused on the development of isolation devices. The research was carried out in early application stage of base isolation in Japan. However, the study did not cover the interaction of the porcelain bushing mounted on top of those facilities. Their test-frame did not contain any bushings.

1.4 Base Isolation for Seismic Protection of Transformer

The base isolation technology has gained popularity in the recent decade as one of the rehabilitation measures for seismic protection of structures. This is especially true in Japan, where over 1000 base-isolated buildings have been constructed or are under construction since the 1995 Kobe earthquake. Many types of isolation systems have been developed, such as high-damping rubber bearing systems, lead-rubber bearing systems, systems of low-damping bearing combined with dampers, and sliding bearing systems. The fundamental period and displacement of such base-isolated buildings are generally over 3.0 seconds and over 300 mm. The reduction of response acceleration to the ground motion is less than 30%. Some of the applications of base isolation include bridges, LNG tanks, warehouses, nuclear plants, and other industry facilities. The first application of an electric facility was the high-voltage condenser system in Haywards, New Zealand, in 1988 (Skinner, 1993). The isolation system consists of low-damping rubber bearings and steel dampers. The bearings are 400 mm x 400 mm in plane dimensions and 254 mm in total height. The load-sustaining capacity of the bearing is 5,000 kgf. The system shifted the effective period from 0.2 second in the fixed-base system to 1.8 seconds. A major difference of design requirements between base isolation of conventional structures and electric facilities (i.e. transformer/bushing system) are the lightweight structure that makes it difficult to make long period-shifting. When a base isolation scheme is planned for a transformer/bushing system, the goal is to protect the transformer and the porcelain bushing that makes up only a few percentage of the entire weight. The small mass of the bushing is sensitive to high-mode frequency even with a small-amplitude acceleration.

1.5 Research Objectives

The objective of this research is to develop a new methodology for seismic protection of power transformer/bushing systems by application of modern base isolation schemes by performing comprehensive analytical and experimental study. Tri-axial earthquake simulator testing with a large-scale model was used for the first time in this field. Design of a base isolation system for the transformer/bushing system presents a unique challenge for the following two reasons.

1. The entire mass of the system is much lighter than a building, making it difficult to lengthen the natural period.
2. The base isolation system should reduce the response acceleration of the bushing and transformer without resulting in a large base displacement. A large displacement is not desired considering the interaction with the cable-connected other facilities.

A task flowchart of this research project is shown in Figure 1-6. First, tri-axial earthquake simulator testing was conducted. The testing program was part of a joint research project between MCEER and the National Center of Research on Earthquake Engineering (NCREE) in Taipei, Taiwan, and the earthquake simulator test was conducted at NCREE. A large-scale 2 m x 2 m x 1.8 m transformer model with a bushing, together with two types of isolation systems were designed and manufactured for the project. Actual porcelain bushings of 161-kV and 69-kV sizes were used in the testing. Two types of isolation systems, one using sliding bearings combined with rubber bearings and the other segmented high-damping bearings, were developed in this project. The testing program was classified into two phases by the type of isolation system. Phase-1 tested the isolation system consisting of sliding bearings and low-damping rubber bearings, while Phase-2 tested a segmented high-damping rubber bearing (SHRB) system.

I. Phase-1 Testing: (Aug. 1999 ～ Sep. 1999)

1. Isolation System :
   4xSliding bearings + 2xLow damping rubber bearings
2. Transformer Model and Bushing:
   235.5 kN Frame-structure with counter weight
   161kV & 69kV bushings
3. Ground Motion :
   1940 El Centro, 1994 Northridge (Sylmar), 1995 Kobe (Takatori)

⇩

II. Phase-2 Testing: (Jan.2002)

1. Isolation System :
   4x Segmented High-damping Rubber Bearings (SHRB)
2. Transformer Model and Bushing:
   145kN Frame-structure with counter weight
   161kV Bushing
   Rubber Ring to elongate the period of bushing
3. Ground Motion :
   1994 Northridge (Sylmar), 1995 Kobe (Takatori)
   1999 Chi-Chi, Artificial wave- ART 693

⇩

III. Analytical Study

1. Numerical Model Calibrated by test results in Phase-1, and Phase-2
2. Parametric Study :
   Effect of bushing mass, natural frequency, stiffness
3. Case Study:
   Numerical simulation of existing transformer with/without base isolation

Figure 1-6 Task-Flow of Research

Next, numerical study of the base-isolated transformer/bushing system was conducted. A simplified mathematical model of the base-isolated transformer/bushing was proposed, where the properties of the isolation system were expressed as non-linear functions. The model was calibrated by the Phase-1 and -2 tests. Finally, the results of experimental and analytical study were reviewed and the effectiveness of the base isolation as the measure of seismic protection of transformer/bushing system was discussed.

1.6 Organization of Technical Report

This report is organized into six sections. Section 2 contains an introduction followed by a review of the design procedure for base isolation systems. Section 3 and 4 discuss the earthquake simulator testing of Phases -1, and -2 including the base isolators, transformer and bushing model, test setup, test programs, and test results. Section 5 presents numerical analysis of base-isolated transformer system, including comparison with the test results and case studies. Finally, Section 6 provides a summary and conclusions of the research. Appendix A presents additional earthquake simulator test results of transformer/bushing system that includes the bushing electrical connection interaction.

SECTION 2
DESIGN OF BASE ISOLATION SYSTEMS FOR POWER TRANSFORMERS

2.1 Overview

In this chapter, the concept of base isolation for transformer/bushing system is proposed. Since the transformer is light compared to a building, it requires a different engineering approach. A large 500-kV transformer can weigh 2400 kN. If four isolators are installed beneath the corner of the transformer-bottom, the weight per isolator is only 600 kN. The diameter of the rubber bearing for 600 kN is estimated at about 400 mm. Generally, the target period of base isolation is over 2.0 seconds and, as a result, displacement for design-basis earthquake (DBE) will reach more than 300 mm. Under the maximum credible earthquake (MCE), the displacement is usually more than 400 mm, and a bearing with 400 mm diameter will loose its stability. Therefore, displacement should be repressed to a certain level by control of period shifting and increase of damping. Actually, the large displacement is not desired for those electric facilities considering interaction in interconnected equipment in the substation system. On the other hand, the reduction of response acceleration is not required to such a level as required in general base isolation. The aim is not to protect the human life or valuable properties inside building but to protect transformers and porcelain bushings from fracture by overturning or over-stress. Based on the above discussion, the design philosophy of a base-isolation plan for the facilities in the substation is summarized as follows:

1. The response acceleration of transformer and bushing shall be reduced.
2. Large displacement is not desirable.
3. Reduction of the acceleration may be smaller than that of base-isolation design for a conventional structure.

The design basis of a base-isolation system for the transformer/bushing is discussed in the following section by showing some design examples and analyses.

2.2 Conventional Base Isolation System

Base isolation is an aseismic design concept to reduce the seismic force transmitted to the structure by supporting it with a flexible element at the base to elongate the natural period of the structure and thereby decouples it from the ground. The first base-isolated building in the United States, Foothill Communities Law and Justice Center in San Bernadino, California, was constructed in 1985 (Clark, 1997). During the 1995 Kobe earthquake (officially known as Hyogo-ken Nanbu earthquake), two base-isolated buildings located in the suburb of Kobe demonstrated excellent performance and verified the effectiveness of the base isolation. Through this experience, base isolation technology has been widely accepted and gained great popularity in Japan. At this time, there are more than 1000 base-isolated buildings and additional 200 base-isolated buildings appear to be scheduled for construction each year.

Basically, base isolation systems provide functions of restoring force and energy dissipation. The rubber bearing, made up with layers of alternating rubber and steel plates, as shown in Figure 2-1, is the most popular device for providing a restoring force. The two components of the rubber bearing are bonded to each other by strong special adhesion materials. The steel plates act as confinement for the rubber layers to support vertical loads with low horizontal stiffness. Generally, the ratio of the vertical stiffness and horizontal stiffness is over 1000.

Ordinarily, there are three types of rubber bearings: 1) Natural Rubber Bearings (NRB); 2) High-damping Rubber Bearings (HRB); and 3) Lead-rubber Bearings (LRB). With NRB, over 60% of total weight of rubber is natural rubber. The NRB has almost linear characteristics in the horizontal force – displacement relationship and low damping. Therefore, when using NRB, additional damping devices such as hydraulic dampers, steel bar dampers or friction dampers, are required in order to control the response displacement. HRB is a type of rubber bearing in which a specially-compounded rubber material is used to provide energy-dissipation capability during deformation, in addition to its restoring function with its stiffness. LRB is another type of rubber bearing that has both spring and damping functions combined. The cylindrical-shaped lead core is vertically inserted at the center of the bearing for energy dissipation.

Recently, extensive research and development work has been carried out for the sliding bearing. The sliding bearing has a sliding surface generally made of PTFE (poly-tetra-fluoro-ethylene) mating with a stainless steel plate. The coefficient of friction of the sliders is 0.10 to 0.20 with normal PTFE and stainless plates, and 0.02 to 0.04 with lubricated PTFE and PTFE-coated stainless plate. Sliding bearings are used mainly in combination with rubber bearings as a restoring force element to control the sliding displacement during an earthquake and to prevent excessive permanent displacement after an earthquake. The merit of this system is to be able to achieve a longer period shifting with larger damping. Also, this system is quite effective in the case of a structure that has relatively lightweight – under 2 MN – such as residential house, industrial equipment, or power transformer.

2.3 Mechanism of Rubber Bearings

Much research of the mechanism of the laminated rubber bearings has been analytically and experimentally conducted in the past two decades (Constantinou, 1990; Gent, 1959). The derivation of governing equations to describe the mechanical behavior of the laminated rubber bearing is omitted for simplicity. The essential equations for practical design procedures are introduced below. Physical parameters of the laminated rubber bearings are presented here. They include: outer rubber diameter D, inner rubber diameter d, unit rubber layer thickness t_r, shim plate thickness t_s, number of rubber layers n_r, and total rubber height h. The horizontal stiffness K_h and vertical stiffness K_v are presented in the following equations.

$$K_v = \frac{E_c \cdot A_{eff}}{h} \tag{2-1}$$

$$K_h = \frac{G_{eq} \cdot A_{eff}}{h} \tag{2-2}$$

where,

$$E_c = \frac{1}{\frac{1}{E_{ap}} + \frac{1}{E_\infty}}, \quad E_{ap} = E_0(1 + 2\kappa S_1^{\,2})$$

$A_{eff} = \frac{\pi}{4} \cdot D^2$ or $\frac{\pi}{4} \cdot (D^2 - d^2)$ is cross sectional area

$S_1 = \frac{D}{4t_r}$ or $\frac{(D-d)}{4t_r}$ is first shape factor

$h = n_r \cdot t_r$

E_0 is Young's modulus
$E\infty$ is bulk modulus of rubber
κ is correction factor
G_{eq} is shear modulus
h is total rubber height
n_r is number of rubber layers
t_r is thickness of unit rubber layers

Among the parameters shown above, first shape factor S_1, or sometime simply called shape factor, is a key factor. S_1 is the ratio of the free surface area of the rubber relative to the load-supporting area of one unit rubber layer of the rubber bearing. In the case of circular rubber bearings without a center hole, S_1 is derived from the following equation.

$$S_1 = \frac{loading\ area}{free\ area} = \frac{\frac{1}{4}\pi D^2}{\pi D t_r} = \frac{D}{4t_r} \qquad (2\text{-}3)$$

When S_1 becomes larger, the rubber pad becomes thinner and as a result, the pad will have a larger stiffness in the loading direction. Generally, S_1 is 20 to 30 for rubber bearings. As shown in the above equations, the apparent Young's modulus for the loading direction of the rubber pad will be affected by the square of S_1 (Thomas, 1982). Vertical stiffness K_v is calculated with the modulus E_c, which is corrected with bulk modulus E_∞ of the rubber material itself. On the other hand, the horizontal stiffness is calculated with shear modulus G_{eq} without any influence from the shape factor S_1. If the bearing also has energy dissipation capability, equivalent damping ratio h_{eq} is generally used as the representative physical property and is calculated by the following equation.

$$h_{eq} = \frac{1}{2\pi} \cdot \frac{W_d}{K_h \cdot X_C^{\ 2}} \tag{2-4}$$

where, W_d is dissipated energy per cycle

X_C is shear amplitude

As introduced in the preceding section, the rubber bearings having energy dissipation capacity are HRB and LRB. Both bearings have h_{eq} from 15% to 25%. Figure 2-2 shows a typical horizontal force-displacement curve of HRB during cyclic loading. Figure 2-3 shows the relationship between shear strain and shear modulus G_{eq}, and equivalent damping ratio h_{eq} of HRB. This non-linear relationship between shear strain, G_{eq} and h_{eq} is generally determined experimentally. In practical design, those functions are provided by manufactures. As an example, some rubber bearing manufactures provide the following polynomial equations for this purpose.

$$G = G_{eq} = f(\gamma) = \sum_{i=0}^{n} a_i \cdot \gamma^i \tag{2-5}$$

$$h_{eq} = g(\gamma) = \sum_{i=0}^{n} b_i \cdot \gamma^i \tag{2-6}$$

where, γ is shear strain

The coefficients a_i and b_i are determined from the force-displacement relationships obtained by both scaled and full-size model testing. Therefore, shear modulus G_{eq} should be understood as effective shear modulus G_{eq}, which means that this is the property determined by particular testing with a certain shape of a test specimen. The certain shape of a test specimen in this case is the alternately laminated rubber bearing. Those force-displacement relationships as shown in Figure 2-2 are generally modeled in a dynamic analysis, either as equivalent linear properties or as an elasto-plastic bilinear model. The equivalent linear model with K_h and h_{eq} will provide a reasonably good approximation with such a simple procedure as response spectrum analysis,

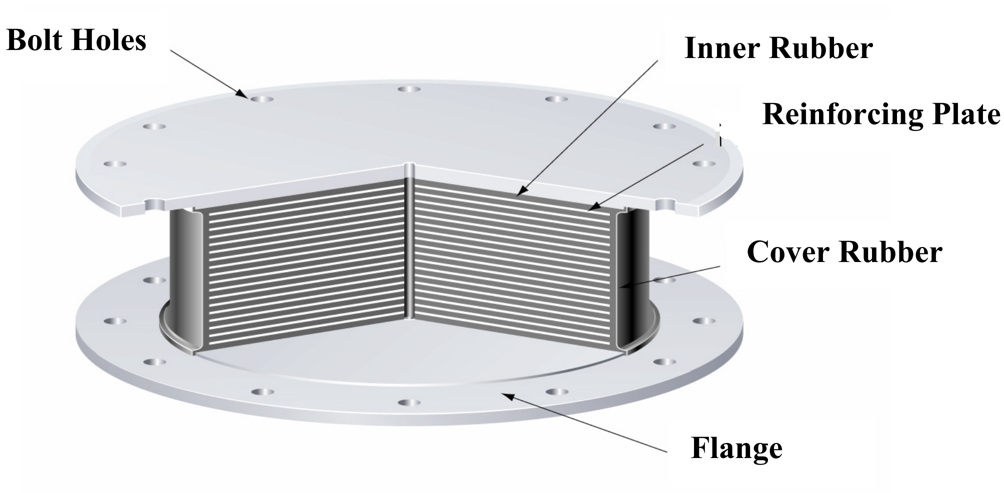

Figure 2-1 Laminated Rubber Bearing

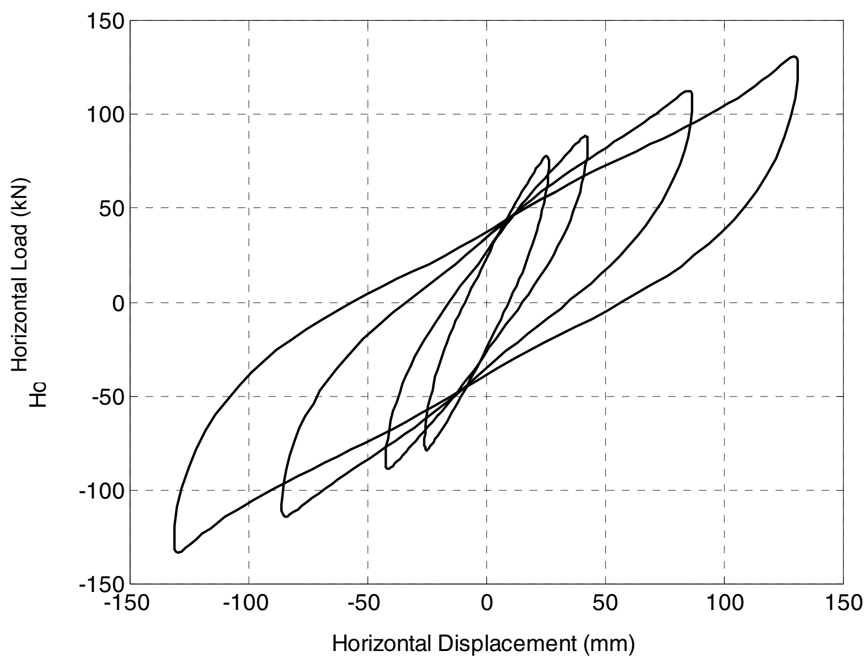

Figure 2-2 An Example of Hysteresis Curve of High-Damping Rubber Bearings

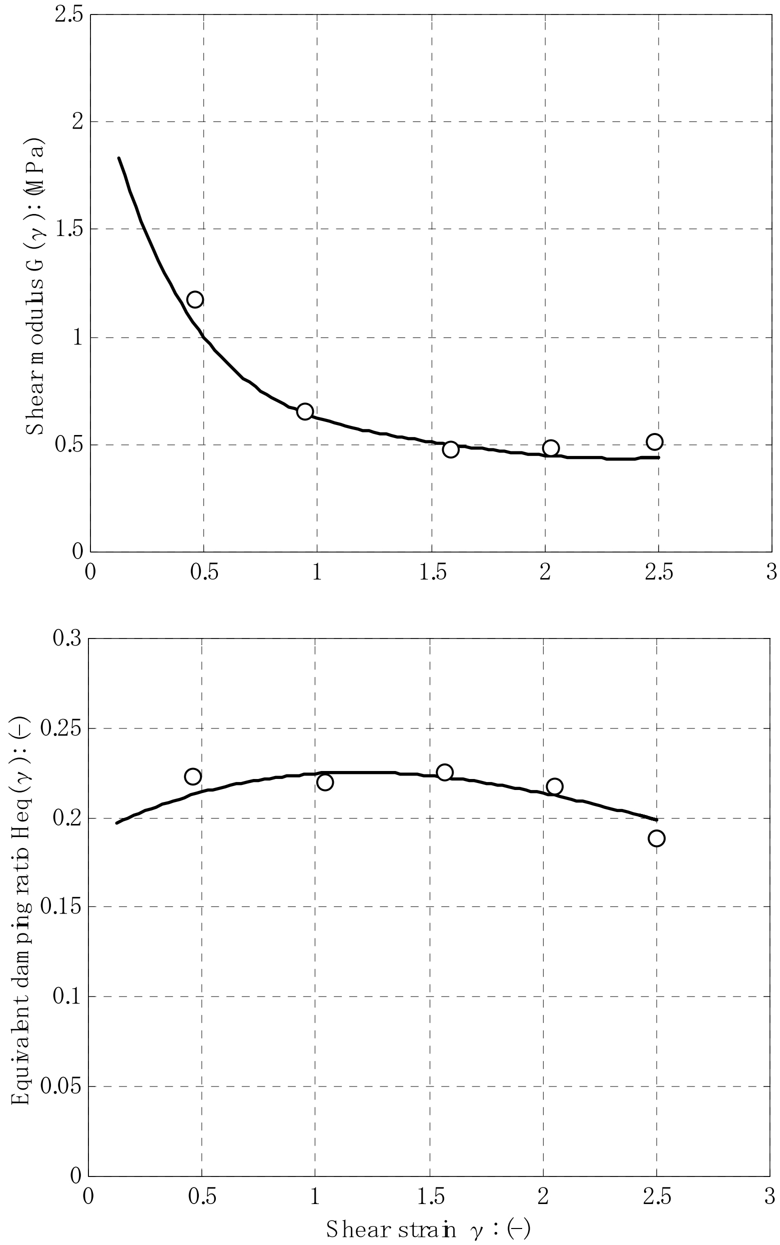

Figure 2-3 Relationship of Shear Modulus and Equivalent Damping Ratio versus Shear Strain

whereas bilinear modeling offers more precise and detailed response information by nonlinear time history analysis. The determination of the bilinear model is shown in Figure 2-4. The force-displacement relationship is modeled with initial stiffness K_1, post yielding stiffness K_2 and yield load Q_y or yield deflection δ_y. In the case of LRB, because the hysteresis curve shows typical elasto-plastic characteristics, the modeling procedure is directly determined from actual performance curve. In the case of HRB, which shows rather viscous-elastic behavior in its hysteresis curve, K_2 and Q_y will be changed according to the loading amplitude. Therefore, the assumption of reasonable loading amplitude is needed to translate the characteristics to a bilinear model. However, the target displacement of the isolation system will not differ much from structure to structure and will be at a similar level with adequate design earthquake levels. If the calculated bearing displacement is significantly different from the assumed displacement, another displacement will be assumed and next calculation will be performed. For a few trial and error procedures, a reasonable solution will be obtained.

2.4 Design of Rubber Bearings

2.4.1 Preliminary Design based on Stiffness Requirement

The dynamic behavior of the structure is mostly characterized by the isolation system. It is a great benefit of the base isolation. Even if the structure has an irregular shape with a large eccentricity in inertia, earthquake response will not be affected so much for the base-isolated structure. The target period of base isolation is generally 2.0 to 3.0 seconds at the design earthquake level. Such period shifting will result in a base displacement of 150 to 300 mm. The first shape factor, S_1, is the influential factor to the vertical stiffness and is determined by the vertical stiffness requirement restricted by the creep performance under long-term vertical load (Thomas, 1982). The vertical frequency, f_v, is generally required over 12 Hz resulting in S_1, practically and empirically, in the range of 20 to 30. The diameter of the bearing, if circular in shape, will be mainly decided by the vertical load to be carried by the bearing. The maximum compressive stress of the rubber area is restricted by the long-term deterioration of the rubber, such as creep, as well as the buckling characteristics of the bearing. Higher compressive stress will result in decreasing ultimate displacement by virtue of buckling. Generally, the long-term

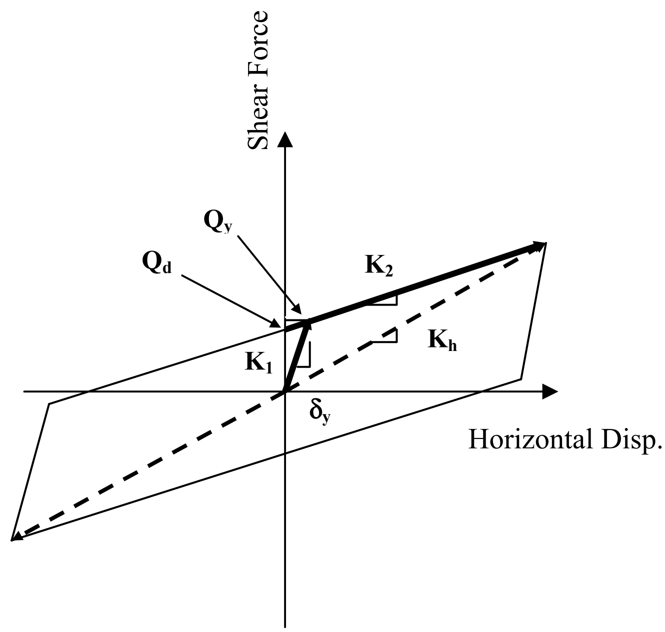

Figure 2-4 Definition of Bi-Linear Model for Isolators

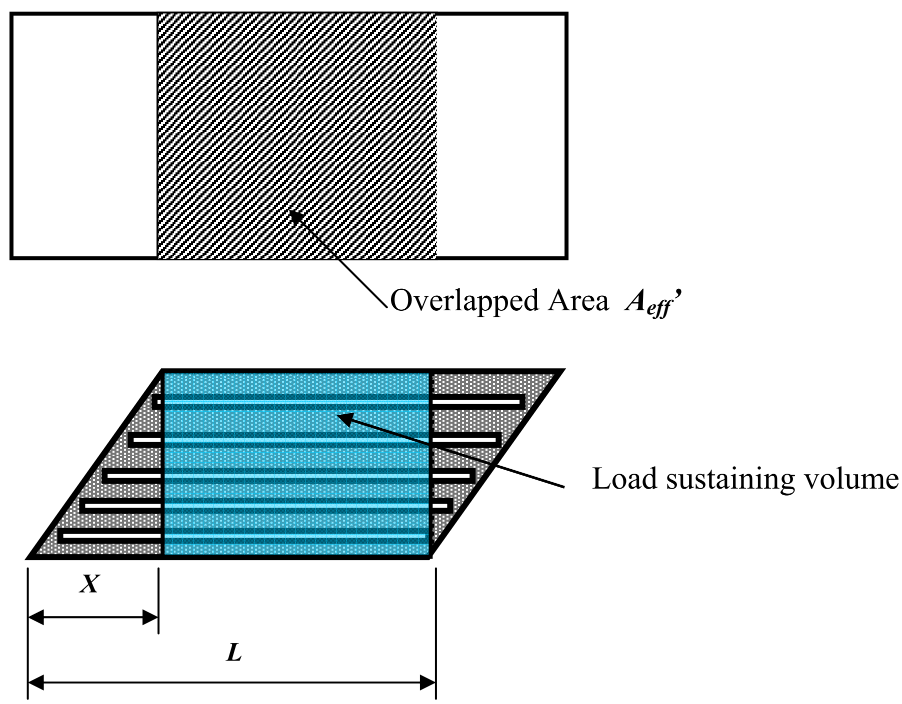

Figure 2-5 Overlapped Effective Area of Rectangular Type Bearing at Displacement *X* [2-8]

compressive stress is in the range of 4 to 10 MPa. The design procedure is summarized as follows.

I. .Design Conditions

· design horizontal frequency f_h $(= \frac{1}{T_h})$

· design vertical frequency f_v

· design base displacement X_D

· maximum displacement X_M

· vertical load P

· maximum allowable shear strain γ_M

· design base shear strain γ_D

· rubber material properties $G (= G_{eq}), E_0, \kappa, E_\infty$

Design base displacement X_D and maximum displacement X_M are generally determined from the response spectrum with assumed design horizontal frequency f_h (or the period T_h).

II. Design Procedure

<u>Step-1 : total rubber thickness h</u>

$$h = \frac{X_D}{\gamma_D} \quad \text{with} \quad h \geq \frac{X_M}{\gamma_M} \tag{2-7}$$

Step-2 : shape factor S_1

$$\left(\frac{f_v}{f_h}\right)^2 = \frac{K_v}{K_h} = \frac{E_c}{G} = \frac{E_0(1+2\kappa S_1{}^2)\cdot E_\infty}{G\{E_0(1+2\kappa S_1{}^2)+E_\infty\}} \tag{2-8}$$

$$\therefore S_1 = \left(\frac{\chi G(1+\frac{E_\infty}{E_0}) - E_\infty)}{2\kappa(E_\infty - \chi G)}\right)^{\frac{1}{2}}, \quad \text{where } \chi = \frac{K_v}{K_h} \tag{2-9}$$

Step-3 : diameter D

$$D = \left(\frac{\pi K_h \cdot h}{4G}\right)^{\frac{1}{2}} \tag{2-10}$$

$$K_h = \frac{4\pi^2 f_h{}^2 P}{g} \tag{2-11}$$

Step-4 : unit rubber layer thickness t_r and number of layer n_r

$$t_r = \frac{D}{4S_1} \ \textit{and} \quad n_r = \mathrm{int}\left|\frac{h}{t_r}\right| \tag{2-12}$$

where, int| **a**| is the integer value closest to the real value of **a**

In Step-2, a reasonable S_1 is decided first and f_v is calculated later. The vertical frequency, f_v, is not an important design factor as long as it falls in a reasonable range, such as, $12 \leq f_v \leq 20$Hz. After the completion of these calculations, the ultimate capacity of the bearings shall be checked as shown below.

2.4.2 Prediction of Ultimate Capacity of Rubber Bearings

The ultimate properties of the rubber bearing may be classified into two types: rubber breaking and buckling. In a typical design, breaking will occur at over 400% shear strain with a corresponding ultimate displacement of over 600 mm. This displacement is usually large enough for base isolation. A bearing with a large diameter to height ratio will have no buckling before the rubber breaks. However, in many cases, the bearings will experience buckling before breaking (Kelly, 1993). Here, we derive a new design factor called the secondary shape factor, S_2, calculated by the following equation:

$$S_2 = \frac{D}{h} \tag{2-13}$$

Many experiments verified that the bearing in the range of $S_2 \geq 5$ is stable until rubber breaking and has no buckling problem. However, to obtain the isolation period over 2.0 seconds, the rubber height becomes at least over 160 mm even if the softest rubber compound is used. It means that the diameter of the bearing will be over 800 mm. A typical compressive stress of a bearing is 6.0 MPa, and the sustaining column load is calculated as 3.0 MN. This corresponds to the vertical load on interior located column of an 8-story reinforced concrete (RC) building. Buildings with less weight would be isolated with the smaller diameter resulting in a smaller S_2. Considering the majority of the structures weigh lighter than 8-story RC building, buckling will be the critical failure mode of a rubber bearing.

The prediction of buckling behavior of a rubber bearing under combined compression and shear loading is not simple because of its geometric and material nonlinearity. The load under zero deflection assumption is considered as the critical buckling load, P_{cr}, by many analytical and experimental studies. Koh and Kelly (1988) derived the critical load, P_{cr}, under zero displacement with linear assumption as follows:

$$P_{cr} = \frac{-P_S + (P_S^2 + 4P_S P_E)^{\frac{1}{2}}}{2} \tag{2-14}$$

$$P_S = GA_S, \quad P_E = \frac{\pi^2 E_b I_S}{H^2} \tag{2-15}$$

where,

$$A_S = A_{eff} \cdot \left(\frac{H}{h}\right), \quad I_S = I_{eff} \cdot \left(\frac{H}{h}\right) \tag{2-16}$$

H is bearing height
($H = n \cdot t_r + (n-1) \cdot t_s$, t_s is thickness of shim plate)

I_{eff} is effective moment of inertia,

$$I_{eff} = \frac{\pi}{64} \cdot D^4 \tag{2-17}$$

When $S_2 > 3$, equation (2-14) will be approximated as follows.

$$P_{cr} = (P_S P_E)^{\frac{1}{2}} \tag{2-18}$$

E_b is the apparent Young's modulus of a thin rubber pad for bending deformation. Fujita (1985) provided the equation for E_b as follows,

$$E_b = \left(\frac{1}{E_0 (1 + \frac{2}{3} \kappa S_1^2)} + \frac{1}{E_\infty} \right)^{-1} \tag{2-19}$$

Then the critical stress for buckling will be derived as follows.

$$\sigma_{cr} = \frac{\pi}{4} S_2 \left(E_b G\right)^{\frac{1}{2}} \tag{2-20}$$

Buckle (1994) introduced P_{cr} under large displacement for rectangular type bearing by reducing P_{cr} at zero displacement with the ratio of the effective overlapped area at the displacement X, as shown in Figure 2-5.

$$P_{cr}' = P_{cr} \cdot \left[1 - \frac{X}{L}\right] \tag{2-21}$$

where, L is bearing length in loading direction

For the circular bearing, the overlapped-area is expressed in more complicated form as shown in (2-23).

$$A_{eff}' = \frac{D^2}{2} \cdot \left(\theta_d - \frac{1}{2}\sin(2\theta_d)\right) \tag{2-22}$$

A_{eff}' is overlapped area at displacement of X

where,

$\theta_d = \arccos(X / D)$

X is horizontal displacement

D is bearing diameter

The critical load is given as follows.

$$P_{cr}' = P_{cr} \cdot \frac{A_{eff}'}{A_{eff}} = \sigma_{cr} \cdot A_{eff}' \tag{2-23}$$

However, many test results verify that the critical load given by the above-mentioned procedure is conservative enough, and even for circular bearings. The simple equation for a rectangular bearing (2-21) is also applicable in practical design, as shown in (2-24).

$$P_{cr}' = P_{cr} \cdot \left[1 - \frac{X}{D}\right] \tag{2-24}$$

where, D is diameter of bearing

Equation (2-24) is translated by introducing A_{eff} and S_2 into (2-25).

$$\sigma_{cr}' = \sigma_{cr}\left(1 - \frac{X}{h} \cdot \frac{h}{D}\right) = \sigma_{cr}\left(1 - \frac{\gamma}{S_2}\right) \tag{2-25}$$

Using (2-25), design criteria of bearings regarding buckling stress is expressed with given design compressive stress σ as (2-26).

$$\gamma \leq S_2\left(1 - \frac{\sigma}{\sigma_{cr}}\right) \tag{2-26}$$

where,

$\gamma = \frac{X}{h}$, is shear strain of rubber, and

$\sigma = \frac{P}{A}$, is design compressive stress on rubber bearing

Another criteria of ultimate properties is breaking of bearing, which is determined by testing. Generally, the breaking property is defined as breaking strain γ_b under given design compressive stress σ. With relationship of equation (2-26) and γ_b, the demand of ultimate properties of bearings can be illustrated in a diagram with σ and γ, as shown in Figure 2-6. The intersection of maximum compressive stress and shear strain must be within the enclosed are bounded by the horizontal-vertical axis, the line expressed by (2-26), and $\gamma = \gamma_b$.

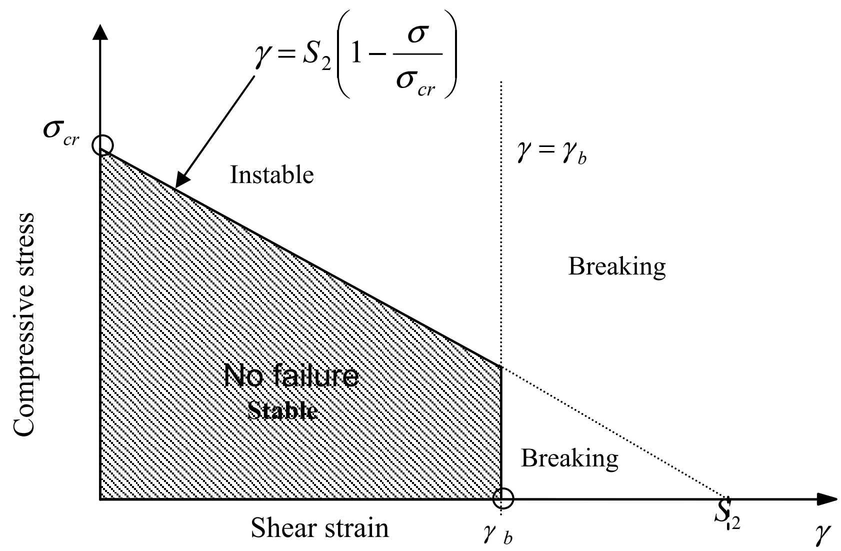

Figure 2-6 Design Diagram for Ultimate Properties of Isolators

2.5 Base Isolation Systems for Lightweight Structures

2.5.1 Sliding Bearing

For a lightweight structure, the small axial load on a bearing makes it impossible to design a rubber bearing which satisfies the requirements for buckling, breaking, and creeping safety, as discussed before. One of the countermeasures is to apply sliding bearings in such an isolation system.

A sliding bearing generally consists of a PTFE disc and a stainless steel plate. A rubber pad is usually attached to the PTFE disc. The general configuration of a sliding bearing is shown in Figure 2-7. Compressive stress on PTFE is designed within the range of 10 MPa to 30 MPa. In order to endure high compressive stresses, PTFE is usually confined with glass fiber or carbon fiber. One of the functions of the rubber pad is to reduce the shock generated when the static friction force is broken and the bearing slides (usually called “breaking away”). If there were no rubber pad, the shock would stimulate the high frequency mode response of the isolated structure. The friction coefficient of PTFE usually depends on sliding velocity and compressive stress. Higher sliding velocity increases the friction coefficient. A typical relationship of sliding velocity and friction coefficient is shown in Figure 2-8. The test data was obtained with a PTFE disc confined with glass fiber. However, as the figure indicates, at the velocity range under earthquake ground motions, such as ≥250 cm/s, the friction coefficient can be considered constant.

Another typical characteristic of sliding bearings is compressive stress dependence. The friction coefficient will be lower when the compressive stress becomes higher. For example, the friction coefficient at 10 MPa is 0.14; whereas at 30 MPa, it becomes 0.090 (see Figure 2-9). The compressive stress is generally limited by the fracture and creep characteristics of the PTFE material.

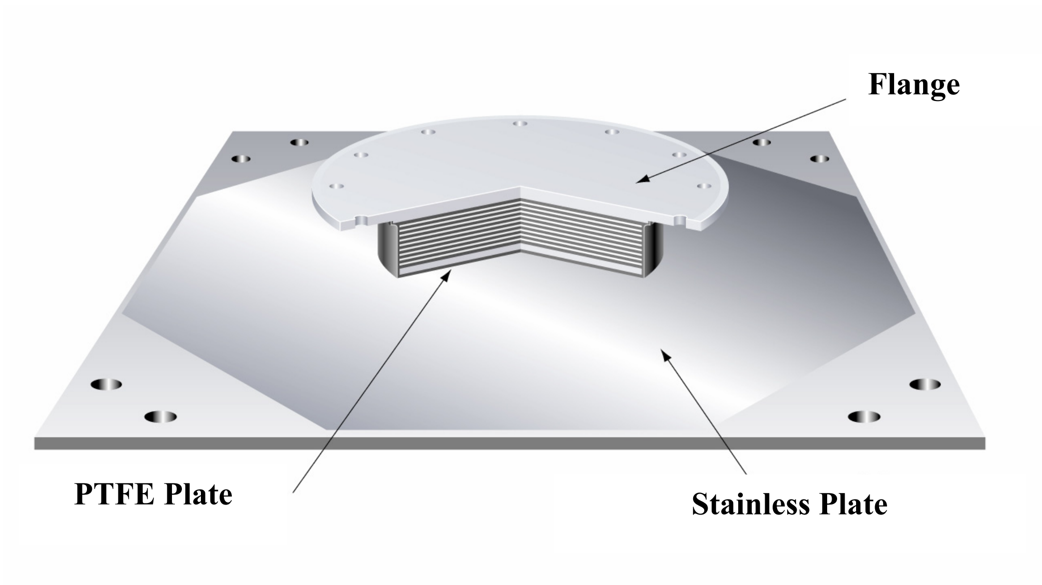

Figure 2-7 Sliding Bearing

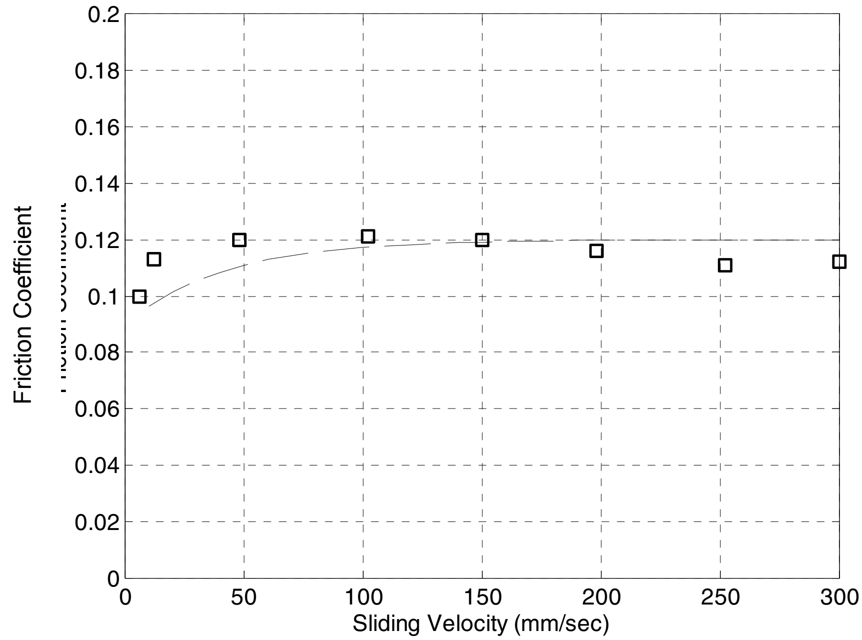

Figure 2-8 Sliding Velocity Dependency of Friction Coefficient: Compressive Stress =12MPa, Confined PTFE

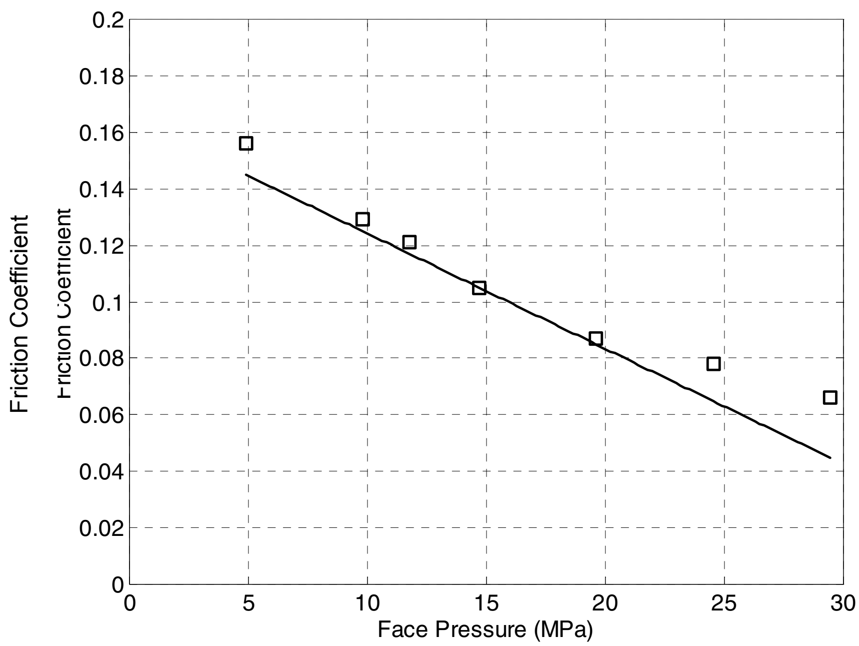

Figure 2-9 Compressive Stress Dependency of Friction Coefficient: Velocity = 200(mm/sec), Confined PTFE

2.5.2 Segmented Rubber Bearing

A segmented rubber bearing is another prospective solution of isolation of lightweight structures. It has a structure of layers consisting of several laminated rubber bearings with stabilizing plates as shown in Figure 2-10. This type of structure has low stiffness, large deformation capability, and good stability. Its main use is a spring element for tuned-mass dampers--vibration controls for high-rise buildings. Masaki (1999) conducted an experimental and analytical study on the application of segmented rubber bearings. Basically, the deformation capability is computed as the deformation of an element bearing multiplied by the number of layers. However, the rotation of the element bearing at the end fixed to the stabilizing plates, and the bending stiffness of the stabilizing plate itself affects the ultimate deformation of the bearing. Masaki studied the instability characteristics of the element rubber bearings with a bending moment at one end and verified that the bending moment causes the reduction of its stability. According to the results of experiments by Masaki, the ultimate deformation of an element bearing in a segmented structure will be reduced to approximately 80% of the individual element. The precise analytical approach will be a topic of future study.

2.6 Proposed Design Procedure of Isolation System for Transformer

The preliminary response-analysis of base-isolated structures can be determined by the statically equivalent method, namely the equivalent linearization method (EQLM). In UBC 97, the EQLM formulas provide displacements and forces and are based on constant-velocity spectra over the period range of 1.0 to 3.0 seconds. In the calculation procedure, the isolation system is modeled with equivalent linear properties. The solution is given by a response spectrum.

In this study, we apply this static analysis, EQLM, to the preliminary design of the base isolation system for a transformer. The isolation system is modeled with a bi-linear characteristic and the solution is obtained by an iterative process with response spectrum, as shown in Figure 2-11. The IEEE 693-1997 Required Response Spectrum (RRS), which is introduced in Chapter 1, is applied as the demand-spectrum. The IEEE 693-1997 RRS (High Level) is defined as follows:

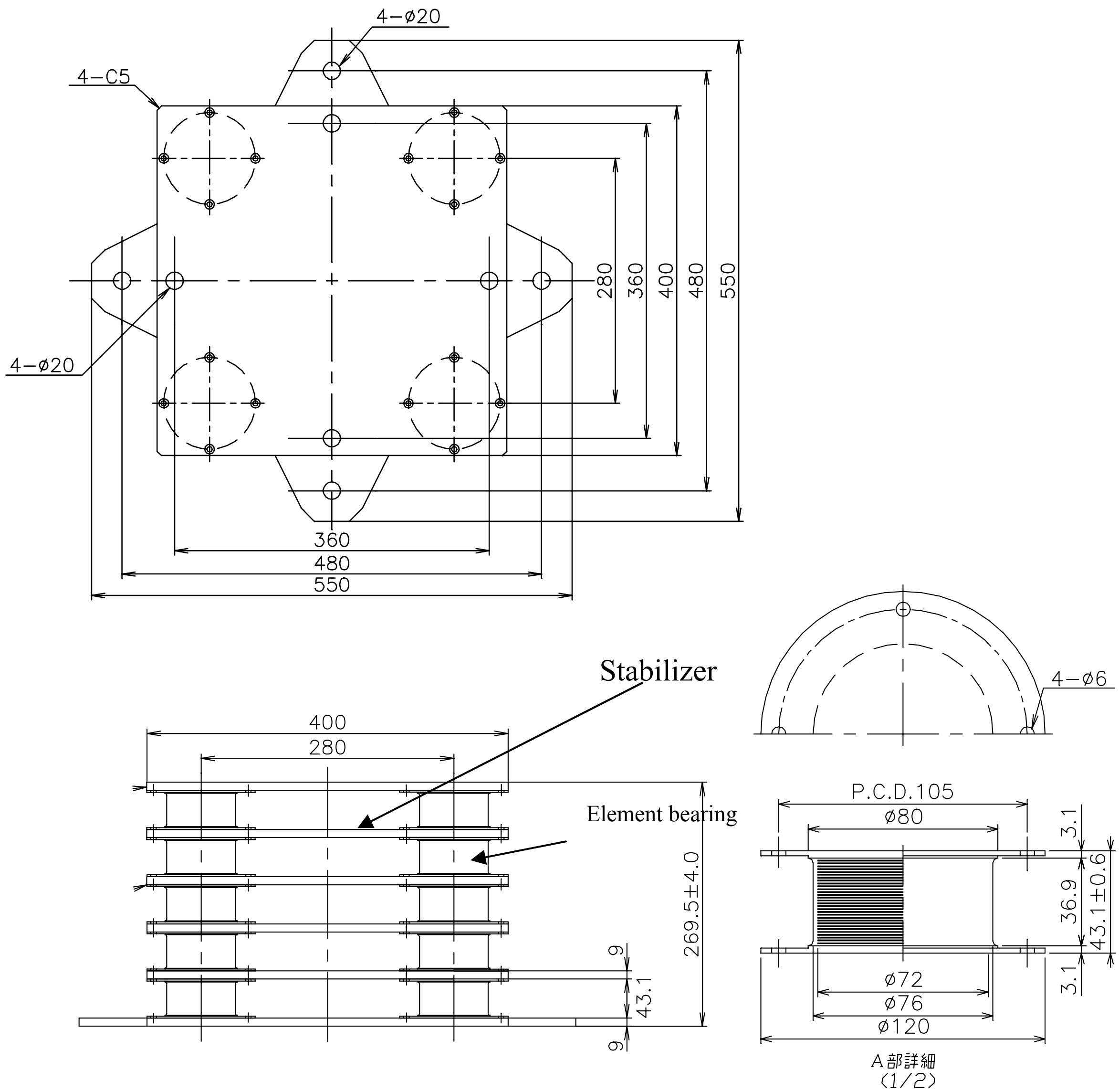

[Element Bearing]

- Low stiffness with stable performance at large displacement

Figure 2-10 Segmented Rubber Bearings

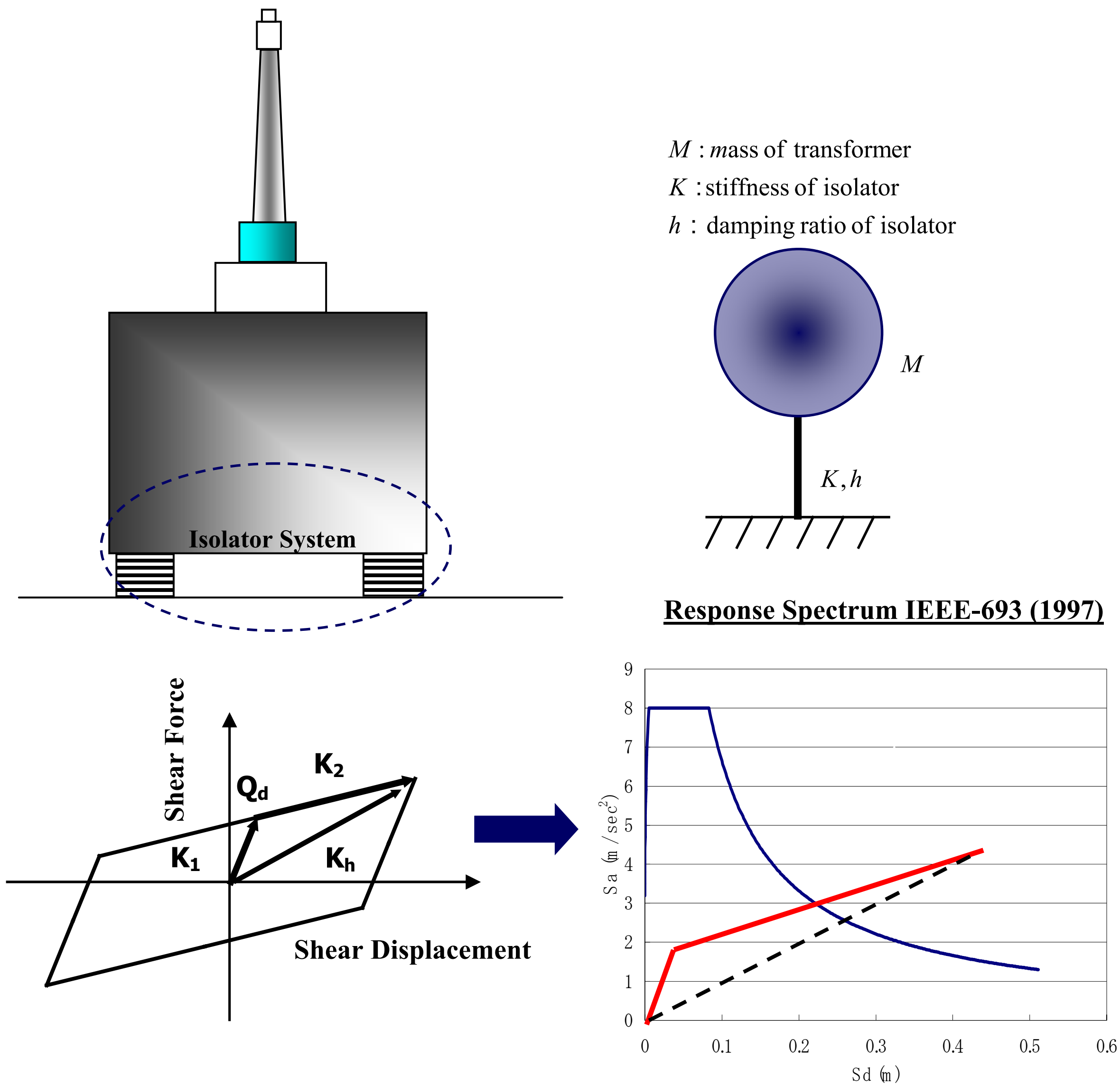

Figure 2-11 Equivalent Linearization Analysis of Base-isolated Transformer/Bushing System

$$\left.\begin{aligned} S_A &= 1.144rf && \text{for} \quad 0 < f \le 1.1\ (\text{Hz}) \\ S_A &= 1.25r && \text{for} \quad 1.1 < f \le 8.0\ (\text{Hz}) \\ S_A &= (13.2r - 5.28)\frac{1}{f} - 0.4r + 0.66 && \text{for} \quad 8.0 < f \le 33.0\ (\text{Hz}) \end{aligned}\right\} \tag{2-27}$$

where,

S_A is Spectrum of response acceleration

ζ is damping ratio of the system

f is natural frequency (Hz)

$r = [3.21 - 0.68Ln(100\zeta)] / 2.1156$

The RRS is specified for the seismic evaluation of the electrical equipment in a substation, such as a porcelain bushing, by a shaking table test using earthquake ground motion. Ground motion shall have spectral ordinates that equal or exceed the RRS. Because the RRS is specified as the input to the bushing, this spectrum already includes the amplification from the transformer body. Therefore, it is conservative to use this RRS for the design of base isolation systems for power transformers.

The spectrum related to the frequency range of base isolation is:

$$S_A = 1.144rf \tag{2-28}$$

S_A and S_D, the spectrum of response displacement, has the following relationship:

$$S_D = \left(\frac{1}{2\pi \cdot f}\right)^2 \cdot S_A \tag{2-29}$$

Substituting (2-28) into (2-29), and erase f from the equation, then the relationship of S_A and S_D is expressed as follows.

$$S_A = {C_0}^2 \cdot r^2 \cdot \frac{1}{S_D} \tag{2-30}$$

where, $C_0 = \dfrac{0.572}{\pi}$

The force-deflection relationship of the bi-linear model for the isolation system is expressed as follows:

$$Q = K_2 \cdot \delta + Q_d = K_h \cdot \delta \tag{2-31}$$

The definition of the each variable is shown in Figure 2.4. In an equivalent linear system, the following relationship is assumed:

$$Q = M \cdot S_A \tag{2-32}$$

$$\delta = S_D \tag{2-33}$$

Substituting (2-31), (2-32), and (2-33) into (2-30),

$$\frac{K_h \cdot \delta}{M} = {C_0}^2 \cdot r^2 \cdot \frac{1}{\delta}$$

$$\therefore \delta = C_0 \cdot r \cdot \sqrt{\frac{M}{K_h}} \tag{2-34}$$

The damping factor r is the function of damping ratio ζ of the bilinear-model at displacement δ as follows.

$$\zeta = \frac{2}{\pi} \cdot \frac{Q_d \cdot \left(\delta \cdot - \dfrac{Q_d}{K_1 - K_2} \right)}{\left(Q_d + K_2 \delta \right) \cdot \delta} \tag{2-35}$$

Damping factor is expressed with ζ as follows.

$$r = \frac{[3.21 - 0.68\ln(100\zeta)]}{2.1156} \qquad (2\text{-}36)$$

The response displacement δ and acceleration S_A are given as the cross point of the curve expressed by (2-37) obtained by substituting (2-36) into (2-30), and performance curve of isolation system. The relationship expressed by (2-37) is called as transit curve.

$$S_A = C_0^{\ 2} \cdot \left\{ \frac{[3.21 - 0.68\ln(100\zeta)]}{2.1156} \right\}^2 \cdot \frac{1}{S_D} \qquad (2\text{-}37)$$

Practically, the solution of response displacement δ that satisfies (2-33) will be given by an iteration process as indicated in Figure 2-12. The capacity curve of the isolation system is modeled as bi-linear characteristics with parameters of yield force ratio α and fundamental period T_f.

$$\alpha = \frac{Q_d}{M \cdot g} \qquad (2\text{-}38)$$

$$T_f = 2\pi\sqrt{\frac{M}{K_2}} \qquad (2\text{-}39)$$

Figure 2-13 shows the relationship of the transit line and capacity curve when the α = 0.08 and T_f =2.0 seconds. Figures 2-14 and 2-15 are the design diagram of isolation system with parameter of α and T_f.

In general base-isolation design of buildings, α varies from 0.04 to 0.06 and T_f varies between 3.0 and 4.0 seconds. However, according to the curves in Figure 2-13, the resulting response displacement will be over 300 mm and it will be too large considering the complicated interconnection with other equipment. The author recommends making the T_f less that 2.0 seconds and increase the α to more than 0.07. These boundaries become part of the design principle in this research for isolators of transformers or other equipment in substations.

In order to verify the proposed procedures, the result of the EQLM was compared with time-history analysis. Nine time-history ground motion were generated based on the target spectrum RRS 693-1997 for 2% damping and PGA=0.5g. Seven records have random phase angles (Art-R1 to Art-R7, respectively), one with phase angle of 1995 Kobe (Takarazuka) EW (Art-KT), and one with phase angle of 1994 Northridge (Sylmar) S11 (Art-NY). Each ground motion has slight difference in its PGA from 0.5g in target spectrum. However, the spectrum agrees better to target spectrum than modify its PGA to 0.5g. The response spectra of acceleration and time histories of Art-R1, Art-KT, and Art-NY are shown in Figures 2-16 and 2-17.

The comparison of time-history analysis results under PGA of 0.25, 0.50, and 0.70g and EQLM was shown in Figure 2-18. The solution line of EQLM covers all of the time history results. It indicates that the proposed method by EQLM gives a good approximated solution with reasonable safety margin in its practical use.

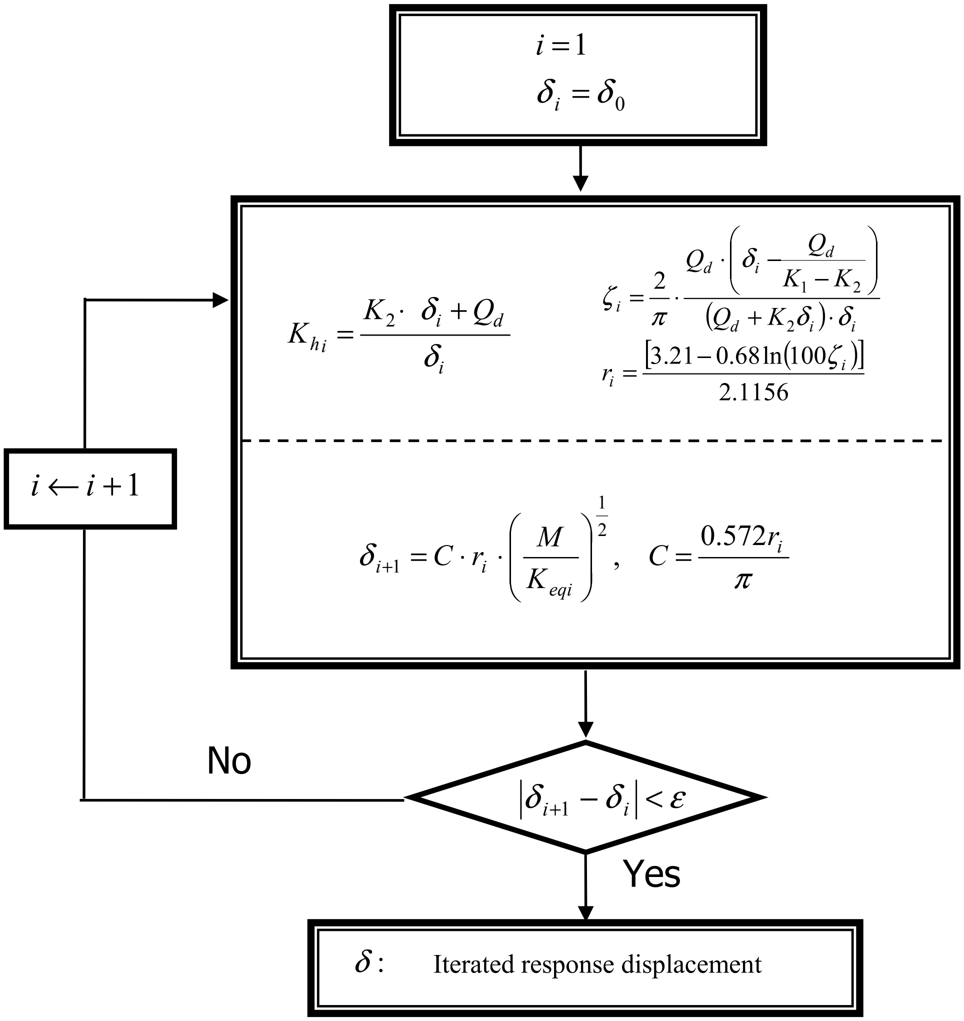

Figure 2-12 Iteration-Flow for Computation of Response Displacement

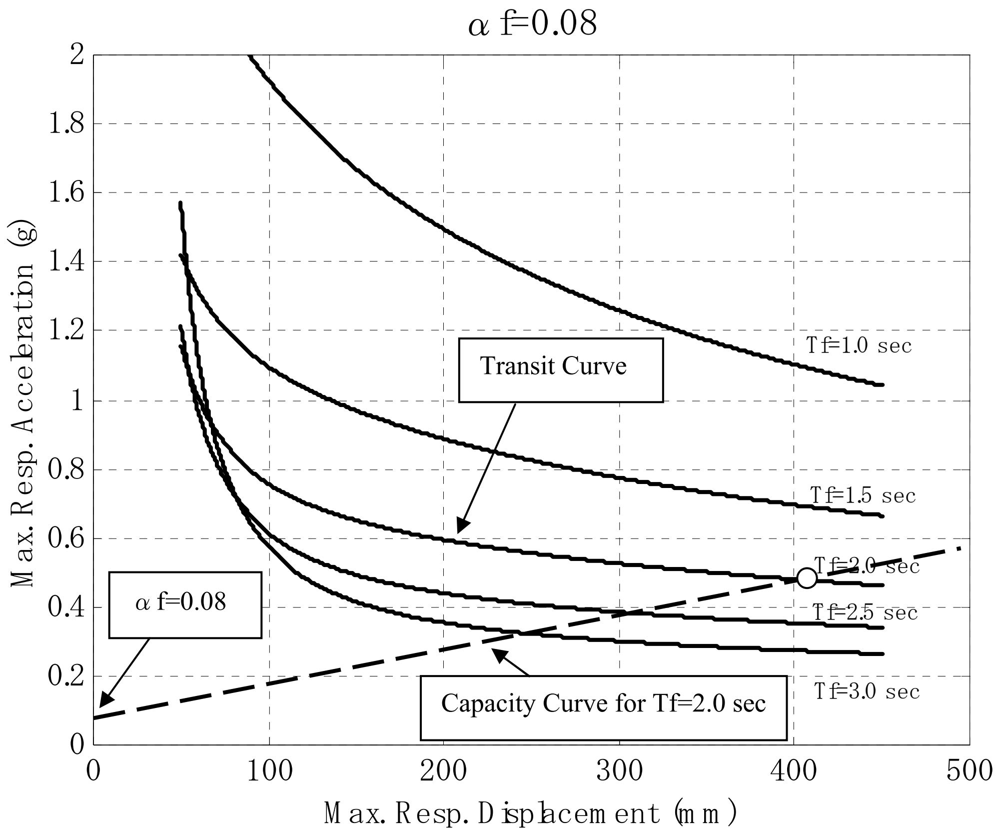

Figure 2-13 Relationship of Transit Line and Capacity Curve

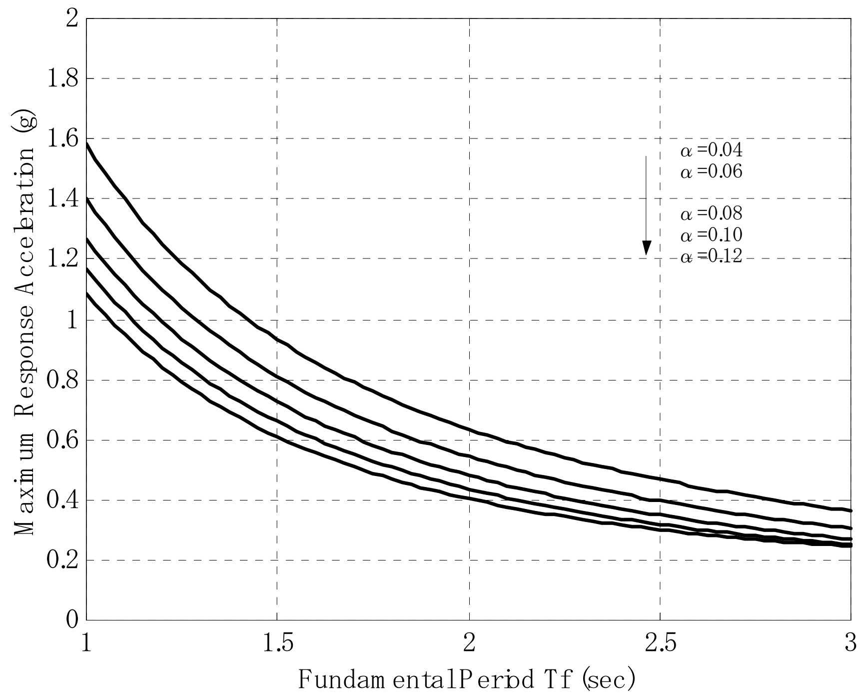

Figure 2-14 Relationship of Fundamental Period and Response Acceleration

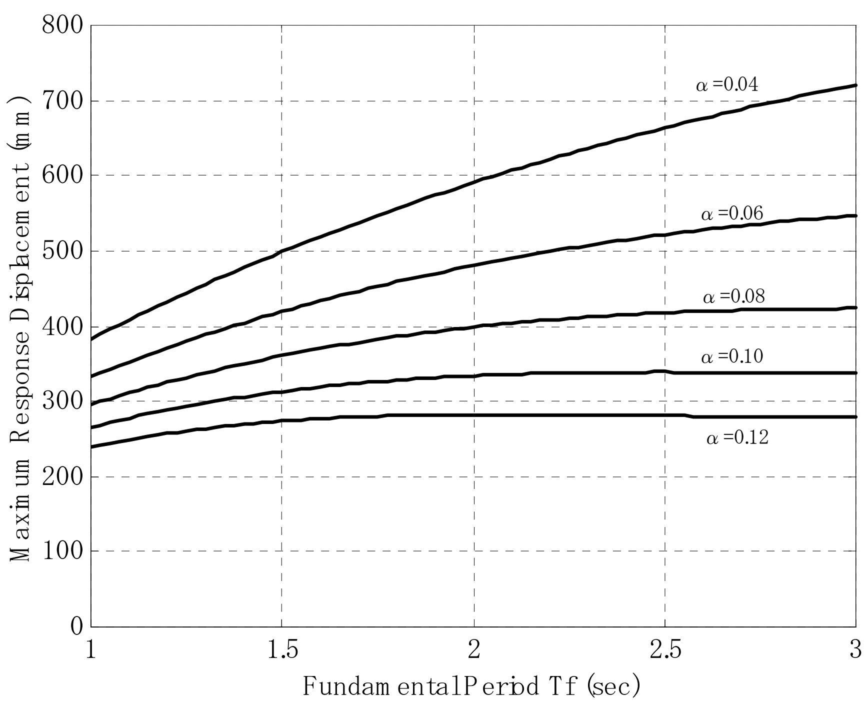

Figure 2-15 Relationship of Fundamental Period and Response Displacement

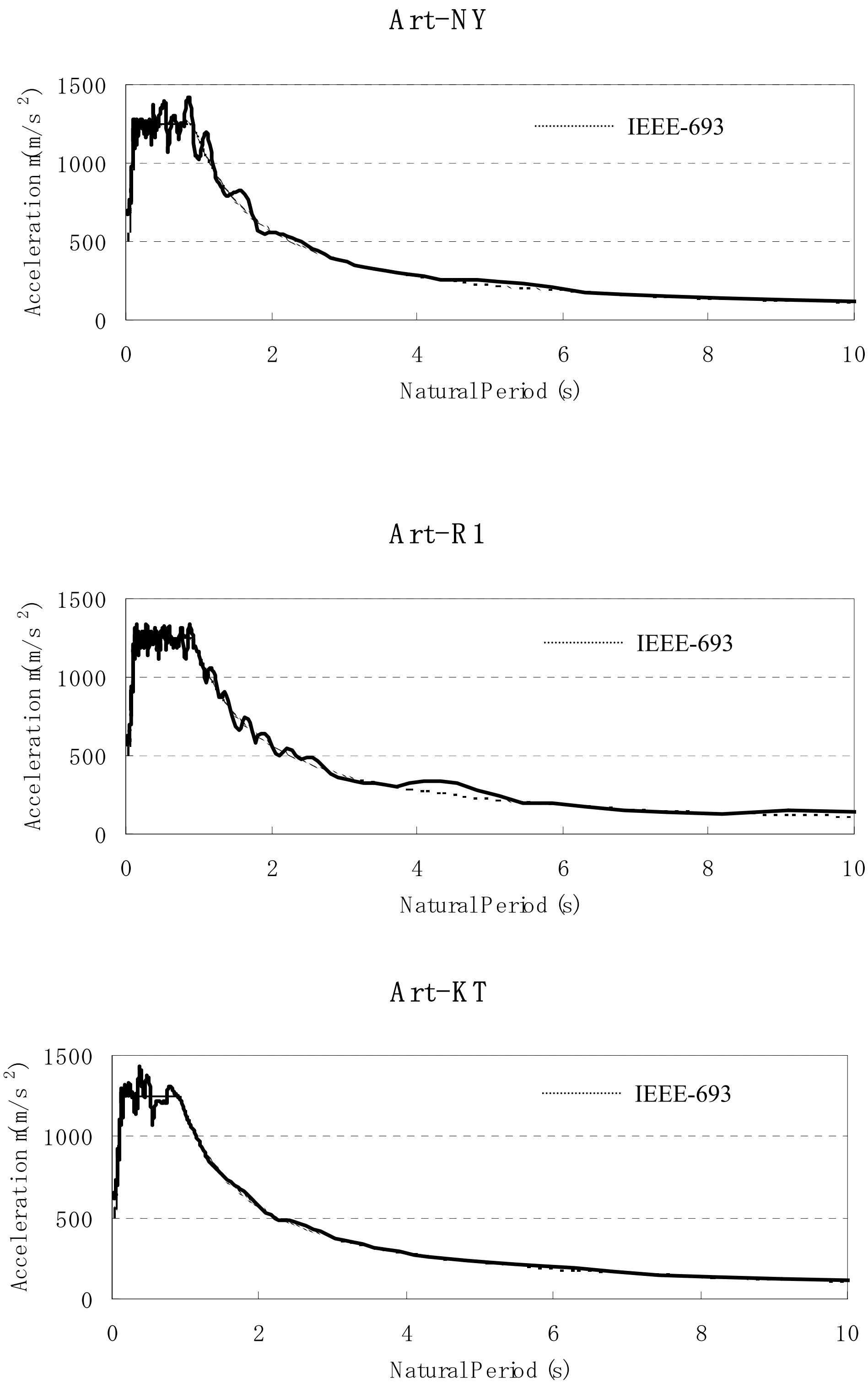

Figure 2-16 Response Spectrum of Artificial Wave: Art-R1, Art-KT, and Art-NY

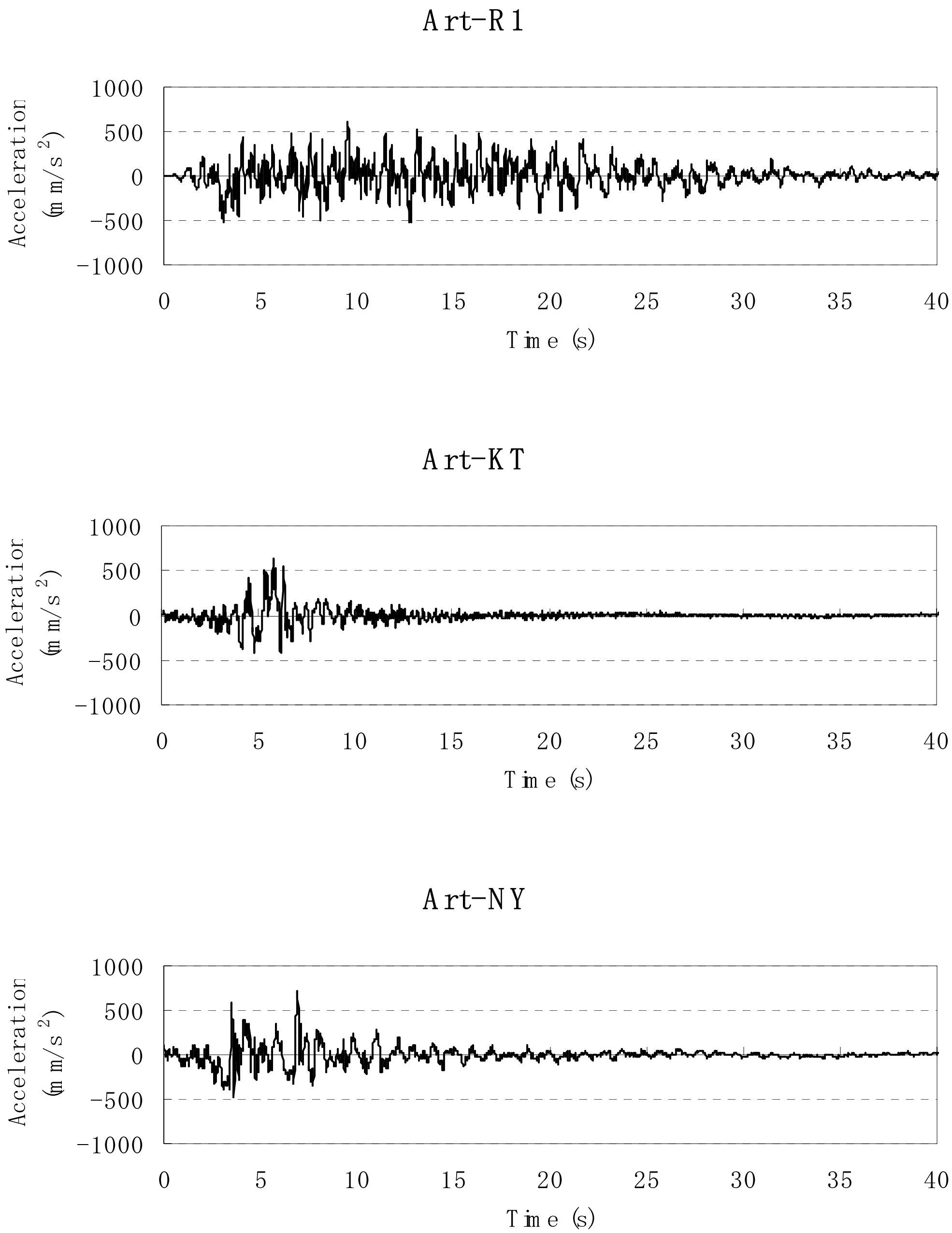

Figure 2-17 Time History Record of Artificial Wave: Art-R1, Art-NY, and Art-KT

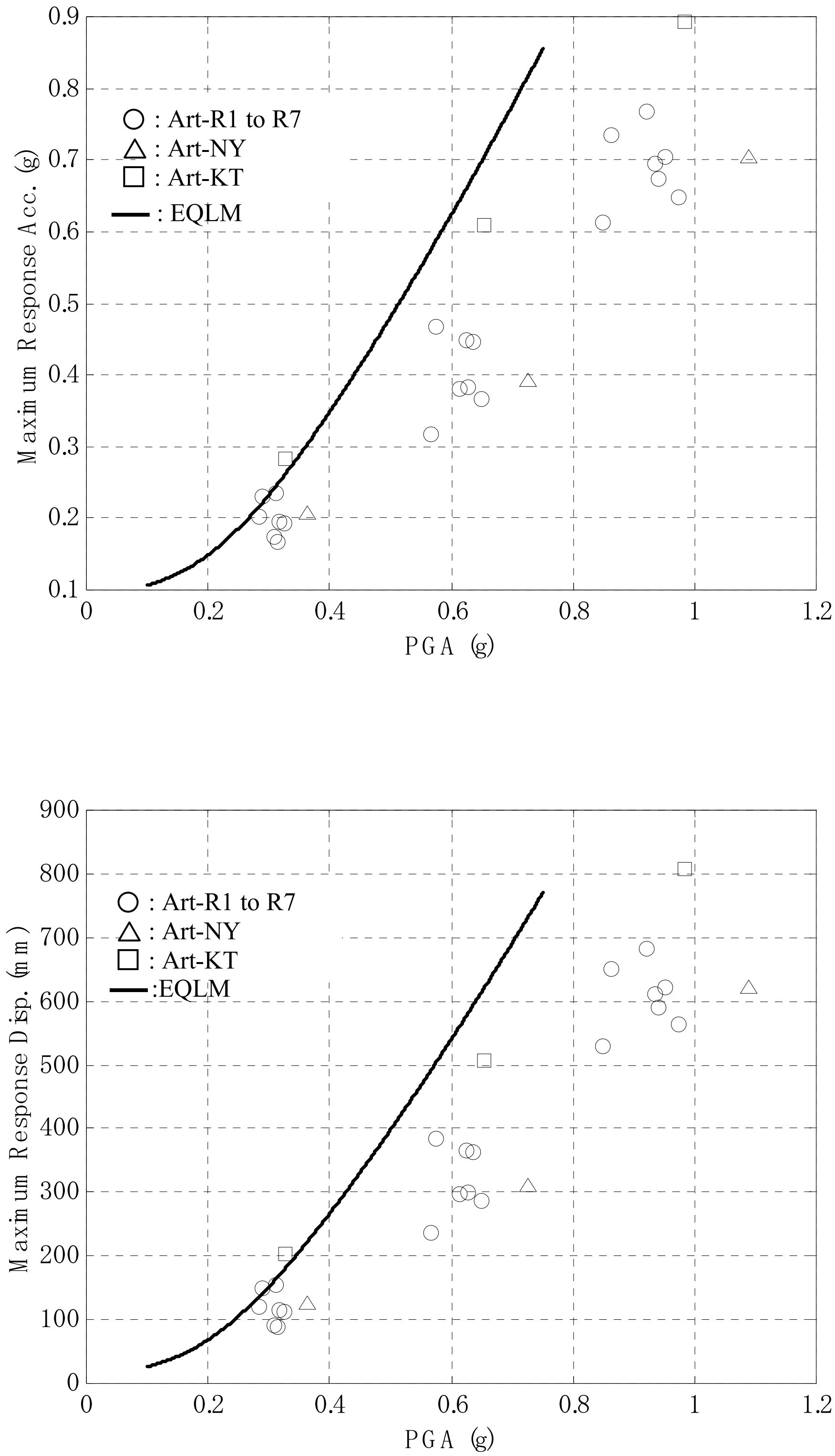

Figure 2-18 Comparison of the Results by EQLM and Time-History Analysis

SECTION 3
EARTHQUAKE SIMULATOR TEST/PHASE-1

3.1 Overview

In this section, the earthquake simulator test /Phase-1 is reported. In this phase, the combined sliding and low-damping rubber bearing system was used. The system consists of PTFE-sliding bearings and low-damping rubber bearings. The test cases were classified into uni-axial (x-direction), bi-axial (x-,y-direction), and tri-axial (x-,y-, and z-direction) shaking. First, dynamic characteristics of each test-component were identified by random vibration tests. After that, tri-axial shaking was conducted using several records of site-motion. The results were analyzed and discussed.

3.2 Experimental Setup

3.2.1 Earthquake Simulator

The size of the earthquake simulator in NCREE is 5m x 5m in plan and the maximum payload is 500 kN. The simulator has six degrees of freedom and the maximum stroke and velocity are ±250 mm and ±1000 mm/sec, respectively. Specifications of this earthquake simulator are summarized in Table 3-1 and a schematic view of the simulator is shown in Figure 3-1.

3.2.2 Transformer Model

The transformer model was a four-layered steel frame structure. It has 80 pieces of lead blocks loaded inside to provide additional weight. The total weight of the transformer model was 235 kN in Phase-1 (Ref: 145 kN in Phase-2). At the top of the frame, a bushing was connected with bolts through the bushing flanges to a column, which was assumed as the turret of the transformer. Figure 3-1 shows a photo of the frame. The transformer model can be assumed as a scaled-model of the actual transformer. The target transformer was a large-size one, such as over

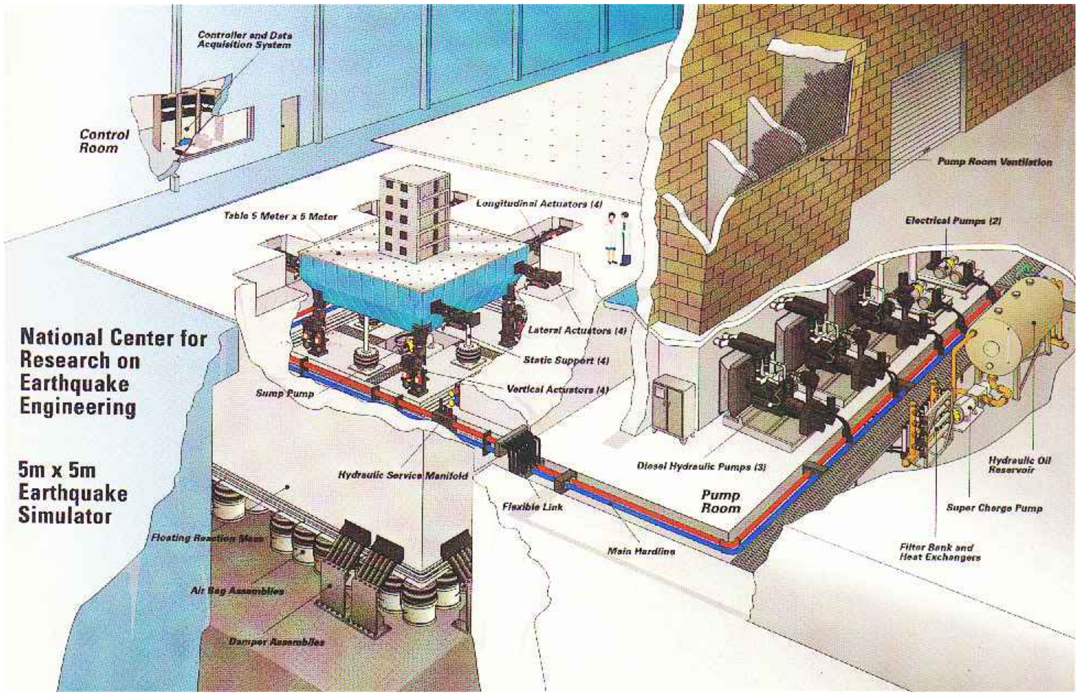

(from NCREE web site [3-1])

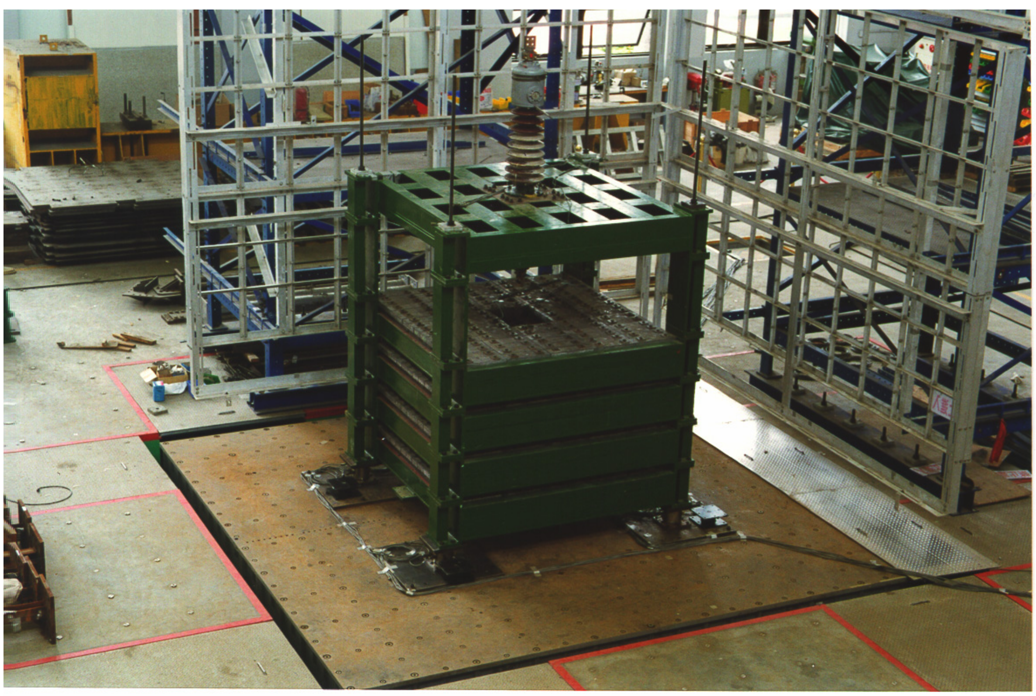

Figure 3-1 Earthquake Simulator in NCREE, Transformer Model and Bushing

500 kV, weighing approximately 2500 kN. In this case, the assumed scale-factor of the transformer model was in the range of 1/3 to 1/4.

Table 3-1 Specification of Earthquake Simulator in NCREE

Table Size	5m x 5m
Specimen Weight Capacity	500kN
Overturning Moment Capacity	150tonf·m
Frequency Range	Min. 0.1Hz , Max 50Hz
Displacement	Longitudinal : ±250 mm Transverse : ±100 mm Vertical : ±100 mm
Velocity	Longitudinal : ±1000 mm/sec Transverse : ±600 mm/sec Vertical : ±500 mm/sec
Acceleration	Longitudinal : ±1.0 g Transverse : ±3.0 g Vertical : ±1.0 g
Actuator Force	Longitudinal : ±220kN Transverse : ±600kN Vertical : ±600kN

3.2.3 Porcelain Bushing

The bushings tested were used in an actual field installation for 15 years and were provided by the Taiwan Power Company. In Phase-1, two types of bushings, 69-kV and 161-kV, were used. Their characteristics and dimensions from the original specifications are shown in Figure 3-2, which were redrawn from the original drawings. According to the description on the drawings, both bushings were manufactured by Toshiba Corporation Japan in 1977. These 161-kV and 69-kV transmission systems are a popular size for power stations in Taiwan. According to JEAG

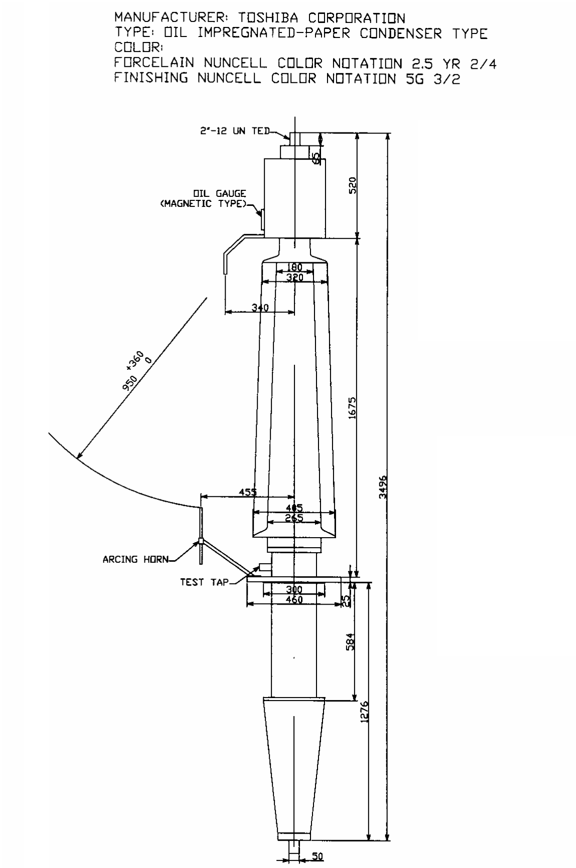

161-kV Bushing

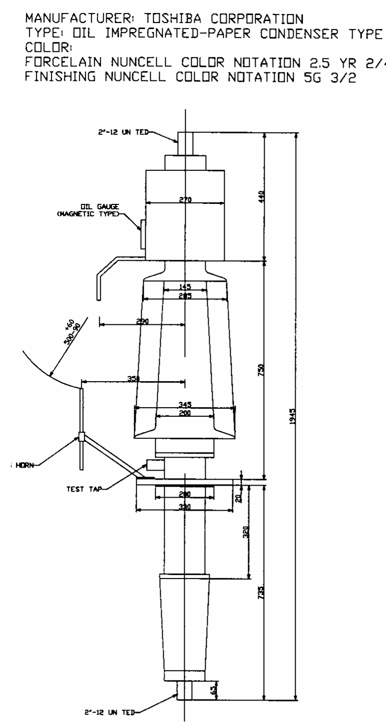

69-kV Bushing

Type Form	VE-60ZN	VEU-140ZT
Insulation Class	69 kV	161 kV
Rated Current	2000 A	1200 A
BIL	350 kV	750 kV
Approximated Weight	1.324kN	3.434kN
Total Length	1945 mm	3496 mm

Figure 3-2 Characteristics of Porcelain Bushings

50003 "Seismic Design Guideline of Electric Facilities in Power Substation" and other references, the typical material properties of porcelain are as follows: Young's modulus is 5.88×10^4 MPa, Poisson's ratio is 0.23, and tensile strength is minimum 40MPa.

3.2.4 Instrumentation

Accelerometers and displacement transducers for x, y and z directions were installed at the simulator platform, at the bottom and top of the transformer model, and at four points on the bushings at the following locations (measured from the middle flange of the bushing):

- 161-kV bushing: 1st node: -112cm .2nd node: –60cm 3rd node: +88cm
  4th node: 197.5cm
- 69-kV bushing: 1st node: -64cm .2nd node: –30cm 3rd node: +41cm
  4th node: 100cm

3-component load cells for the measurement of the reaction forces of the sliding and rubber bearings were installed above each of the bearings. The detailed information of the instruments and their locations are shown in Figure 3-3, together with Table 3-2 and Table 3-3.

Table 3-2 Symbols of Measurement Instruments for Acceleration and Displacement

Measurement Point	Acceleration (g)			Displacement (mm)		
	x-dir.	y-dir.	z-dir.	x-dir.	y-dir.	z-dir.
Table	AX1	AY1	AZ1	long	lateral	transverse
Bottom of transformer	AX2	AY2	-	DX2	DY2	-
Top of transformer	AX3	AY3	AZ2	DX3	DY3	DZ2
Middle of bushing	ABX3	ABY3	ABZ3	DBX3	DBY3	DBZ3
Top of bushing	ABX4	ABY4	ABZ4	DBX4	DBY4	DBZ4

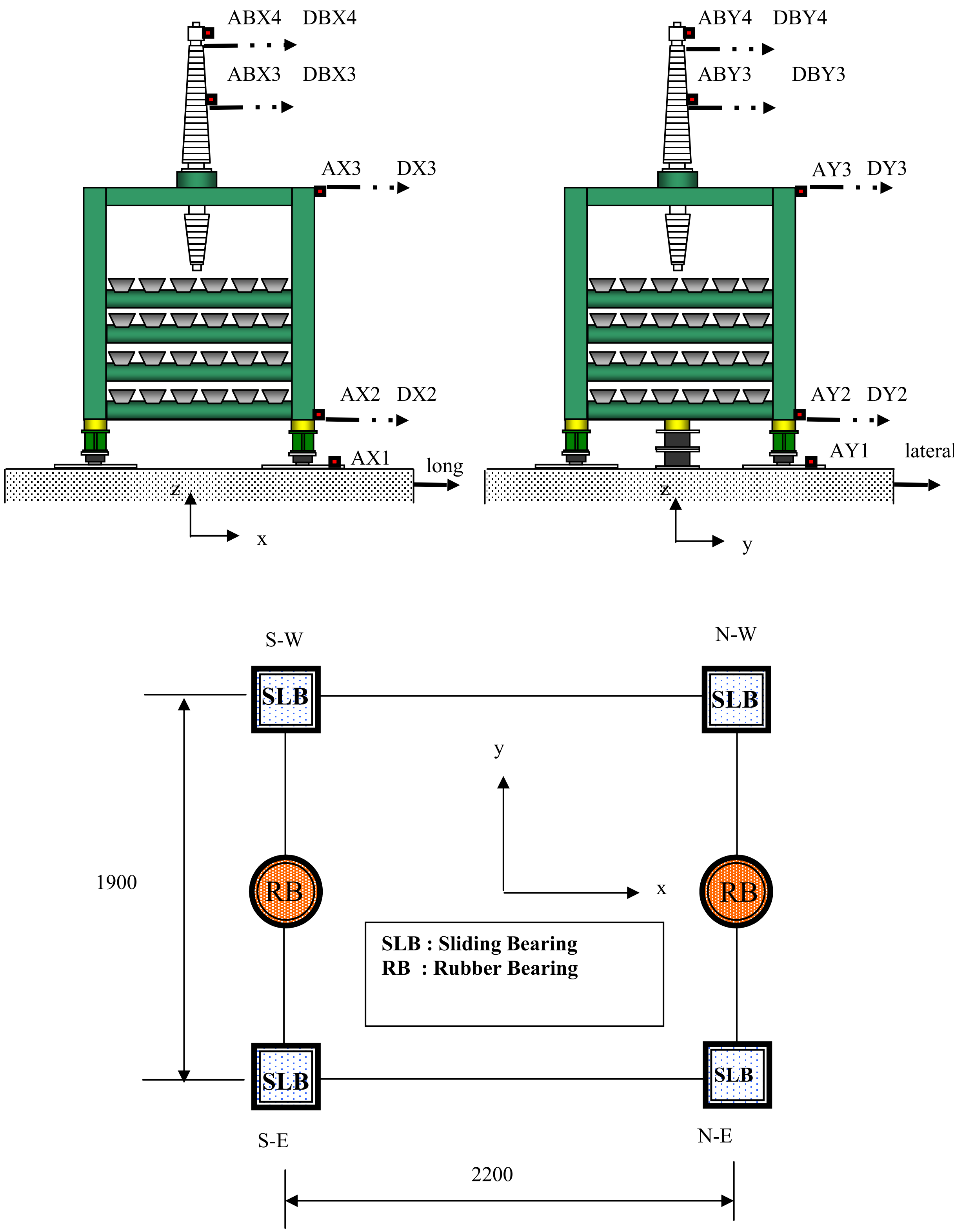

Figure 3-3 Layouts of Sliding Bearings and Rubber Bearings

Table 3-3 Symbols of Measurements in Load Cells Installed

Load Cell ID	x-dir.	y-dir.	z-dir.
SLB-SE	SESX	SESY	FES
SLB-SW	SWSX	SWSY	FWS
SLB-NE	SENX	SENY	FEN
SLB-NW	SWNX	SWNY	FWN
RB-S	SWESX	SWESY	-
RB-N	SWENX	SWENY	-

3.3 Combined Sliding-Rubber Bearing Isolation System

An isolation system combining sliding bearings with low-damping rubber bearings was designed and applied for the transformer. This system enables reasonable period shifting and allows large displacement without buckling problems, which rubber bearings with a small diameter usually possess. A sliding bearing was installed under each of the four corners of the transformer model and two rubber bearings were installed at the midpoint of opposite sides, as shown in Figure 3-3. Coordinate axes were mapped on the simulator platform with the N-S direction as the x-axis and the E-W direction as the y-axis. The positions of the sliding bearings were identified as N-E, N-W, S-E, S-W and the positions of the rubber bearings were identified N and S. The sliding bearings carried the entire weight of the transformer model, including the bushing. The rubber bearings worked only as horizontal restoring force elements, sustaining no vertical load. An experimental study on a similar system was performed by Feng (1994) and Constantinou (1990). Such a system has an advantage for isolation of lightweight structures like small office buildings and residential houses.

3.3.1 Low-Damping Rubber Bearing

In order to reduce the stiffness and to maintain a large deflection capability, each rubber bearing unit actually consisted of two stacked rubber bearings, which were fixed with bolts through mating flange plates as shown in Figure 3-4. The designed characteristics of the rubber bearings

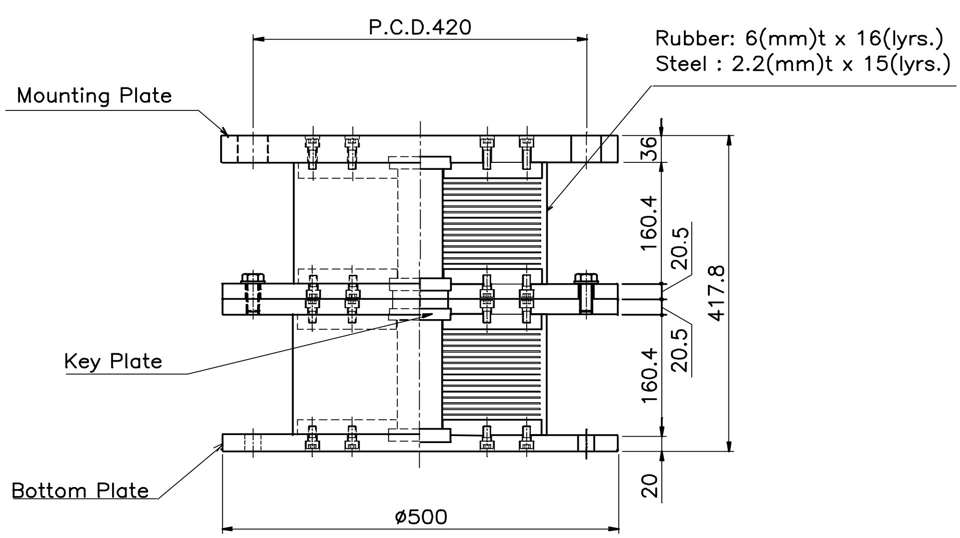

Low-damping Rubber Bearing

Figure 3-4 Low-Damping Rubber Bearing

are summarized in Table 3-4, and the typical physical properties of the rubber compound are shown in Table 3-5. The natural rubber compound shows a clear linear relationship in the stress-strain curve with a small degree of damping. The natural rubber compound used in these bearings had a shear modulus, G, of 0.45 MPa and a damping ratio, h_{eq}, of about 3%. In this system, the energy dissipation function was provided mainly by the sliding bearings. Because the rubber bearings carried no vertical load, the ratio of the thickness of a unit rubber layer to the diameter was relatively large, resulting in a first shape factor of 10.2. The absence of a vertical load allowed for a slim shape of the rubber bearing. As a result, the second shape factor for the double-decked bearing was 1.58. In order to prevent any vertical loading (either compression or tension) on the rubber bearing during the testing, a 10 mm clearance between the bearing flange and the transformer bottom was maintained. Instead of fixing bolts, loose pins were used to transmit the horizontal load.

3.3.2 Sliding Bearing

A sliding bearing consists of a laminated rubber pad and a PTFE disc fixed together with keys and bolts (See Figure 3-5). The purpose of using the laminated rubber pad is to alleviate the degree of shock due to the stick-slip action of the sliding bearing (Iizuka, 1998). The characteristics of the sliding bearing are summarized in Tables 3-6 and 3-7. The rubber compound used in the rubber pad was a high modulus natural rubber compound whose shear modulus, G, was 1.2 MPa. The high modulus rubber compound produces a design with small breaking-away displacement and a compact size. The rubber pad used in the sliding bearing does not require a large deformation capacity such as a conventional rubber bearing. The physical properties of the compound are summarized in Table 3-8.

Table 3-4 Dimensions and Properties of Rubber Bearing

Outer Diameter ***D***	304mm
Inner Diameter ***d***	58.5mm
Unit Rubber Thickness t_r	6.0mm
Number of Layers n_r	16
Shim Plate Thickness t_s	1.6mm
Total Rubber Height ***h***	96mm for NB 192mm for DNB
Rubber Compound Type	Natural Rubber(NR):G5
Apparent Shear Modulus ***G***	0.44MPa
1^{st} Shape Factor S_1	10.2
2^{nd} Shape Factor S_2	3.17 for Single Bearing 1.58 for Doubled Bearing
Horizontal Stiffness K_h	0.321kN/mm

Table 3-5 Physical Properties* of Rubber Compound for Rubber Bearing

Property	Specification
Hardness	39+4
100% Modulus	0.69+0.2MPa
Tensile Strength	> 17.7MPa
Breaking Strain	>600%

* by JIS K 6301

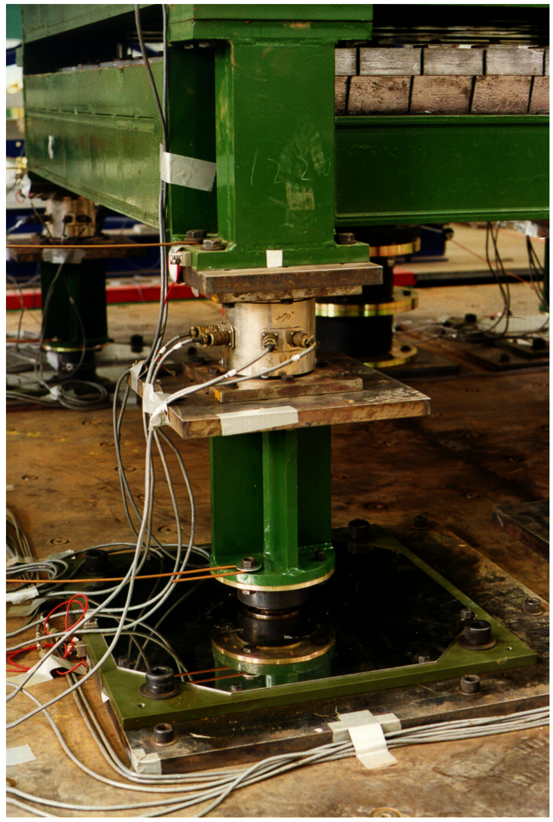

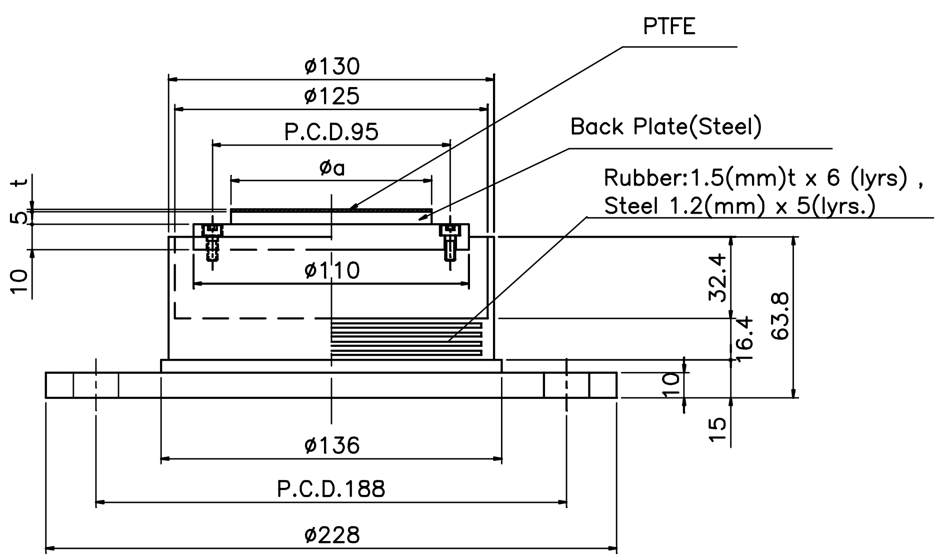

(In above figure, a=60mm, and t=1.0mm)

Figure 3-5 Sliding Bearing

The PTFE disk used in this test had a specially designed reinforcement to endure high axial stress. The PTFE disk consisted of a 0.2 mm thick PTFE sheet that is reinforced by an Aramid-chipped fiber. The fiber was bonded to the glass-fiber fabric with an epoxy resin-type adhesive. The whole sheet was finally bonded to the steel plate with the same type of adhesive. By reducing the thickness of the PTFE sheet and reinforcing it with the Aramid fiber, the PTFE disk can sustain a compressive stress of 30 MPa without fracture or creep. The physical properties of PTFE are summarized in Table 3-9. A stainless steel plate embedded in the back-plate was used as the mating surface of the sliding bearing.

Table 3-6 Dimensions and Properties of PTFE Disc

Diameter D_p	55 mm
Thickness t_p	2.0 mm
Shape Factor S_1	13.8
Friction Coef. μ	0.10 – 0.15

Table 3-7 Dimensions and Properties of Rubber Pad for Sliding Bearing

Property	Rubber Pad
Outer Diameter D	120mm
Inner Diameter d	0mm
Unit Rubber Thickness t_r	2.0mm
Number of Layers n_r	5
Shim Plate Thickness t_s	2.2mm
Total Rubber Height h	10.0mm
Rubber Compound Type	Natural Rubber(NR):G12
Apparent Shear Modulus G	1.18MPa
1st Shape Factor S_1	15
2nd Shape Factor S_2	12
Horizontal Stiffness K_h	1.33kN/mm
Vertical Stiffness K_v	1372kN/mm

Table 3-8 Physical Properties* of Rubber Compound for Sliding Bearing

Property	Specification
Hardness	65+5
Modulus at 25%	0.72+0.2MPa
Tensile Strength	> 14.7MPa
Breaking Strain	> 600%

* by JIS K 6301

Table 3-9 Physical Properties of PTFE Material for Sliding Bearing

Property	Specification
Hardness D-1706	D52 to D55
Tensile Strength D638	> 14.7 MPa
Breaking Strain D638	> 200%

3.3.3 Design Performance

The design characteristics of the complete isolation system are summarized in Table 3-10. The initial stiffness, K_1, is the summation of the initial stiffness of the rubber bearings and the stiffness of the rubber pads in the sliding bearings. After the horizontal load reaches the maximum static friction load, sliding bearings start to slide (sometimes called "break away") and the stiffness decreases to post-sliding stiffness, K_2, which is basically the summation of the post-yield stiffness of the rubber bearings. The designed natural period, T_{eq}, of the system was 1.32 seconds at a deflection of 100 mm, calculated with the effective stiffness, K_h, which corresponds to the gradient of the line from peak to peak of the bi-linear loop. With the post-sliding stiffness, K_2, the period of the system was calculated as 1.75 seconds. The former natural period is called the equivalent natural period, T_{eq}, whereas the latter is called the fundamental natural period, T_f. In general, the natural period, T_{eq}, of a base-isolated building varies from 2.0 to 3.0 seconds. However, in this case, the small dead load of the transformer model limited the period to less than 2.0 seconds. The equivalent damping ratio, h_{eq}, at 100 mm displacement was 27%, which is relatively large damping compared with typical isolation systems.

Table 3-10 Design Parameter Values of Isolation System

Characteristics	Designed Value
Pre-yield Stiffness K_1 (kN/mm)	5.32
Post-yield Stiffness K_2 (kN/mm)	0.323
Effective Stiffness K_h (kN/mm)	x=100mm : 0.568
	x=200mm : 0.441
Equivalent Damping Ratio h_{eq}	x=100mm : 0. 269
	x=200mm : 0.174
Vertical Stiffness K_v (kN/mm)	3360
Effective Period T_{eq} (sec)	x=100mm : 1.32
	x=200mm : 1.49
Fundamental Period T_f (sec)	1.75
Vertical Natural Freq. F_v (Hz)	58.3

3.3.4 Preliminary Performance Test

The sliding bearings and low-damping rubber bearings were manufactured by Bridgestone Corporation in Japan. Before shipping to NCREE, all of the rubber bearings were tested for quality assurance and evaluation of initial performance. The testing conditions and results from those initial tests are shown in Table 3-11. The testing was carried out individually on all four rubber bearings. Therefore, the results cannot be directly compared with the results of the earthquake simulator testing, where each of the rubber bearing units consisted of two stacked bearings.

The sliding bearings used in this testing were not subjected to an initial performance test. However, the PTFE disc itself was tested and the results showed that the friction coefficient was 0.08 under a compressive stress of 10 MPa and a very low sliding velocity. In the earthquake simulator testing, the sliding bearing was subjected to dynamic motion and the friction coefficient was approximately 0.12.

Table 3-11 Initial Performance Test of Rubber Bearing

Testing Condition :

(1) Vertical Load : 29.4 kN (3.0tf)

Compressive stress : 0.32MPa

(2) Horizontal Displacement (Amplitude) : $\pm$96mm

(3) Number of Cycle : 3

(4) Horizontal Stiffness K_h is determined from the 3rd cycle.

Bearing No.	K_h (kN/mm)	G (MPa)
RB-1	0.319	0.438
RB-2	0.307	0.436
RB-3	0.330	0.453
RB-4	0.332	0.456

3.4 Testing Program

Three actual earthquake records were applied as the input earthquake ground motion. They were 1940 El Centro, 1994 Northridge (Sylmar), and 1995 Kobe (Takatori). Their response spectra under 5 % damping are shown in Figure 3.6 together with the IEEE-693 Required Response Spectrum. Each time-history record was normalized to PGA = 0.5 g. The dominant frequency is high for El Centro (2 to 5 Hz) and for Northridge (Sylmar) (1.5 to 3.0 Hz), and very low for Kobe (Takatori) (0.8 to 2 Hz). The Kobe (Takatori) record was considered as a "disadvantageous" input for the isolated system because its dominant frequency was close to the natural frequency of the isolated system and would cause large displacement in the isolation bearings. Although PGA is still the most popular and convenient parameter to characterize the earthquake intensity for general design purposes, the Peak Ground Velocity (PGV) is considered to be another parameter to express intensity of an earthquake, representing the energy of the seismic motion. The PGV of each motion with PGA normalized to 0.5g in the x-direction is as follows:

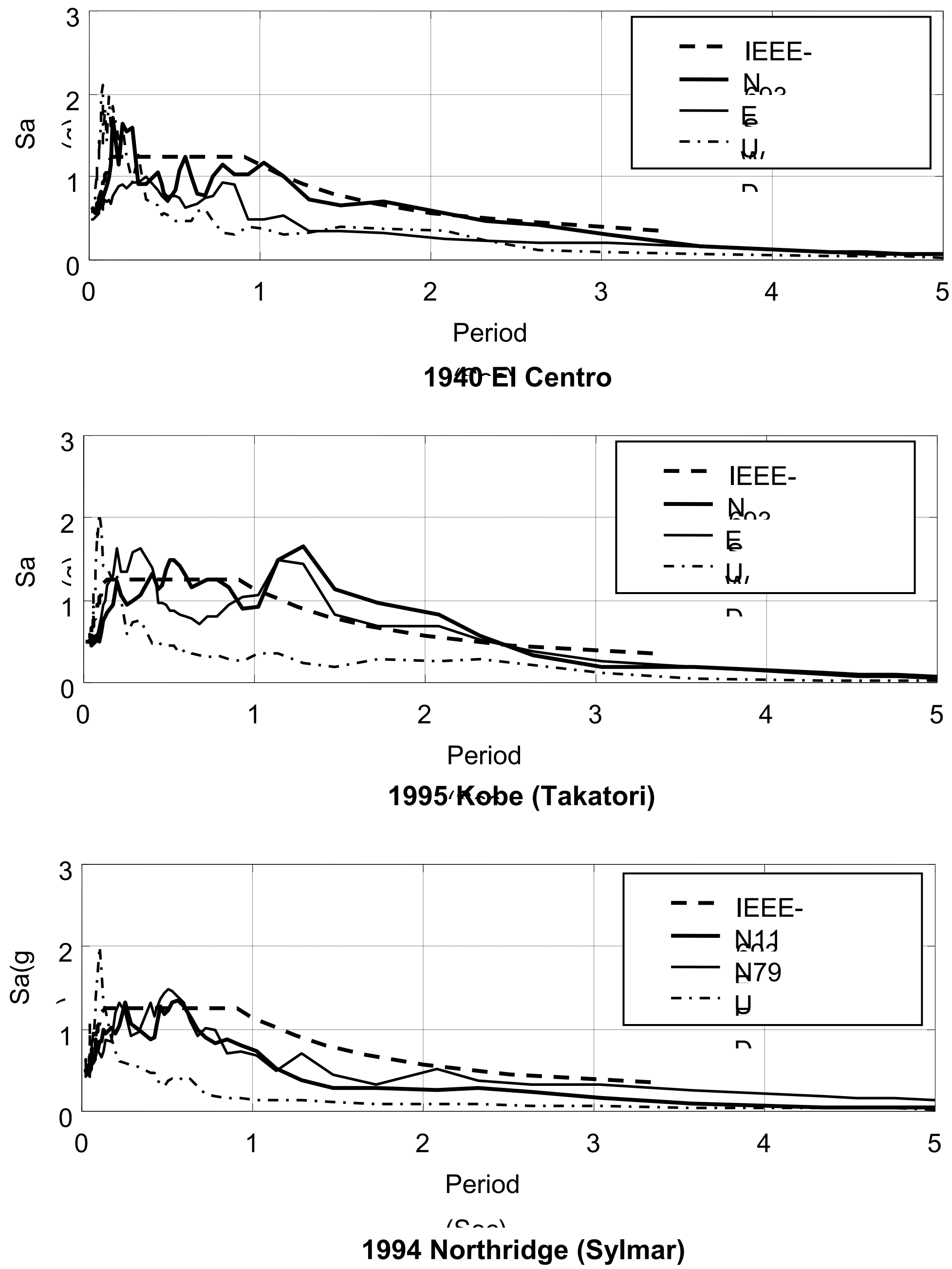

Figure 3-6 Response Spectrum of Input Ground Motion

1940 El Centro NS	: 48.1cm/sec
1994 Northridge (Sylmar) NS	: 79.3cm/sec
1995 Kobe (Takatori) EW	: 105.7cm/sec

The earthquake simulator was excited in the x, x-y and x-y-z directions. The x-direction was set as the main direction for excitation and the component with the largest PGA of each motion was set as the x-direction excitation. The other components in the horizontal direction were set as the y-direction motion and the up-down component as the z-direction motion.

Because the conventional seismic design parameter for electric facilities was PGA, it was used to indicate the intensity of the earthquake motion in the tests. PGA was varied from 0.125g to 0.50g when using intervals of 0.125g. The detailed information about PGA in the earthquake simulator testing is shown in Table 3-12. Because there were no spare bushings, a high PGA that might damage the bushings during the testing was avoided. As a result, the maximum PGA for the fixed-based cases was limited to 0.375g, where the maximum PGA for the base-isolated cases was 0.5g. Only for the Northridge (Sylmar) input, a maximum PGA of 0.625g was tried.
Time scale was not applied to input ground motion.
The test case is identified with the code as follows.

[Example-1]
Bushing: 161 -kV
System: Fixed-base
Earthquake: El Centro, Target PGA 0.375g in x-direction
Code: 161kV/F/El Centro/x375

[Example-II]
Bushing: 69 kV
System: Base-isolated
Earthquake: Northridge (Sylmar), Target PGA 0.375g in x-direction,
0.25g in y-direction, and 0.25g in z-direction
Code: 69kV/B/Northridge/xyz375

Table 3-12 Target PGA of Earthquake Simulator Testing in Phase-1

(1) *Base-isolated Case:*

unit, g

1940 El Centro			1994 Northridge (Sylmar)			1995 Kobe (Takatori)		
NS	EW	UD	NS	EW	UD	EW	NS	UD
X	y	z	x	Y	z	x	Y	z
			0.125			0.125		
0.250			0.250			0.250		
0.375			0.375			0.375		
0.500			0.500			0.500		
			0.625					
0.250	0.125		0.250	0.125		0.250	0.250	
0.375	0.250		0.375	0.250		0.375	0.250	
0.250	0.125	0.125	0.250	0.125	0.125	0.250	0.250	0.125
0.375	0.250	0.250	0.375	0.250	0.250	0.375	0.250	0.250
0.500	0.250	0.250	0.500	0.250	0.250			

(2) *Fixed-based Case:*

1940 El Centro			1994 Northridge (Sylmar)			1995 Kobe (Takatori)		
NS	EW	UD	NS	EW	UD	EW	NS	UD
x	y	z	x	Y	z	x	y	z
			0.125			0.125		
0.250			0.250			0.250		
0.375			0.375			0.375		
0.250	0.125		0.250	0.125		0.250	0.250	
0.375	0.250		0.375	0.250		0.375	0.250	
0.250	0.125	0.125	0.250	0.125	0.125	0.250	0.250	0.125
0.375	0.250	0.250	0.375	0.250	0.250	0.375	0.250	0.250

3.5 Dynamic Characterization of Transformer Model and Bushing

The dynamic characteristics of the transformer model and bushings were evaluated by random wave excitation (Chopra). The transformer model, carrying the lead block weight without the bushing, was subjected to a random wave with peak acceleration of 0.05g. The response acceleration at the top of the transformer was measured and analyzed through Fast Fourier Transform. Then, the transfer function was calculated against the input random wave and the natural frequency was determined.

The dynamic characteristics of the bushings were investigated by mounting the bushings on the upper part of the frame, which was designed as removable, in the transformer model as shown in Figure 3-7. An example of the transfer function for the bushing is also shown in Figure 3-7. The peak of the transfer function curve indicates the natural frequency for the 161-kV bushing was in the range of 12-13 Hz for the x-, y-, yaw-x- and yaw-y- directions. For the 69-kV bushing, the natural frequency was found to be around 27 Hz in the x-direction, 29.5Hz in the y-direction, and 25-30 Hz in yaw-x- and yaw-y- directions. The damping ratio was estimated around 1 to 2 % for each mode of the bushings by the half-power bandwidth method. The natural frequencies in each direction from the random shaking test are summarized in Table 3-13.

Table 3-13 Dynamic Characteristics of Transformer Model and Bushings

Unit, Hz

	x-dir.	y-dir.	yaw-dir.
Transformer Model	12.5	12.5	x-12.5, y-13
161kV Bushing	12-13	12-12.5	x-, y- 12-13
69kV Bushing	27.0	29.0	x-, y- 25-30

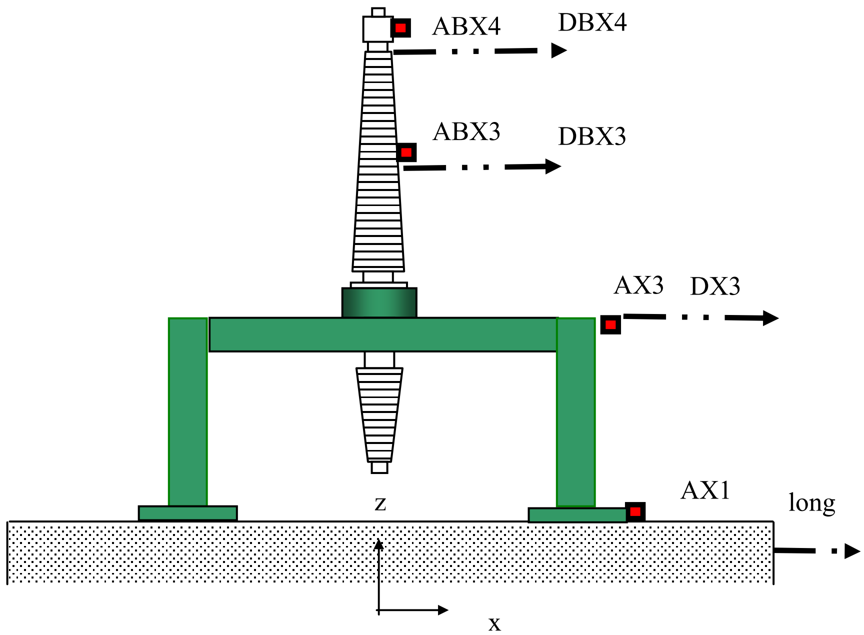

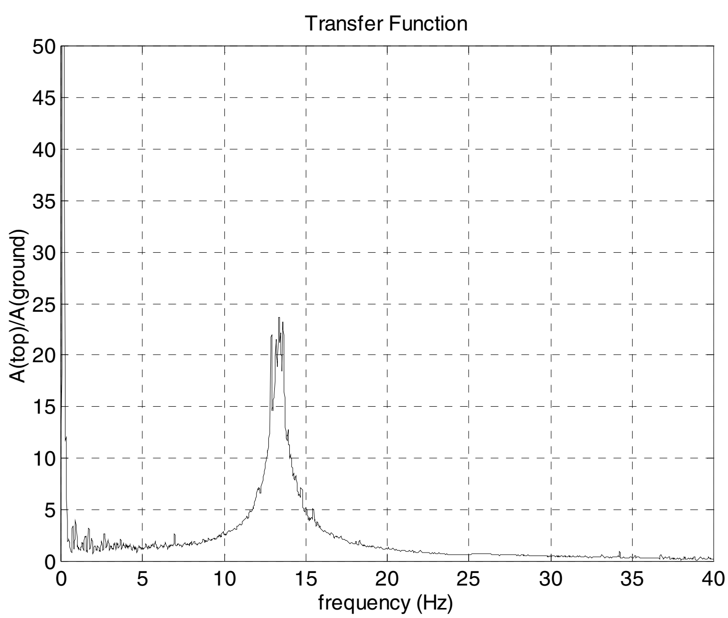

Figure 3-7 Dynamic Characterization Test of Bushings

3.6 Test Results

The differences of response between base-isolated and fixed-base, between 161-kV and 69-kV bushings, and between uni-, bi-, and tri-axial shakings are compared and discussed. In the section of uni-axial shaking, fundamental performance of each element of the system was analyzed and evaluated. In the sections of bi-axial shaking and tri-axial shaking, much attention was paid to the difference between the responses under the bi-axial and tri-axial ground motions.

3.6.1 Uni-Axial Shaking

Under uni-axial shaking, the behavior of the system is straightforward and the fundamental properties of each element in the system can be easily evaluated, whereas the force-displacement relationship under bi- and tri-axial shaking revealed complicated locus caused by multi-directional loading.

3.6.1.1 Response of Transformer/Bushing System

161 -kV Bushing:

Figure 3-8 shows the comparison of response acceleration time histories at the transformer model with and without base isolation under the El Centro 0.375g. In the fixed-base model, the peak response acceleration at the top of the transformer was amplified to 0.747g from the PGA of 0.339g.

Figure 3-9 shows the comparison of response acceleration time histories at node-3 (upper middle) and node-4 (top) of the 161-kV bushing with and without base isolation under the El Centro 0.375g. Without base isolation, the peak acceleration at the top of the bushing reached 3.66g resulting in an amplification factor to PGA of 10.80. On the other hand, with base isolation, the peak response acceleration at the top of bushing was 0.354g and the resulting amplification factor was 1.05. Similar testing results under the Kobe (Takatori) excitations are shown in Figures 3-10 and 3-11. Peak response accelerations at transformer-bottom, transformer-top, and bushing-top are plotted as a function of PGA in Figures 3-12 to 3-14. The effectiveness of base isolation was clearly observed, especially in terms of the response of the bushing top. Base isolation becomes more effective as PGA becomes larger, which is typical of an isolation system with sliding bearings. Among the three earthquake motions, the largest response in the base-isolated system was observed under the Kobe (Takatori) earthquake, as predicted. The peak response acceleration was 1.0g at the top of the bushing and less than 1/3 of that in the fixed-base system.

Figures 3-15 and 3-16 plot the distribution of the response acceleration at different measurement points including platform (ground), bottom, and top of the transformer and top of the bushing, under Northridge and Kobe. The effectiveness of base isolation is very evident in the plots. In the base-isolated system, the amplification of the response acceleration is very small from the bottom to the top of transformer. These results indicate the base-isolated transformer body can be considered as a single mass. The response displacement of each measurement point is also plotted in Figures 3-17 and 3-18. Large displacement was observed in the isolation system.

The Fourier amplitudes of the response accelerations at the tops of the transformer and the 161 kV bushing are compared in Figure 3-19. In the base-isolated system, it was observed that the transformer was not sensitive to the ground motion. In the fixed-base system, the interaction of the transformer and the bushing was observed. The response accelerations at different measurement points on the bushing under the Kobe (Takatori) 0.375g are displayed in Figure 3-20. The shape of the response acceleration distribution indicates that the rocking motion around the fixed end is the dominant movement of the bushing during shaking. The rocking stiffness at the fixed end will characterize the frequency of the bushing.

In Figure 3-21, the change of axial load on each sliding bearing caused by overturning of the transformer/161-kV bushing system is plotted under the Northridge (Sylmar) 0.375g. The maximum change of the vertical load occurred at Slider-WN-- 40% of the initial load. Initial vertical load of each bearing was 41.3kN for NW, 76.0kN for NE, 73.8kN for SW, and 44.4kN for SE. The reason of the initial load distribution is assumed that the stiffness of transformer model is extremely high and the small difference of column height generated the distribution of the load.

69-kV Bushing:

Figures 3-22 and 3-23 compare the peak response accelerations of the transformer/69-kV bushing system with and without base isolation. The peak response acceleration at the bushing top in the fixed-base system was reduced to 1/3 of that in the 161-kV system. The difference in responses between the base-isolated and fixed-base system was relatively small.

The 69-kV bushing, whose fundamental frequency is over 25 Hz, was totally insensitive to the seismic excitations, according to the dynamic characterization results shown in Table 3-13. Therefore, the acceleration amplification factor in the fixed-base system with the 69-kV bushing was also small, showing that little improvement can be made by the base isolation system. The results proved that those bushings with a high frequency have few problems in seismic damage.

3.6.1.2 Performance of Isolation System

Figures 3-24 and 3-25 show examples of horizontal force-displacement loops for a sliding bearing and a rubber bearing. Because the weight of the transformer model was not uniformly distributed to each column, the friction force generated at each sliding bearing differs. The axial load, friction coefficient, and compressive stress on each PTFE disc are summarized in Table 3-14. The compressive stress varied from 17.4 to 32.0 MPa and the friction coefficient from 0.145 to 0.102, as a function of the stress. The change in vertical load due to the overturning moment made the loops of each sliding bearing asymmetrical.

An example of the force-displacement loop of the rubber bearings under the Kobe (Takatori) 161kV/x0375g is shown in Figure 3-26. The maximum displacement was 124 mm, corresponding to a rubber shear strain of 64.6%. The rubber bearing exhibited a linear-elastic behavior, typical of its natural rubber compound.

The total force-displacement loops of the isolation system, including the rubber and sliding bearings, are plotted in Figure 3-23 by superposition of the force-displacement loops of all the bearings. The system performance for K_1, K_2 and Q_d were estimated from the curve and listed in Table 3-15. They agreed very well with the designed values in Table 3-8.

Table 3-14 Friction Coefficient and Compressive Stress on Sliding Bearing

(Evaluated from the performance loops in case of 161kV/Kobe (Takatori),x0.375g)

Location	Axial Load (KN)	Friction Coef.	Compressive Stress (MPa)
E-N	76.0	0.105	32.0
E-S	44.4	0.130	18.7
W-N	41.3	0.145	17.4
W-S	73.8	0.102	31.1

Table 3-15 Total Performance of Isolation System

(Evaluated from the performance in case of 161kV/Kobe (Takatori), x0.375g)

K_1 (kN/mm)	5.17
K_2 (kN/mm)	0.356
Q_d (kN)	27.3
Q_d/P_v	0.116 (=average friction coef.)
T_f (sec)	1.63

P_v: Total Axial Load =235.5kN

T_f: Fundamental Period

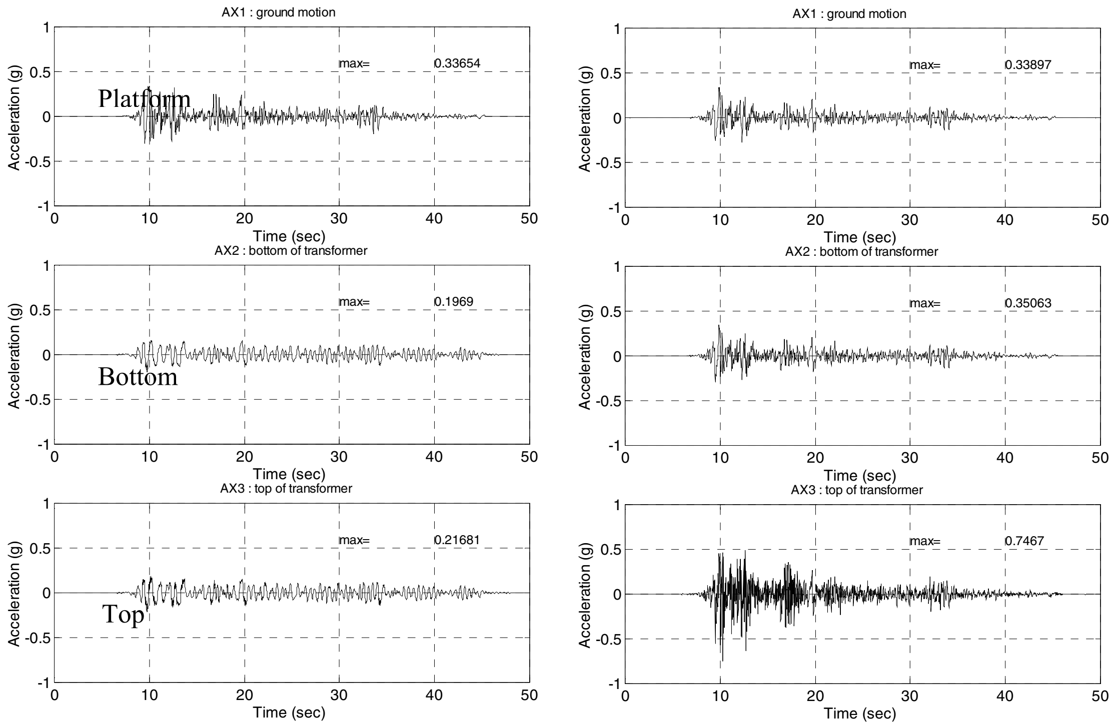

Base-isolated **Fixed-base**

Figure 3-8 Time History of Transformer Response Acceleration: 161kV/El Centro/x375

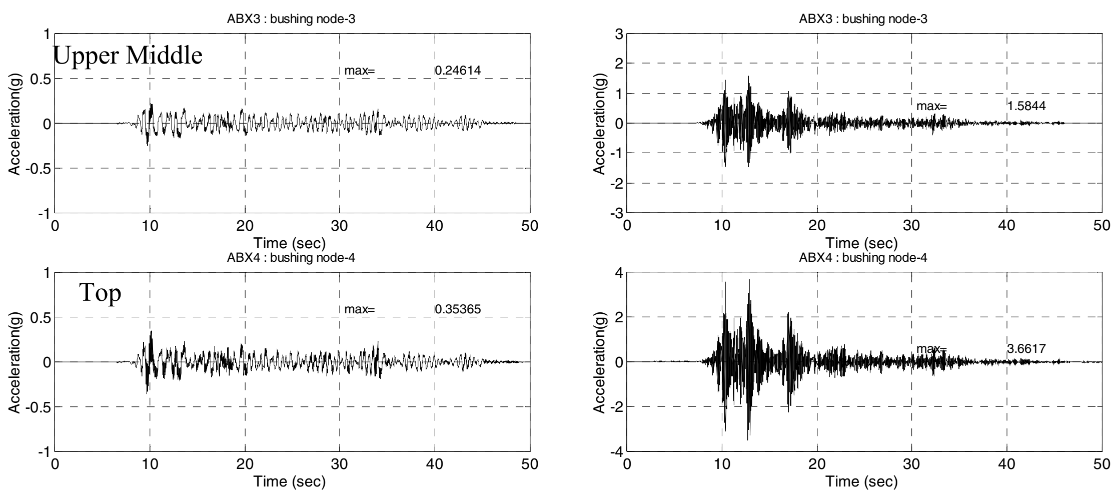

Base-isolated **Fixed-base**

Figure 3-9 Time History of Bushing Response Acceleration: 161kV/El Centro/x375

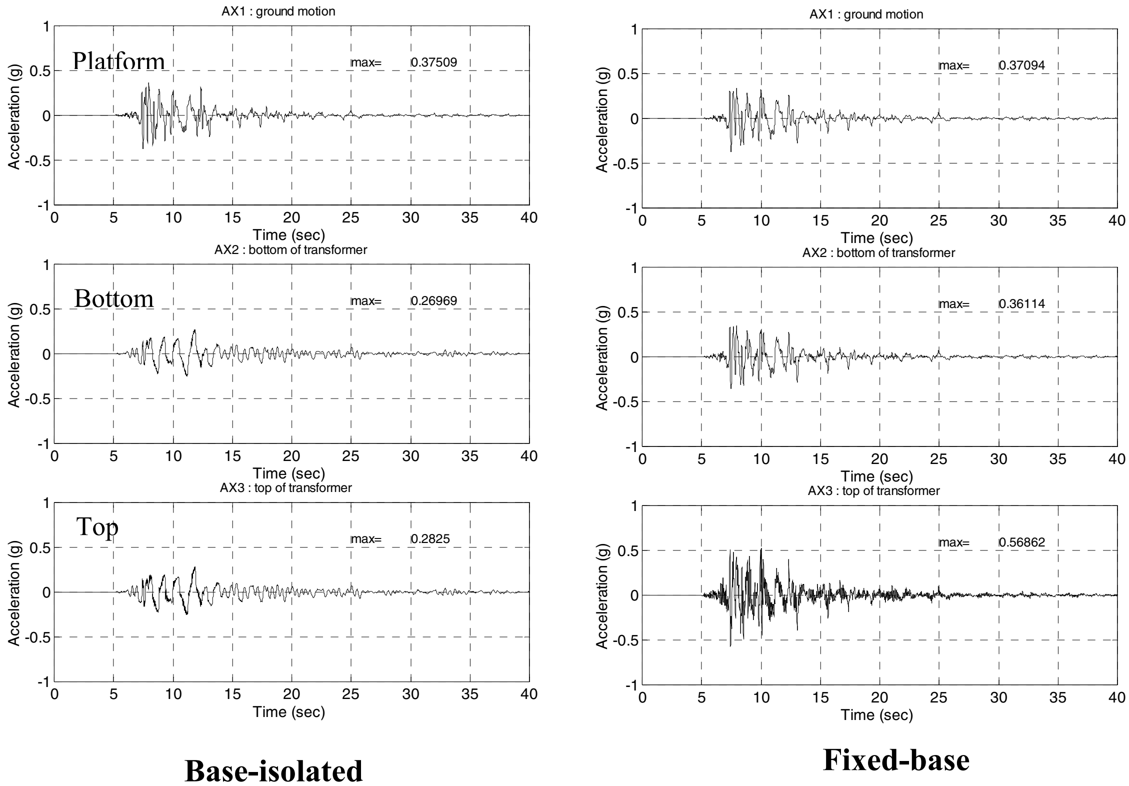

Figure 3-10 Time History of Transformer Response Acceleration: 161kV/Kobe/x375

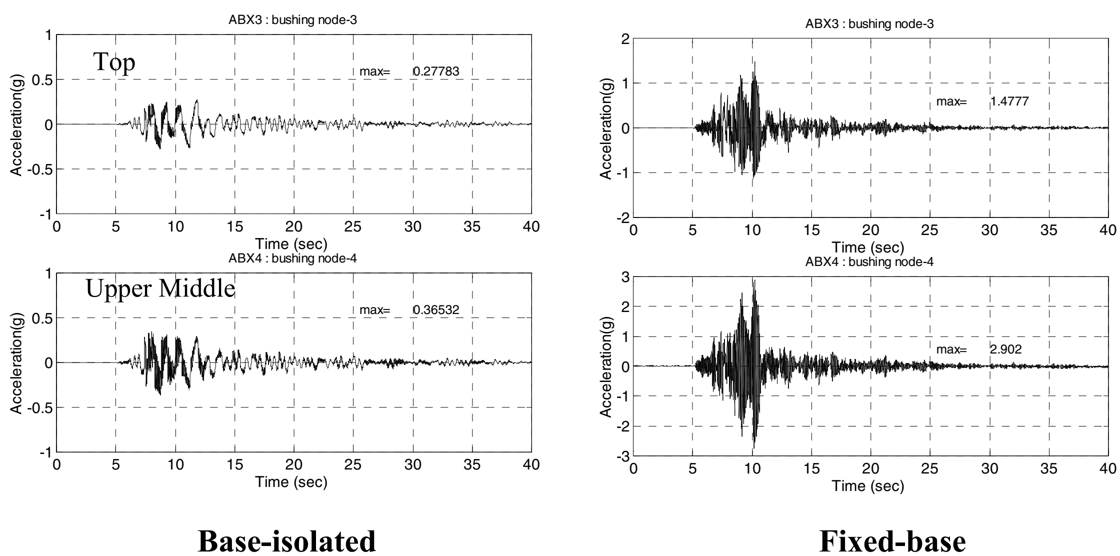

Figure 3-11 Time History of Bushing Response Acceleration: 161kV/Kobe /x375

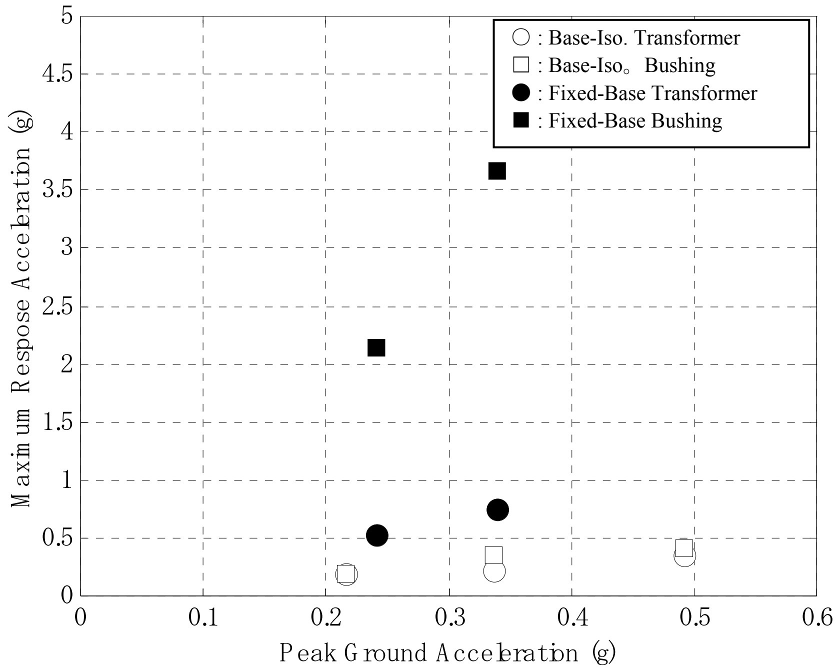

Figure 3-12 Response Acceleration vs. Peak Ground Acceleration in 161kV/ElCentro/ Uni-Axial shaking

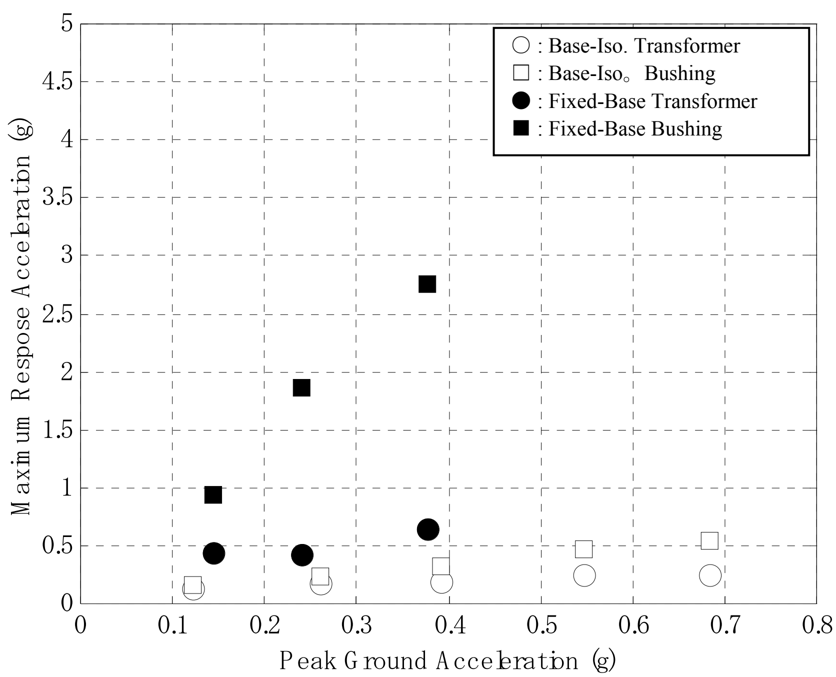

Figure 3-13 Response Acceleration vs. Peak Ground Acceleration in 161kV/Northridge/ Uni-Axial shaking

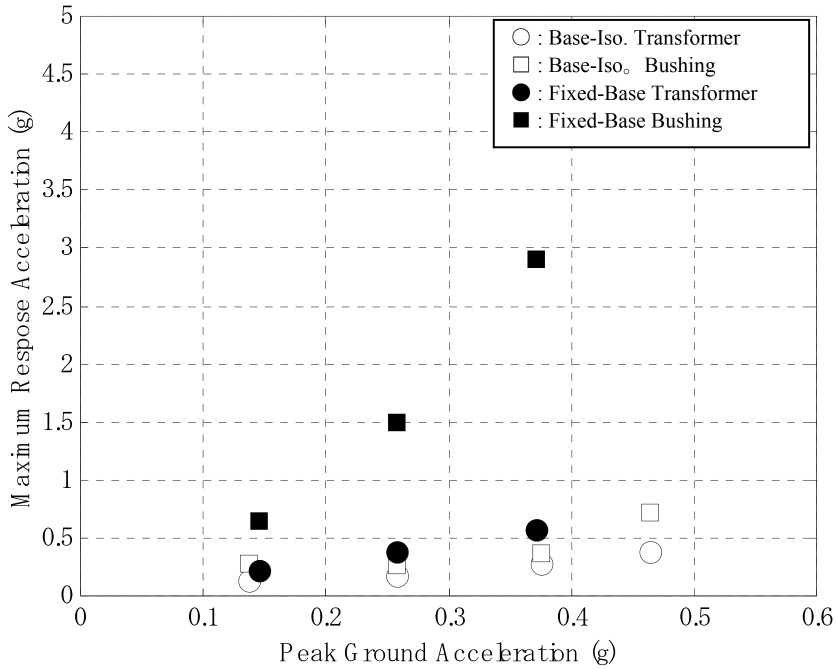

Figure 3-14 Response Acceleration vs. Peak Ground Acceleration in 161kV/Kobe/ Uni-Axial shaking

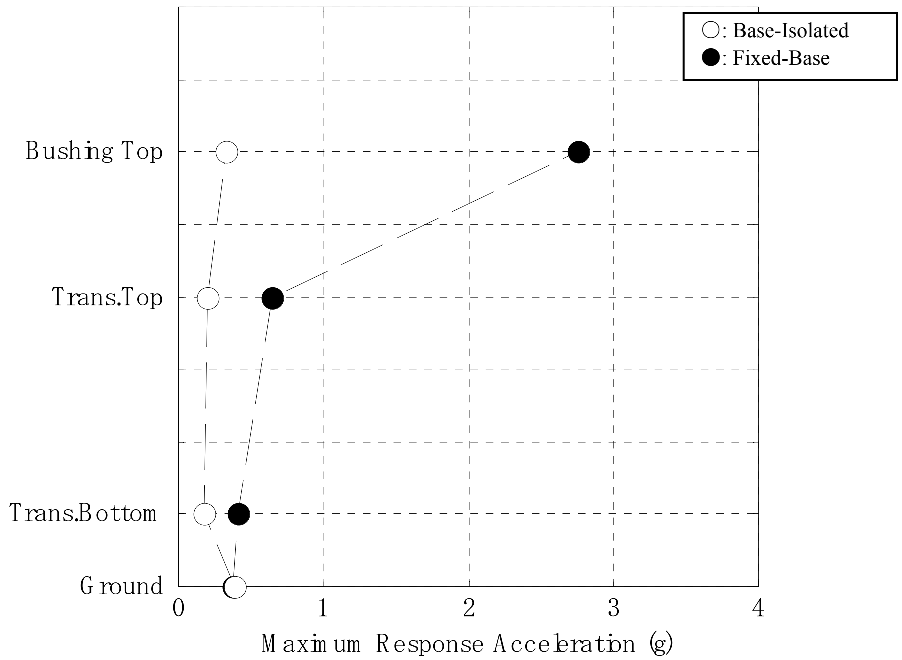

Figure 3-15 Maximum Response Acceleration: 161kV/Northridge/x375

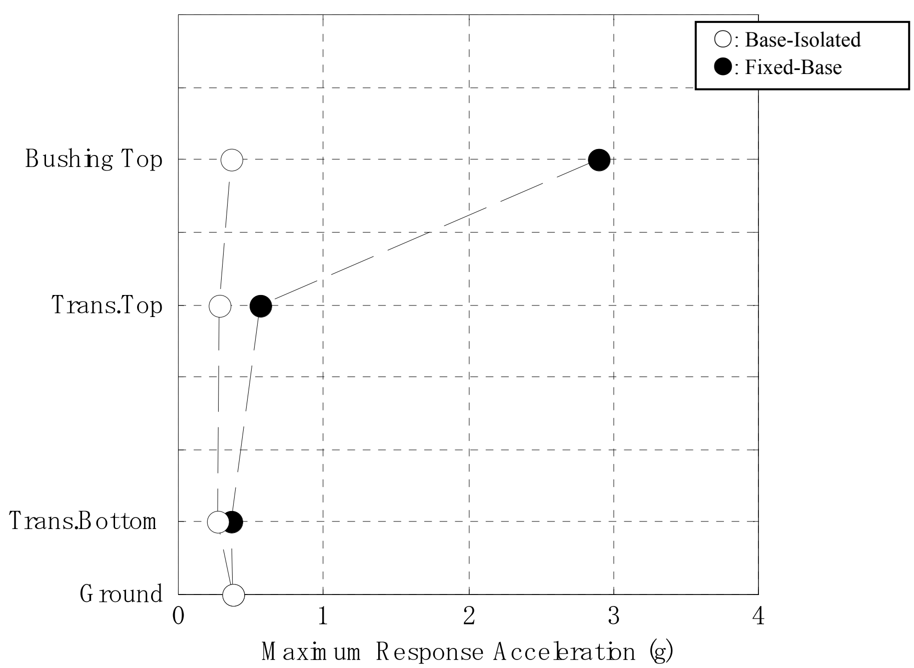

Figure 3-16 Maximum Response Acceleration: 161kV/Kobe/x375

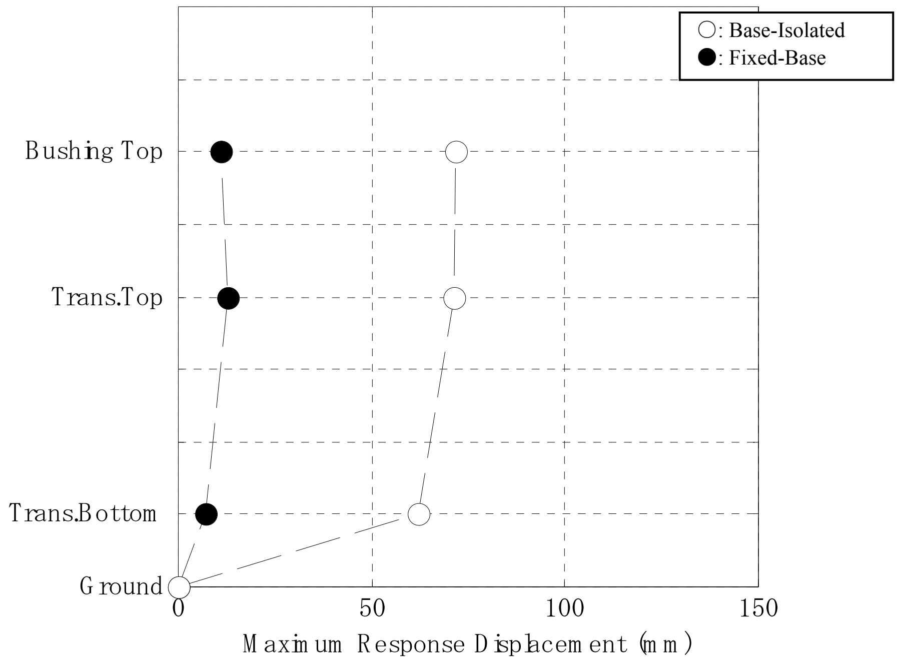

Figure 3-17 Maximum Response Displacement: 161kV/Northridge/x375

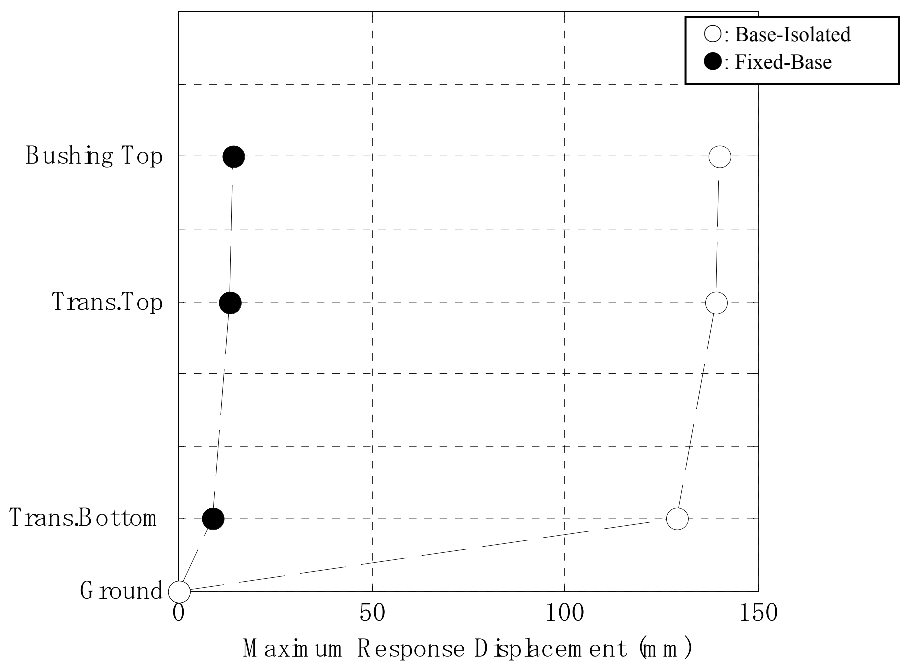

Figure 3-18 Maximum Response Displacement: 161kV/Kobe/x375

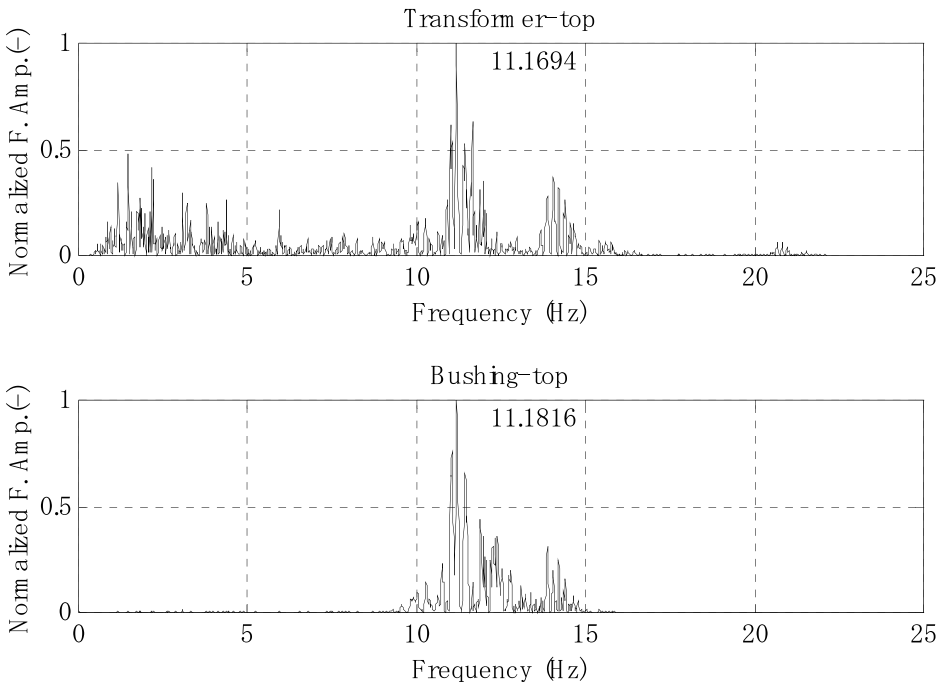

[Fixed-base]

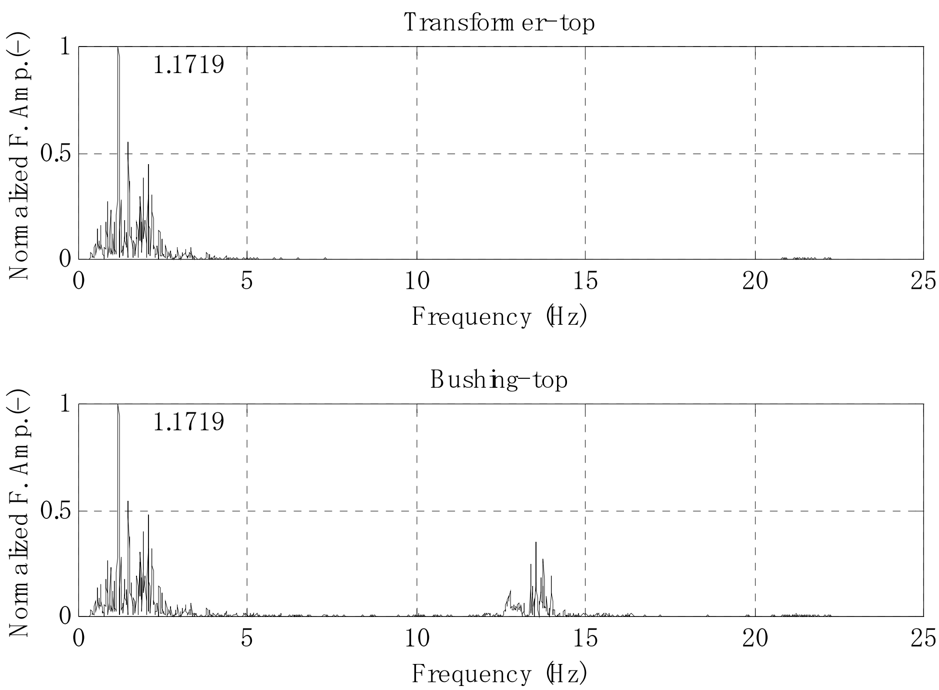

[Base-isolated]

Figure 3-19 FFT Analysis of Response Acceleration in 161kV/ El Centro/x375

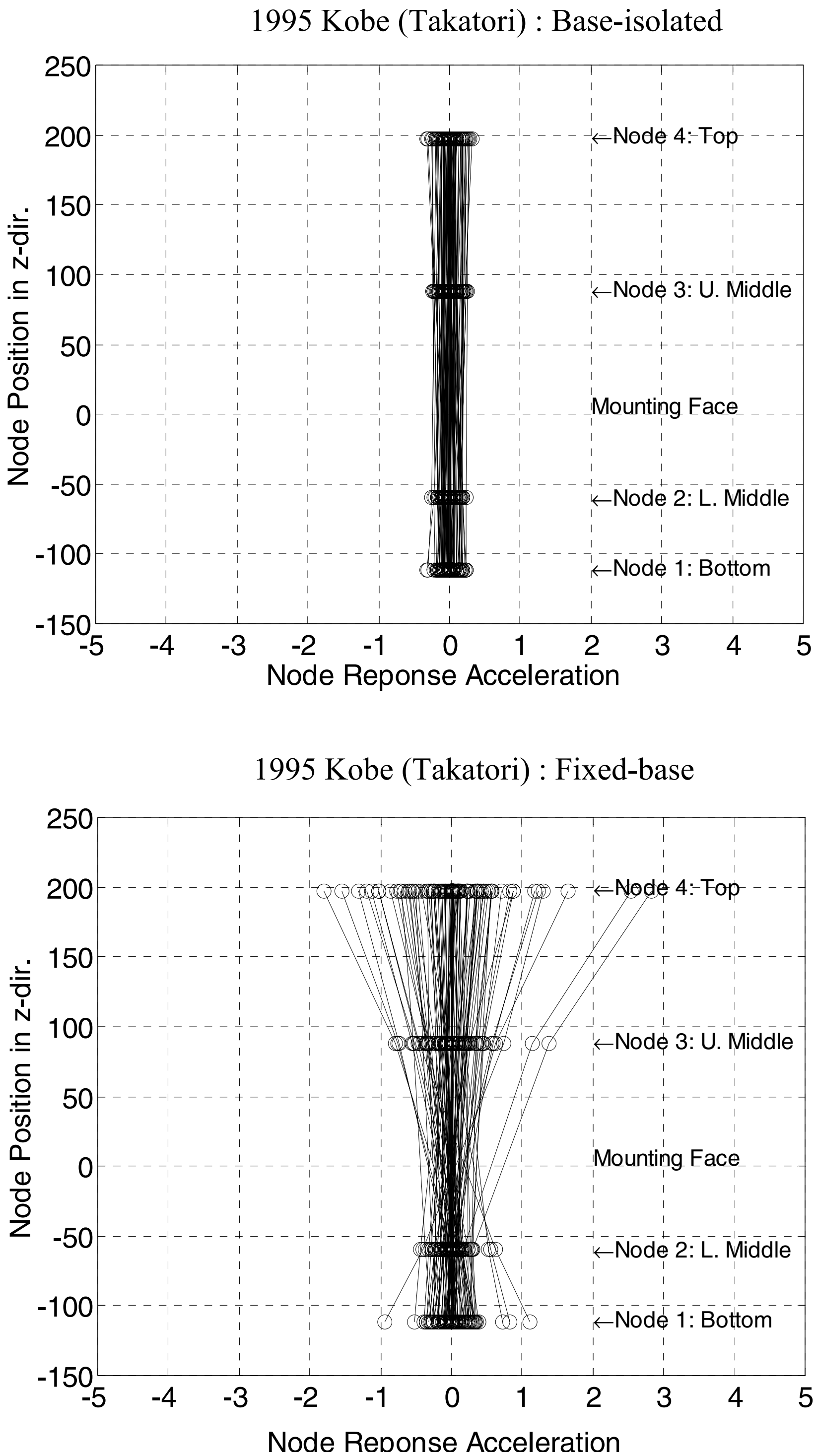

Figure 3-20 Distribution of Response Acceleration at Bushing,161kV/Kobe/x375

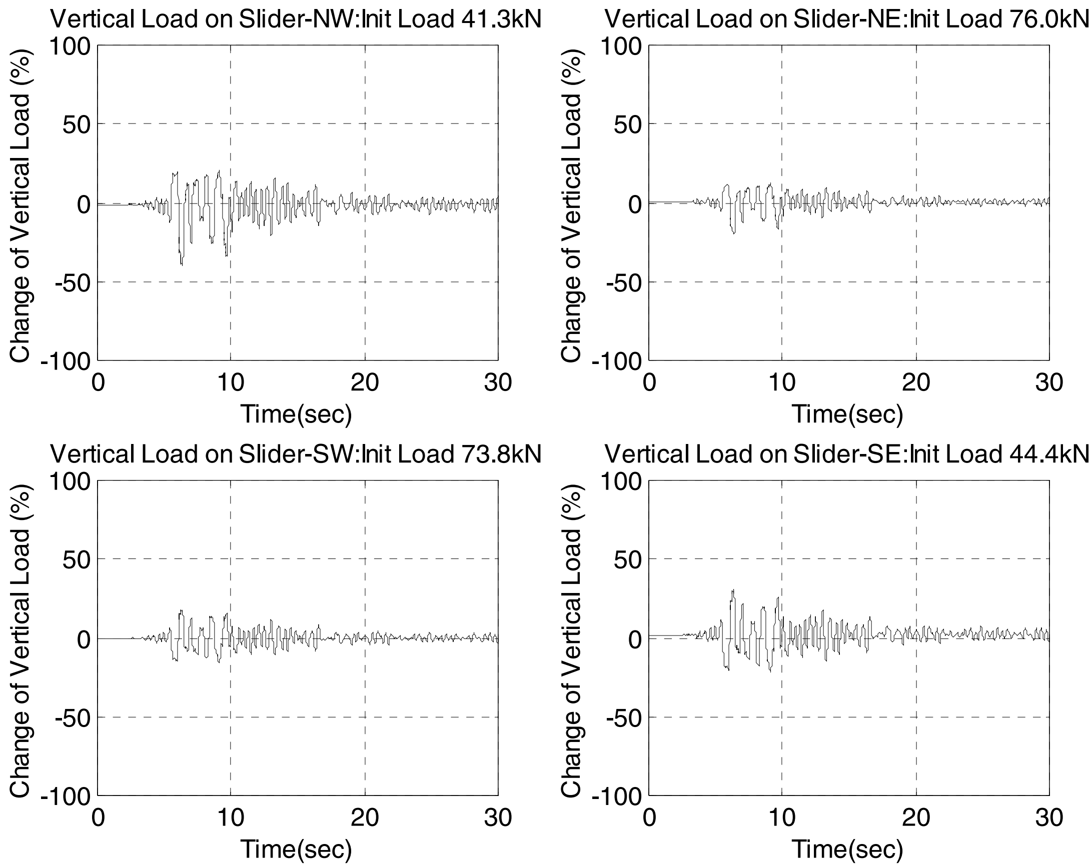

Figure 3-21 Change of Vertical Load on Sliding Bearings: 161kV/ Kobe/x375

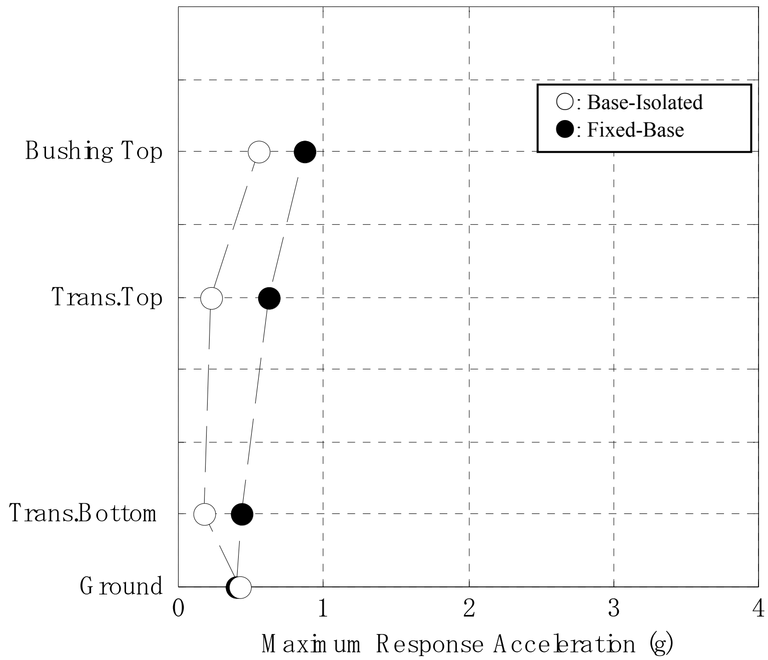

Figure 3-22 Maximum Response Acceleration: 69kV/Northridge/x375

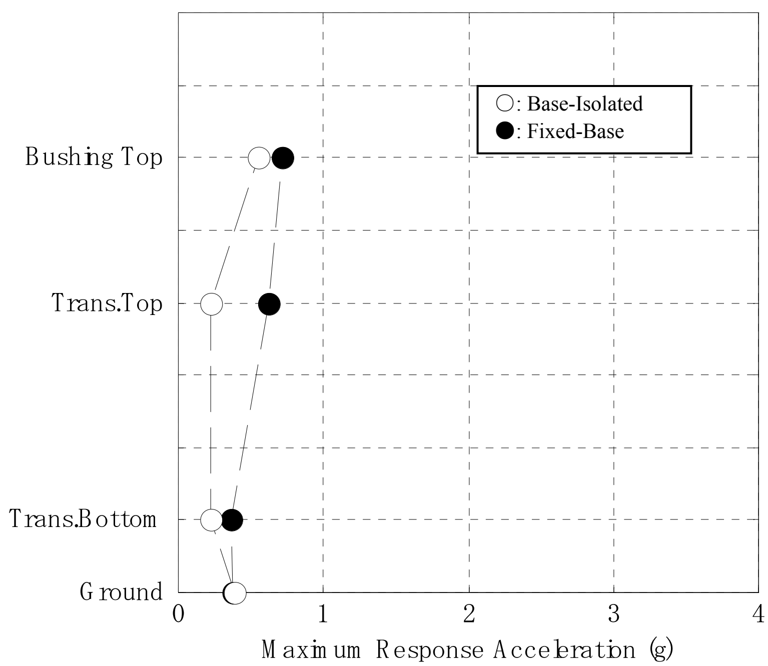

Figure 3-23 Maximum Response Acceleration: 69kV/Kobe/x375

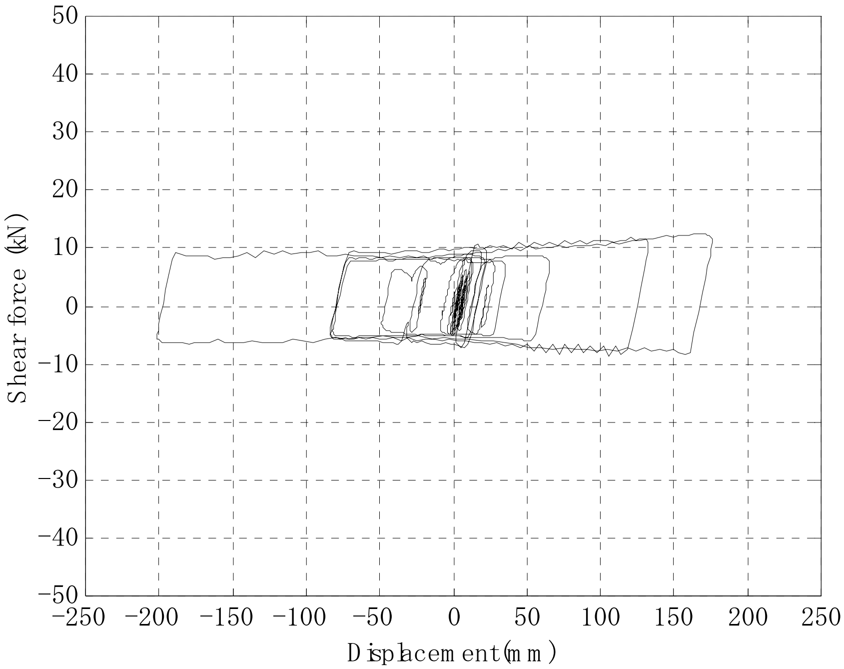

Figure 3-24 Force-Displacement Curve of Sliding Bearing: 161kV/B/Kobe/x500

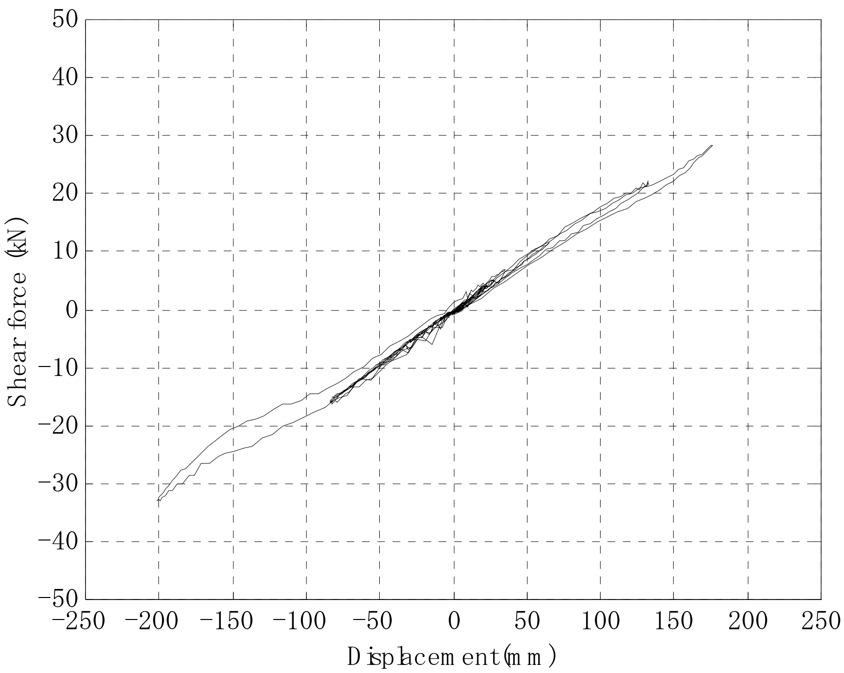

Figure 3-25 Force-Displacement Curve of Low-damping Rubber Bearing: 161kV/B/Kobe/x500

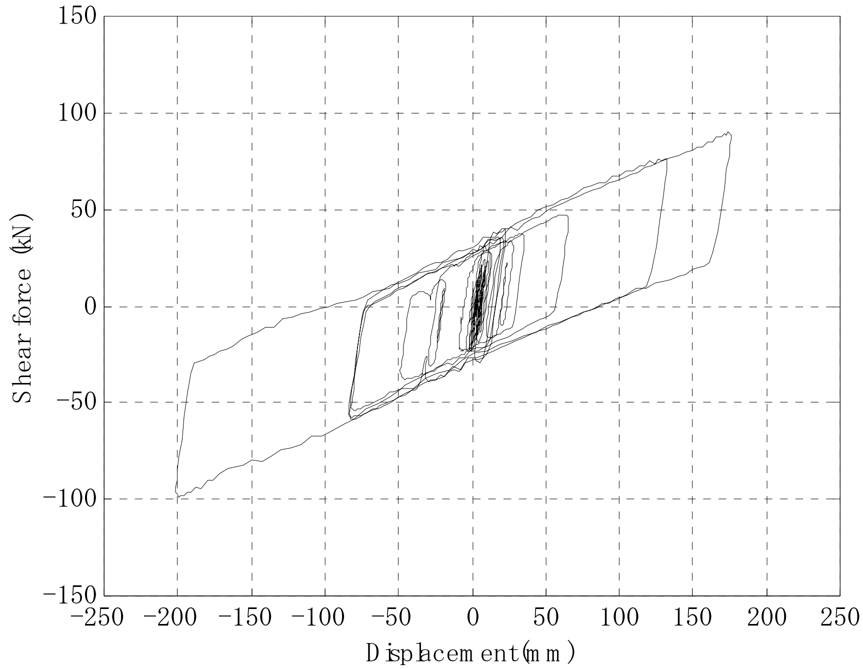

Figure 3-26 Total Force-Displacement Curve of Isolation System in 161kV/B/Kobe/x375

3.6.2 Bi-Axial Shaking

The bi-axial shaking test showed similar results to those of the uni-axial shaking. Figure 3-27 shows the correlation between the response accelerations at the top of the bushing (AB4) and the transformer (A3), in the x-direction under the uni- and bi-axial excitations. Each point plotted on the figure is the result under uni- and bi-axial excitations with the same PGA in the x-direction. In the fixed-base system, a strong correlation was demonstrated both fixed and isolated systems at top of transformer. In the base-isolated system, however, a weak correlation was observed at top of bushing.

The force-displacement curves of the sliding bearings and the rubber bearings under the Kobe (Takatori) x0375gy025g are shown in Figure 3-28. The sliding bearings exhibited complicated loops caused by the plane movement of the transformer model. Assume that the force-displacement loops for the sliding bearing under uni-axial shaking is a rectangular shape with a friction force of Q_S. When the sliding bearing moves in the x-y plane, the x-component of the friction force Q_x at time *t* is expressed as follows:

$$\left.\begin{aligned} & Q_x = Q_S \times \alpha_x, \quad Q_y = Q_S \times \alpha_y \\ & \alpha_x = \frac{\Delta x}{\sqrt{\Delta x^2 + \Delta y^2}}, \quad \alpha_y = \frac{\Delta y}{\sqrt{\Delta x^2 + \Delta y^2}} \end{aligned}\right\} \qquad (3\text{-}1)$$

where,

$\Delta x = x(t) - x(t-1), \Delta y = y(t) - y(t-1)$

Applying (3-1), $Q_x(t)$ was calculated using the actual locus(x,y) measured during the Kobe (Takatori) x0375gy025g excitation and plotted in Figure 3-29. The loops show very good agreement with the actual test results and verified the relationship expressed in (3-1). The total force-displacement curves in x- and y-directions under the Kobe (Takatori) x0375gy025g are shown in Figure 3-30. Compared with Figure 3-26 under the uni-axial shaking, the effect of multi-axial shaking on the performance of the isolation system can be observed.

The locus of the gravity center under Kobe (Takatori) x0375gy025g, the largest input to the base-isolated system, is shown in Figure 3-31. The maximum deflection of the rubber bearing under the Kobe (Takatori) was 177.6 mm, corresponding to a rubber shear strain of 92.5%.

3.6.3 Tri-Axial Shaking

Under the tri-axial (tri) shaking, the responses of the transformer/bushing system showed significant difference from those under the uni and bi-axial shaking. The response accelerations at the tops of the bushing for both 161-kV and 69-kV bushings on the isolated transformer were amplified and, in some cases, the response exceeded that of the fixed-base system.

Figure 3-32 shows the time-history of the response acceleration in the x-direction of the case 161kV/Northridge/xyz375, for the base-isolated and fixed-base systems. The acceleration at the bushing top with base isolation reached 1.0g and the amplification of the input was about 3. Amplification on the bushing was not observed in uni-axial and bi-axial shaking in the base-isolated system. This phenomenon was a very significant finding through Phase-1 testing. Figures 3-33, 3-34 and 3-35 compare the peak response acceleration along the height of the transformer under uni-, bi-, and tri-axial shaking in the cases of 161kV/Northridge, 161kV/Kobe, and 161kV/El Centro.

Figure 3-36 shows the correlation between the response accelerations at the tops of the bushing and the transformer under the bi- and tri-axial shaking. In the fixed-base system, there was a linear correlation between the bi- and tri-axial shaking. In other words, the vertical ground motion had little effect on the responses in the horizontal directions. However, in the base-isolated system, there was no linear correlation between the bi- and tri-axial shaking. The response under the tri-axial excitation was much larger than that under the bi-axial shaking with the same intensity of ground motion.

Figure 3-37 shows the comparison of the vertical load on the sliding bearings under bi- and tri-axial shaking for the 69kV system. The vertical load change under bi-axial shaking was caused by overturning of the transformer, whereas under tri-axial shaking the vertical load change was caused by the combination of overturning-load and vertical ground motion.

In Figure 3-38, the total force-displacement curves of the sliding bearings under the bi- and tri-axial shaking are compared. The loops under tri-axial shaking were obviously affected by the change of vertical load due to the vertical excitation. From the above discussion, it was deduced that the high frequency factor on the friction force of the sliding bearings, which was caused by the vertical excitation, affected the bushing response. The 161kV bushing showed better results because the natural frequency of this bushing was lower than that of the 69-kV bushing.

3.7 Summary

The uni-axial, bi-axial and tri-axial seismic simulator testing was carried out for both the fixed-base and the based-isolated transformer/bushing systems. The input motions were the 1940 El Centro, 1994 Northridge (Sylmar), and 1995 Kobe (Takatori) earthquake ground motion records.

Under the uni-axial shaking, the response of the base-isolated transformer/bushing system showed obvious improvement compared to the fixed-base system. Particularly in the 161kV bushing/transformer system, the response acceleration observed on the bushing attached on the fixed-base transformer showed severe amplification, whereas the corresponding amplification in the base-isolated system remained well confined.

Under the bi-axial horizontal shaking, the base-isolated system in general showed improved responses, although in some cases the amplification at the top of the bushing increased compared with those under the uni-axial shaking.

Under the tri-axial shaking with the vertical ground motion introduced, the response acceleration at the top of the bushing was amplified more in the base-isolated system than the same system under bi-axial horizontal shaking with the same x and y intensities. In some cases, the base-isolated system showed larger response accelerations than those of the fixed-base system.

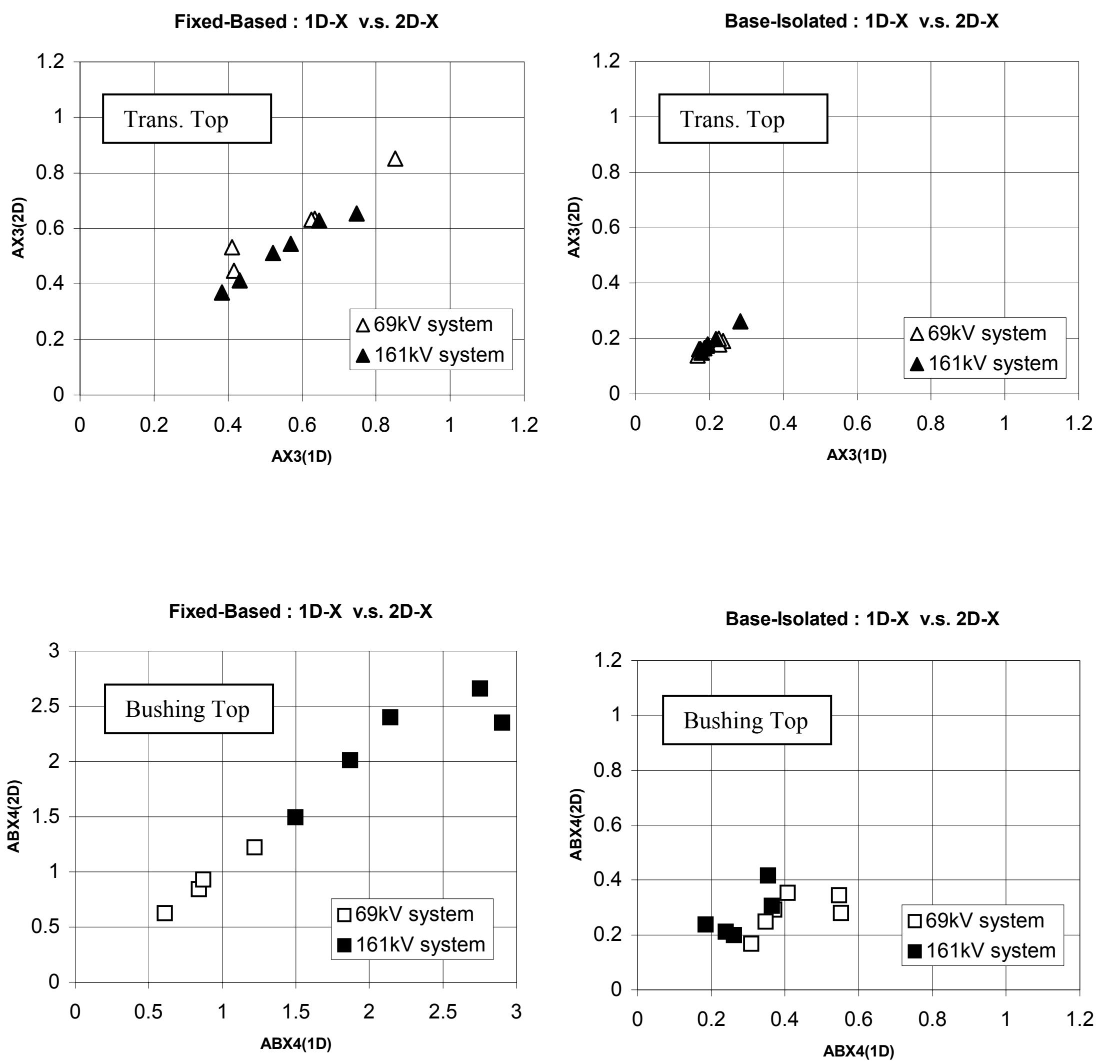

Figure 3-27 Correlation between Response Accelerations under Uni- and Bi-Axial Shaking

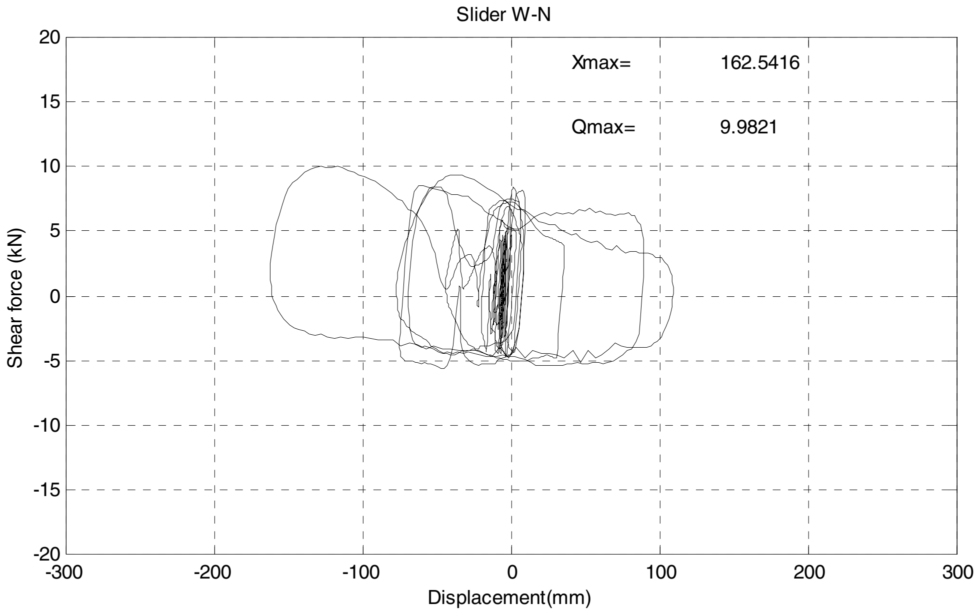

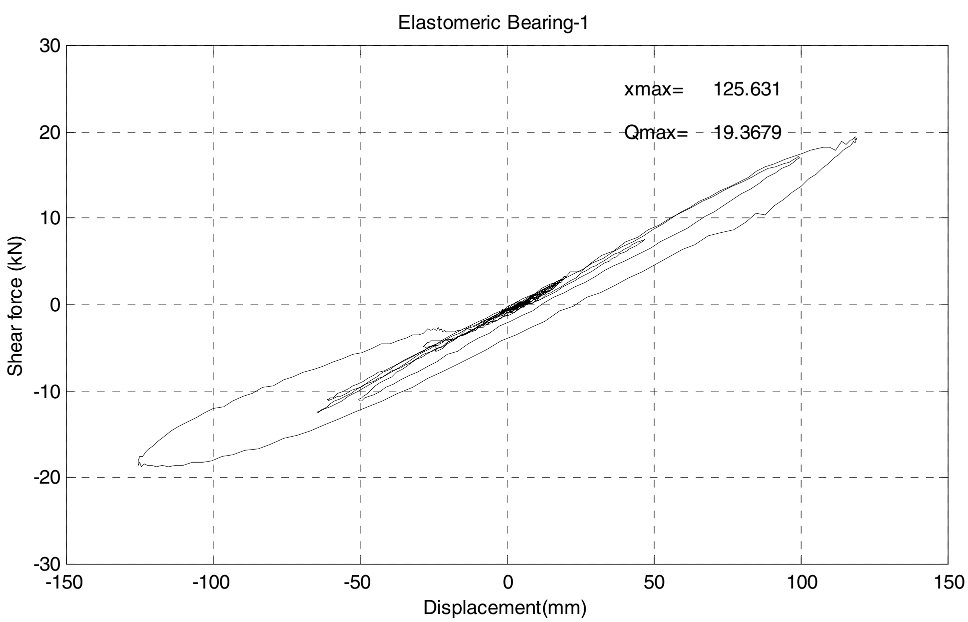

Figure 3-28 Force-Displacement Curve of Sliding Bearing and Low-Damping Rubber Bearing under Bi-Axial Shaking: 161kV/B/Kobe /xy375, x-dir., W-N, W-S

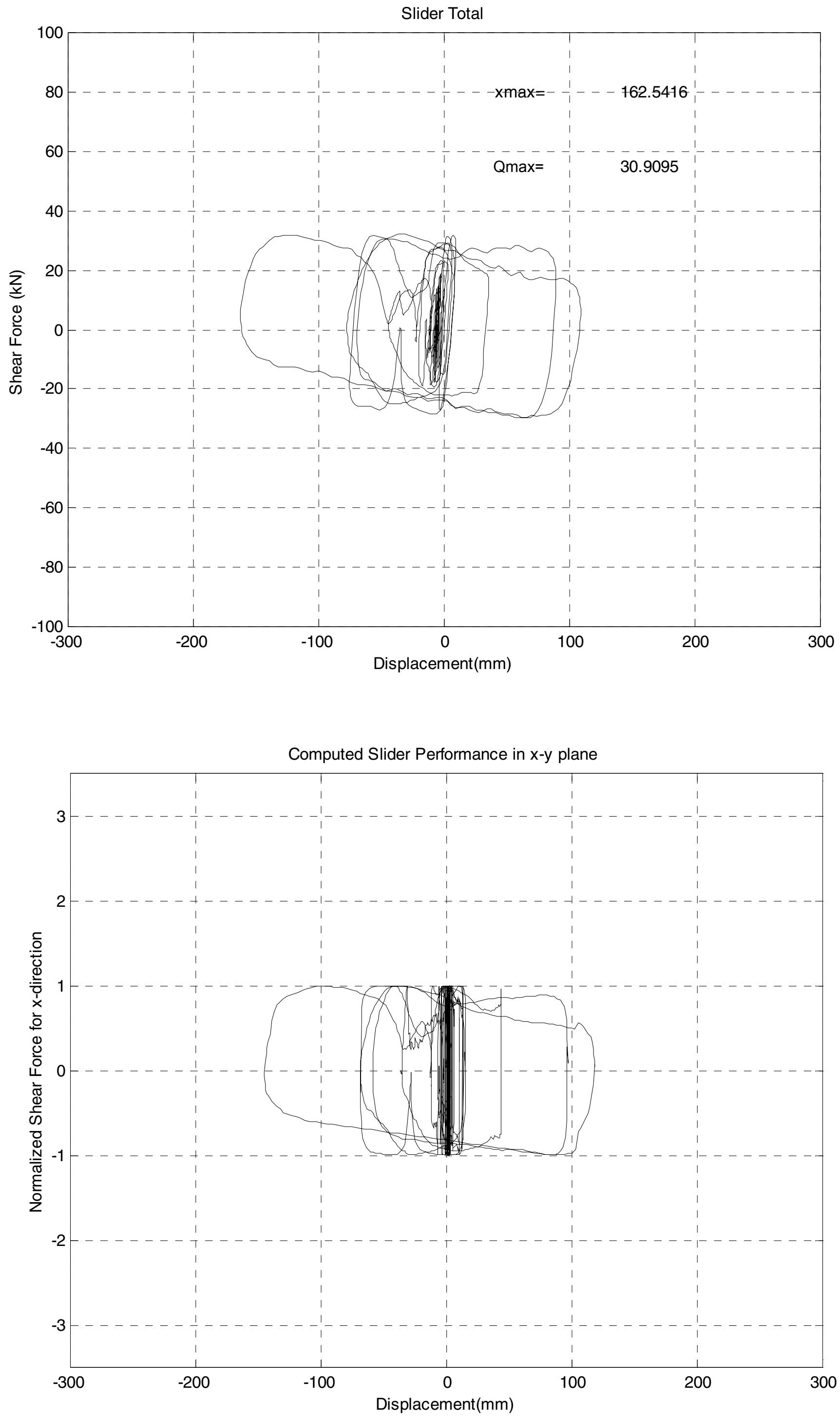

Figure 3-29 Comparison of Experimental and Analytical Force-Displacement Curves of Sliding Bearing

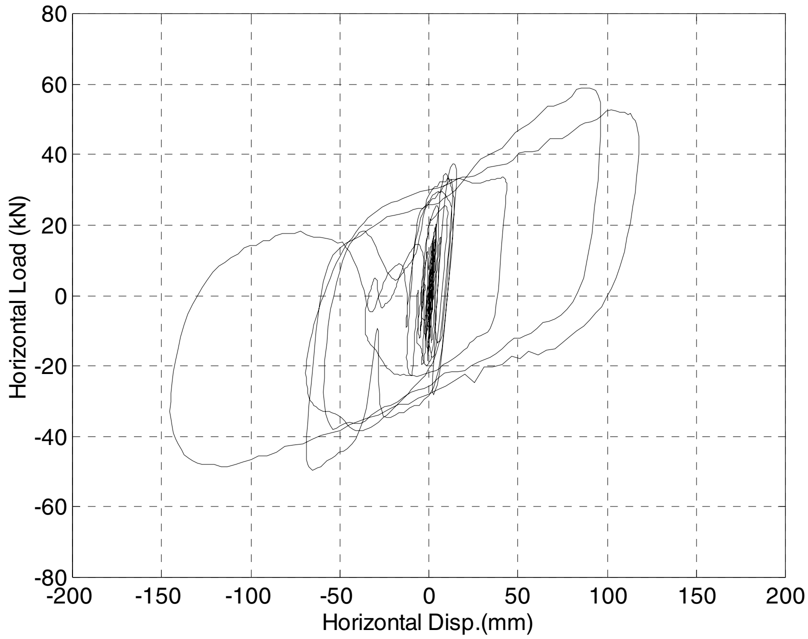

Figure 3-30 Total Force-Displacement Curve under Bi-Axial Shaking: 161kV/B/Kobe /xy375

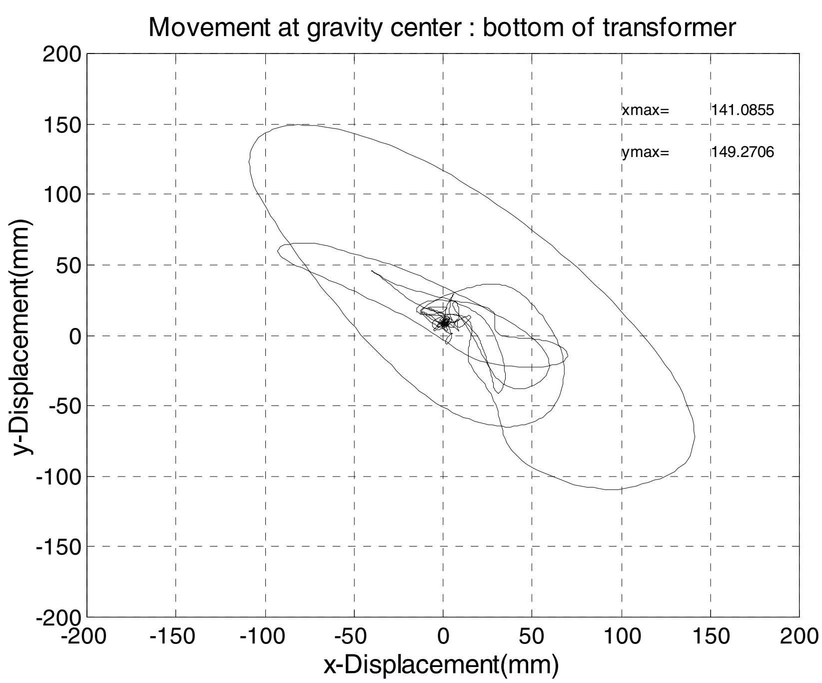

Figure 3-31 Locus of Center at Transformer Bottom under Bi-Axial Shaking: 161kV/B/Kobe/xy375

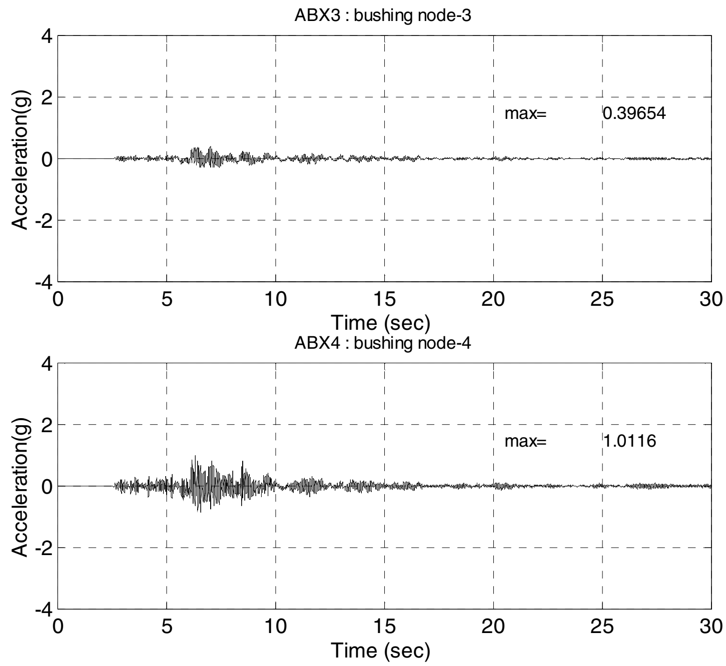

Base-isolated

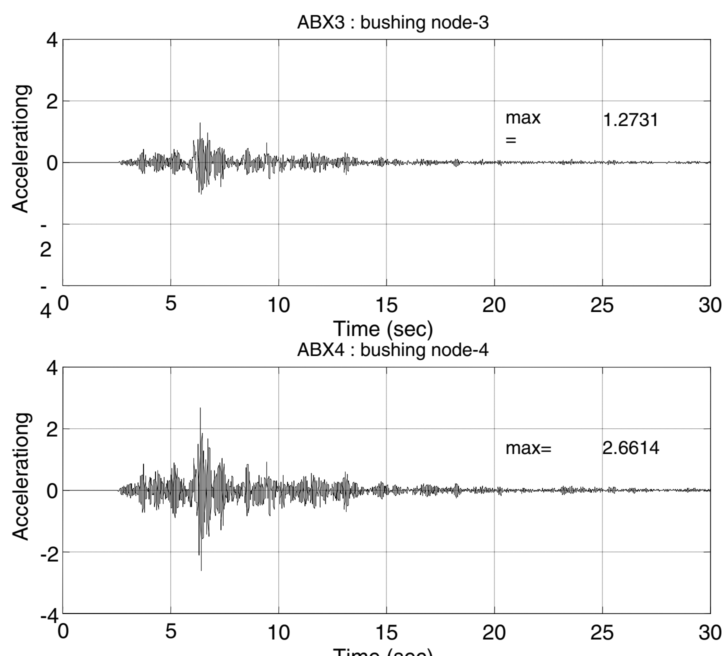

Fixed-base

Figure 3-32 Response Acceleration at the Top of 161kV Bushing under Tri-Axial Shaking: 161kV/B/Northridge / xyz375, Acceleration in x-dir.

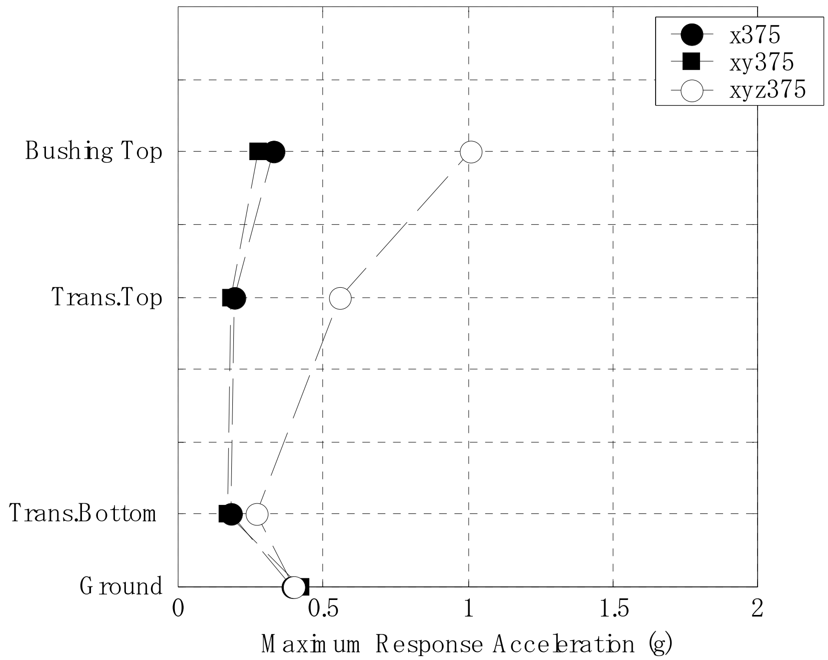

Figure 3-33 Comparison of Maximum Response Acceleration in Uni-, Bi-, and Tri-Axial Shaking: 161kV/B/Northridge/x, xy, xyz375

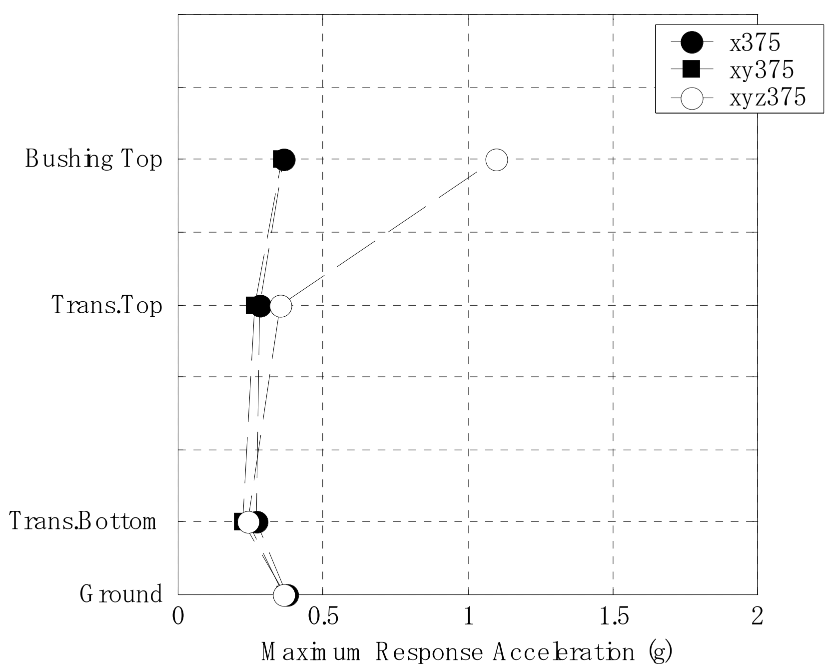

Figure 3-34 Comparison of Maximum Response Acceleration in Uni-, Bi-, and Tri-Axial Shaking: 161kV/B/Kobe/x, xy, xyz375

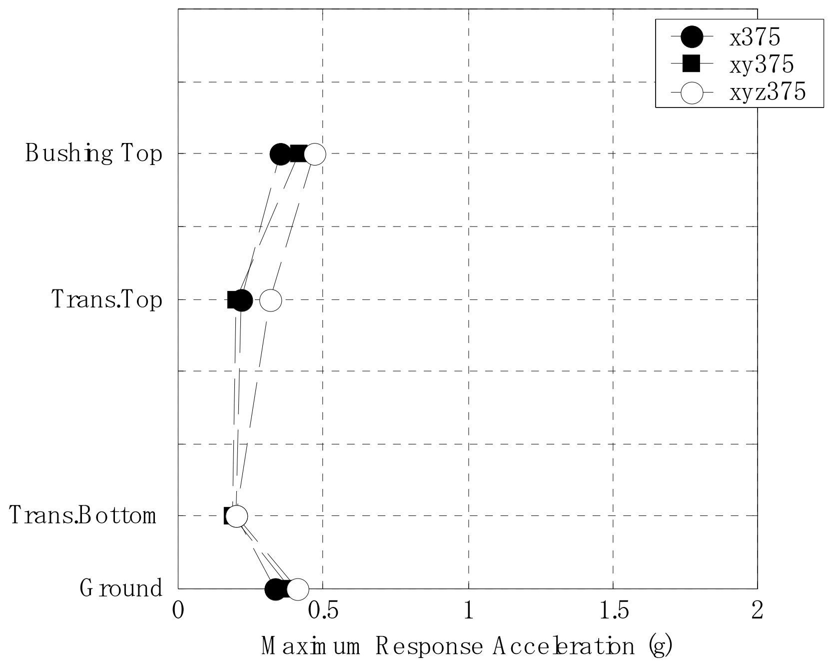

Figure 3-35 Comparison of Maximum Response Acceleration in Uni-, Bi-, and Tri-Axial Shaking: 161kV/B/El Centro/x,xy,xyz375

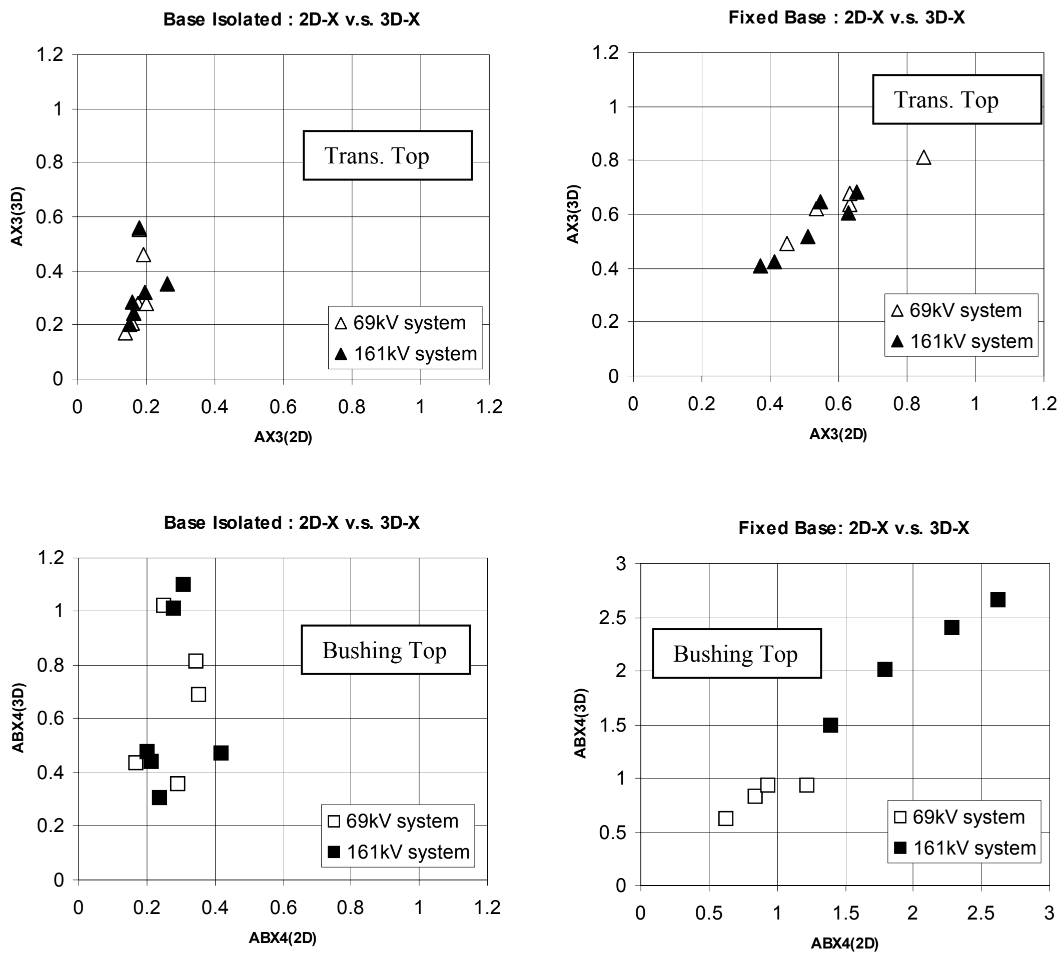

Base-isolated | Fixed-base

Figure 3-36 Correlation between the Response Accelerations under Bi and Tri-Axial Shaking

bi-axial shaking : 69kV/Northridge (Sylmar) x0375gy025g, Base-isolated

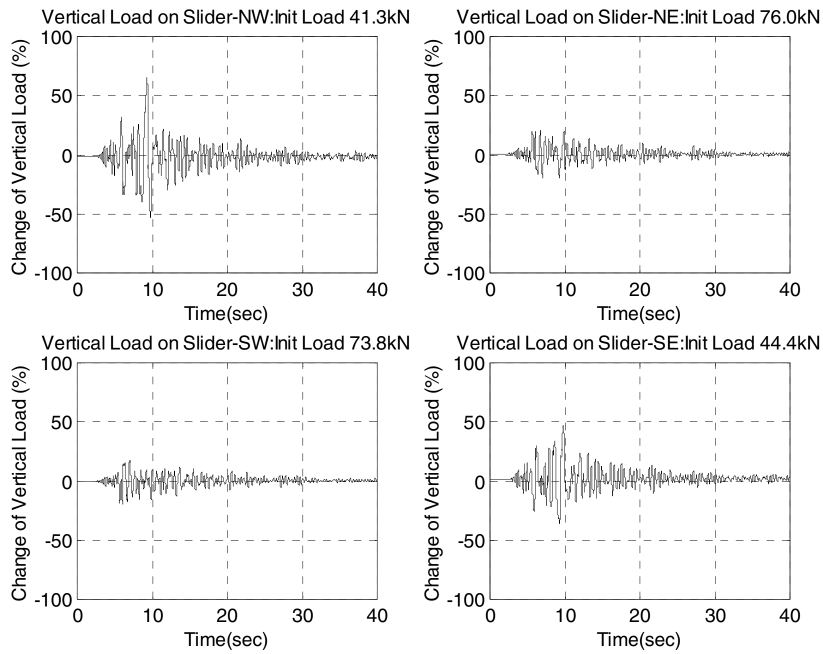

tri-axial shaking : 69kV/Northridge (Sylmar) x0375gy025gz025g, Base-isolated

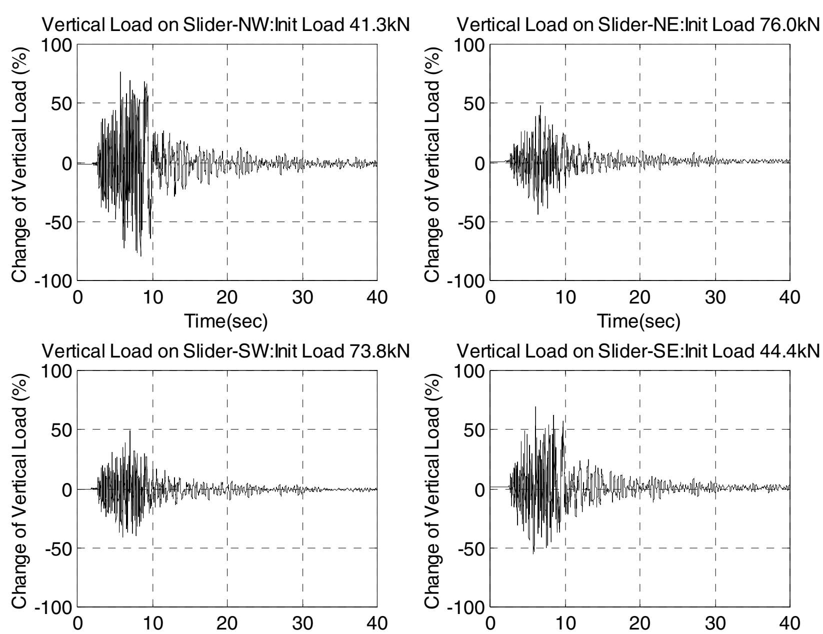

Figure 3-37 Comparison of the Vertical Load on Sliding Bearing under Bi- and Tri-Axial Shaking

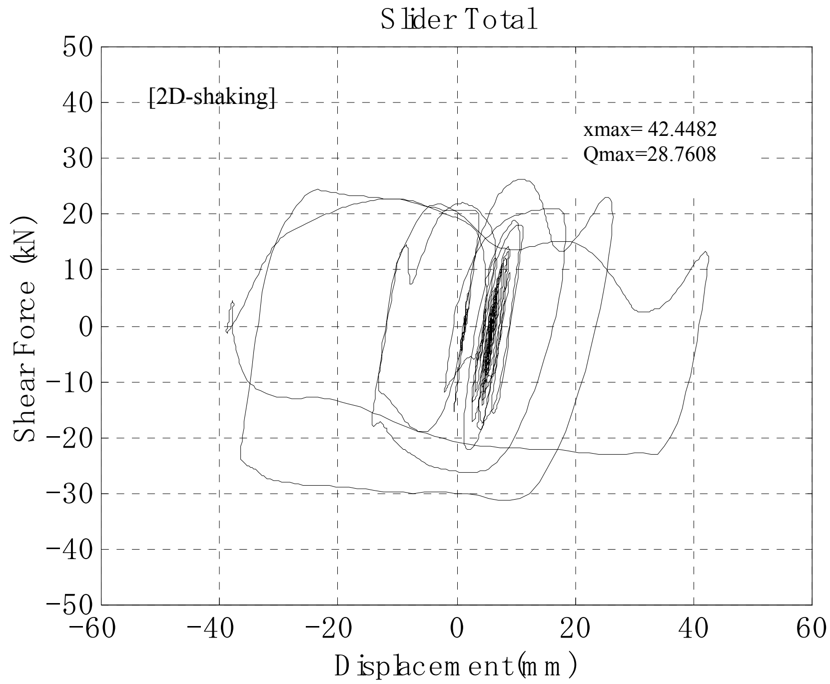

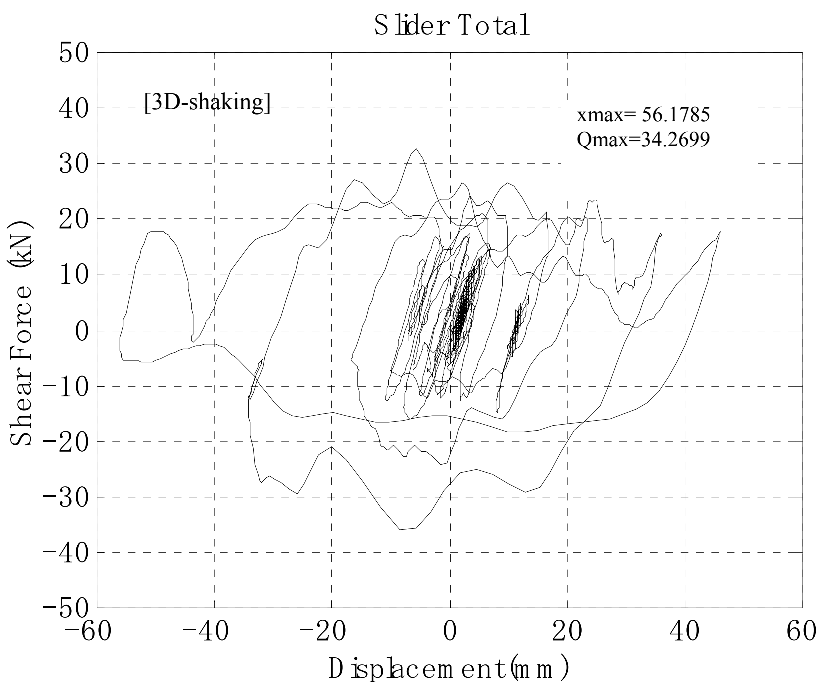

Figure 3-38 Force-Displacement Curve of Sliding Bearing under Bi- and Tri-Axial Shaking: 69kV/B/Northridge /xy375,xyz375, x-dir.

SECTION 4
EARTHQUAKE SIMULATOR TEST/PHASE-2

4.1 Overview

In Phase-2, the segmented high-damping bearings were used as isolators, and a flexible rubber ring was developed and installed between the flanges of bushing and transformer top to change the dynamic characteristics of the bushing. The frequency was shifted to low-range (assuming a large-size bushing such as 500-kV) that is generally sensitive to ground motion. The artificial wave matching to IEEE693-1997 REQUIRED RESPONSE SPECTRUM was generated and applied.

4.2 Experimental Setup

The basis of the experimental setup of Phase-2 was almost the same as that of Phase-1. As described later, the weight of the transformer model was reduced and a scale factor was introduced. Figure 4-1 shows the test setup of base-isolated model.

4.2.1 Transformer Model

The total weight of the transformer model was decreased from 241kN in Phase-1 to 141kN considering the stability of the segmented isolators. The other dimensions were the same as that of Phase-1. According to the dynamic identification test results, the natural frequencies of the 1^{st} and 2^{nd} modes were 12.3 Hz and 28.9 Hz, respectively.

4.2.2 Porcelain Bushing

From the results of Phase-1, it is concluded that the 69-kV bushing had a frequency high enough to be insensitive to ground motion. Therefore, only the 161-kV bushing was used in Phase-2.

Figure 4-1 Test Set-Up of Phase-2 Testing

4.3 Segmented High-Damping Rubber Bearing Isolation System

Figure 4-2 shows the segmented high-damping rubber bearing (SHRB) used in this test (Masaki, 1999). The isolation system consisted of four stacks of three element bearings. The thick plates between each bearing layer were designed to work as stabilizers during large displacement. The element bearings had a maximum shear-strain capacity of 250%. The total maximum displacement of SHRB was around 200 mm. The nominal compressive stress was 4.0 MPa. The design shear modulus and equivalent damping ratio at 100% shear strain was 0.61 MPa and 16%, respectively. The diameter of the element bearing was 72 mm and the thickness of the unit rubber layer was 0.9 mm. The number of layers was 31 and the total rubber height was 27.9 mm. The first and second shape factors, S_1 and S_2, of the element bearings were 20 and 2.58. The element bearing itself had poor stability characteristics because of its slim shape, or a small S_2. Therefore, the stabilizing plates installed between each layer of SHRB allow large displacement without instability. The design fundamental period of the transformer model sustained by the four SHRB was computed as 1.32 seconds. The design properties are summarized in Table 4-1.

Table 4-1 Design Properties of Segmented Rubber Bearings

1. Element bearing			
Unit rubber thickness	t_r	0.9	(mm)
Number of layers	n_r	31	(-)
Total rubber height	h_r	27.9	(mm)
Rubber diameter	D	72	(mm)
First Shape Factor	S_1	20	(-)
Second Shape Factor	S_2	2.58	(-)
Effective area	A_{eff}	4071.50	(mm^2)
Shear modulus	G	0.418	(N/mm^2)
Shear stiffness	K_h	60.99	(N/mm)
Shear force at 300%	Q_{max}	5615.7	(N)
2. Assembled bearing			
Shear stiffness	K_{hT}	81.3	(N/mm)
Total rubber height	Hr	111.6	(mm)
3. Design compressive force		141	(kN)
4. Fundamental period	T_f	1.32	(sec)

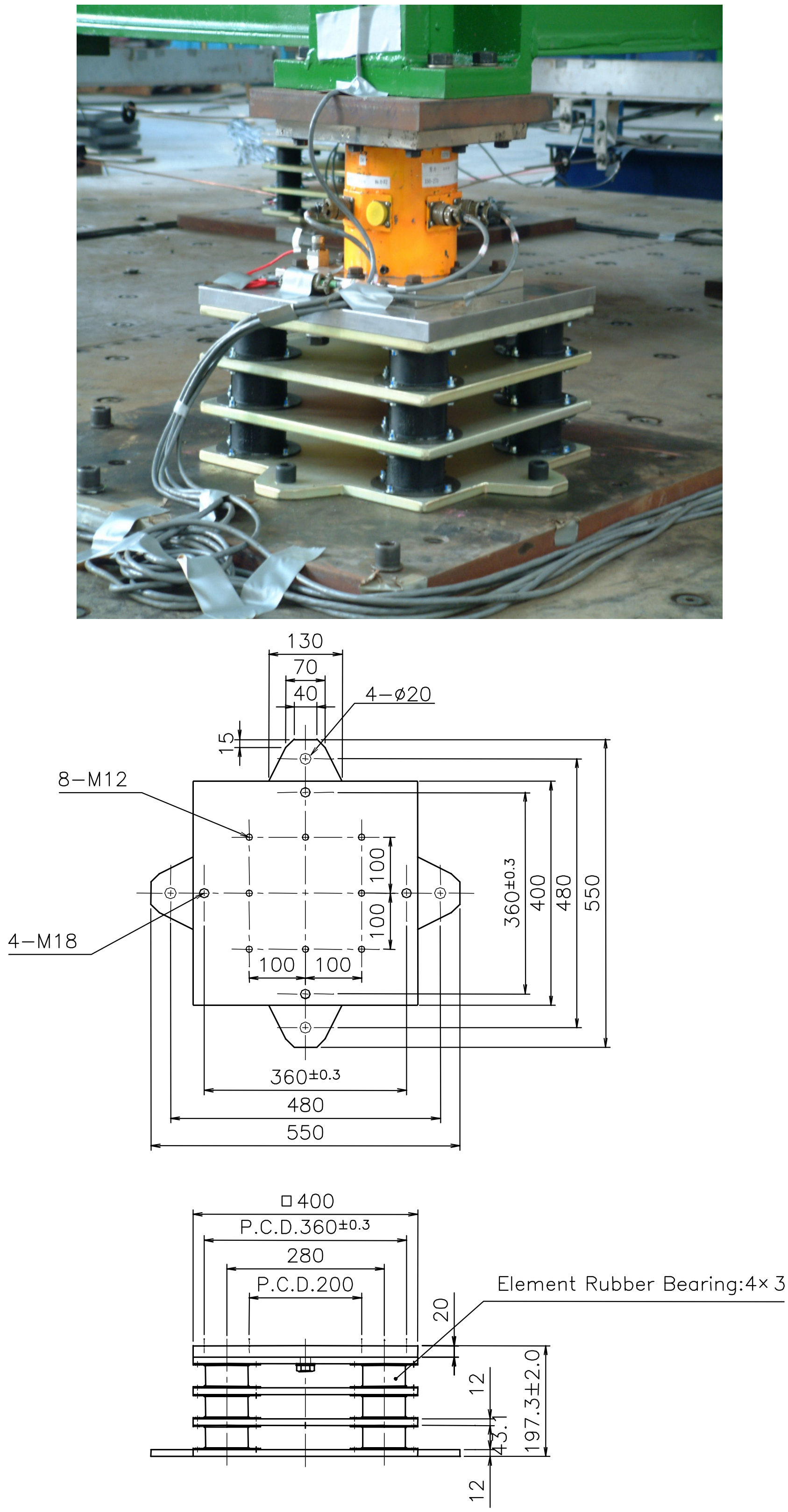

Figure 4-2 Segmented High-Damping Rubber Bearing

4.4 Flexible Rubber Ring

In order to evaluate the response of the bushing under a low frequency, like 3.0 Hz, a flexible rubber ring (shown in Figure 4.3) was specially designed and manufactured, and was mounted between the top of the turret and the flange of the bushing. The rubber ring was designed to contribute to the rocking motion of the bushing and shift the fundamental period of the bushing with its low tilting stiffness. The tilting stiffness K_r of the rubber ring is calculated by the following equation:

$$K_r = \frac{E_{bent} \cdot I}{t} \quad (4\text{-}1)$$

$$\frac{1}{E_{bent}} = \frac{1}{E_0 (1 + \frac{2}{3} \kappa S_1^{\,2})} + \frac{1}{E_\infty} \quad (4\text{-}2)$$

where,

E_{bent}	is the apparent Young's modulus of rubber
E_0	is Young's modulus of rubber $(\approx 3G, G: shear\ modulus)$ =2.2MPa
E_∞	is bulk modulus of rubber =1200 MPa for this compound
S_1	is first shape factor of rubber ring
κ	is correction factor, =0.85 for this compound
t	is rubber-layer thickness
I	is second section modulus of the ring

A low damping rubber compound was used, with a shear modulus of 0.4 MPa--one of the softest compounds in practical use for isolation bearings. The design characteristics of the rubber ring are shown in Table 4-2.

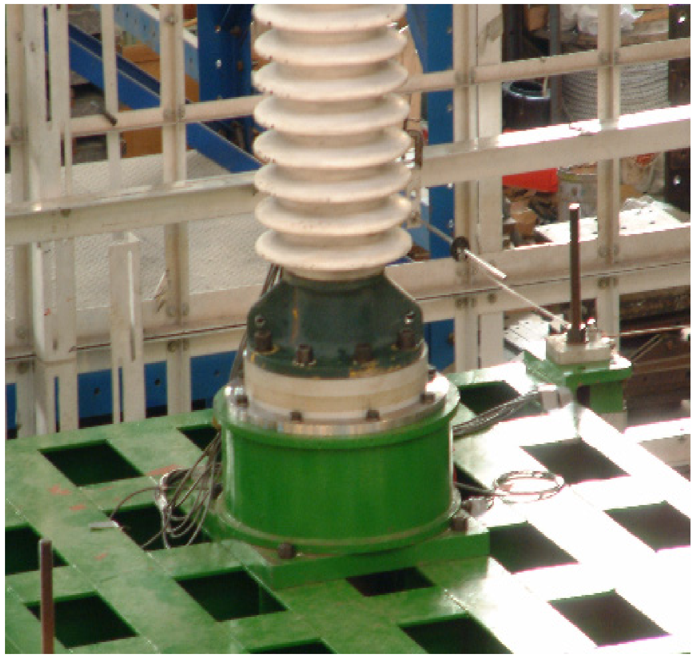

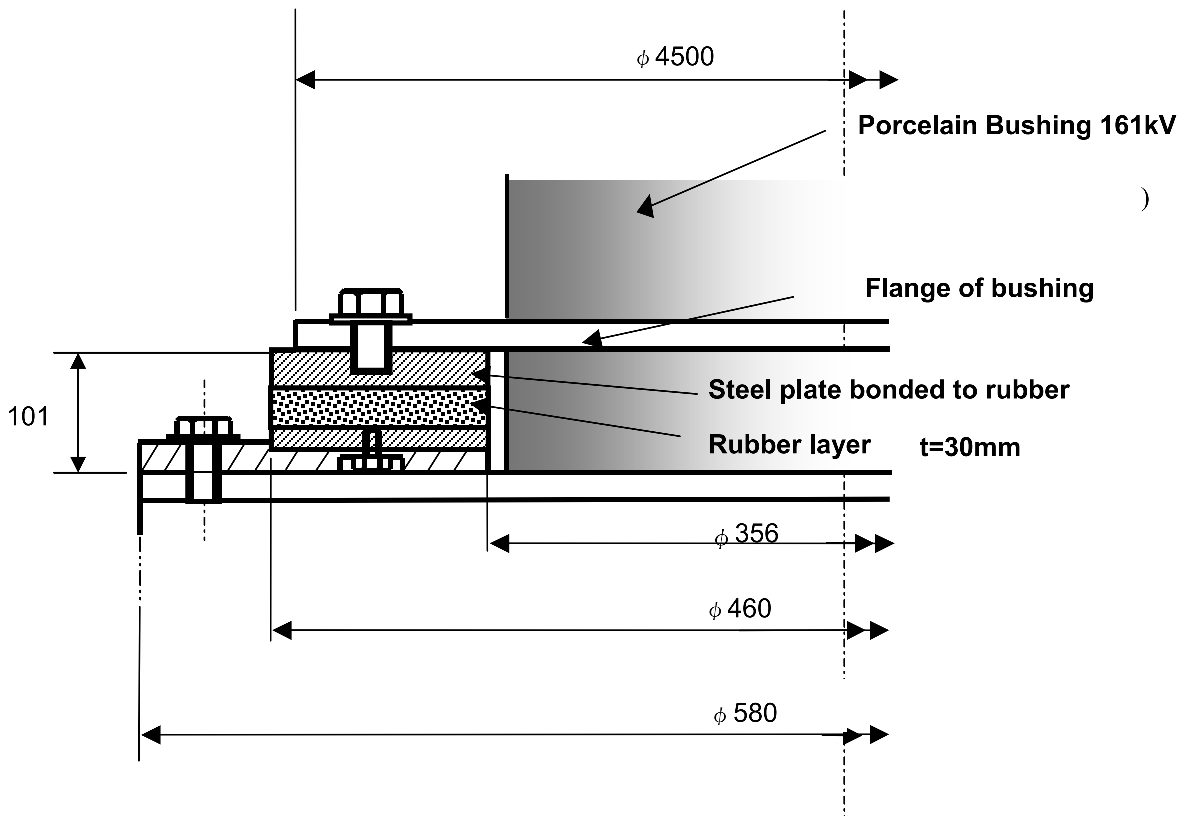

Figure 4-3 Flexible Rubber Ring

Table 4-2 Design Parameters of Flexible Rubber Ring

t_r	30	(mm)	E_b	2.845	(MPa)
D	460	(mm)	I	1.4094e+9	(mm^4)
d	356	(mm)	K_r	133636.9	(kN· mm)
A	66652.0	(mm^2)	W	3.43	(kN)
S_1	0.867	(-)	σ	0.05199	(MPa)
E	2	(MPa)	h_g	1000	(mm)
k	0.85	(-)	$W h_g^2$	3430000	(kN· mm^2)
E_m	1200	(MPa)	T_r	0.32	(sec)
E_b'	2.851	(MPa)	f	3.11	(Hz)

4.5 Testing Program

The differences between the Phase-2 and the Phase-1 testing programs were the isolator system, the input ground motion, the total weight of the model, the application of the flexible rubber ring, and the application of a scale factor. The scaling chosen in the test was based on constant stress and constant acceleration. The scale factor applied was 0.6 for length and displacement, and $0.6^{0.5}$=0.775 for velocity and time. The relationship of constant stress scaling is summarized in Table 4-3.

Table 4-3 Constant Stress Scale of Testing

	0.6 scale model
Length L	0.6
Time $L^{1/2}$	0.775
Mass L^2	0.36
Displacement L	0.6
Velocity $L^{1/2}$	0.775

	Real model	**Test set-up**
Weight	391.7 kN	141 kN
Natural period	1.76 sec	1.36 sec
Bushing frequency	11.6 Hz	15 Hz
Compressive stress on SHRB	2.3 MPa	

Prior to the earthquake simulator tests, dynamic identification of the system was conducted. The procedure of this test was the same as that of Phase-1, page 65, so the explanation is omitted.

The parameters of the earthquake simulator tests were: 1) base-isolated or fixed-base; 2) with rubber ring (low- frequency mode) or without rubber ring (high-frequency mode); 3) earthquake record; 4) intensity of earthquake record; 5) direction of shaking. The earthquake records used in Phase-2 were 1995 Kobe (Takatori), 1999 Chi-Chi (TCU-129), and Art-693. The 1999 Chi-Chi (TCU-129) is similar to 1940 El Centro in its frequency characteristics. Art-693 was the artificially-generated wave based on the Required Response Spectrum IEEE-693. The phase angles of the composed waves were randomly chosen and superimposed. The response spectrum and Fourier spectrum of Art-693 are shown in Figure 4-4. The typical dynamic characteristics of Art-693 is the high intensity in the low frequency range, similar to 1995 Kobe (Takatori), close to the fundamental frequency of the base-isolated transformer. The shaking direction was uni-axial in the x-direction, bi-axial in the x- and y-directions, tri-axial in the x-, y-, and z-directions, the same as Phase-1. Bi-axial shaking in the x- and z-directions was added in Phase-2. The combination of the record, intensity, and shaking direction in each test case is shown in Table 4-4.

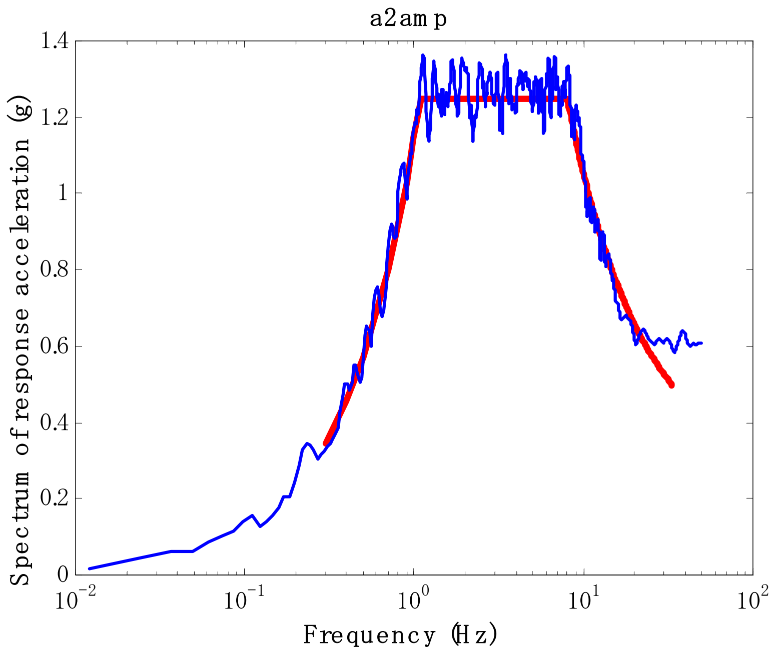

Art-693: N-S Component

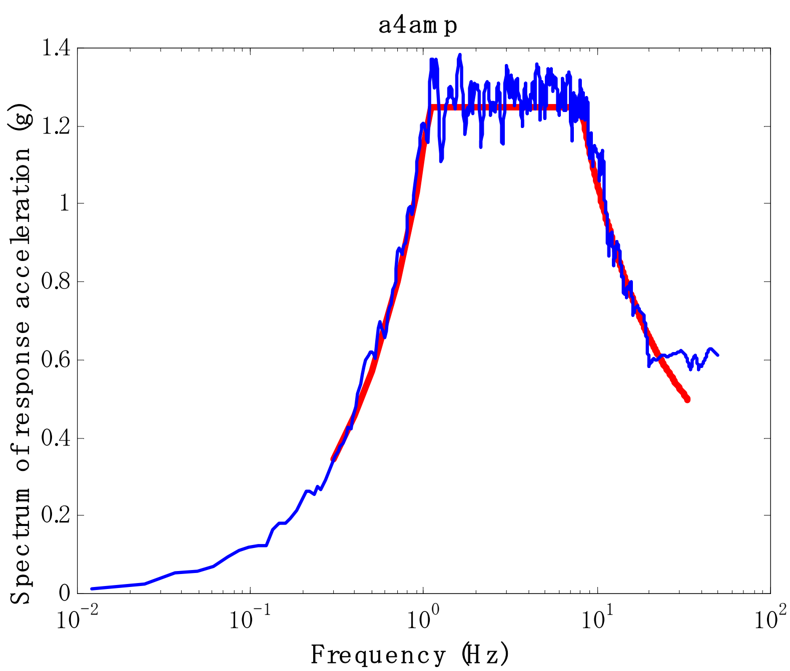

Art-693: E-W Component

Figure 4-4 Response Spectrum of Artificial Wave: N-S and E-W Components of ART-693

Table 4-4 Target PGA of Earthquake Simulator Testing in Phase-2

(1) *Base-isolated Case:*

Unit, g

Art-693			1999 Chi-Chi (TSU-129)			1995 Kobe (Takatori)		
NS	EW	UD	NS	EW	UD	EW	NS	UD
x	y	z	x	y	z	x	Y	z
0.250			0.250			0.250		
0.375			0.375			0.375		
			0.500					
0.250	0.125		0.250	0.125		0.250	0.250	
0.375	0.250		0.375	0.250		0.375	0.250	
0.25		0.125				0.25		0.125
0.375		0.25						
0.250	0.125	0.125	0.250	0.125	0.125	0.250	0.250	0.125
0.375	0.250	0.250	0.375	0.250	0.250	0.375	0.250	0.250
			0.500	0.250	0.250			

(2) *Fixed-base Case:*

Art-693			1999 Chi-Chi (TSU-129)			1995 Kobe (Takatori)		
NS	EW	UD	NS	EW	UD	EW	NS	UD
x	y	z	x	y	z	x	y	z
0.250			0.250			0.250		
0.375			0.375			0.375		
0.250	0.125		0.250	0.125		0.250	0.250	
0.375	0.250		0.375	0.250		0.375	0.250	
0.250	0.125	0.125	0.250	0.125	0.125	0.250	0.250	0.125
0.375	0.250	0.250	0.375	0.250	0.250	0.375	0.250	0.250

Each test case is identified by following parameters:

- *Earthquake record*: Art-693, Chi-Chi, Kobe
- *Shaking direction and target-PGA in x-direction*:

  x375 = uni-axial shaking in x-direction, target PGA =0.375g, xyz250=tri-axial shaking in x-,y-, and z-direction, target PGA in x-direction is 0.250g
- *System*: with (R) or without (F) rubber ring + base-isolated(B) or Fixed-base(F)

  RB = with rubber ring in base-isolated system, FR=without rubber ring in base-isolated system

An example of the notification of a test case is as follows.

RF/Art/xz375: EQ record is Art-693, bi-axial shaking in x- and z-directions, target PGA of platform in x-direction is 0.375g, with rubber ring in fixed-base system

4.6 Dynamic Characterization of Transformer Model and Bushing

The dynamic identification of the transformer model and bushing was performed by a random vibration test using the same procedure as in Phase-1. As predicted, the results were almost the same as Phase-1. The 1st and 2nd mode of the transformer model without the bushing was around 16.4 Hz, and 29.6 Hz in x, y, and yaw direction. The 1st and 2nd mode of the 161-kV bushing without the rubber ring was 12.7 Hz and 16.3 Hz, whereas with rubber ring it was as follows: 1st mode - 3.9 Hz; 2nd mode - 12.6 Hz; and 3rd mode - 26.1 Hz. The results are summarized in Table 4-5.

The most interesting point is that the fundamental frequency of the bushing was shifted to 3.9 Hz by the rubber ring, as expected. Considering the scale factor, the equivalent frequency of the bushing in the real scale is 3.9 x 0.775 = 3.02 Hz. According to a field investigation, the largest size bushing in the field (500-kV) sometimes had around 3.0 Hz of dominant frequency (Villaverde, 1999). The transfer function of the bushing with and without the rubber ring is shown in Figure 4-5.

Table 4-5 Dynamic Identification Test Results

	x	y	yaw-x	yaw-y
Bushing without RR	12.7	12.7	12.7	12.7
Bushing with RR	3.9	3.9	3.9	3.9
Transformer only	16.4	16.4	26.5	26.0
Rigit Frame only	23.1	26.3	23.4	29.4

4.7 Test Results

4.7.1 Uni-Axial Shaking

4.7.1.1 Response of Transformer/Bushing Systems

Figures 4-6 and 4-7 show the time histories in cases of RB/Art693/x375 and RF/Art-693/x375. The effect of base isolation was observed comparing both records. The FFT analysis of the data at the bottom of the transformer and the top of the bushing, in RB, RF, FB, and FF/Art-693/x375 are shown in Figures 4-8, 4-9, 4-10, and 4-11. The isolation-period of the RB and FB systems estimated by FFT analysis varied from 0.69 Hz (FB) to 1.20 Hz (RB). Tests were conducted first for RB and then for FB. The stiffness of the isolators in the FB system was lower than in the RB system, caused by the load-history effect of high-damping rubber bearings. In Figure 4-12, the maximum response acceleration at the transformer-bottom, transformer-top, and bushing-top under uni-axial shaking in each system is plotted for the cases of Art-693 and Kobe. The order of response acceleration under all motions was FF > RF >> RB $\approx$ FB. In the FF system, the response acceleration in the bushing top was significantly amplified. The amplification factor of the bushing in the fixed-base system became larger as PGA increased. On the other hand, the amplification factor of the bushing top in the RF system remained small even as PGA increased. Figures 4-13 to 4-15 show the distribution of the response acceleration and response relative displacement along the height of the system under Art-693/x375. The result shows the interaction effect between the bushing and the transformer model. In the FF system, the fundamental frequency in the transformer (16 Hz) was close enough to that of the bushing (12 Hz) to cause amplification, while in the RF system they were almost decoupled since the fundamental frequency of the bushing was reduced to 3.0 Hz by the rubber ring. According to a survey by this author, the fundamental frequency of a transformer body generally varies from 15 Hz to over 30 Hz. The results in this study indicate the relationship of the bushing frequency to the transformer frequency has significant influence in the amplification of the response in the bushing and will be one of the major reasons for severe damage in bushings. The results in the RB and FB systems show good reduction in acceleration. There was no obvious difference in the accelerations between the RB and FB systems, regardless of the difference in the fundamental frequency of the bushing.

The response displacements in four systems under each input motion were compared. The displacement at the bottom of the transformer in the RB and FB systems, which indicate the shear deflection of SHRB, is around 85 mm under Art-693/x375g in a scaled system. In real-scale, this 85 mm is translated to 85/0.6 = 142 mm. Considering the many cable connections in actual transformer systems, this response displacement was controlled in a quite reasonable range. As summarized in Chapter 2, a major difference between base-isolation for transformer systems versus conventional isolation, such as building isolation, is the higher stiffness for limiting the displacement in a transformer. As a result, the isolation period will be less than 1.5 seconds, whereas the period of a conventional system is generally over 2.5 seconds.

Figure 4-16 shows a performance curve of the flexible rubber ring under Kobe (Takatori), uni-axial shaking. The force-displacement curve represents the relationship between the rotation angle and the assumed bending moment computed from the response acceleration at the top of the bushing. The maximum horizontal displacement at the top of the bushing was 20 mm. The damping ratio computed from the force-displacement curve was around 5%. The initial purpose of applying this rubber ring was to reduce the apparent fundamental frequency of the bushing and to evaluate the base-isolation effect in the flexible bushing system. However, the results in the fixed-base system with the rubber ring (RF-system) indicated that this flexible-joint system itself had significant effect in reducing the response of acceleration in the bushing. If there are no other problems in mounting these joints on the turret in an actual transformer, the rubber ring can be one of the effective measures in improving the seismic performance of transformer/bushing systems.

4.7.1.2 Performance of Isolation System

Figures 4-17 and 4-18 show the force-displacement curve of the total SHRB system under uni-axial shaking. The shapes of these plots demonstrate visco-elastic characteristics. These shapes were more rounded and each plot did not trace the same path, whereas the curve in Phase-1 showed a reasonable bi-linear curve. This phenomenon can be explained by the load-history dependency and velocity-dependency in the restoring force of the high-damping rubber compound.

In Figure 4-19, the force-displacement curves of RB/Art-693/x375 (Test-A, hereafter) and FB/Art-693/x375 (Test-B) are plotted and compared. Test-A was performed first and Test-B followed one day later. The curve of Test-A shows higher load than Test-B at the same horizontal displacement. This indicates the stiffness was softened by the load-history effect of the high-damping rubber bearing during Test-A, which is called the "scragging" effect or Mullins's effect (Mullins, 1962). In this test, carbon and resin are physical links between polymers and fillers that are added for damping and reinforcement. When the vulcanized rubber in the virgin state is first subjected to loading, these physical links are destroyed and the stress will be relaxed upon the next loading. After some time interval (10 to 24 hours), a percentage of the destroyed links will re-generate and, as a result, the restoring force characteristics will partially recover, but never to the virgin state. This is called the recovery phenomena. Murota (1994) studied the recovery phenomena of a 450 mm-diameter high-damping rubber bearing for over 100 days. It was concluded that the bearing recovered to almost 90% within seven days, with full recovery in about three months. According to the FFT analysis for Test-A (Figure 4-8) and for Test-B (Figure 4-10), the fundamental frequency was 1.2 Hz in Test-A and 0.69 Hz in Test-B. This difference was obviously caused by the difference in stiffness of the bearing during each test.

The maximum shear-strain experienced during the entire test program was 178% in FB/Kobe/x375, as shown in Figure 4-20. The predicted ultimate shear strain of the SHRB was around 200%, corresponding to a ratio of the diameter to the displacement of 0.8.

The initial sustaining load of each SHRB was 39.5 kN at EN, 37.8 kN at ES, 36.8 kN at WN, and 38.7 kN at WS, for an average of 38.2 kN. The average compressive stress was 2.35 MPa. The change of vertical load on each SHRB in FB/Kobe/x375 is shown in Figure 4-21. The load change due to the overturning moment of the transformer was approximately ±20 kN. Therefore, approximately ±50% of the static vertical load changed during Kobe/x375.

4.7.2 Bi-, and Tri-Axial Shaking

Figure 4-22 shows the comparison of response acceleration in uni-, bi-, and tri-axial shaking of RB/Art-693 and RB/Chi-Chi. There was no significant difference in these responses. In Phase-1, there were obvious differences in the response acceleration between uni-axial shaking and bi-, or tri-axial shaking. A large difference was particularly noted in the bushing response observed during tri-axial shaking in Phase-1. However, in Phase-2 with SHRB, the response in tri-axial shaking did not show any amplification at the bushing top.

Figure 4-23 compares the curves of the total system under FB/Kobe/x250 and FB/Kobe/xz250. There is no significant difference between these curves. This fact indicates the effect of z-motion was negligible in SHRB systems as long as the compressive stress was kept low enough, whereas z-motion significantly affected the characteristics of the slider system in Phase-1. Figure 4-24 compares the force-displacement curves in the Phase-1 and Phase-2 tests. The force and displacement of SHRB in Figure 4-24 was corrected to the same loading conditions.

4.8 Summary

The isolation system consisting of segmented high-damping rubber bearings performed very well during testing, as well as the sliding system in Phase-1. With SHRB, the response acceleration of the bushing was reasonably reduced even in tri-axial shaking. So, the problem observed in the Phase-1 test with the sliding bearing system did not occur. The shear restoring force characteristics of the SHRB was not entirely affected by the ground motion because the design compressive stress was relatively low.

The rubber ring worked well as designed. The initial purpose of applying the ring was to study the difference in the bushing response with a low-frequency type (3 Hz) and a high-frequency type (12 Hz). Before testing, it was predicted that the bushing would show a larger response with the rubber ring. However, the test results showed the rubber ring worked to decouple the frequency of the bushing from the transformer body and the response was dramatically improved. It is deduced from the results that the interaction of the transformer body and the bushing is one of the significant reasons for amplification of the bushing-response, and the flexible joint for the bushing will be an effective countermeasure. A new idea of seismic protection for the bushing will be proposed as a result of these tests. A rubber ring of high-damping material may be more effective than the standard material used in these tests.

Load-history dependence of high-damping rubber bearings was seen during the entire test program, which is typical of these compounds. The difference in the stiffness affected the isolation period and the response of the system. The characteristics should be carefully considered at the design stage of the isolation system with high-damping rubber bearings.

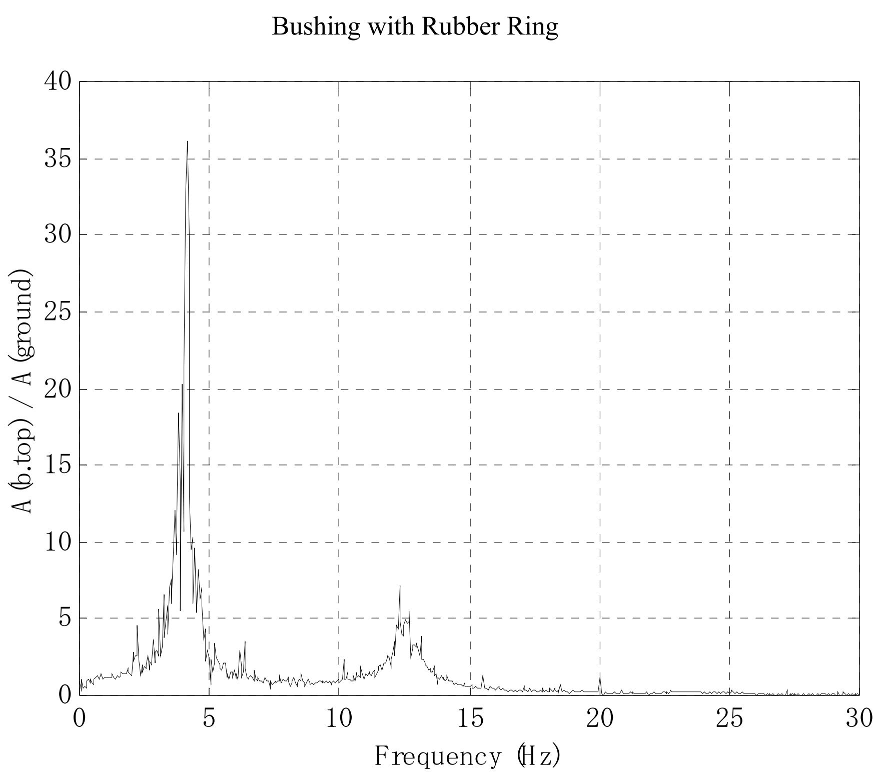

Figure 4-5 Dynamic Identification Test Results of Bushing with/without Flexible Rubber Ring

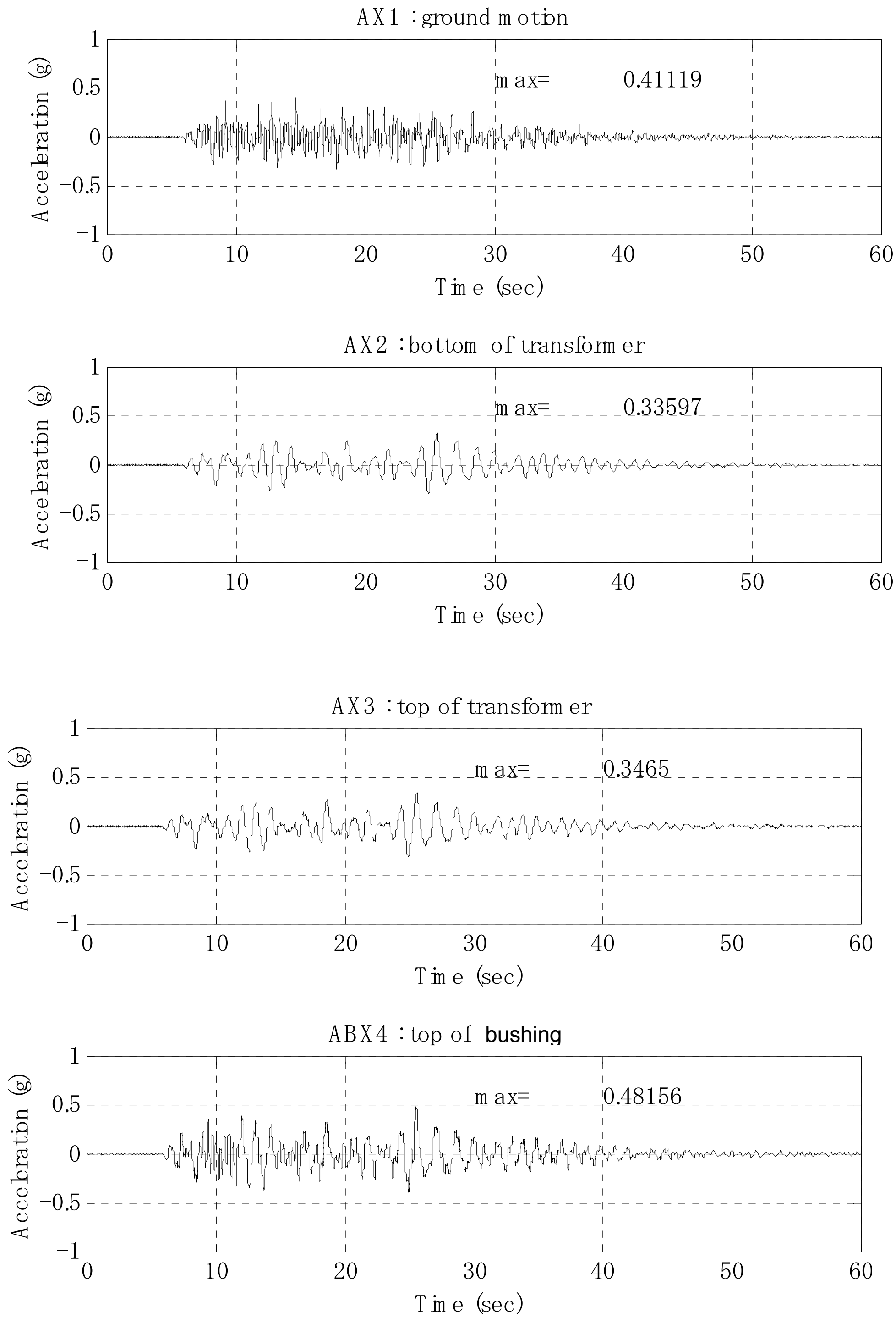

Figure 4-6 Time Histories of Response Acceleration in RB/Art-693/x375

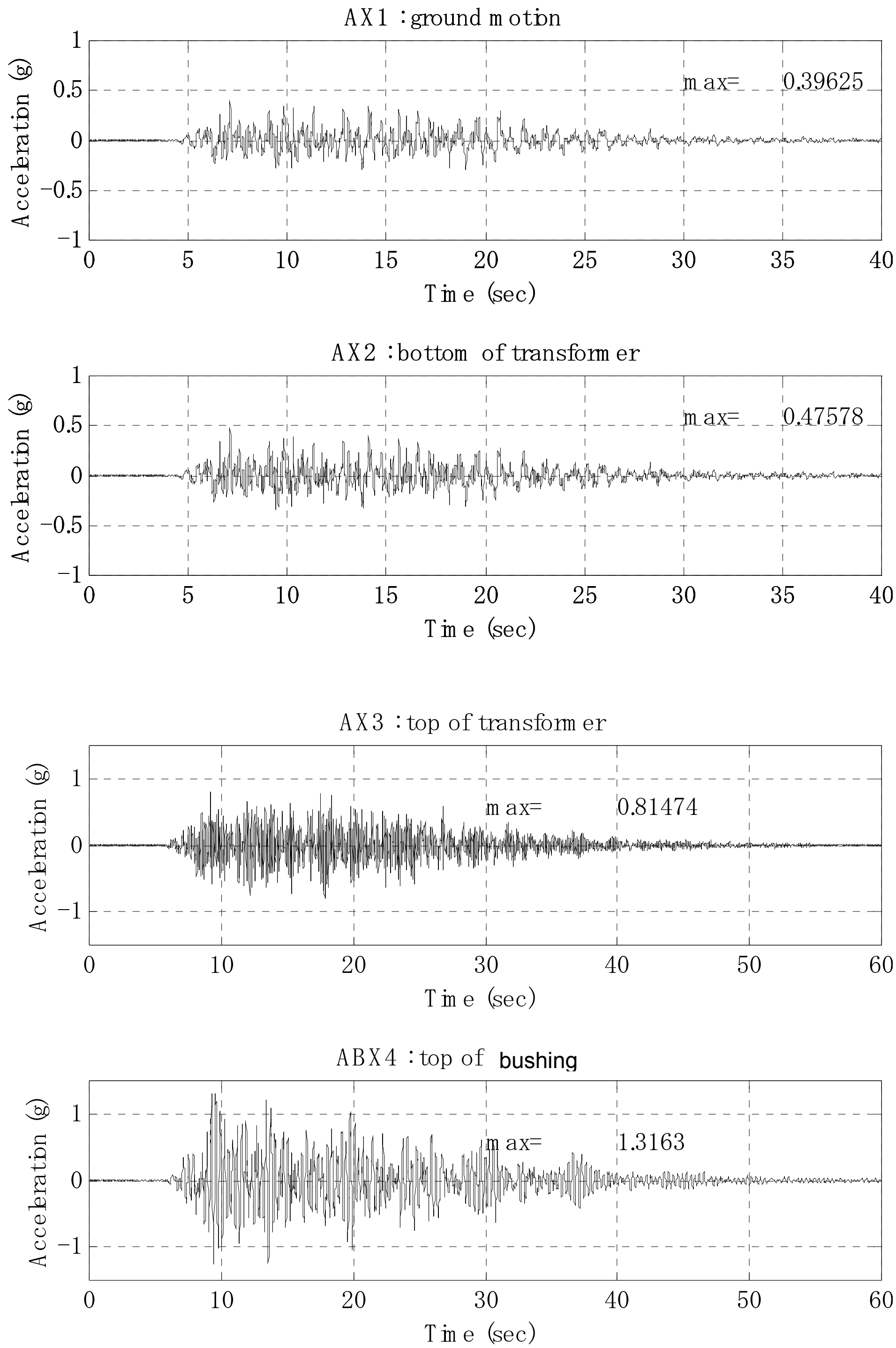

Figure 4-7 Time Histories of Response Acceleration in RF/Art-693/x375

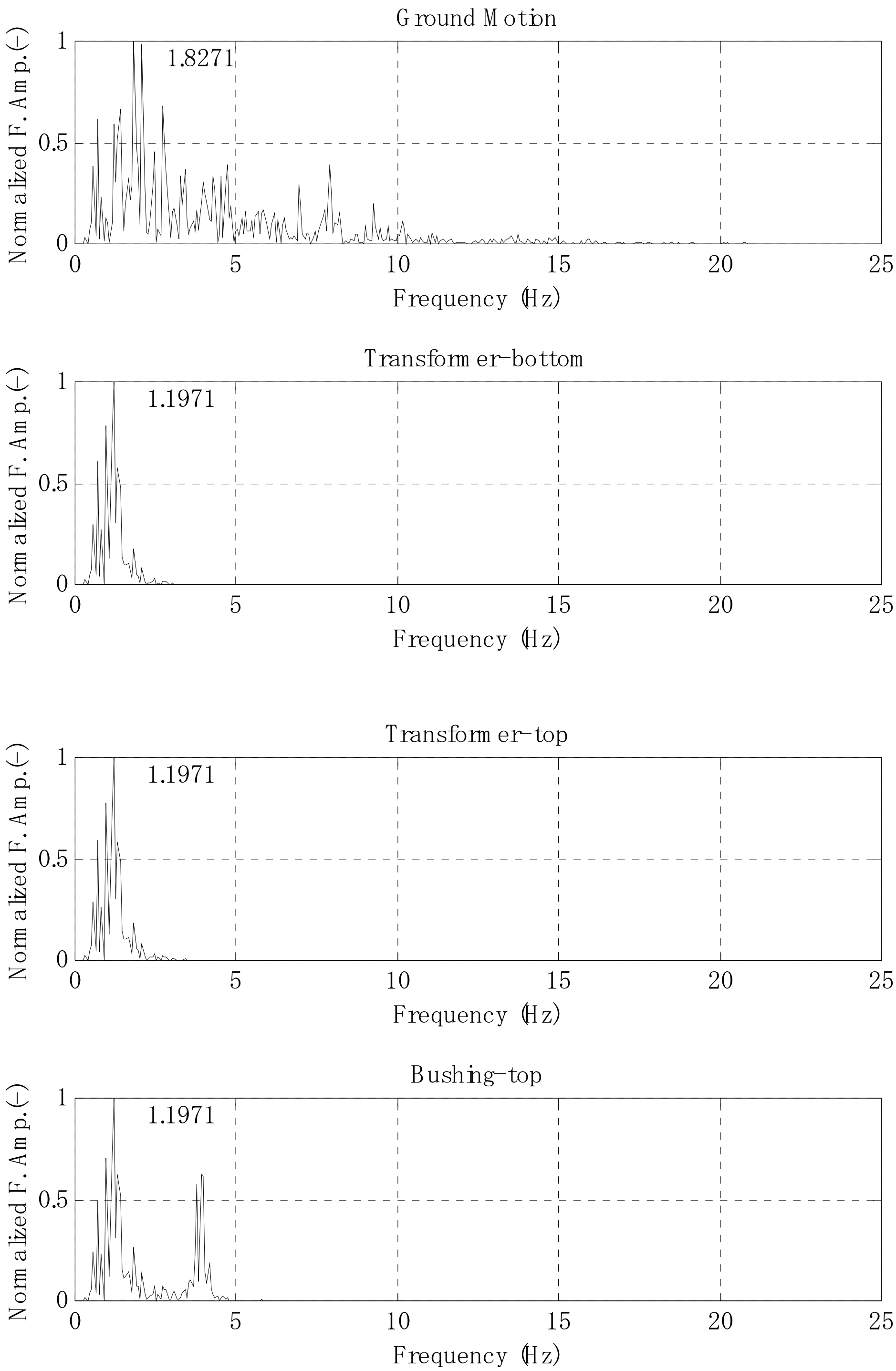

Figure 4-8 Normalized Fourier Amplitude of RB/Art-693 /x375

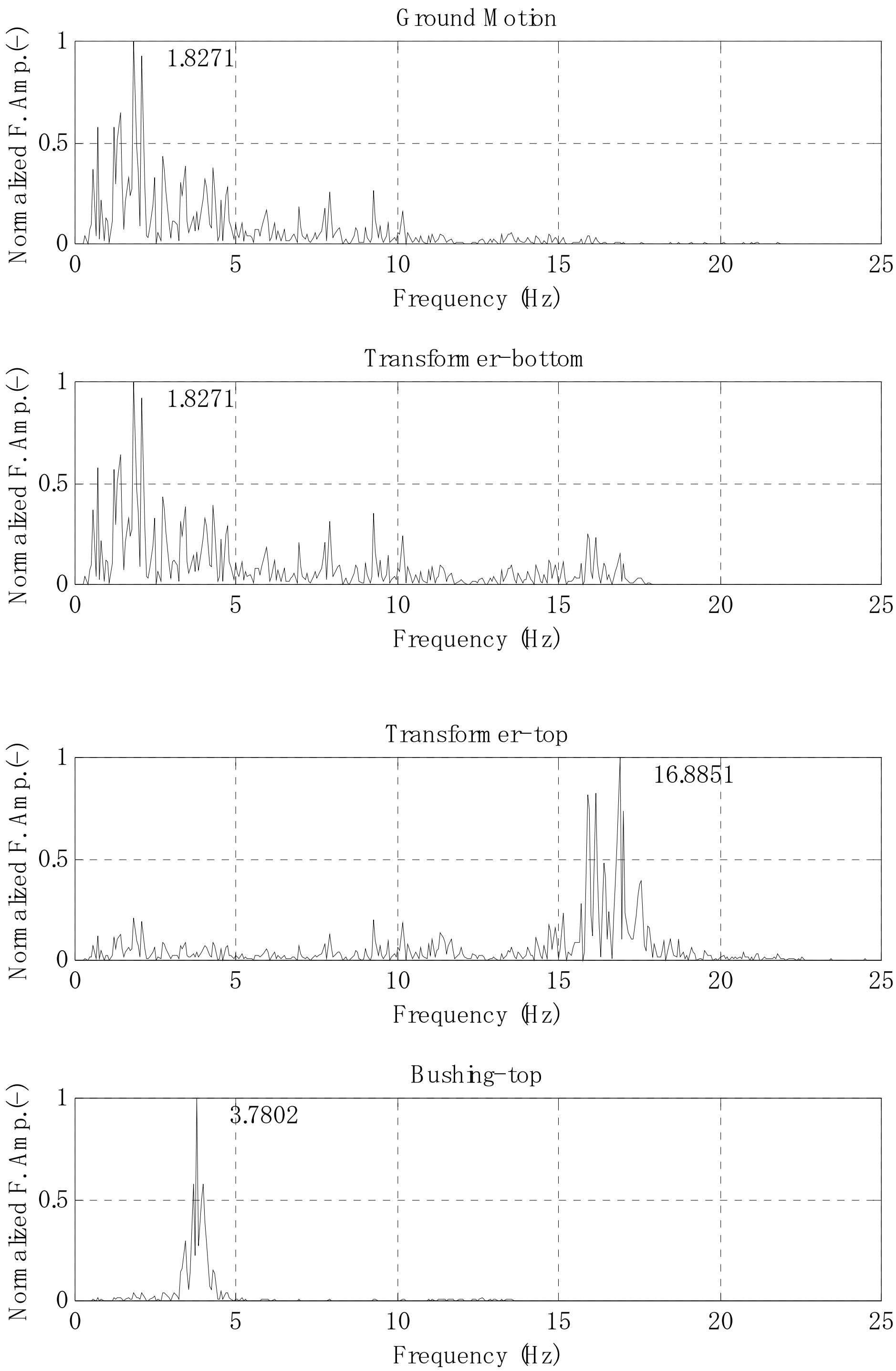

Figure 4-9 Normalized Fourier Amplitude of RF/Art-693 /x375

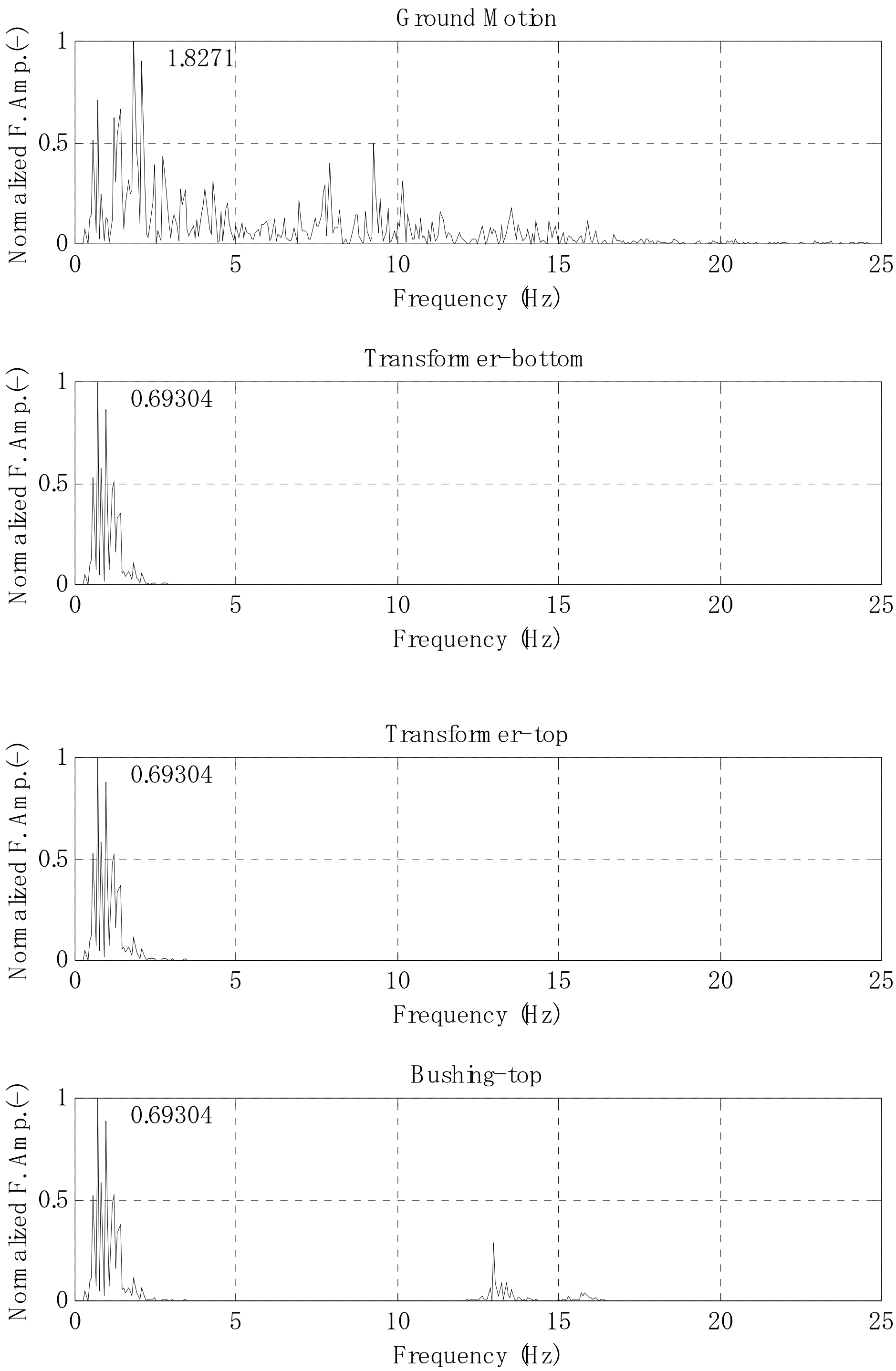

Figure 4-10 Normalized Fourier Amplitude of FB/Art-693 /x375

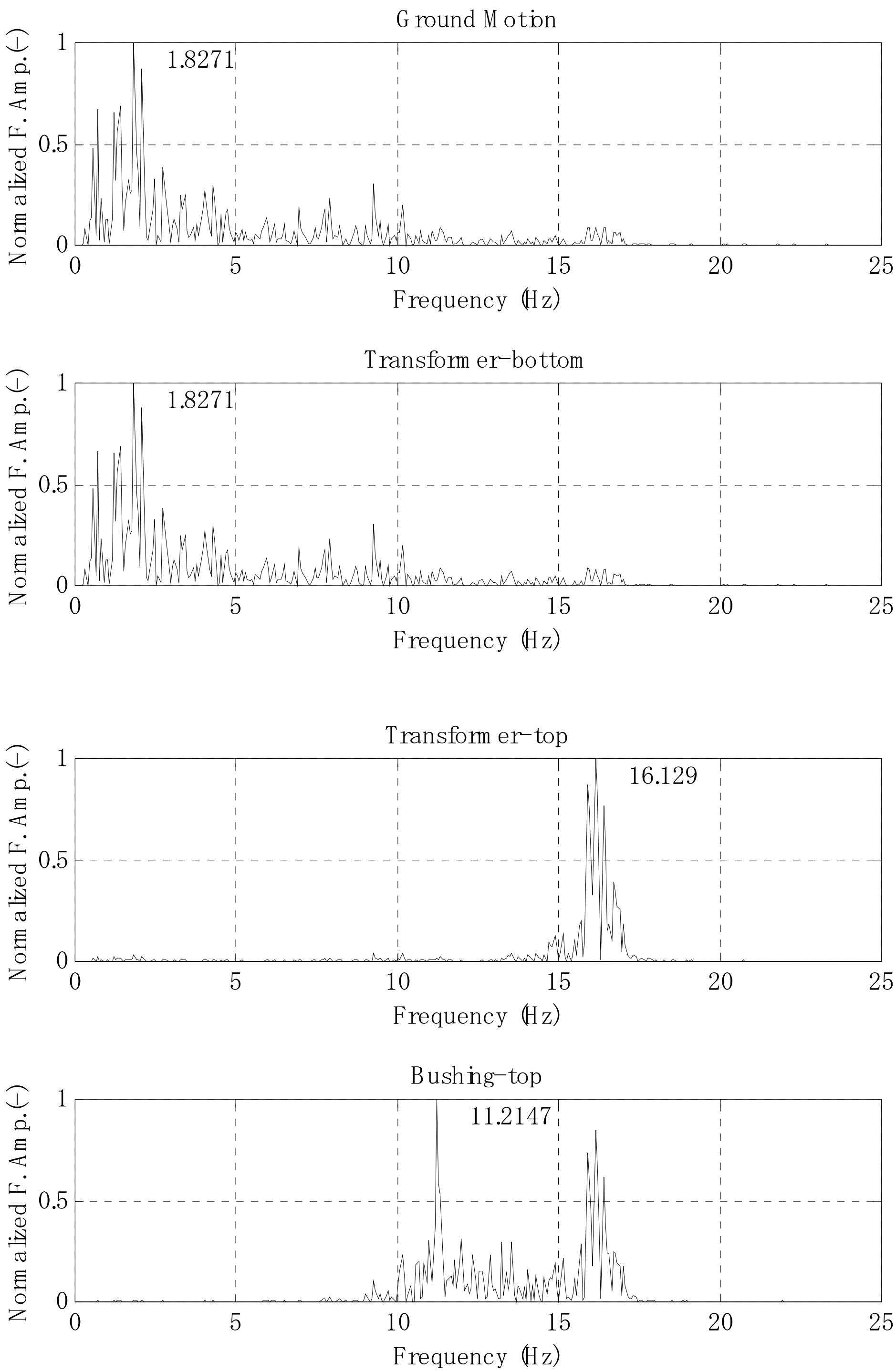

Figure 4-11 Normalized Fourier Amplitude of FF/Art-693 /x375

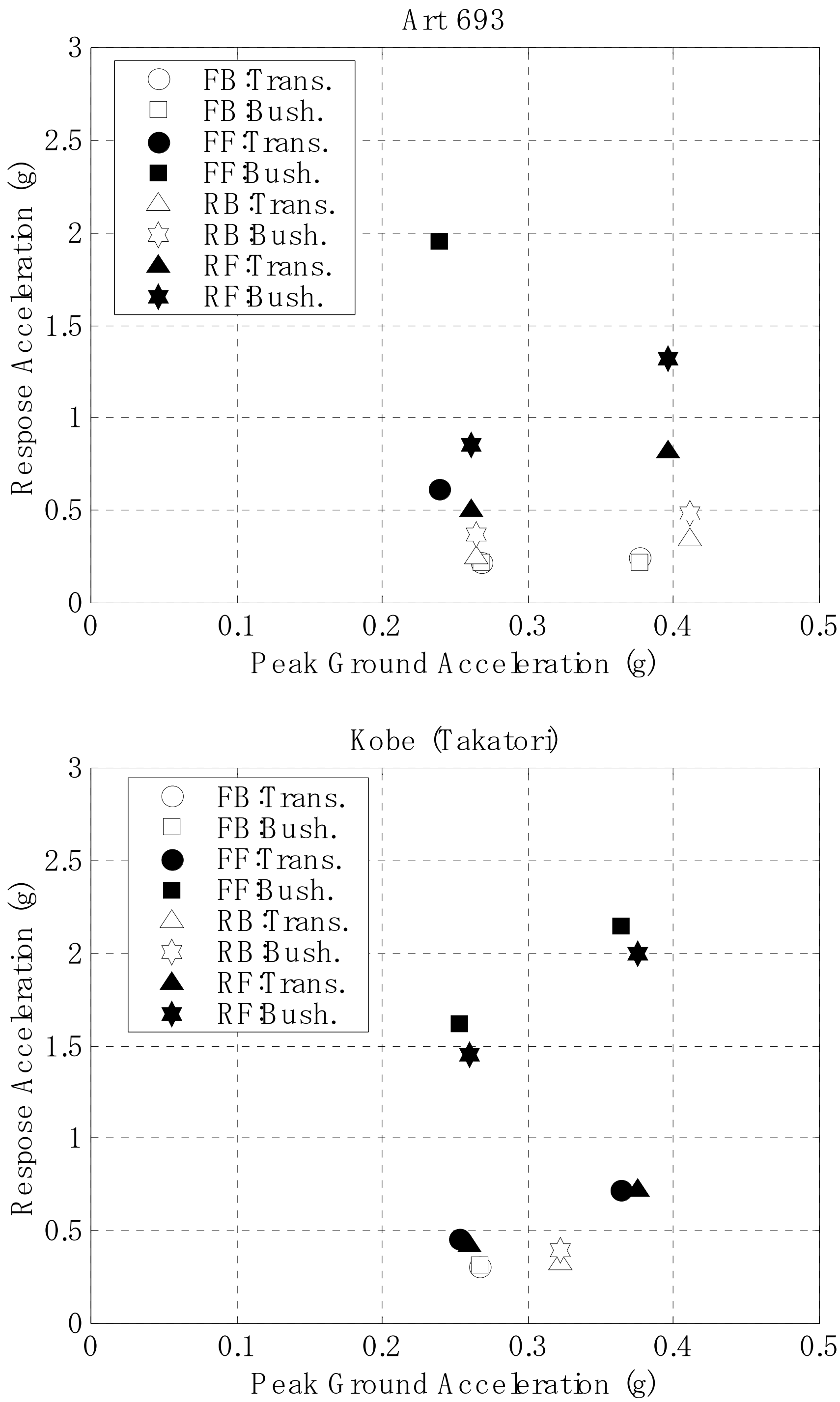

Figure 4-12 Maximum Response Acceleration in Art-693 and Kobe

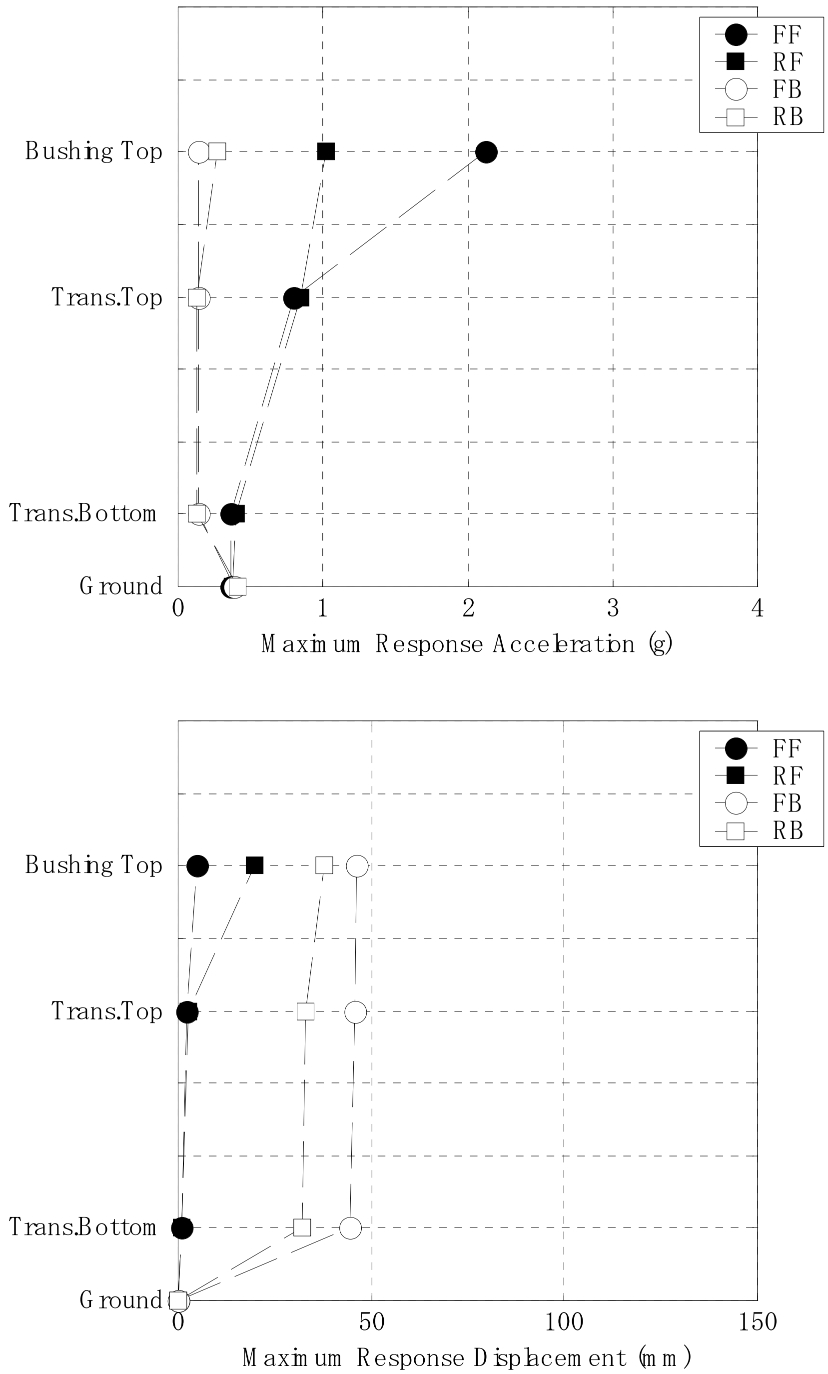

Figure 4-13 Maximum Response Acceleration and Displacement at each Measurement Point:Chi-Chi/x375

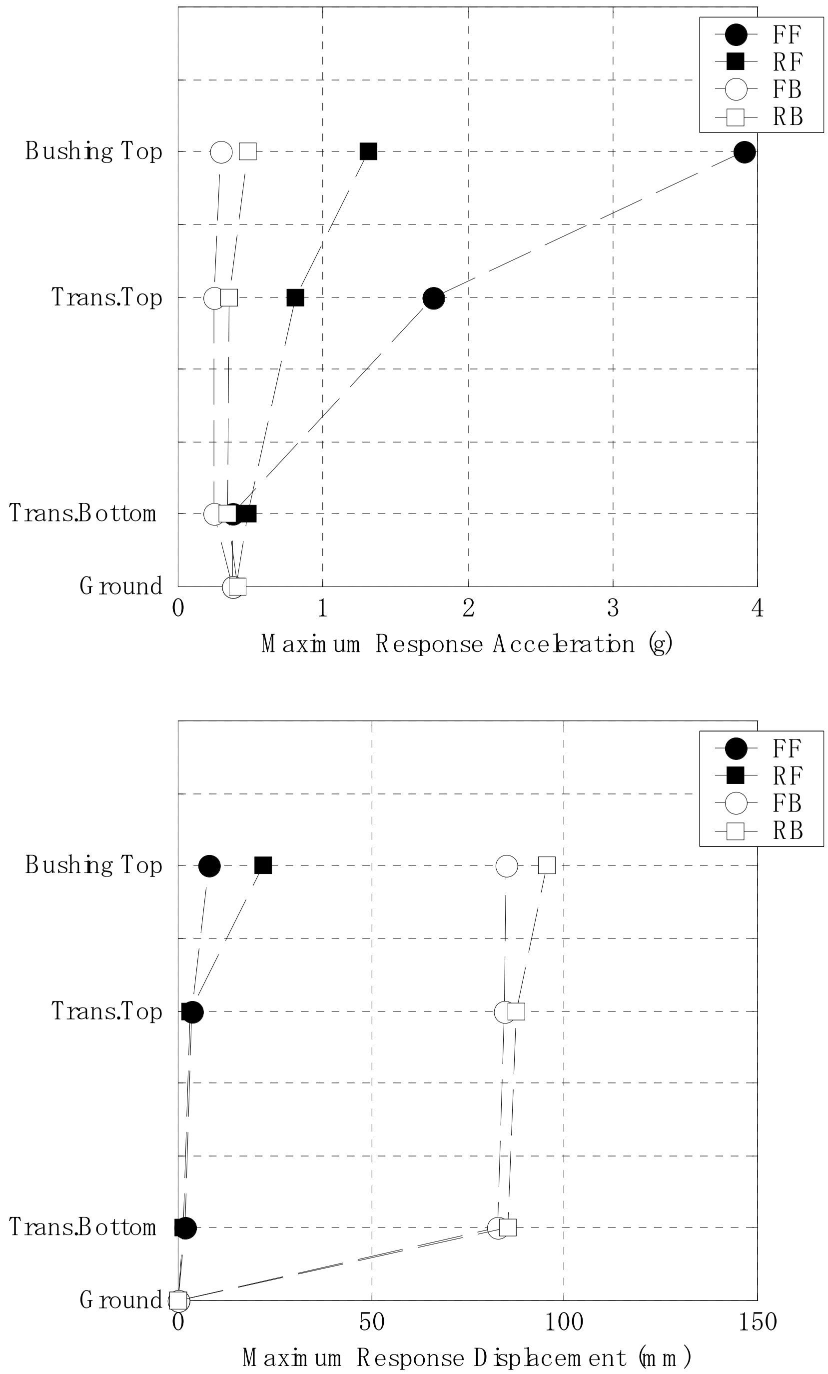

Figure 4-14 Maximum Response Acceleration and Displacement at each Measurement Point: Art-693/x375

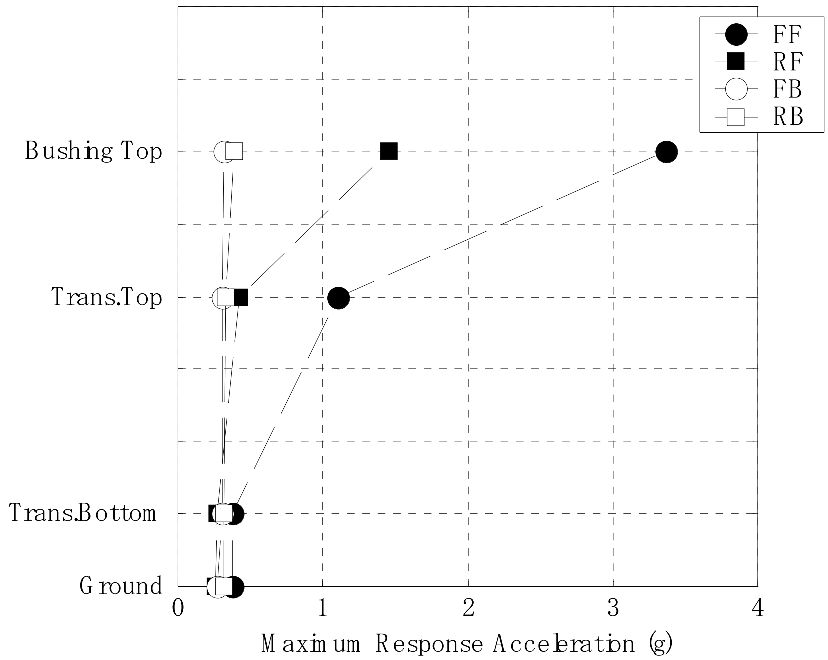

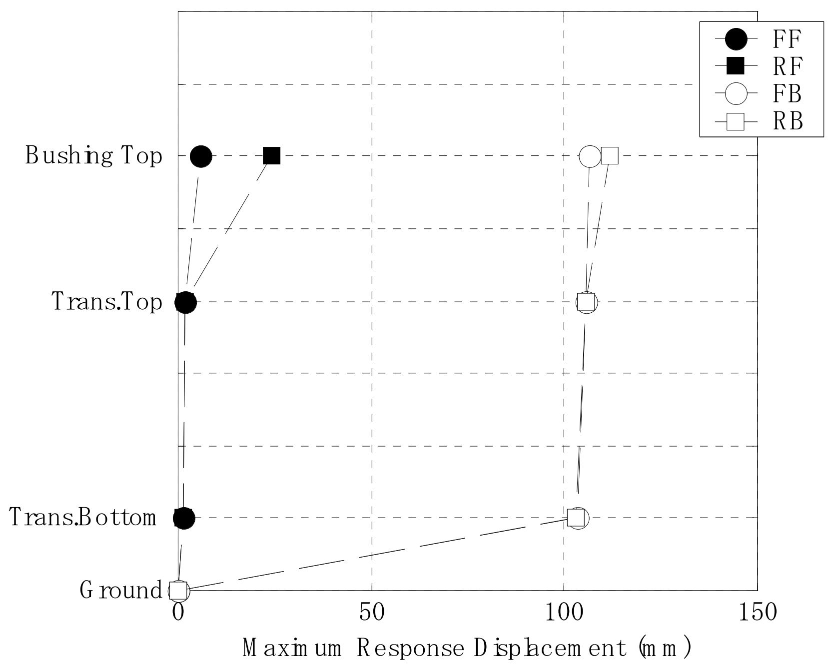

Figure 4-15 Maximum Response Acceleration and Displacement at each Measurement Point: Kobe/x375

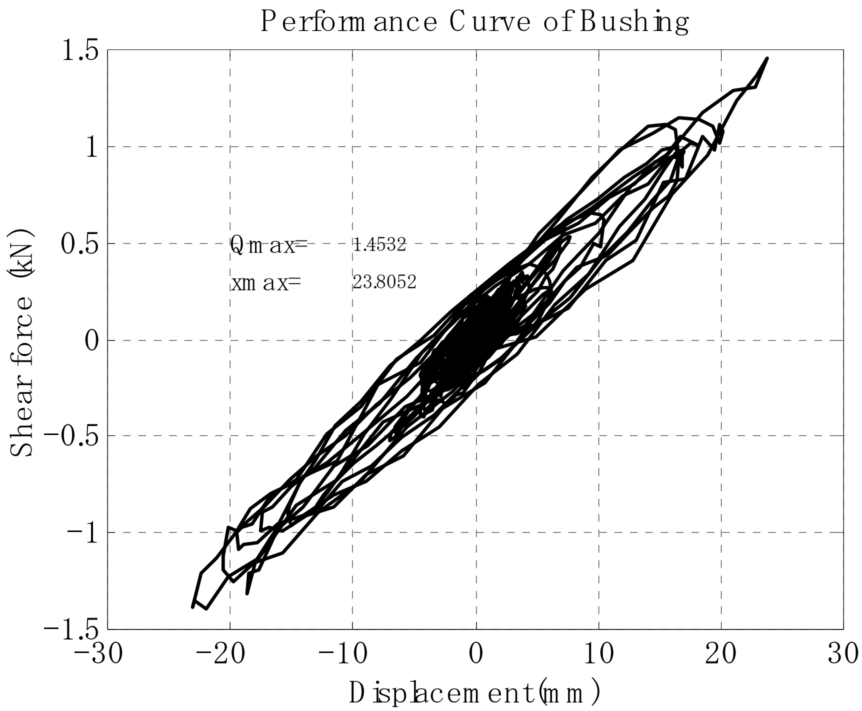

Figure 4-16 Shear Force-Horizontal Displacement Relationship of Bushing with Rubber Ring: RB/Kobe/x375

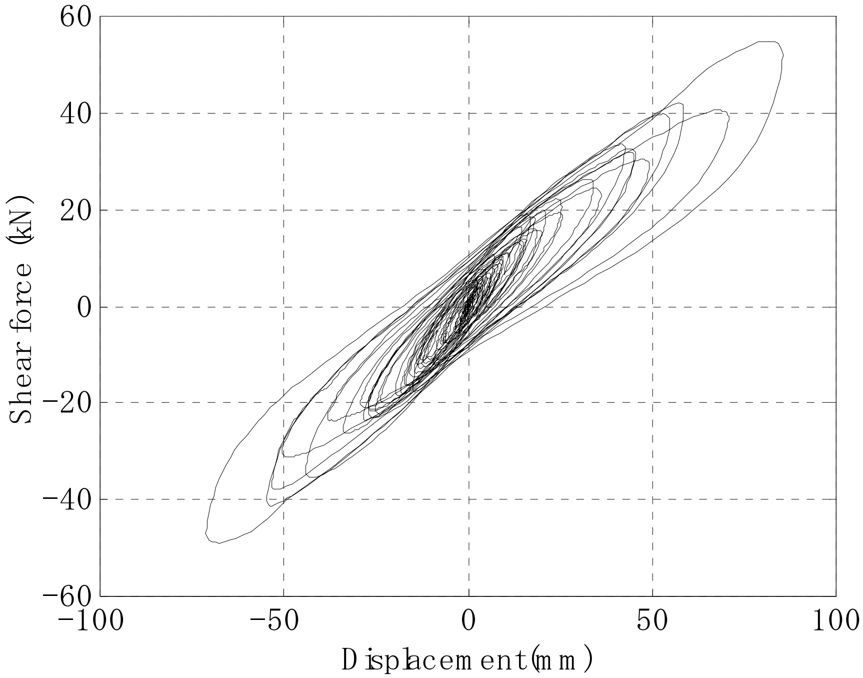

Figure 4-17 Force-Displacement Curve of Isolation System in RB/Art-693/x375

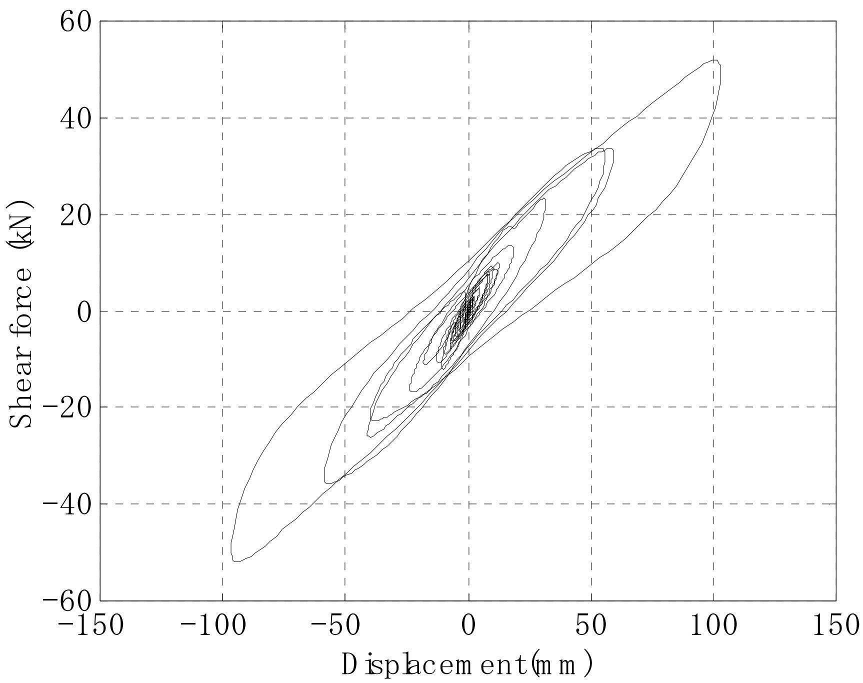

Figure 4-18 Force-Displacement Curve of Isolation System in RB/Kobe/x375

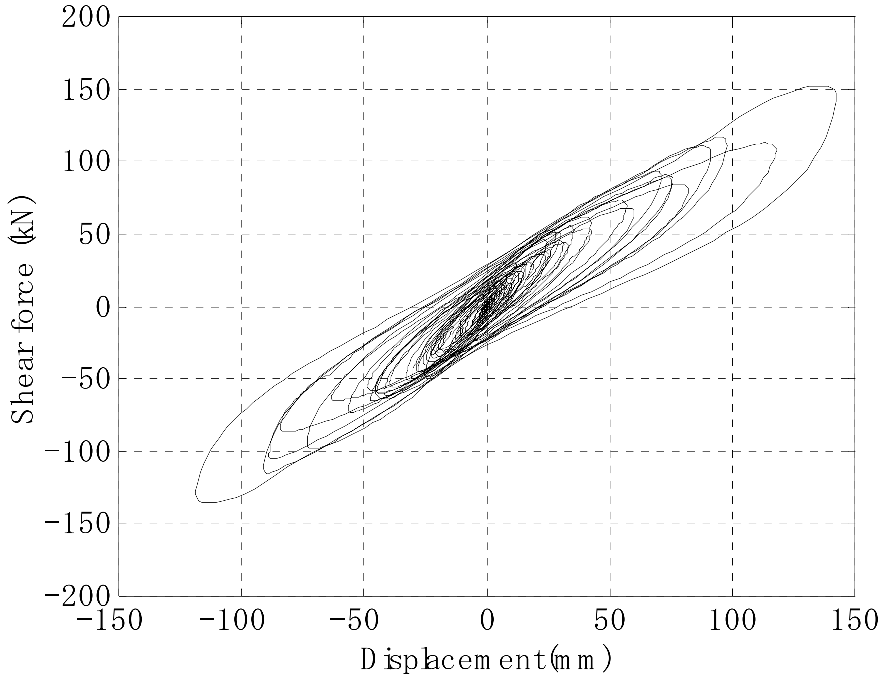

RB/Art-693/x375

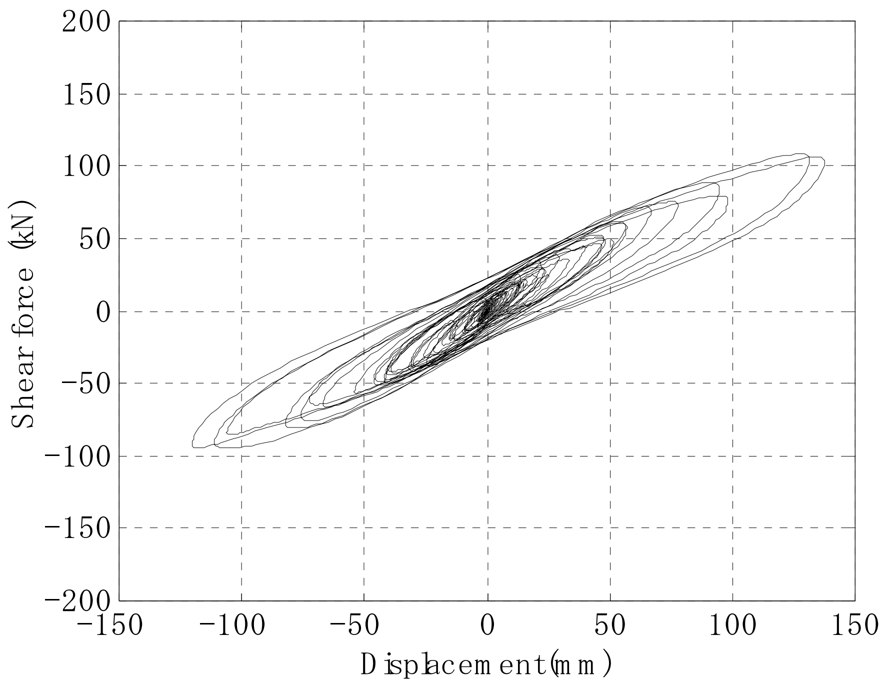

FB/Art-693/x375: (1 day after RB/Art-693/x375)

Figure 4-19 Load History Dependence of High-damping Rubber Bearing

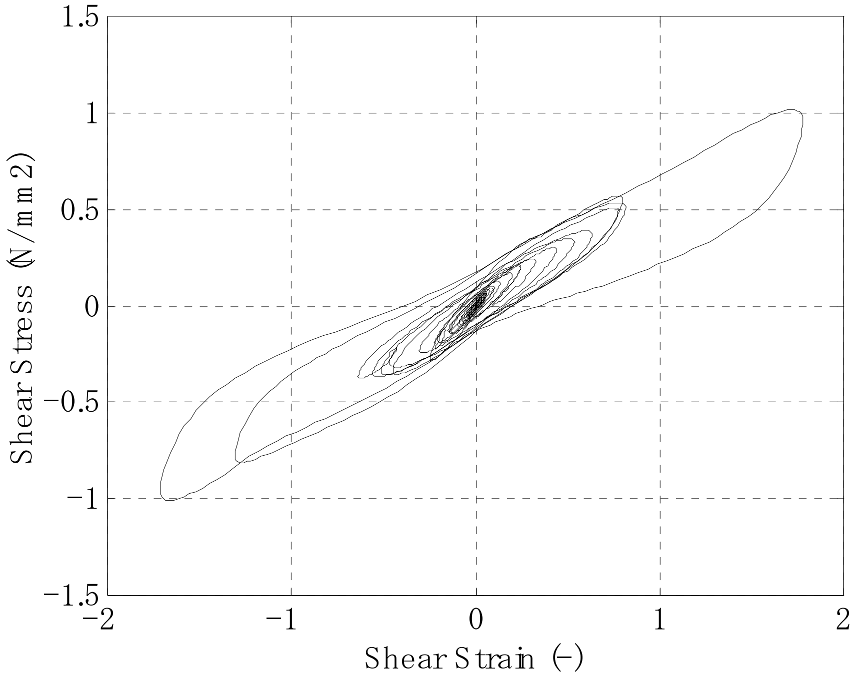

Figure 4-20 Force-Displacement Curve of SHRB in RB/Kobe/x375

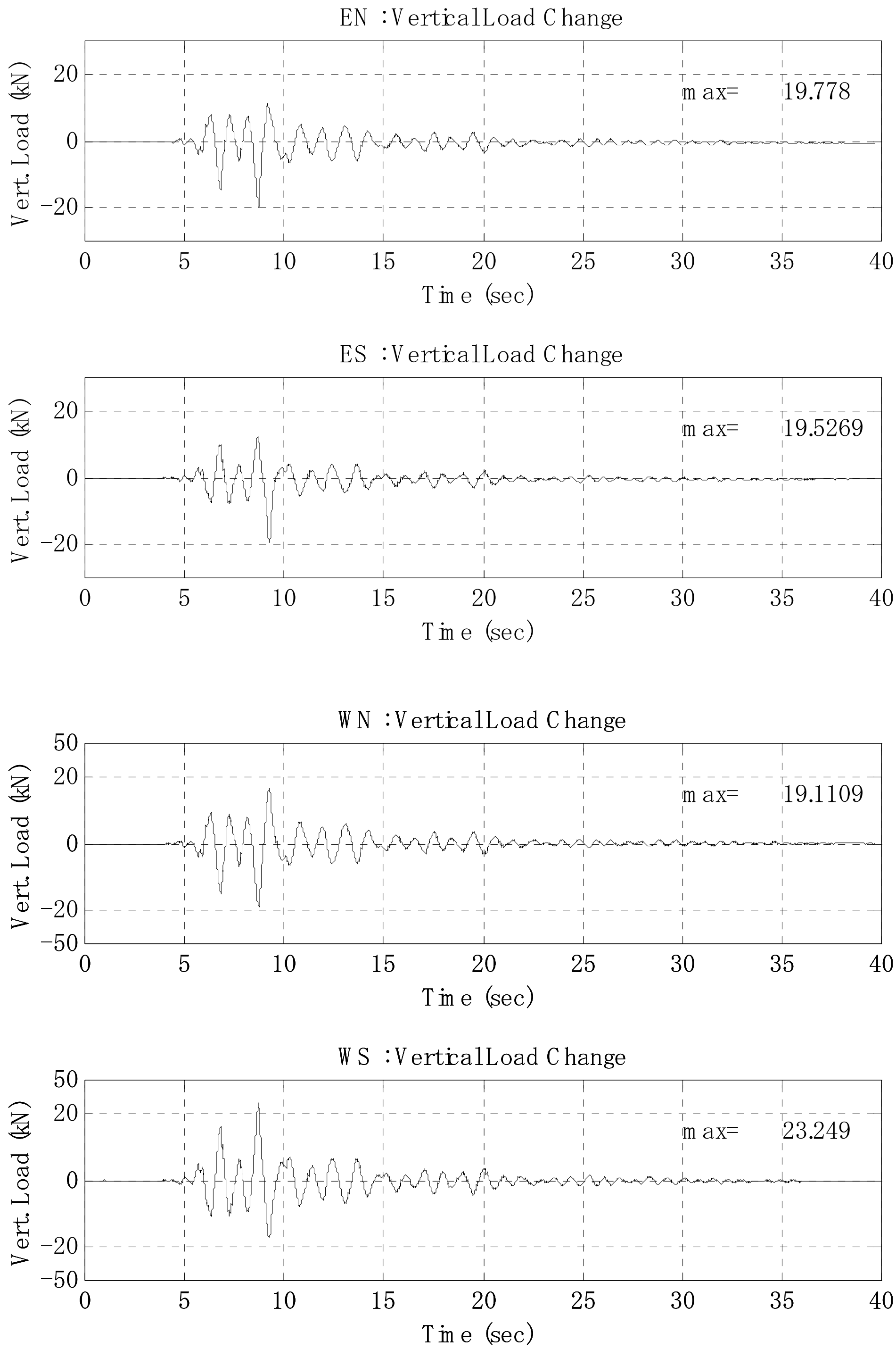

Figure 4-21 Vertical Load Change of each SHRB in FB/Kobe/x375

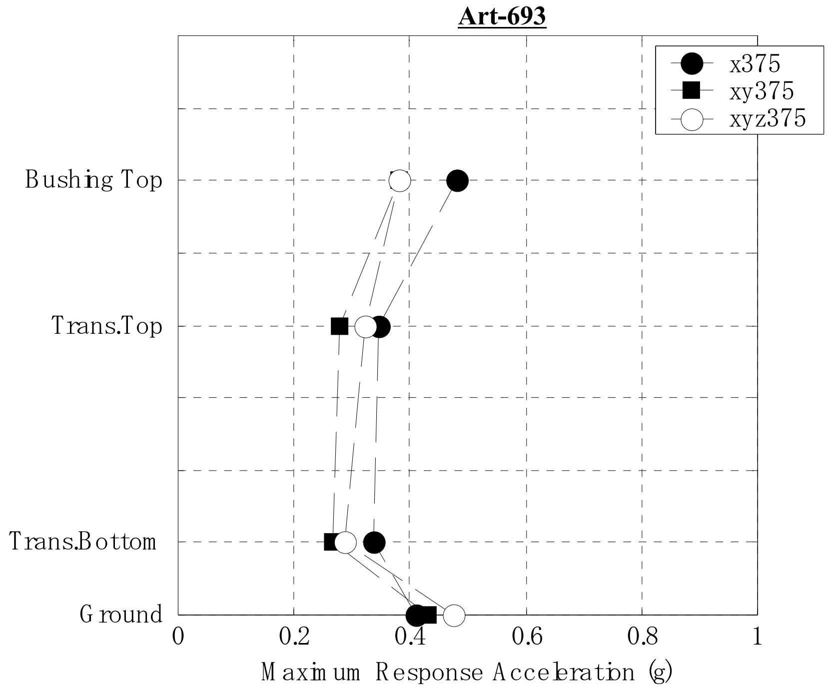

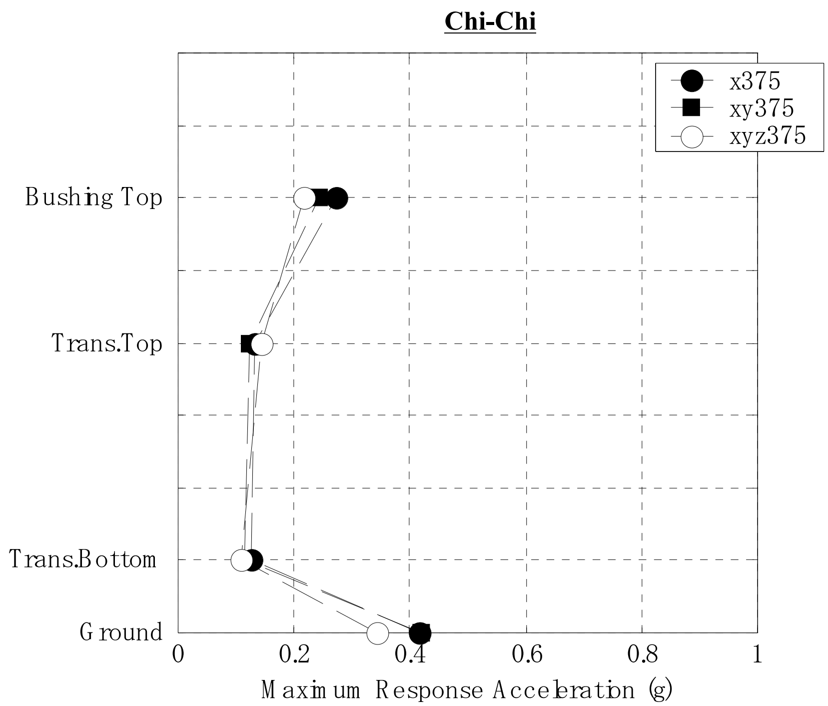

Figure 4-22 Comparison of Maximum Response Acceleration in Uni-, Bi-, and Tri-Axial Shaking : RB/Art-693, and RB/Chi-Chi

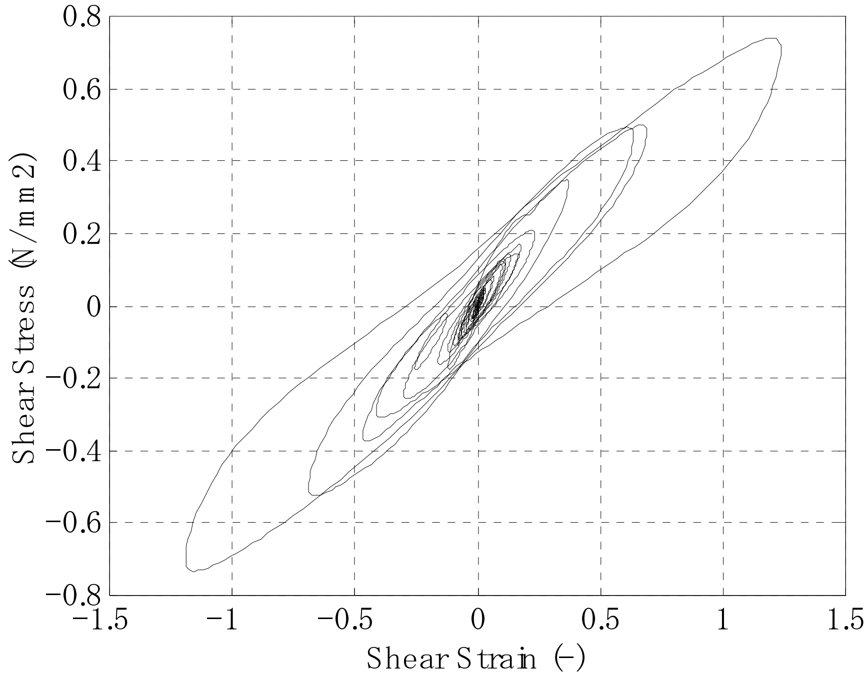

RB/Kobe/x375

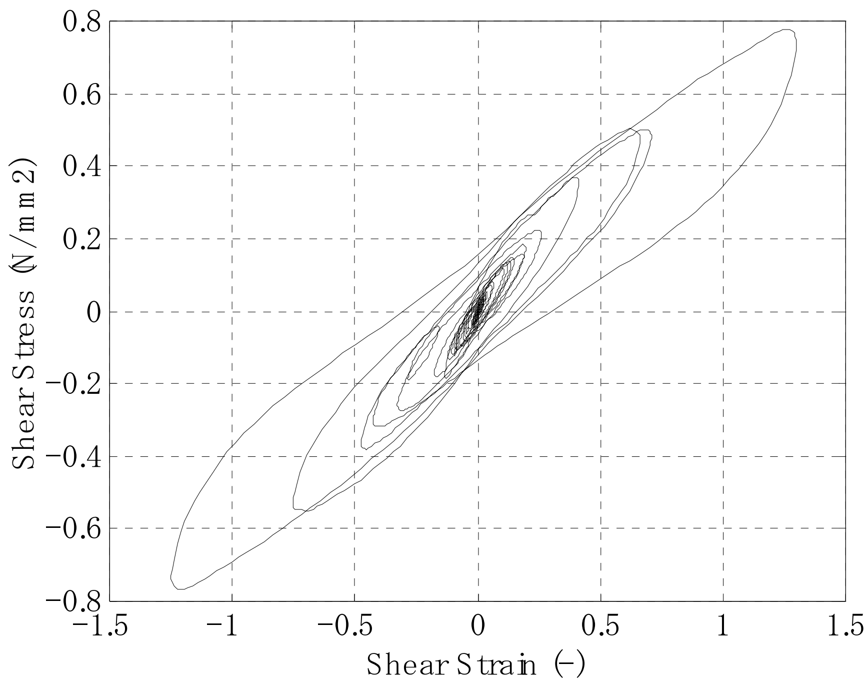

RB/Kobe/xz375

Figure 4-23 Comparison of Force-Displacement Curve under x-, and xz-Shaking

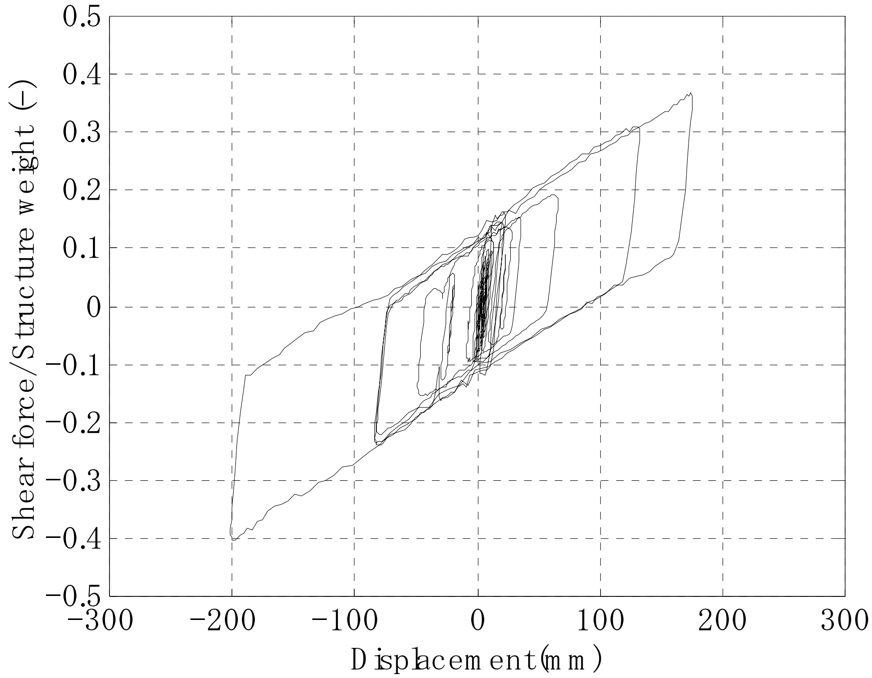

Corrected Force-Displacement Curve at Phase-1: Kobe/FB/x500

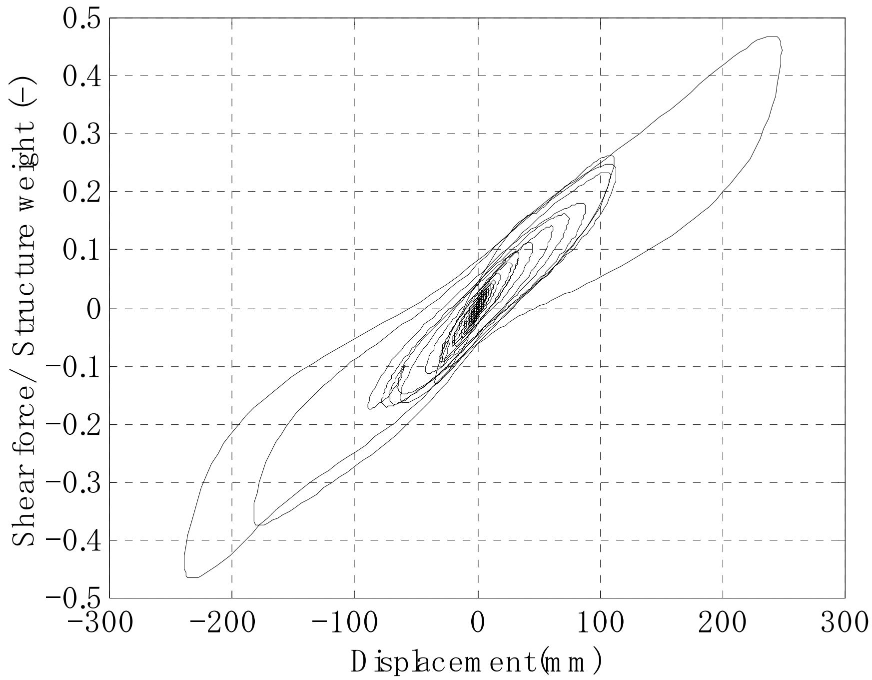

Corrected Force-Displacement Curve at Phase-2: Kobe/FB/x375

Figure 4-24 Comparison of Force-Displacement Curve of Slider System (Phase-1) and SHRB System (Phase-2)

SECTION 5
NUMERICAL ANALYSIS

5.1 Overview

In this chapter, the numerical analysis of the base-isolated transformer/bushing system is studied and discussed. The simulation was carried out with a commercial program called SAP2000 Nonlinear. With this tool we can develop a numerical model of the test set-up in Phase-1 and –2 to verify the test results, especially focusing on the response of the bushing and the performance of the isolator system. The main focus of the analytical study is the problem of interaction with vertical motion and bushing response, which was observed in Phase-1 testing with hybrid isolation system.

5.2 Mathematical Model of the System

The mathematical model of the transformer/bushing systems tested in Phase-1 and Phase-2 was basically defined as shown in Figure 5-1. The transformer was considered as a single mass supported by a linear spring in the shear direction. In other directions, the model was considered rigid. The bottom of the transformer was modeled as a rigid beam/shell, and isolators were installed beneath the corners. The bushing was modeled as a rigid beam with several lumped masses and was supported by a linear-rotation spring attached to the transformer. The stiffness for the other directions was considered rigid.

According to the analysis of the test data, the movement of the porcelain bushing during shaking was dominated by the rotation at the mounting flanges connected to the turret of the transformer. The rotational flexibility of the bushing is determined by the rubber-gasket installed at the interface of mounting face, which is usually installed for the prevention of oil spills. The results of dynamic identification of the bushing revealed that the 2nd mode frequency is over 25 Hz and its contribution to the entire response was considered very low. Therefore, in this simulation, the bushing was simply modeled as a rigid beam supported by rotational spring at the interface of the transformer top and the bushing flange.

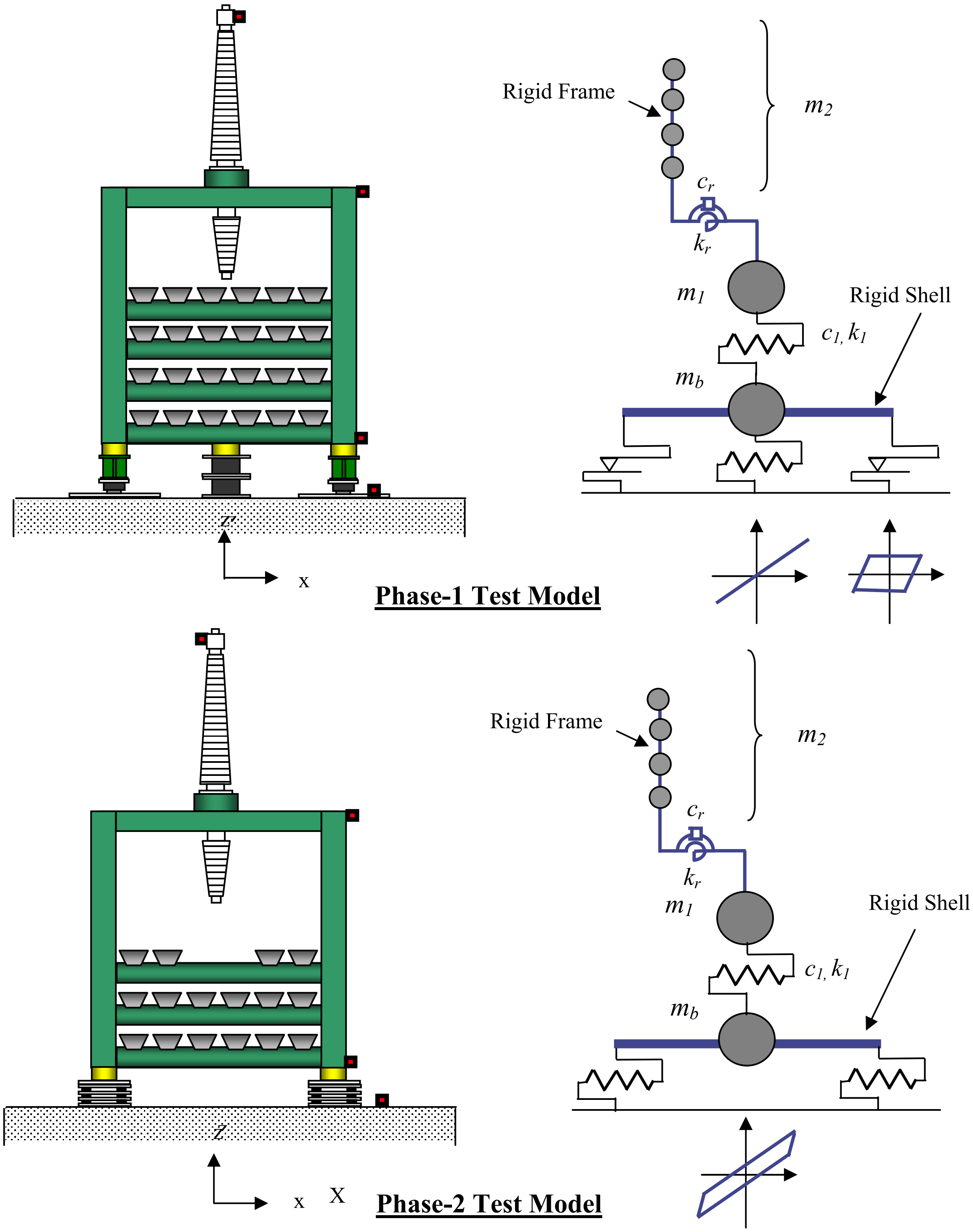

Figure 5-1 Numerical Model of Transformer/Bushing System in Phase-1 and –2

The equations of motion governing the test system in the x-direction are defined below (the rotational motion of the transformer and the shear motion of the bushing are neglected in these equations):

$$\left.\begin{aligned}
&m_b\ddot{x}_b + \Sigma R_i + k_1(x_b - x_1) + c_1(\dot{x}_b - \dot{x}_1) = -m_b\ddot{x}_g \\
&m_1\ddot{x}_1 + c_1(\dot{x}_1 - \dot{x}_b) + k_1(x_1 - x_b) + k_2(x_2 - x_1) = -m_1\ddot{x}_g \\
&m_2\ddot{x}_2 + c_r\frac{(\dot{x}_2 - \dot{x}_1)}{\bar{h}^2} + k_r\frac{(x_2 - x_1)}{\bar{h}^2} = -m_2\ddot{x}_g
\end{aligned}\right\} \qquad (5\text{-}1)$$

The equation of motion in the z-direction was simplified by assuming the stiffness of bushing and transformer in the z-direction is rigid:

$$(m_1 + m_2 + m_b)\ddot{z}_1 + c_v\dot{z}_1 + k_v z_1 = -(m_1 + m_2 + m_b)(\ddot{z}_g + G) \qquad (5\text{-}2)$$

where,

m_b, x_b is mass and absolute displacement of basement, expressed as a rigid beam/shell

m_1, x_1 is mass and relative displacement of upper part of transformer

m_2, x_2 is representative mass and relative displacement of bushing

R_i is the horizontal reaction force of i^{th} isolator, which is expressed as a function of the deflection δ_i and the deflection rate $\dot{\delta}_i$ as $R_i = f(\delta_i, \dot{\delta}_i)$

k_1, c_1 is the shear stiffness and damping coefficient of the transformer,

k_r, c_r is the rotation stiffness and damping coefficient of the bushing,

$\bar{h}$ is the representative height of bushing = height from end to gravity center of the bushing

G is gravity

Furthermore, the rotation angle of the bushing is assumed small enough to have a linear relationship with the displacement in the x-direction as follows:

$$x_2 - x_1 = \bar{h} \cdot \theta_2 \qquad (5\text{-}3)$$

where,

θ_2 is the rotation angle of the bushing from vertical axis.

5.3 Numerical Expression of Isolator Characteristics

The characteristics of isolators are dependent on deflection (or strain rate of deflection) and compressive force. Many analytical models have been developed and proposed by researchers. The nonlinear element for isolators used in this analysis was based on the research of Nagarajaiah for the development of the computer code 3D-BASIS. The isolator devices in that report were classified into elastic element, hysteretic element, frictional element, and viscous element. The elastic element is generally called the bi-linear model, and is determined with the parameters of initial stiffness, ratio of post-yield stiffness to initial stiffness, and yield load. The hysteretic element is the model for high-damping rubber bearings and lead-rubber bearings, while the frictional element is for sliders. A viscous damper is the model for energy dissipation in visco-elastic dampers and hydraulic dampers. In this study, the sliders for Phase-1 were modeled with a frictional element.

5.3.1 Friction Force of Sliding Bearing

The friction force characteristics of sliding bearings are expressed in the following equation:

$$F_s = \mu_d \cdot P_v \qquad (5\text{-}4)$$

where, F_s is the friction force generated along the locus of bearings in x-y plane, μ_d is the dynamic-friction coefficient during sliding motion. Static-friction (μ_s), generally called "break-away" coefficient, is the friction at the start of sliding. P_v is the compressive force on the bearings.

As many experimental data have shown, μ_d is dependent on compressive stress σ and sliding rate v. It is also sometimes defined by the following function:

$$\mu_d = f(v) \cdot g(\sigma) \cdot \mu_0 \tag{5-5}$$

where, functions of $f(v)$ and $g(\sigma)$ are empirically derived from test data which was introduced in Chapter 3, and μ_0 is the base friction coefficient at a very low sliding rate. Among many expressions proposed for $f(v)$ and $g(\sigma)$ in the literature, the author chose the following expression:

$$f(v) = \psi - (\psi - 1) \cdot \exp(-a \cdot v) \tag{5-6}$$

$$\psi = \frac{\mu_{\max}}{\mu_0}$$

where, μ_{max} is the maximum friction at large rate of sliding, a is a constant.

$$g(\sigma) = \left(\frac{\sigma}{\sigma_0} \right)^b \tag{5-7}$$

where, σ_0 is the nominal compressive stress and b is a constant.

In this simulation, to make the model simple, the effect of the change of compressive stress to the friction coefficient, the function of $g(\sigma)$ in (5-7), was neglected.

In bi-lateral shaking, the friction forces in the x- and y-directions, F_x and F_y, are expressed with F_s as follows:

$$\begin{aligned} F_x &= \Gamma_x \cdot F_s \\ F_y &= \Gamma_y \cdot F_s \end{aligned} \tag{5-8}$$

where, Γ_x and Γ_y are the direction factor and are expressed as follows:

$$\left. \begin{aligned} \Gamma_x &= \frac{\dot{u}_x}{\dot{u}_s} = \cos\phi \\ \Gamma_y &= \frac{\dot{u}_y}{\dot{u}_s} = \sin\phi \\ \dot{u}_s &= \sqrt{\dot{u}_x^{\,2} + \dot{u}_y^{\,2}} \end{aligned} \right\} \tag{5-9}$$

5.3.2 Restoring Force Characteristics of High-Damping Rubber Bearings

High-damping rubber bearing was treated as hysteretic model in this analysis. The governing equation for load-deflection is expressed by the following equation developed by Wen 1976:

$$Q = \alpha_c \cdot K_u + (1-\alpha_c) \cdot Q_Y \cdot \Omega \qquad (5\text{-}10)$$

where,

$K_u = \dfrac{Q_Y}{u_Y}$ is the initial stiffness , Q_Y is the yield strength and u_Y is yield displacement.

α_c is the ratio of post-yield stiffness to initial stiffness, and Ω is a hysteretic dimensionless quantity which is governed by the following equation:

$$\dot{\Omega} \cdot u_Y = \left\{ C - |\Omega|^n \left(\tau \cdot Sign(u \cdot \Omega) + \eta_c \right) \right\} \cdot \dot{u} \qquad (5\text{-}11)$$

where, τ , η_c , C , and n are dimensionless quantities that control the shape of the force-displacement curve.

The bi-axial model of the hysteretic element was developed by Park (1986), which was derived from the extension of the uni-axial equation as follows:

$$\begin{Bmatrix} Q_x \\ Q_y \end{Bmatrix} = \begin{pmatrix} \alpha_x \cdot K_{ux} & 0 \\ 0 & \alpha_y \cdot K_{uy} \end{pmatrix} \cdot \begin{Bmatrix} u_x \\ u_y \end{Bmatrix} + \begin{pmatrix} (1-\alpha_x) \cdot Q_{Yx} & 0 \\ 0 & (1-\alpha_y) \cdot Q_{Yy} \end{pmatrix} \cdot \begin{Bmatrix} \Omega_x \\ \Omega_y \end{Bmatrix} \qquad (5\text{-}12)$$

where, α_x and α_y are the ratio of post-yield stiffness to initial stiffness in the x, and y directions, Q_{Yx} and Q_{Yy} are the yield strength, $K_{ux} = \dfrac{Q_{Yx}}{u_{Yx}}, K_{uy} = \dfrac{Q_{Yy}}{u_{Yy}}$ are the initial stiffness for x, and y directions, respectively. Ω_x and Ω_y , the hysteretic dimensionless quantities, are governed by the following coupled differential equations:

$$\begin{Bmatrix} \dot{\Omega}_x \cdot u_{Yx} \\ \dot{\Omega}_y \cdot u_{Yy} \end{Bmatrix} = C \cdot \boldsymbol{I} \cdot \begin{Bmatrix} \dot{u}_x \\ \dot{u}_y \end{Bmatrix} - \begin{pmatrix} \Omega_x^2 \left(\varepsilon \cdot Sign(\dot{u}_x \cdot \Omega_x) + \eta \right) & \Omega_x \cdot \Omega_y \left(\varepsilon \cdot Sign(\dot{u}_y \cdot \Omega_y) + \eta \right) \\ \Omega_x \Omega_y \left(\varepsilon \cdot Sign(\dot{u}_x \cdot \Omega_x) + \eta \right) & \Omega_y^2 \left(\varepsilon \cdot Sign(\dot{u}_y \cdot \Omega_y) + \eta \right) \end{pmatrix} \cdot \begin{Bmatrix} \dot{u}_x \\ \dot{u}_y \end{Bmatrix} \qquad (5\text{-}13)$$

where, $\boldsymbol{I}$ is unit matrix , and C and η is dimensionless quantities that control the shape of the hysteresis loop.

5.4 Comparison with Phase-1 Test Results

Numerical simulation was conducted for several selected cases in Phase-1 and Phase-2 in order to calibrate the numerical model by the test results, especially focusing on the phenomenon in tri-axial shaking observed in Phase-1.

At first, simulation of a fixed-base system under uni-axial shaking was carried out to calibrate the model of the transformer/bushing system. The stiffness' for both the transformer and bushing were chosen according to the results of the dynamic characterization test described in Chapter 4. Each element was modeled to match the fundamental frequency of the 1st mode obtained in the tests. The damping ratio was defined as modal damping of 2% for all modes. The ground motion measured on the shake table, AX1 in Figure 3-3 Chapter 3, was applied as the input data for the simulation.

The selected cases used for the simulations were, Northridge/x375, Kobe/x375, and El Centro/x375. The comparison of test results and numerical simulation in time histories of response acceleration at transformer bottom, transformer top, and bushing top, are shown in Figures 5-2, 5-3, and 5-4.

The maximum values of response acceleration in each case are summarized in Table 5-1. Although the results of the numerical simulation and the test have some degree of difference in maximum response acceleration, the time history data show good agreement in the shape of the envelope.

Table 5-1 Comparison of Test Results and Numerical Simulation of Fixed-Base System in Uni-Axial Shaking

Unit: g	El Centro/x375		Northridge/x375		Kobe/x375	
	Test	Simulation	Test	Simulation	Test	Simulation
Tr. Bottom	0.351	0.347	0.416	0.376	0.361	0.372
Tr. Top	0.747	0.476	0.646	0.431	0.569	0.709
Bush. Top	3.66	3.21	2.75	2.65	2.90	3.74

The simulation results of the base-isolated system under uni-axial shaking are shown in Figures 5-5, 5-6, and 5-7. Basically, the results show good agreement at all measurement points, although there were some differences at the transformer top. The response of the test results includes the high-frequency mode in its wave-configuration, which was not observed in the results of the numerical simulation because the higher mode was neglected in this simplified model. Performance curves of the isolation system in the test results and the numerical simulation are compared in Figures 5-8 and 5-9. The simulation results agree with the test results and prove that the bilinear model was adequate enough to express the properties of sliders. The maximum response acceleration is shown in Table 5-2.

Table 5-2 Maximum Response Acceleration of Test Results and Numerical Simulation of Base-Isolated System in Uni-Axial Shaking : Phase-1

Unit: g	El Centro		Northridge		Kobe	
	Test	Simulation	Test	Simulation	Test	Simulation
Tr. Bottom	0.197	0.187	0.182	0.181	0.270	0.212
Tr. Top	0.217	0.188	0.195	0.184	0.283	0.214
Bush. Top	0.352	0.391	0.326	0.361	0.344	0.337

Next, the response acceleration under bi-axial shaking in the base-isolated system was simulated and compared with the test results. Figures 5-10 and 5-11 show the comparison of the Kobe and Northridge test results and simulation results. The simulation results of acceleration at each measurement point basically show good agreement with the test results. There remained some degree of difference in peak response acceleration at the bushing-top. Figure 5-12 shows the comparison of the performance curves between the test and the simulation. The result shows that the numerical model adequately expresses bilateral performance of sliders. The maximum response acceleration at each component is shown in Table 5-3.

Table 5-3 Maximum Response Acceleration of Test Results and Numerical Simulation of Base-Isolated System in Bi-Axial Shaking : Phase-1

Unit: g	El Centro		Northridge		Kobe	
	Test	Simulation	Test	Simulation	Test	Simulation
Tr. Bottom	0.184	0.184	0.179	0.167	0.227	0.202
Tr. Top	0.197	0.185	0.179	0.170	0.262	0.203
Bush. Top	0.416	0.345	0.279	0.257	0.257	0.307

Figures 5-13 and 5-14 show the comparison of acceleration in tri-axial shaking. The simulation results also show good agreement. The maximum acceleration is shown in Table 5-4. In Figure 5-15, the force-displacement curves of the isolation system in tri-axial shaking, Kobe/xyz375, were compared. Although there are some differences in maximum displacement, overall agreement is seen.

Table 5-4 Maximum Response Acceleration of Test Results and Numerical Simulation of Base-Isolated System in Tri-Axial Shaking : Phase-1

Unit: g	El Centro		Northridge		Kobe	
	Test	Simulation	Test	Simulation	Test	Simulation
Tr. Bottom	0.198	0.181	0.270	0.178	0.241	0.213
Tr. Top	0.319	0.190	0.558	0.186	0.353	0.246
Bush. Top	0.471	0.442	1.012	0.869	1.100	0.898

In summary, the numerical simulation with the proposed model compared well to the test results.

5.5 Study on Amplification in Bushing under Phase-1 Tri-Axial Shaking

In order to study the amplification phenomenon of the bushing response in tri-axial shaking with the hybrid system in Phase-1, a parametric simulation was conducted.

5.5.1 Response under Sinusoidal Wave Input

At first, to simplify the problem, the response to the sinusoidal wave was evaluated. The transformer was considered a rigid body. The natural period of the bushing in rotation was fixed as 15 Hz. Assumptions for the isolation system were as follows:

1) Friction coefficient = 0.12 at maximum velocity
2) Linear restoring element with fundamental period of 2.0 sec. in x-direction
3) Compressive stiffness was assumed rigid

The numerical model of the system is shown in Figure 5-16.

The input motions were applied to the x- and z-directions. These inputs were 0.5g of amplitude with a frequency of 2 Hz in the x-direction, and 0.4g with 15 Hz in the z-direction. They are expressed as follows:

x-direction: $\ddot{x}_g = 0.5g\sin(2\pi f_1 t), \quad f_1 = 2Hz$, z-direction: $\ddot{z}_g = 0.4g\sin(2\pi f_2 t), \quad f_2 = 15Hz$

The simulations were conducted for xz-shaking and x-shaking. The maximum response accelerations are summarized in Table 5-5. In the case of xz-shaking, the maximum acceleration at the bushing was amplified 1.98 times the acceleration at the transformer, whereas it was amplified 1.25 times in the case of x-shaking.

Table 5-5 Maximum Response Acceleration under Sinusoidal Wave Input

Unit: g	x0.5gz0.4g	x0.5g
Transformer	0.198	0.151
Bushing Top	0.392	0.189

Figures 5-17 and 5-18 show the time history of the input and the response for both cases. The response acceleration at the transformer under xz-shaking shows high-mode vibration corresponding to the vertical motion of the ground. This component was transmitted from the vibration of the slider frictional force. The response at the bushing-top shows a complicated form--the motion with its natural period stimulated by inertia force at the change of direction of the sliding force, and the motion influenced by the high-mode vibration transmitted from the transformer. This is considered the mechanism of amplification of the bushing response with the sliding bearing system.

5.5.2 Response under Earthquake Input

Next, the response to earthquake inputs with various combinations of frequency characteristics of the components was investigated. The bushing natural frequency and vertical natural frequency of the isolation system were considered as variable parameters of the system to be investigated. The structure of the numerical model was the same as that used in the former sinusoidal input investigation. The following parameters were fixed:

1) Ground motion:
   a) x-direction=Northridge (Sylmar) N11E 0.5g
   b) z-direction= Northridge (Sylmar) UD 0.4g (or 0 for reference)

2) Mass of bushing: 0.5% of transformer-mass

3) Sliding isolation system properties:
   a) Friction coefficient = 0.12 at maximum velocity
   b) Linear restoring element with fundamental period of 2.0 sec. in x-direction

The variable parameters were as follows:

Natural frequency of bushing, f_b: 5 to 40 Hz.

Natural frequency of isolation system in vertical dir. f_{sv}: 3 to 30 Hz, and rigid.

The simulation cases are summarized in Table 5-6.

Table 5-6 Cases of Parametric Study

f_{sv} (Hz) / f_b (Hz)	10	15	20	25	30	∞
3			○			
5			○			
10			○			
15			○			
20			○			
25	○	○	○	○	○	○
30			○			
40			○			

Note: ○ = to be conducted

The simplified governing equation of motion in the x-z plane is shown below:

$$\left.\begin{aligned}
&m_1\ddot{x}_1 + k_1 x + \mu Sign(\dot{x}_1)\cdot P_v = -m_1\ddot{x}_g \\
&m_2\ddot{x}_2 + \frac{c_{2r}}{L^2}(\dot{x}_2 - \dot{x}_1) + \frac{k_{2r}}{L^2}(x_2 - x_1) = -m_2\ddot{x}_g \\
&(m_1 + m_2)\ddot{z}_1 + c_v\dot{z}_1 + k_v z_1 = -(m_1 + m_2)(\ddot{z}_g + G) \\
&P_v = c_v\dot{z}_1 + k_v z_1
\end{aligned}\right\} \quad (5\text{-}15)$$

where,

The equations indicate that there is a coupling term in the motions of the x- and z-directions through the friction force of the sliders, expressed as:

$$\mu Sign(\dot{x})\cdot P_v = \mu Sign(\dot{x})\cdot(c_v\dot{z}_1 + k_v z_1) \quad (5\text{-}16)$$

Figure 5-19 shows the relationship of the maximum response acceleration at the bushing-top and at the transformer, versus the natural frequency of the bushing in the x- and in the xz-shaking. In the x-shaking, the response acceleration of the bushing shows peak-values at 3 Hz and at 25 Hz. The peak at 3 Hz is considered as the frequency close to the resonance of the dominant frequency of ground motion in the x-direction, and is regardless of the ground motion in the z-direction. On the other hand, the peak at 25 Hz indicates the influence of the vertical motion. The second mode frequency of the system is around 20 Hz with a bushing frequency of 25 Hz, and corresponds to the natural frequency of the system in the z-direction. Figure 5-20 shows the relationship of the maximum response acceleration at the bushing-top and at the transformer, versus the natural frequency of the system in the z-direction. The peak at 20 Hz indicates the resonance to the 2^{nd} mode frequency of the system. These results clearly explain the phenomenon of amplification of the bushing top with the sliding bearing system, observed in Phase-1 testing.

Finally, the effect of the friction coefficient to the response of each component was investigated. The friction coefficient of the sliding bearing varied from 0.04 to 0.16. The bushing natural frequency and the vertical natural frequency of the total system were 25 Hz and 20 Hz, respectively. The simulation results are plotted in Figure 5-21. The maximum response acceleration of the bushing top increases as the friction coefficient increases, whereas the response of the transformer increases slightly. The maximum response displacement increases as the friction coefficient decreases. The results indicate that the friction coefficient has a significant influence on the amplification of the bushing, and reasonable design of the friction coefficient in the balance of the displacement will mitigate this problem by using sliding bearings. Recently, many types of sliding bearings with different friction coefficients have been developed. The low-friction type bearings are also available.

This problem of amplification of the response acceleration in the superstructure component is not only present in the transformer/bushing system, but also in other similar equipment in substations on which relatively small mass components are mounted. According to the results of the parametric study, the following conclusions are made:

1) When the natural frequency of the bushing is close to the natural frequency of the system in the vertical direction, amplification occurs.
2) Designing sliding bearings with lower frictions coefficients may control the amplification.

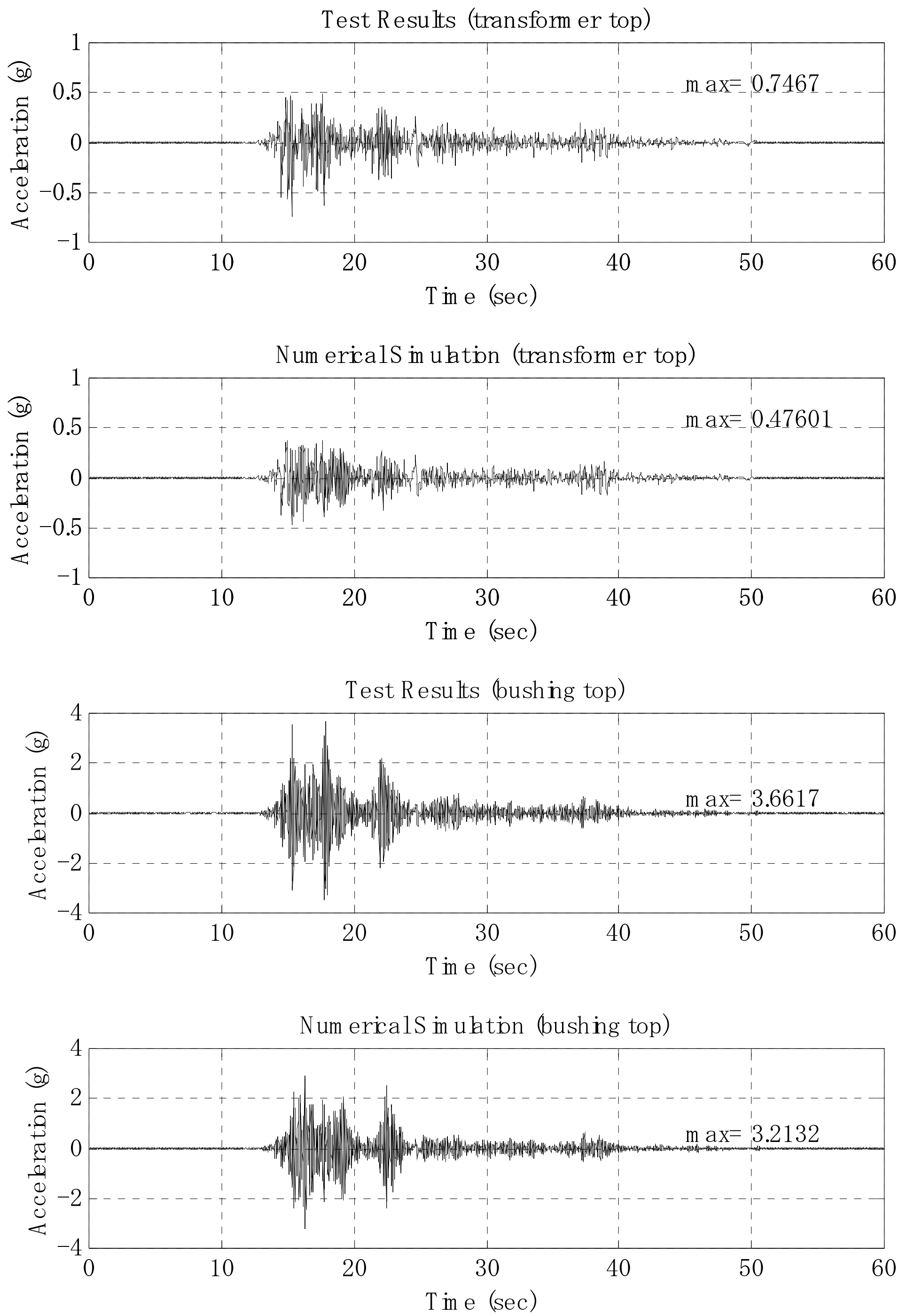

Figure 5-2 Comparison of Test Results and Numerical Simulation: 161kV/F/El Centro/x375, Fixed-Base System

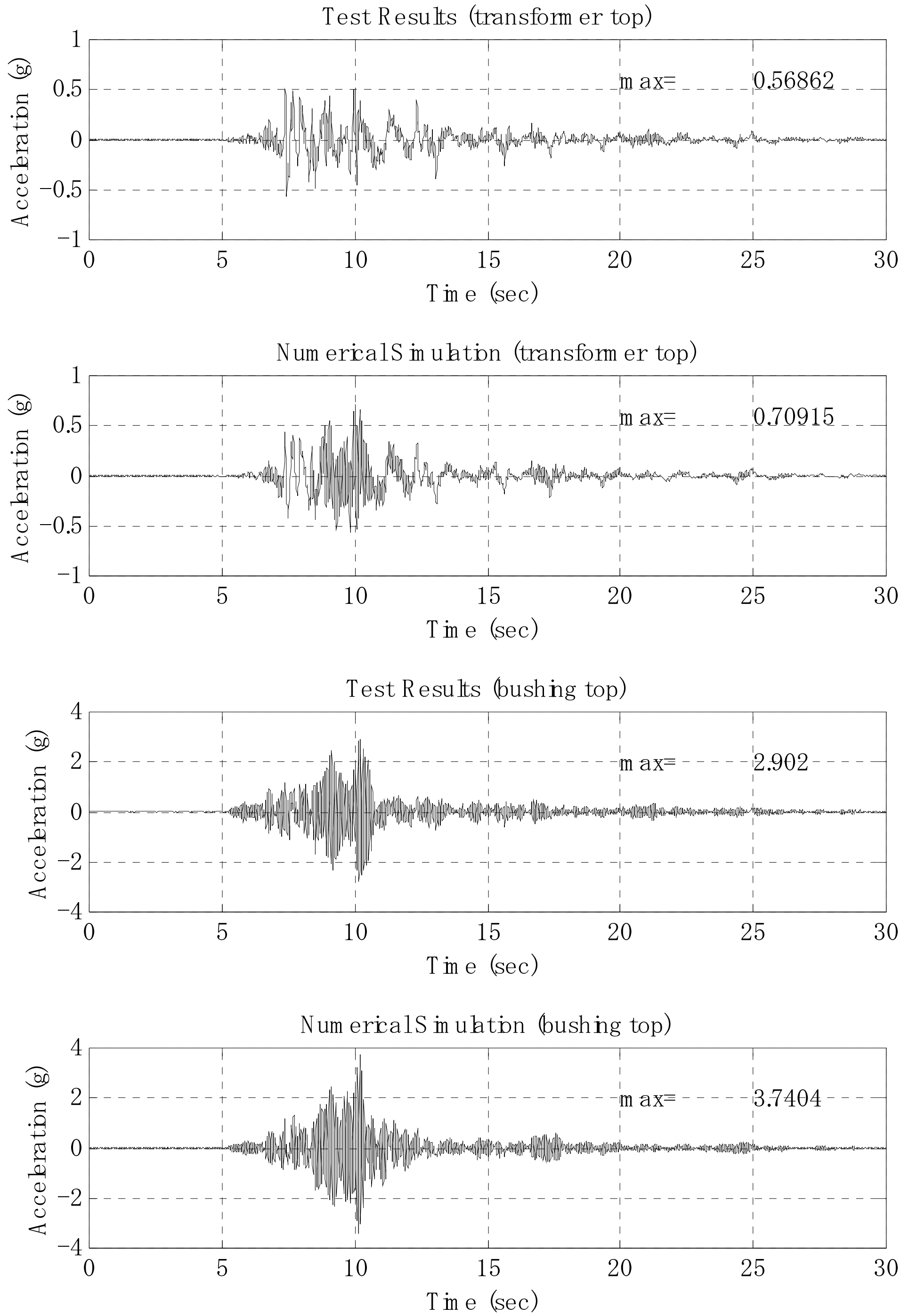

Figure 5-3 Comparison of Test Results and Numerical Simulation: 161kV/F/Kobe/x375, Fixed-Base System

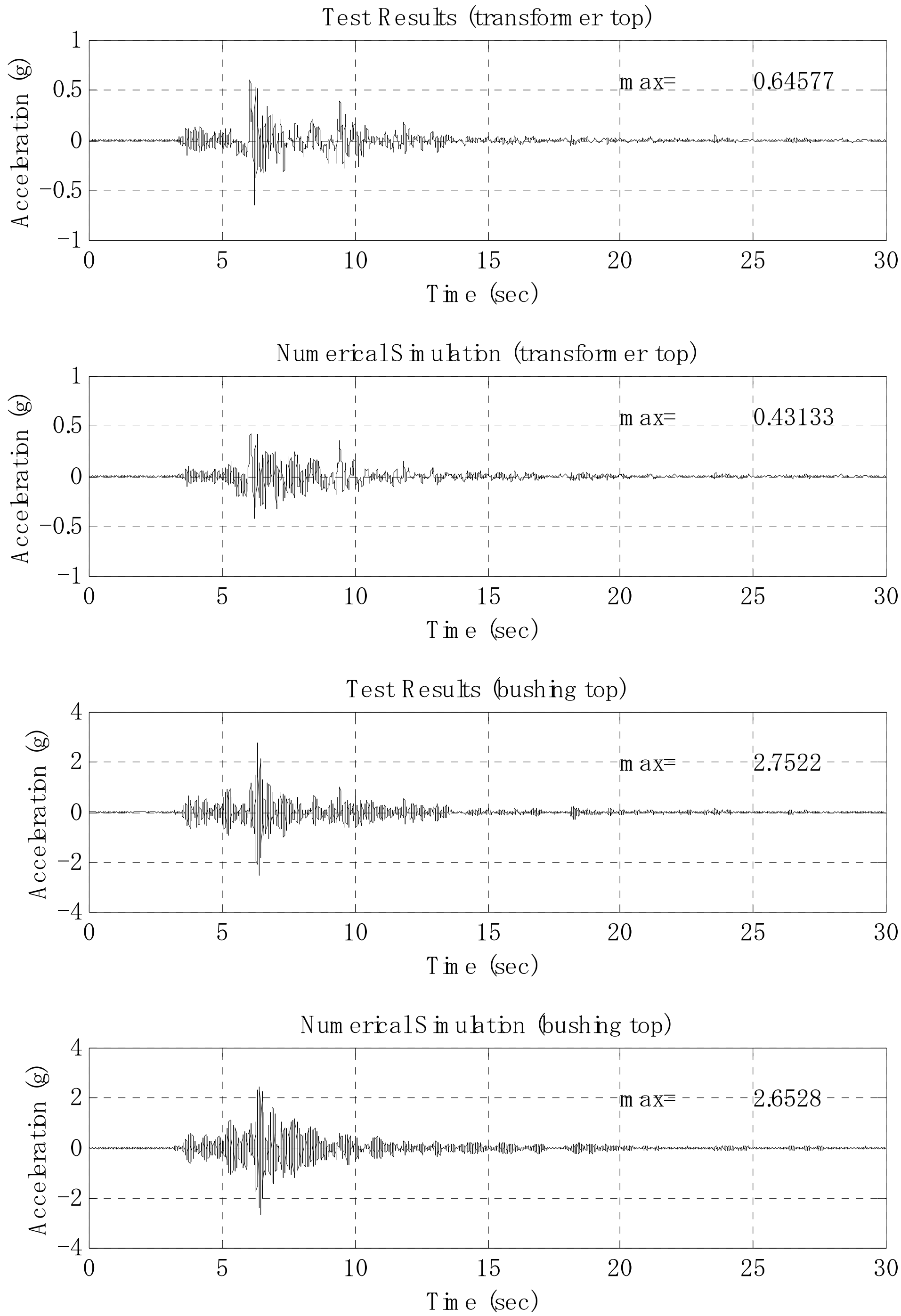

Figure 5-4 Comparison of Test Results and Numerical Simulation: 161kV/F/Northridge/x375, Fixed-Base System

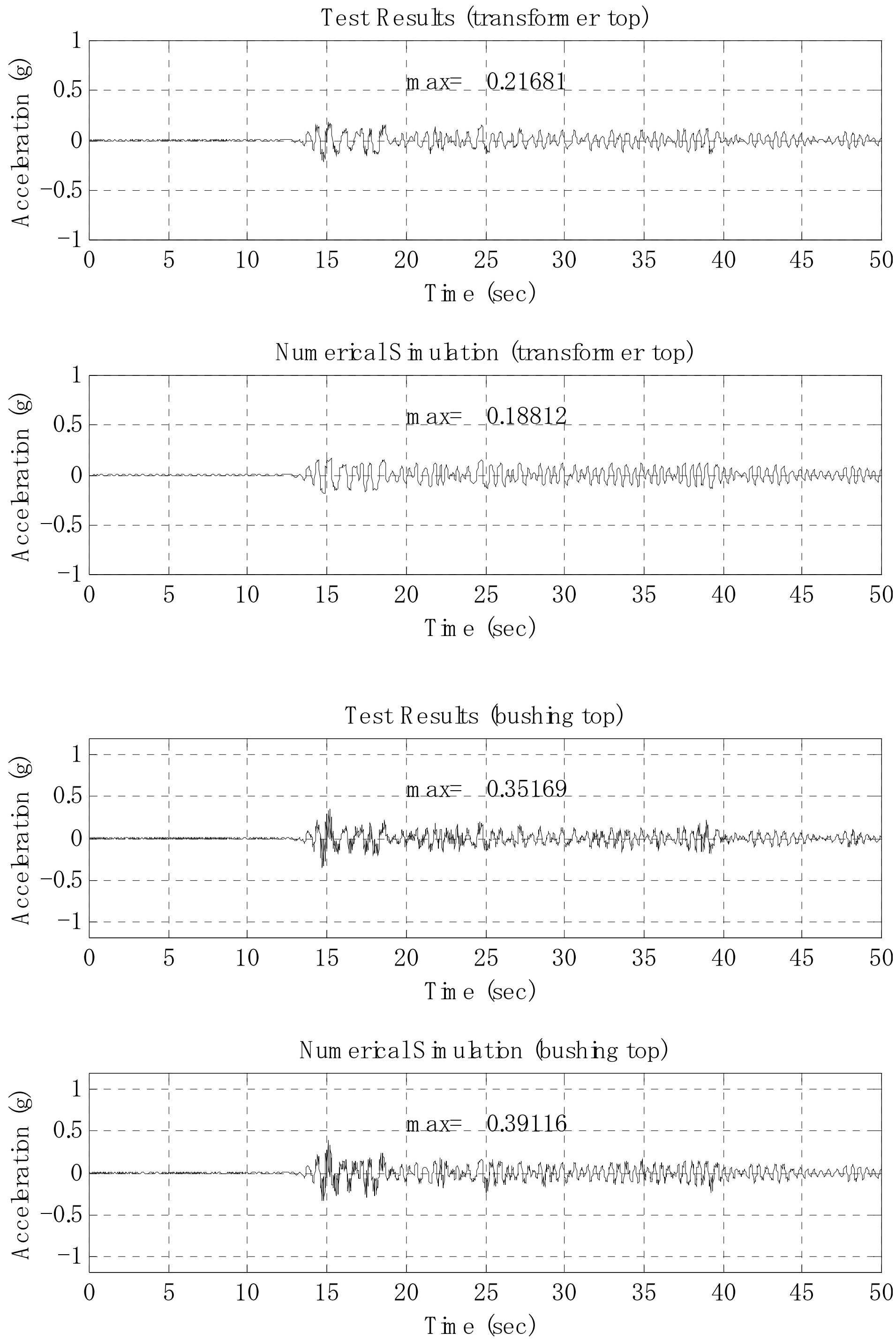

Figure 5-5 Comparison of Test Results and Numerical Simulation: 161kV/B/El Centro/x375, Base-Isolated System

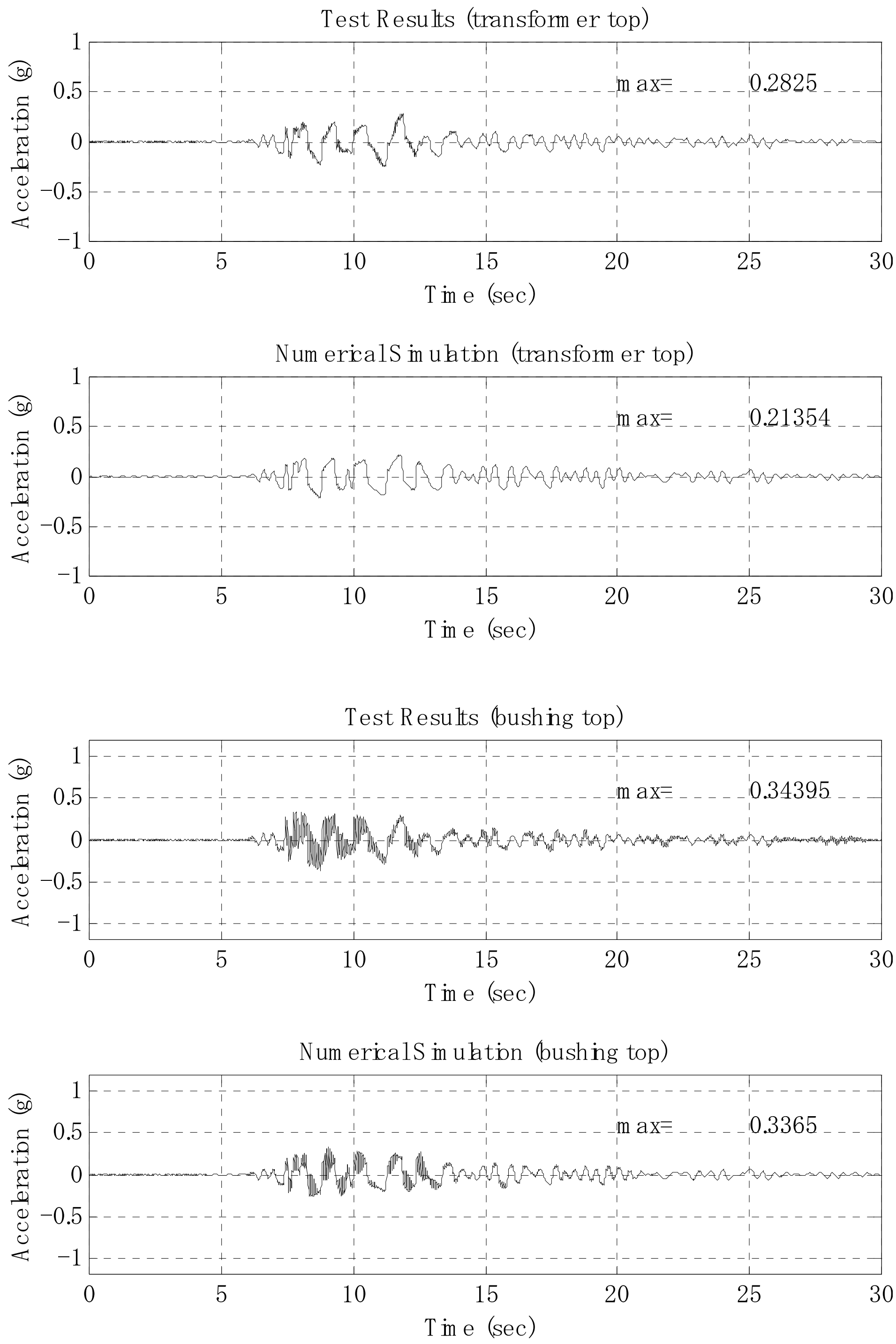

Figure 5-6 Comparison of Test Results and Numerical Simulation: 161kV/B/Kobe/x375, Base-Isolated System

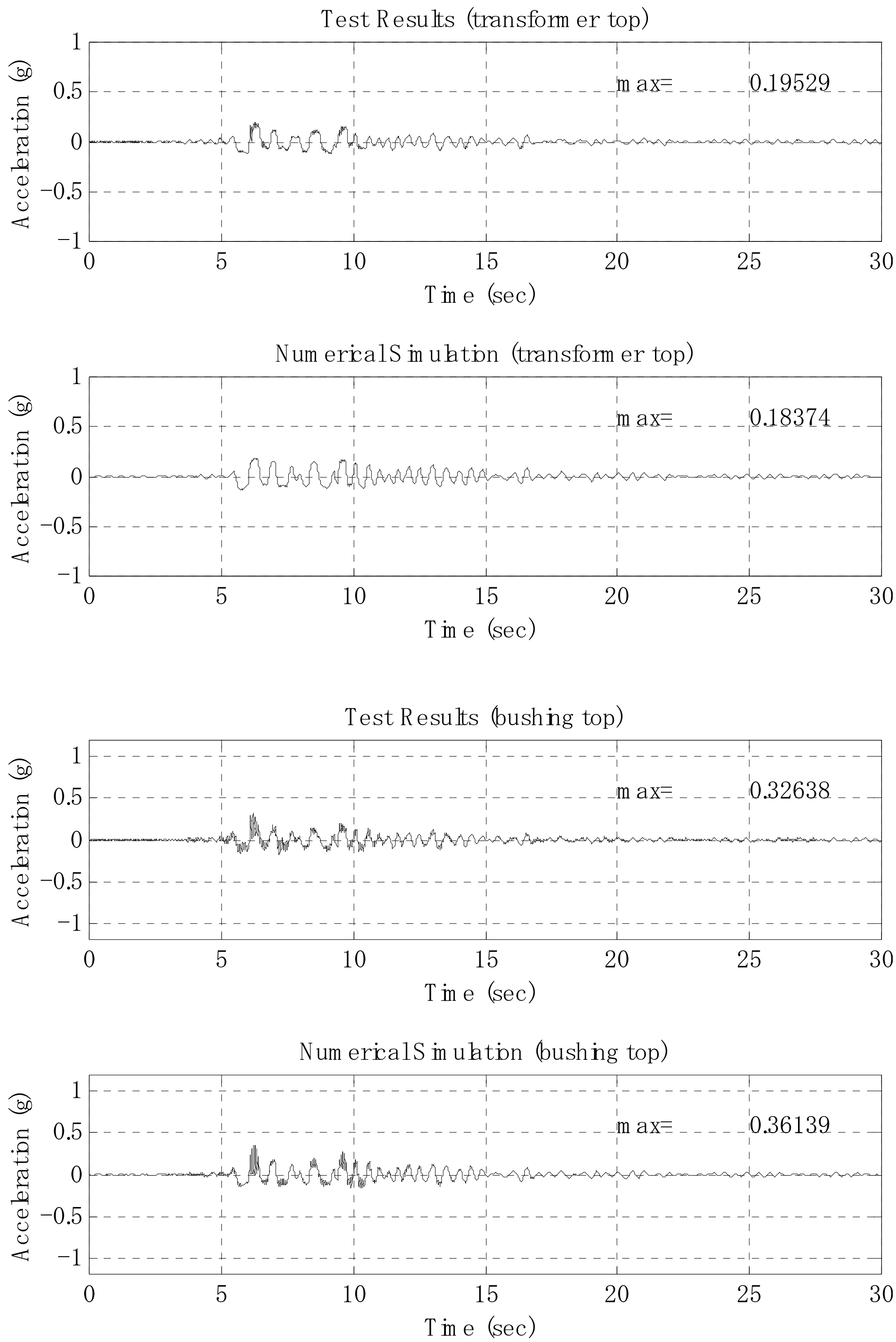

Figure 5-7 Comparison of Test Results and Numerical Simulation: 161kV/B/Northridge/x375, Base-Isolated System

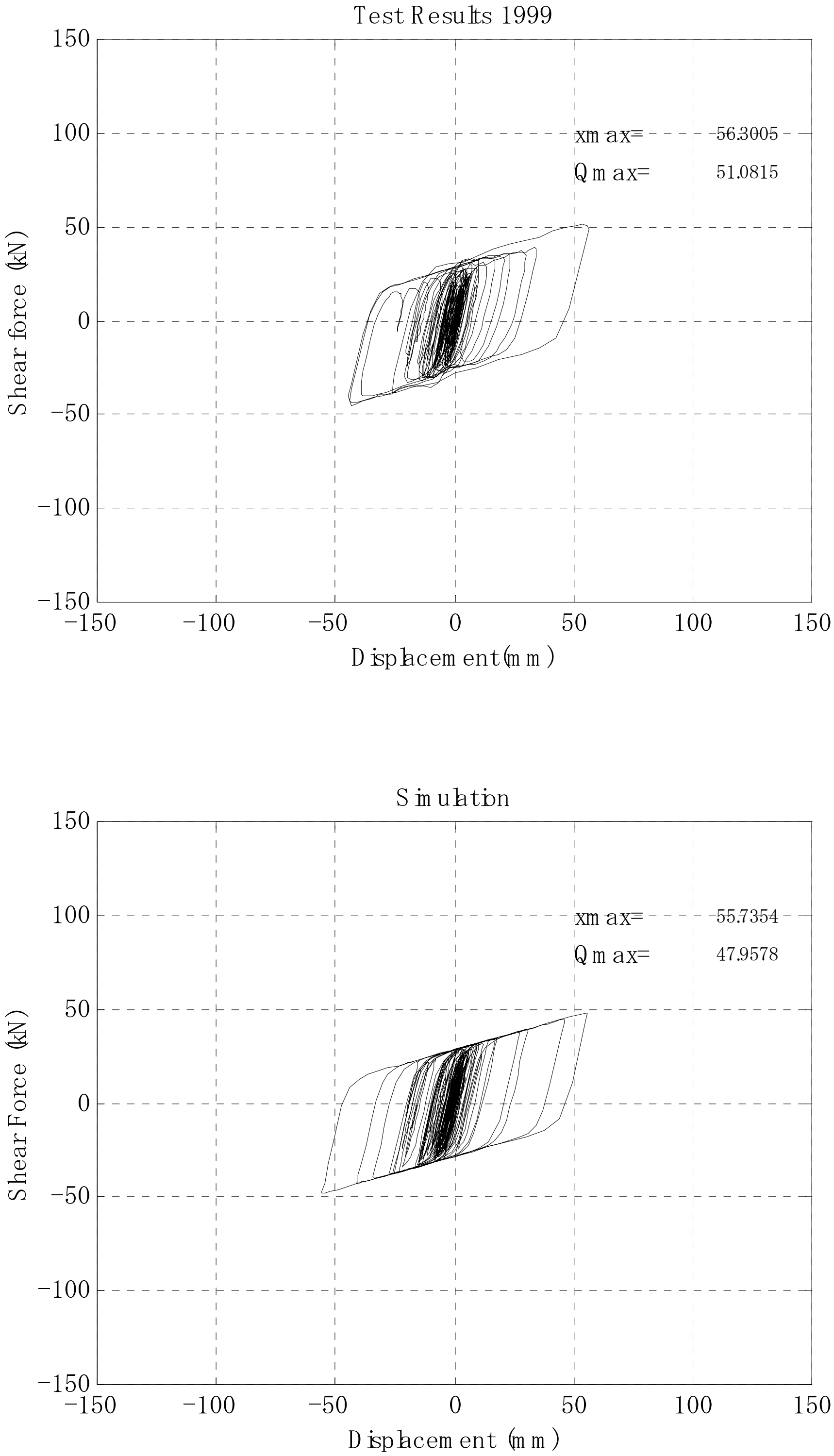

Figure 5-8 Force-Displacement Curve of Isolation System : 161kV/B/El Centro/x375

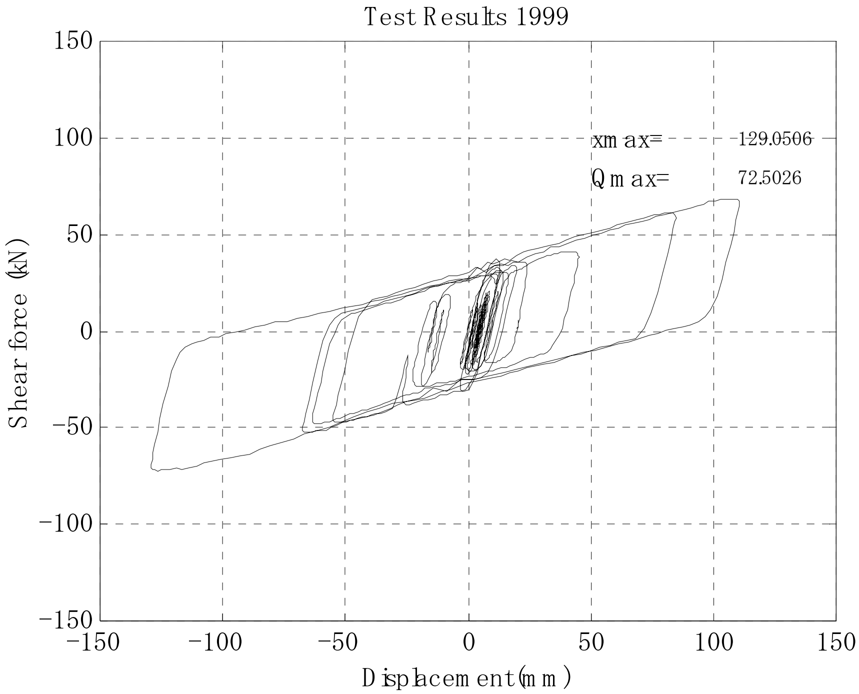

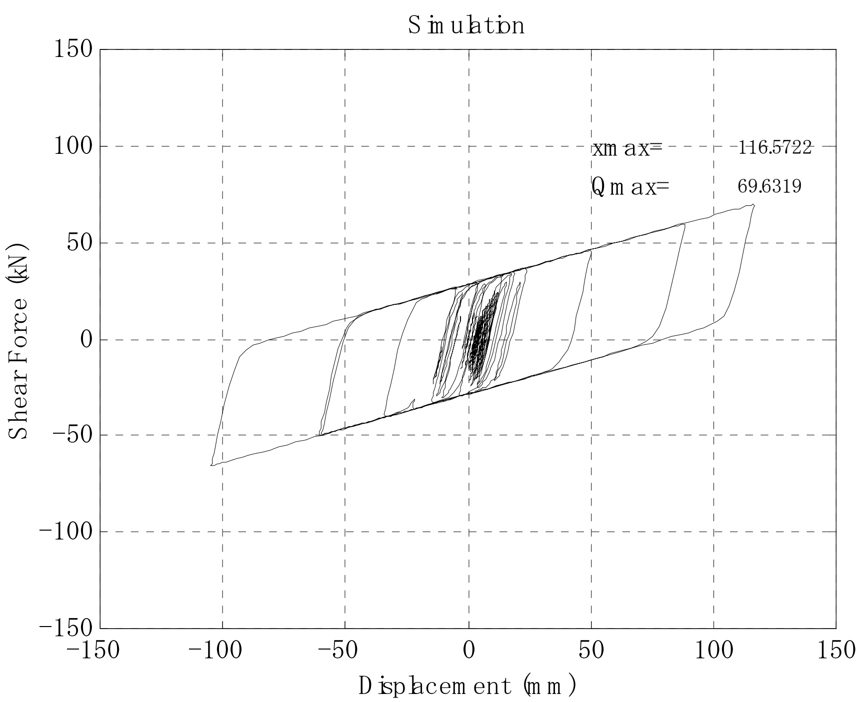

Figure 5-9 Force-Displacement Curve of Isolation System : 161kV/B/Kobe/x375

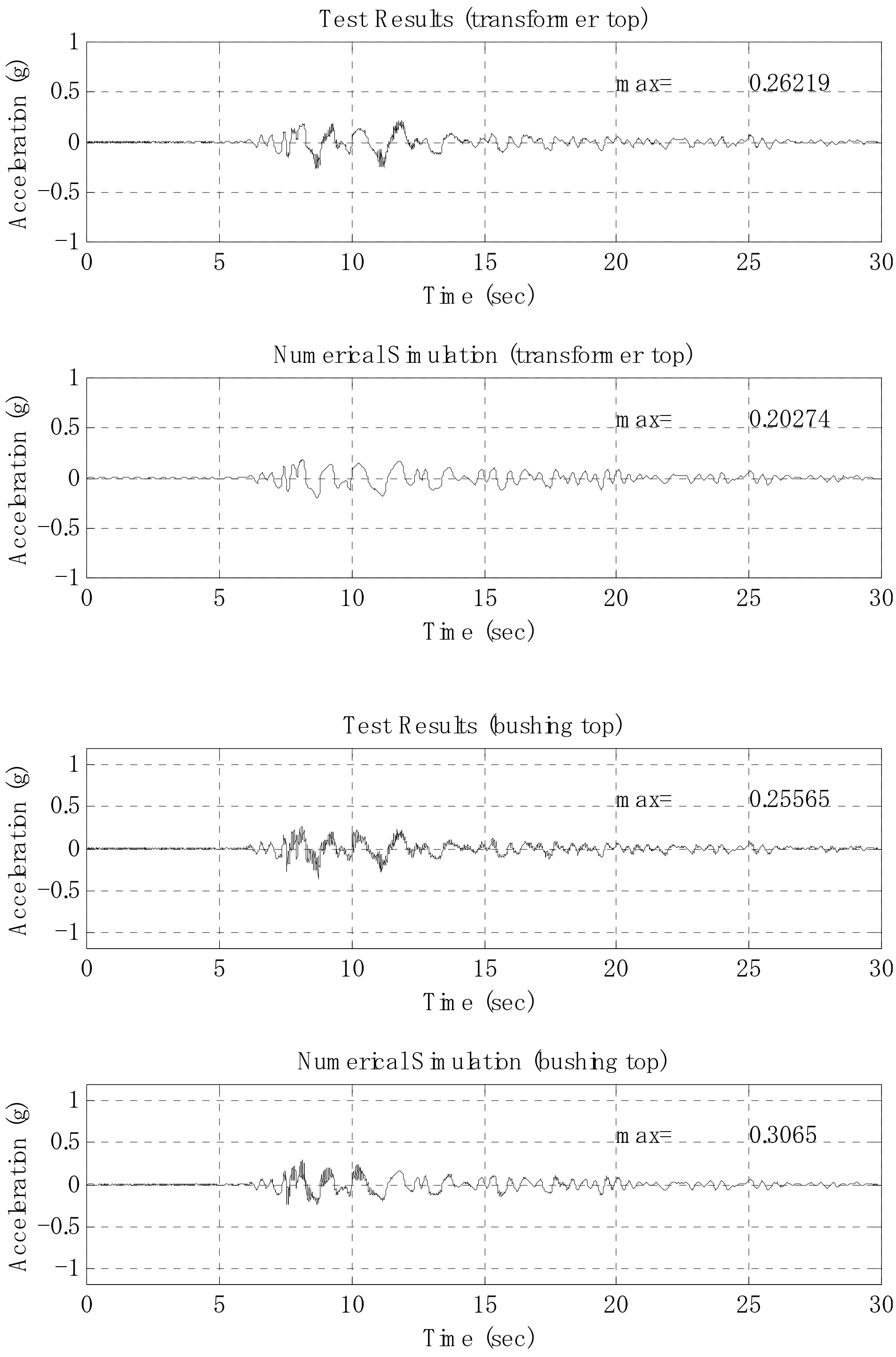

Figure 5-10 Comparison of Test Results and Numerical Simulation: 161kV/B/Kobe/xy375, Base-Isolated System

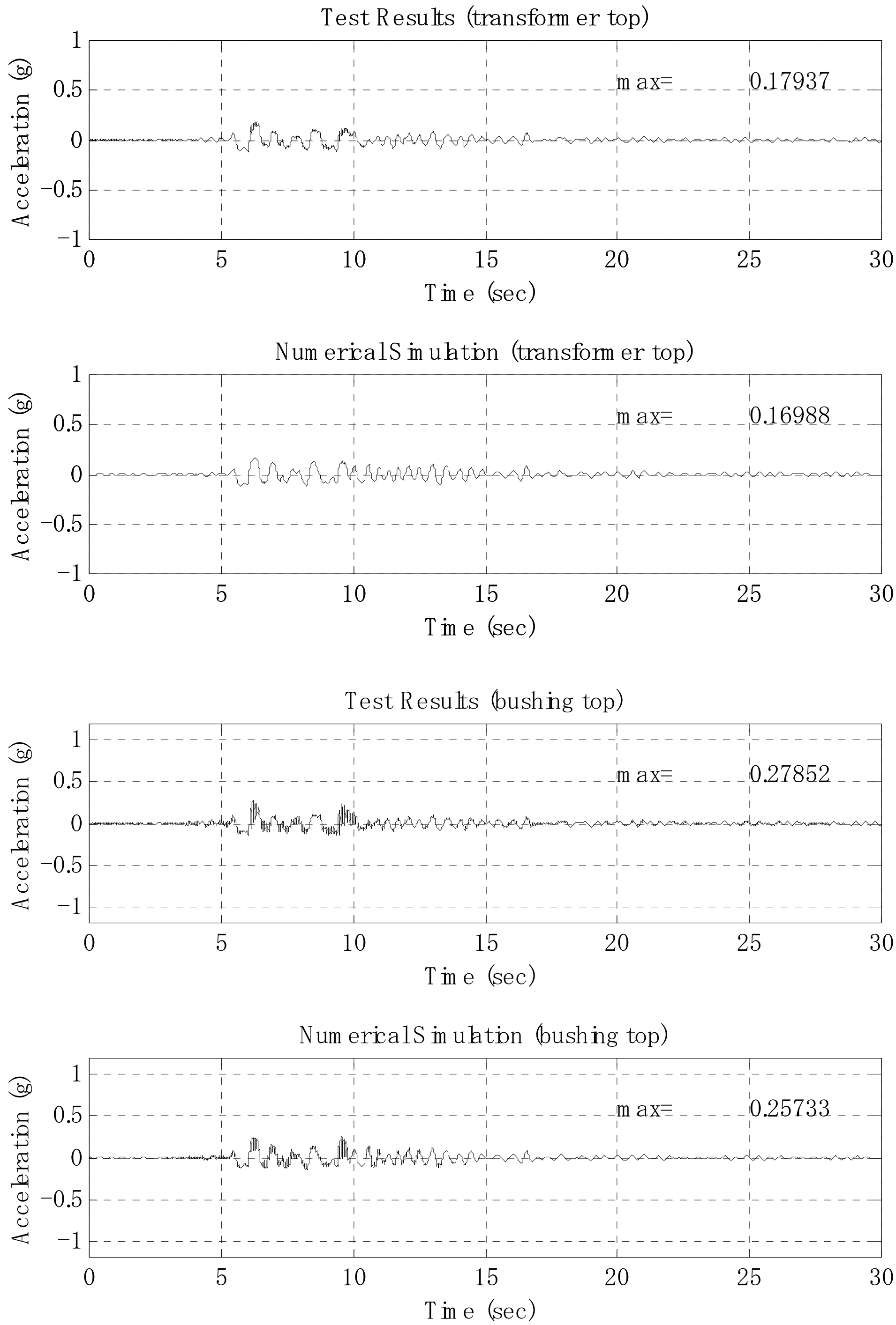

Figure 5-11 Comparison of Test Results and Numerical Simulation: 161kV/B/Northridge/xy375, Base-Isolated System

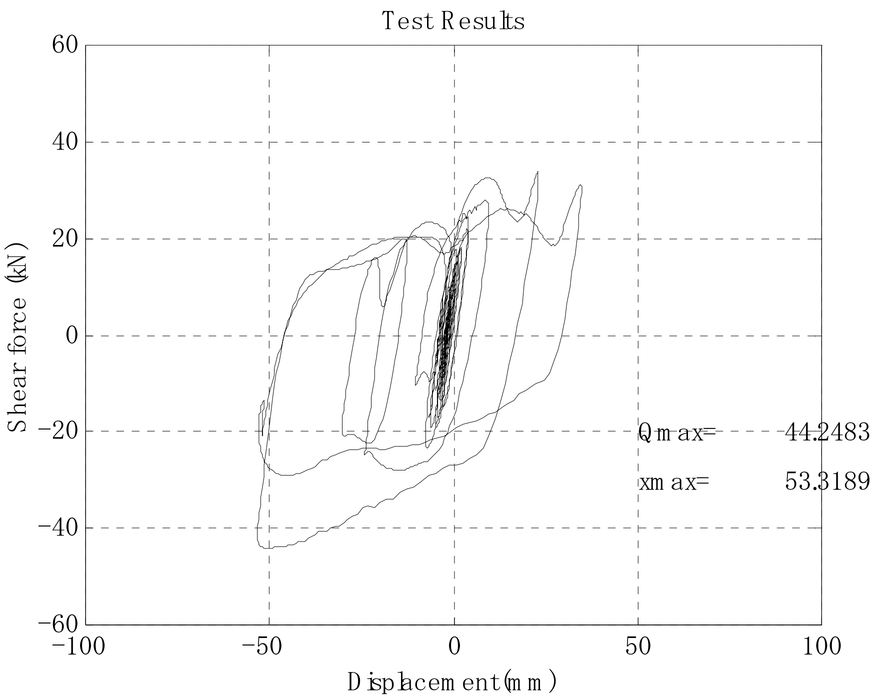

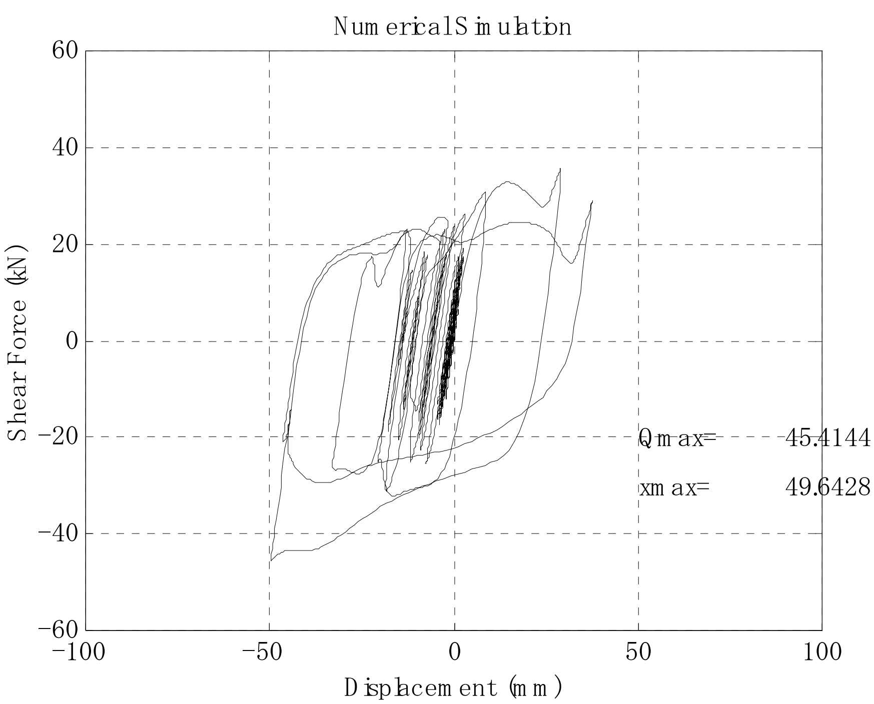

Figure 5-12 Force-Displacement Curve of Isolation System: 161kV/B/Northridge/xy375

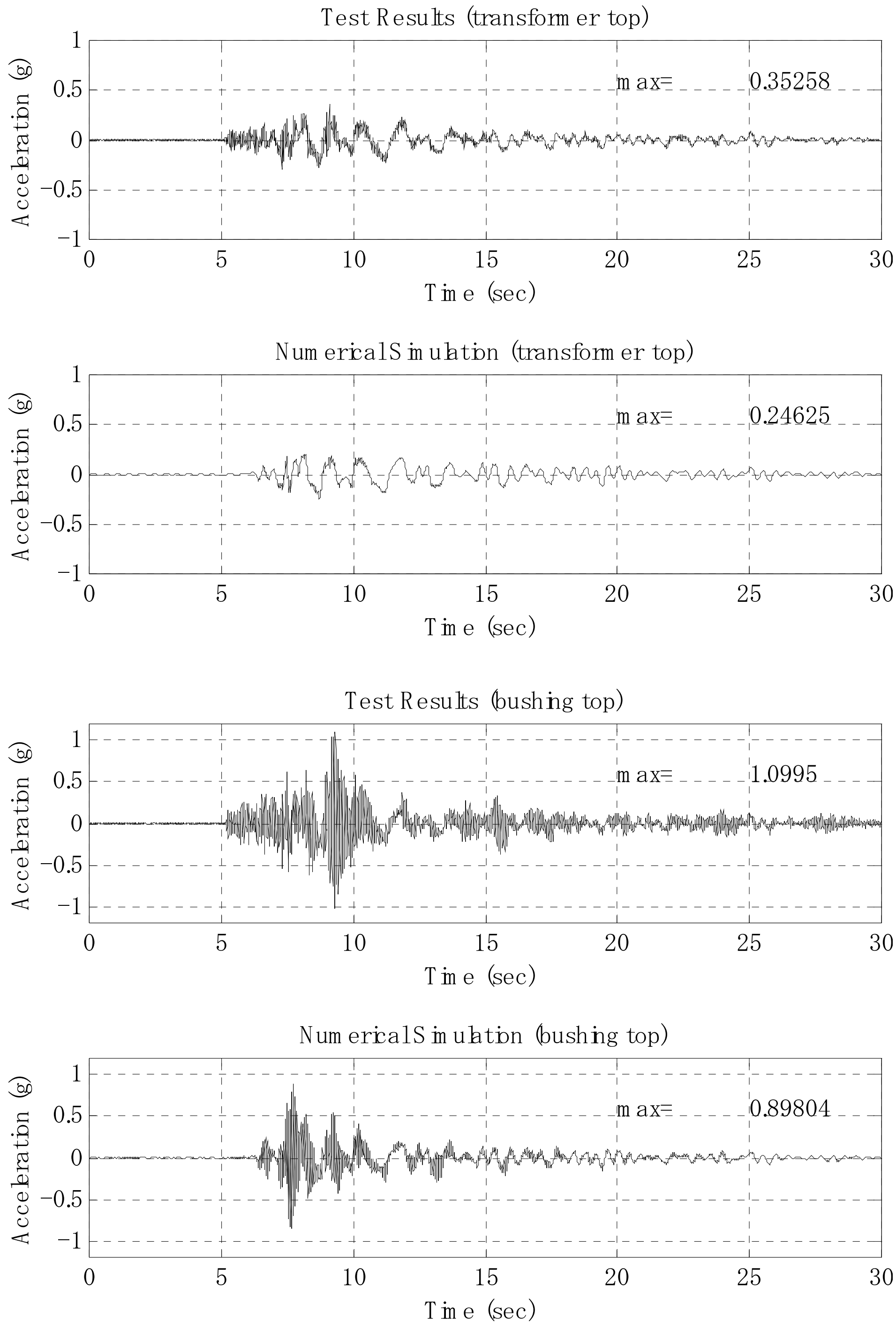

Figure 5-13 Comparison of Test Results and Numerical Simulation: 161kV/B/Kobe/xyz375, Base-Isolated System

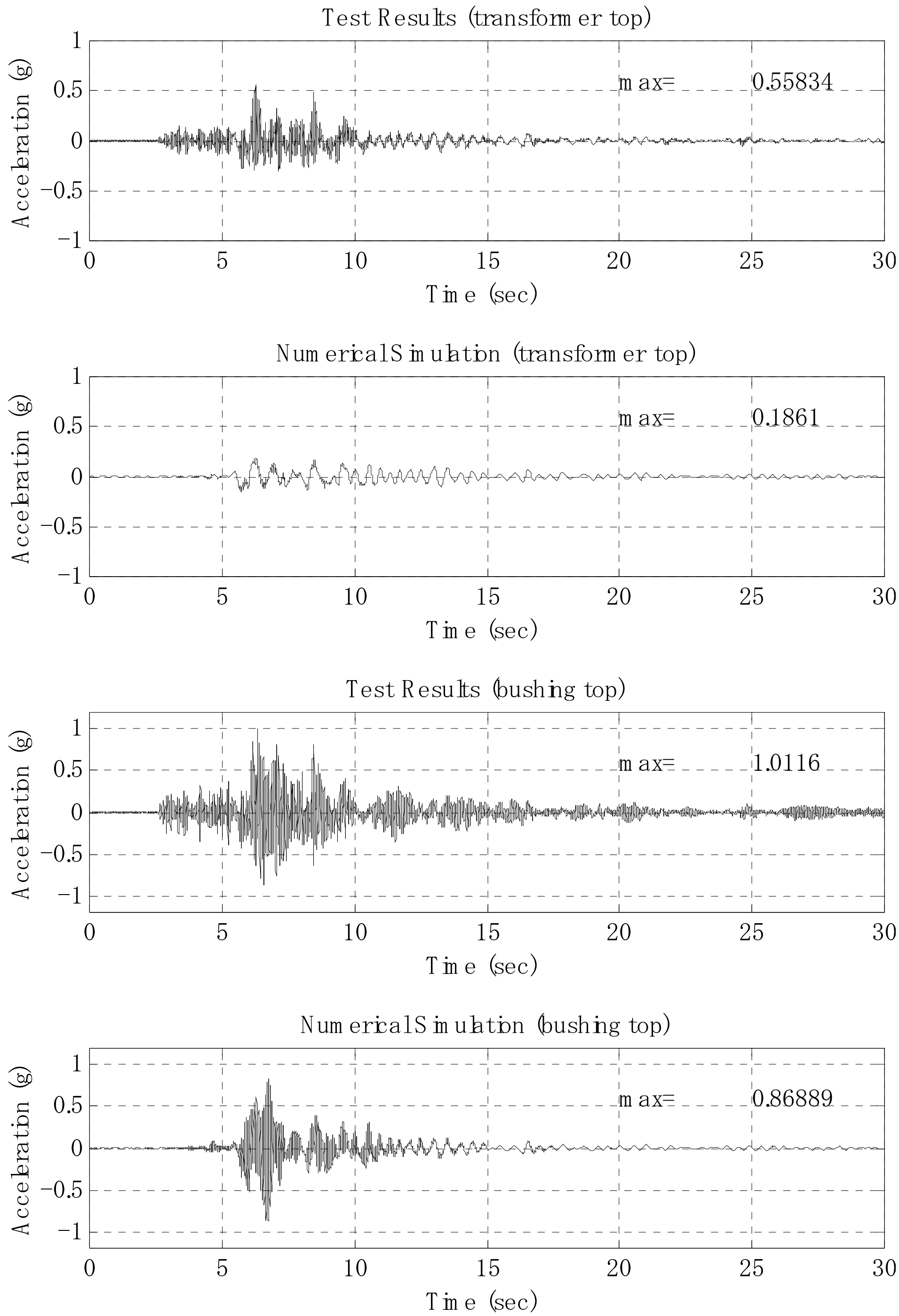

Figure 5-14 Comparison of Test Results and Numerical Simulation: 161kV/B/Northridge/xyz375, Base-Isolated System

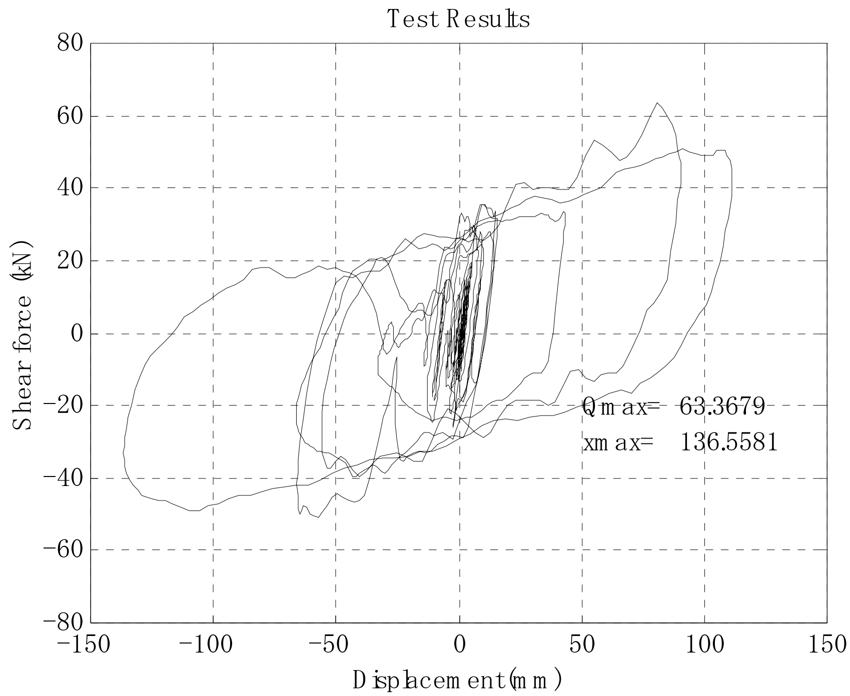

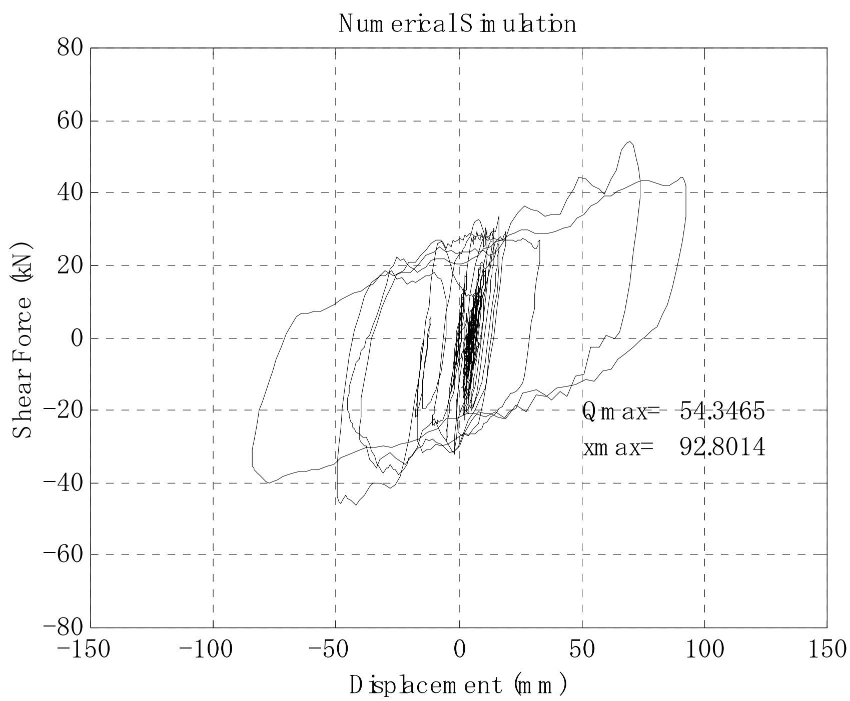

Figure 5-15 Force-Displacement Curve of Isolation System: 161kV/B/Kobe/xyz375

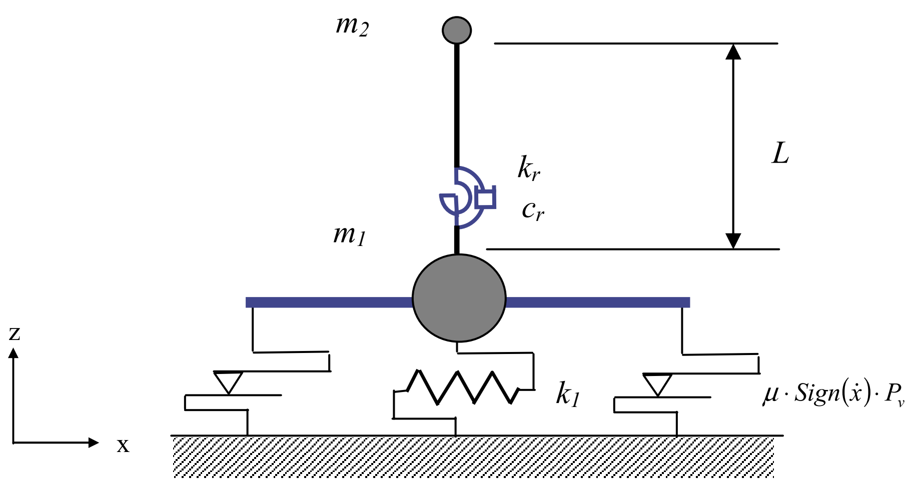

Figure 5-16 Simplified Model for Parametric Study

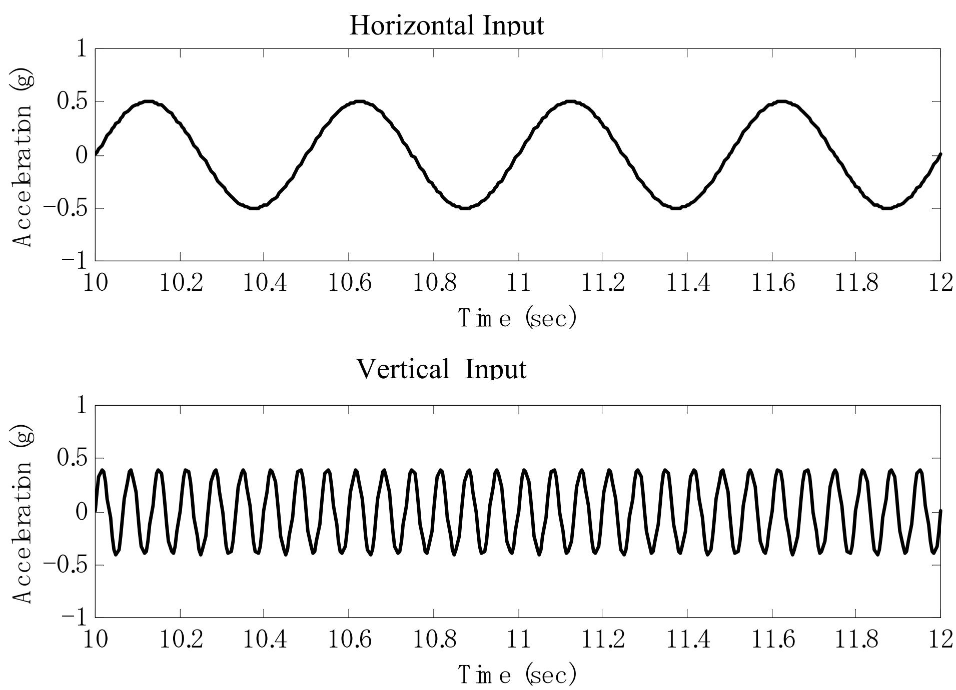

Figure 5-17 Sinusoidal Wave Input in Horizontal and Vertical Direction

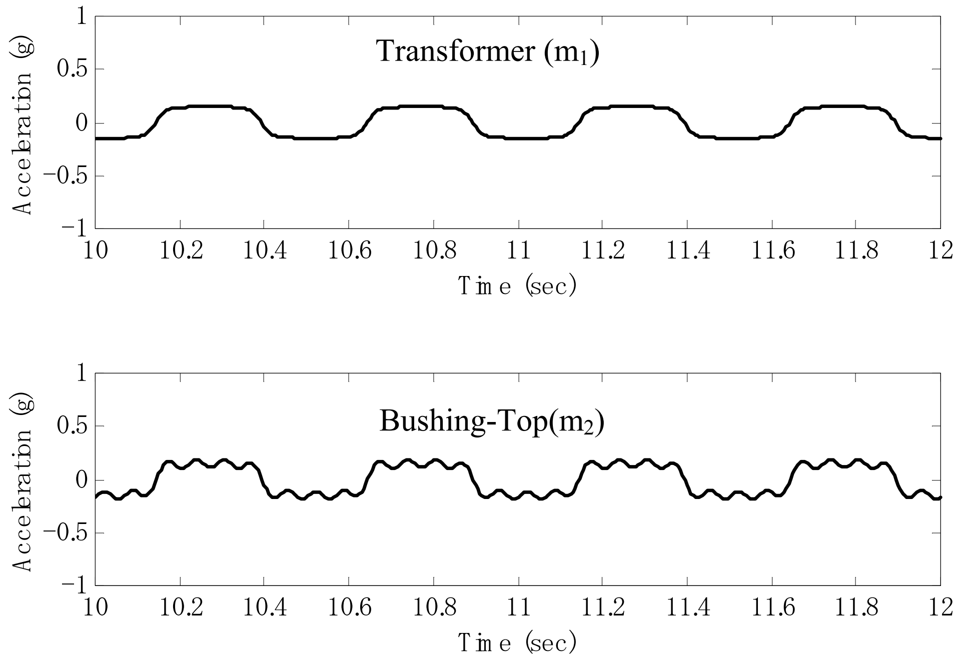

Uni-Axial Shaking: x0.5g

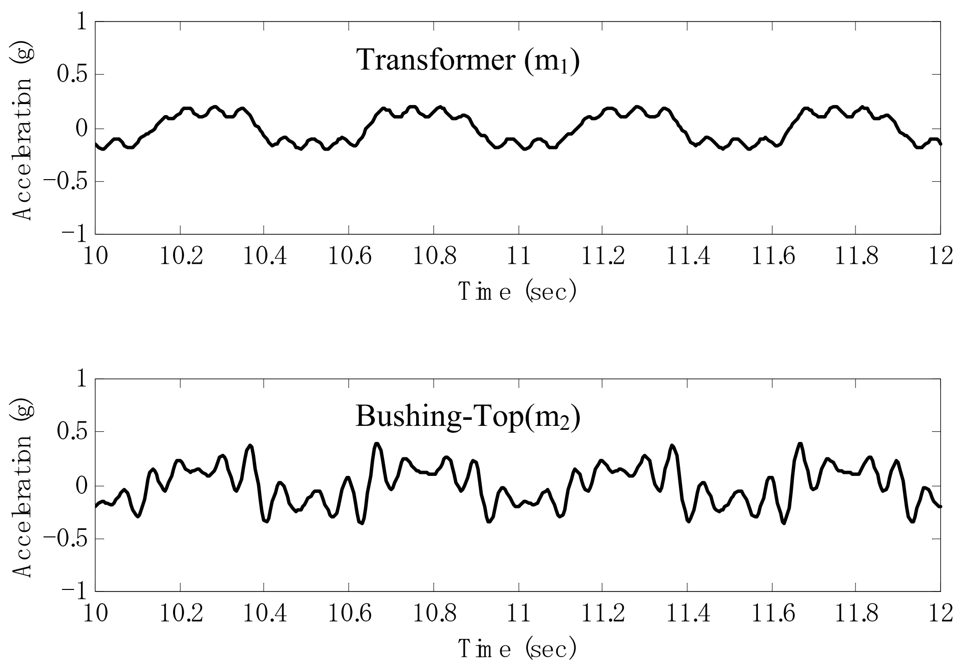

Bi-Axial Shaking: x0.5g-z0.4g

Figure 5-18 Comparison of Response Acceleration under x-, and xz-Shaking

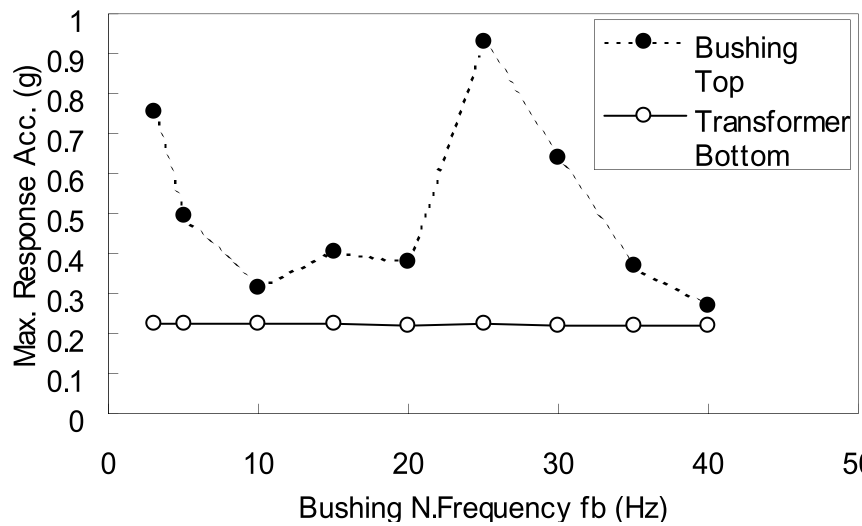

Figure 5-19 Relationship of Bushing Natural Frequency in Horizontal Direction and Maximum Response Acceleration in x-direction

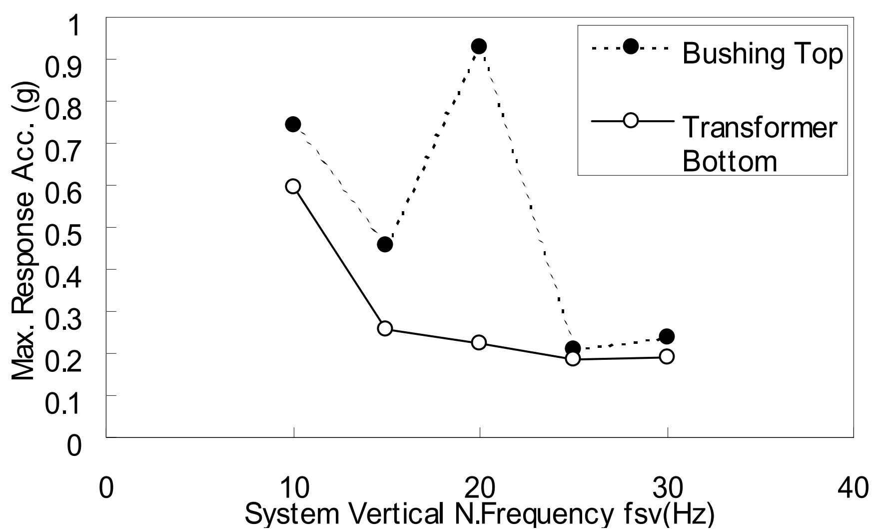

Figure 5-20 Relationship of System Natural Frequency in Vertical Direction and Maximum Response Acceleration in x-direction

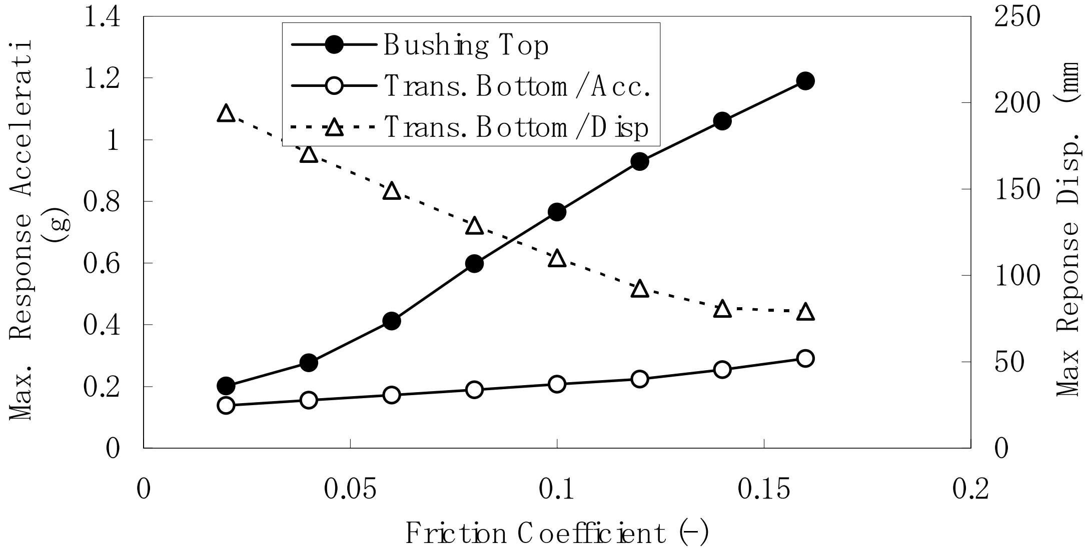

Figure 5-21 Relationship of Friction Coefficient versus Maximum Response Acceleration and Maximum Response Displacement

5.6 Comparison with Phase-2 Test Results

Since the load-deflection curve of Segmented High-Damping Rubber Bearing (SHRB) shows non-linear and visco-elastic behavior, the bi-linear model is not a precise model to express the shear characteristics. However, considering the practical use of a commercial program for dynamics structures, a normal bilinear model was applied for simulation in this study. The bilinear model was defined to nearly match the actual curve chosen from the data obtained during earthquake simulator test in Phase-2. Figure 5-22 shows the definition of the bilinear model overlaid on the force-displacement curve in the test case FB/Kobe/x375, which was selected as the master curve for modeling. The parameter of the bilinear model was set as follows:

1. Post-yield Stiffness: 0.4 (kN/mm)
2. Characteristic Strength: 8.0 (kN)
3. Initial Stiffness: 1.6 (kN/mm)

The same numerical model for the transformer/bushing in calibration of Phase-1 was applied. The mass and stiffness of each element was defined so that the fundamental frequency matches the results of the dynamic identification tests in Chapter 4. At first, the simulation of the fixed-base system was conducted. Figure 5-23 shows the comparison of both results in the Rubber Ring / Fixed-Base RF-system for Art-693/x375, which has a rubber ring installed between the bushing end and the turret mounting face, and also shows good agreement with the test results. The other fixed-base cases overall agree with these test results.

Next, the simulation of base-isolated cases was conducted. Figures 5-24 to 5-27 show the comparison of the results in the test and simulation in Rubber Ring / Base-Isolated RB-system/ Art-693/x375 and Kobe/x375, and without Rubber Ring Base-Isolated FB-system/ Art-693/x375 and Kobe/x375. All of the results show good agreement. In Figures 5-28 and 5-29, the performance curve in tests and simulation was compared. The behavior for small displacement levels, as shown in Figure 5-28, shows good traceability whereas for large displacement levels, as shown in Figure 5-29, some differences are seen in the skeletons of the curve. The SHRB shows high non-linearity in its load-deflection relationships. The peak response acceleration value of the uni-axial shaking is summarized in Table 5-7.

Table 5-7 Maximum Response Acceleration of Test Results and Numerical Simulation in Uni-Axial Shaking : Phase-2

a) Without rubber ring system;

Unit: g	FB/Art-693/x375		FB/Kobe/x375	
	Test	Simulation	Test	Simulation
Tr. Bottom	0.266	0.246	0.401	0.463
Tr. Top	0.277	0.229	0.430	0.464
Bush. Top	0.181	0.240	0.444	0.494

b) With rubber ring system;

Unit: g	RB/Art-693/x375		RB/Kobe/x375	
	Test	Simulation	Test	Simulation
Tr. Bottom	0.336	0.265	0.320	0.282
Tr. Top	0.347	0.249	0.328	0.277
Bush. Top	0.482	0.454	0.392	0.446

Figures 5-30 and 5-31 show the comparison between the response acceleration and the performance curves in simulation and the test results in the cases of RB/Art-693/xy250. In this case, the simulation result agreed sufficiently. However, in the case of RB/Kobe/xy375 as shown in Figure 5-32, the locus of the force-displacement curve shows some difference from the test results. In bi-axial and tri-axial shaking, the numerical model of SHRB was insufficient to express the multi-directional performance. More accurate modeling of high-damping rubber bearings in multi-direction loading is still under development by many researchers.

5.7 Case Study of Existing Transformer/Bushing System

Through the comparison with test results, the accuracy of numerical simulation method was basically proven. Using the same concept of modeling, numerical simulation of real transformer/bushing system in the field was carried out and the seismic response was examined. The selected system was in the Tottori-prefecture, Japan, damaged in the 2000 Tottori-ken Seibu Earthquake, as introduced by Constantinou (1990). The transformer system was a 500 kV/220 kV size installed in an ultra-high voltage substation, located about 5 km to the northeast of the epicenter. The secondary-bushings (220 kV) of three similar transformer systems were all fractured at the fixed end. The model of the system is shown in Figure 5-33. The bushings had lengths of 5.788 m and a total weight of 5.99 kN. These bushings were modeled as a lumped-mass beam, and the sleeve and turret were modeled as a beam element. Rotation-springs were connected between the bushing-end and the sleeve, the sleeve-end and turret, and the turret-end and the transformer-top. The weight of the transformer body was 1784.7 kN. Modal damping of 5 % was considered for all modes. The material constants and geometric constants of the bushing-element and each rotation-spring constant, are listed in Tables 5-8, 5-9, and 5-10.

Table 5-8 Material Constants of Beam Element

	Young's Modulus (MPa)	Poison's Ratio	Damping Ratio
Bushing	5.88E+04	0.23	0.05
Sleeve	7.06E+04	0.28	0.05
Turret	2.06E+05	0.33	0.05

Table 5-9 Geometric Properties of Beam Element

Element	Cross-sectional Area (m^2)	Moment of Inertia (m^4)
Bushing-1	1.17E-02	8.62E-05
Bushing-2	2.44E-02	1.35E-04
Bushing-3	3.21E-02	2.68E-04
Bushing-4	4.10E-02	4.81E-04
Bushing-5	4.83E-02	7.57E-04
Bushing-6	4.83E-02	9.06E-04
Sleeve-1	2.34E-02	2.54E-04
Sleeve-2	2.34E-02	2.54E-04
Turret-1	1.52E-02	1.08E-03
Turret-2	1.52E-02	1.08E-03
Turret-3	1.52E-02	1.08E-03

Table 5-10 Stiffness of Rotation Spring

Position of Spring	Stiffness (N*m/rad)
Bushing-Sleeve	2.42E+07
Sleeve-Turret	4.90E+07
Turret-Transformer	4.90E+07

Segmented high-damping rubber bearings were designed for the isolator system. A sliding bearing system was also designed, modeled and simulated for comparison. The design parameters for the high-damping rubber bearings are listed in Table 5-11.

Table 5-11 Characteristics of Element Bearing of SHRB

Diameter	225 (mm)
Effective Area	39760.782 (mm^2)
Rubber Height	45 (mm)
Shear Modulus	0.61 (MPa)
Equivalent Damping Ratio	0.168 (-)
Characteristic Strength	8.16 (kN)
Post-Yield Stiffness	0.359 (kN/mm)
Initial Stiffness	2.87 (kN/mm)

One SHRB consists of 4 pieces of element bearings per one layer by 3 layers. Therefore, the properties of the assembled SHRB was calculated as follows;

1) Post yield stiffness K_2 = 0.479 kN/mm
2) Initial stiffness K_1 = 3.83 kN/mm
3) Characteristic Strength Q_d = 32.6 kN

Four SHRBs were installed beneath the corner of the transformer. Therefore, the total performance of the isolation system is as follows;

1) K_2-total = 1.92 kN/mm
2) K_1-total = 15.3 kN/mm
3) Q_d-total = 130.4 kN

The natural period of the system at displacement of 135 mm, which agree with shear strain of 100% of the rubber bearing, was computed as 1.60 seconds. The compressive stress on each element bearing was 2.86 MPa.

The period of each mode for fixed-base and base-isolated systems was calculated as follows:
(Fixed-base)
1st mode: 0.126 sec, 2nd mode: 0.0550 sec, 3rd mode: 0.0290 sec
(Base-isolated with SHRB)
1st mode: 1.59 sec, 2nd mode: 0.126 sec, 3rd mode: 0.0630 sec

Next, the sliding bearing system was designed as follows. The friction coefficient was designed as 0.073 and the stiffness of low-damping rubber bearing was set as 0.958 kN/mm so as to have same bi-linear model of SHRB system. The vertical stiffness was designed as 458 kN/mm, corresponding to a vertical frequency of 7.94 Hz, which is the 1st mode frequency of the system in the horizontal direction.

Time-history analysis was conducted under the following ground motions:

1) Art-693: NS in x-direction | UD in z-direction (used in Phase-2 test)
2) El Centro: NS in x-direction | UD in z-direction
3) Kobe (Takatori): EW in x-direction | UD in z-direction

Acceleration and displacement at the bushing-top, the transformer-top, and the transformer-bottom (just above isolation system) under Art-693 in SHRB system, for a PGA of 0.25g, 0.5g, 0.75g, and 1.0g are shown in Table 5-12, and time histories of the response acceleration in Art-693/x0.5gz0.4g for both fixed-base and base-isolated systems are shown in Figures 5-34 and 5-35.

Table 5-12 Summary of Time History Analysis :

Art-693:PGA x0.5g + z0.4g

PGA(g)	Node	Acceleration (g)	Displacement (mm)
x0.25	Bushing-top	0.192	104
	Transformer-top	0.184	103
	Transformer-bottom	0.182	103
x0.5	Bushing-top	0.361	254
	Transformer-top	0.339	252
	Transformer-bottom	0.339	251
x0.75	Bushing-top	0.533	416
	Transformer-top	0.511	413
	Transformer-bottom	0.508	411
x1.0	Bushing-top	0.705	579
	Transformer-top	0.684	575
	Transformer-bottom	0.680	573
x0.5z0.4	Bushing-top	0.362	254
	Transformer-top	0.342	252
	Transformer-bottom	0.339	251
Fixed-base x0.5	Bushing-top	2.55	10.6
	Transformer-top	0.837	2.87
	Transformer-bottom	0.677	0.810

The results under uni-axial shaking x0.5g and tri-axial shaking x0.5gz0.4g show no significant difference. For the SHRB system, the z-motion does not affect the response in the x-direction. In the fixed-base system, the amplification of the bushing-top exceeded 5.0. This level of acceleration will cause damage on the connection of the bushing to the sleeve. With the base-isolation system, the amplification was about 0.65. The displacement of the isolator was 250 mm at a PGA=0.5g, and 411 mm at a PGA=0.75g. The total rubber height of the SHRB is 45x3=135 mm. Therefore, at a PGA=0.75g, the rubber shear strain is around 300%. At a PGA=1.0g, the displacement of the isolator was 573 mm, a shear strain of 424 %, which exceeded the ultimate strain of the bearings. If a conventional bearing, either circular or square in shape, is applied, the minimum diameter, or length of a side, must be 600 mm to have enough stability for a 411 mm displacement under a PGA=0.75g. A diameter of 600 mm will result in a higher stiffness and will increase the response acceleration. In Table 5-13, results of three different earthquakes for fixed-base, SHRB, and slider systems under x0.5g z0.4g shaking are compared.

Table 5-13 Summary of Time History Analysis in Fixed-Based, SHRB System, and Sliding Bearing System: x0.5g z0.4g Shaking

Fixed-Base System

Input	Node	Acceleration (g)	Displacement (mm)
Art-693	Bushing-Top	2.55	10.6
	Transformer-Top	0.837	2.87
	Transformer-Bottom	0.677	0.810
El Centro	Bushing-Top	2.79	10.2
	Transformer-Top	1.02	2.49
	Transformer-Bottom	0.833	7.86
Kobe	Bushing-Top	1.82	9.15
	Transformer-Top	0.794	2.64
	Transformer-Bottom	0.637	0.80

Base-Isolated with SHRB System

Input	Node	Acceleration (g)	Displacement (mm)
Art-693	Bushing-Top	0.362	254
	Transformer-Top	0.342	252
	Transformer-Bottom	0.339	251
El Centro	Bushing-Top	0.201	93.6
	Transformer-Top	0.176	92.6
	Transformer-Bottom	0.171	92.0
Kobe	Bushing-Top	0.502	385
	Transformer-Top	0.485	383
	Transformer-Bottom	0.479	382

Base-Isolated with Sliding Bearing System

Input	Node	Acceleration (g)	Displacement (mm)
Art-693	Bushing-Top	1.17	234
	Transformer-Top	0.413	231
	Transformer-Bottom	0.328	229
El Centro	Bushing-Top	1.12	95.5
	Transformer-Top	0.371	92.4
	Transformer-Bottom	0.272	90.6
Kobe	Bushing-Top	2.40	323
	Transformer-Top	0.883	315
	Transformer-Bottom	0.648	311

Table 5-14 Comparison of Results of Slider System under x-, and xz- Shaking: Art-693

PGA(g)	Node	Acceleration (g)	Displacement (mm)
x0.5	Bushing-Top	0.375	234
	Transformer-Top	0.334	231
	Transformer-Bottom	0.321	229
x0.5z0.4	Bushing-Top	1.17	230
	Transformer-Top	0.413	226
	Transformer-Bottom	0.328	223

Compared with the results of the SHRB system, the results for x0.5g were almost the same because their bilinear models were the same. However, in the xz-shaking (x0.5z0.4), as shown in Table 5-14, the response at the bushing-top was stimulated up to 1.17 g, which was already indicated in the Phase-1 test and the prescribed parametric study in this chapter. In Figure 5-36, the response acceleration under tri-axial shaking x0.5gz0.4g in the fixed-base, SHRB, and sliding bearing systems at each node is plotted and the distribution along the z-coordinate is presented. The amplification of the bushing response in sliding bearing system is clearly observed.

The effect of friction coefficient of sliding bearing to the response of transformer/bushing system was studied. The results are summarized in Table 5-15, and the time histories, force-displacement curves are shown in Figures 5-37 and 5-38. It is interesting to note the response amplification becomes smaller when the friction coefficient becomes smaller. Displacement becomes larger as friction coefficient becomes smaller. However, the displacement with a friction coefficient of 0.03 was 262mm, and is still acceptable for the isolation system. The lower friction coefficient, such as 0.029, may be better for sliding bearing system for transformer/bushing system.

Table 5-15 Effect of Friction Coefficient to Response of Transformer/Bushing System

f.coef. μ	Node	Acceleration (g)	Displacement (mm)
0.03	Bushing-Top	0.560	267
	Transformer-Top	0.343	264
	Transformer-Bottom	0.315	262
0.073	Bushing-Top	1.17	230
	Transformer-Top	0.413	226
	Transformer-Bottom	0.328	223
0.12	Bushing-Top	1.82	199
	Transformer-Top	0.502	196
	Transformer-Bottom	0.376	194

Finally, an analysis was conducted for the system equipped with a rubber ring, as tested in Phase-2 testing. The initial natural frequency of the bushing was 17 Hz. The rubber ring was designed to shift the frequency to 2 Hz. The results are summarized in Table 5-16.

Table 5-16 Simulation Results with Rubber Ring / Fixed-Base : Tri-Axial Shaking x0.5g z0.4g

Input	Node	Acceleration (g)		Displacement (mm)	
		without RR	with RR	without RR	with RR
Art-693	Bushing-Top	2.55	1.51	10.6	99.0 (0.036)
	Transformer-Top	0.837	1.19	2.87	2.37
	Transformer-Bottom	0.677	0.738	0.810	0.758
El Centro	Bushing-Top	2.79	2.20	10.2	116.2 (0.042)
	Transformer-Top	1.02	1.84	2.49	2.70
	Transformer-Bottom	0.833	0.90	7.86	0.811
Kobe	Bushing-Top	1.82	1.16	9.15	79.2 (0.029)
	Transformer-Top	0.794	0.752	2.64	1.60
	Transformer-Bottom	0.637	0.630	0.80	0.719

NOTE: ( ) in Bushing-Top with RR = Rotation Angle in radian

The reduction of acceleration compared to the bushing without the rubber ring was approximately 40% in Art-693, 20% in El Centro, and 36% in Kobe. The purpose of the rubber ring is to absorb energy by deformation of the flexible rubber ring inserted between the bushing and the turret, and to protect the bushing from the damage of the mounting interface, where the "weak link" of the system occurs. Even if there is no reduction of acceleration, the rubber ring can be expected as an effective measure to protect the bushing by absorbing energy. The rotation angle was 0.029 to 0.042 radian (1.7 to 2.4 degrees), as shown in Table 5-16, and was small enough for the ring.

5.8 Summary

Through the study of numerical simulation of Phase-1 and Phase-2 testing, the applicability of the proposed simplified analytical model, consisting of two masses for the transformer and bushing and shear-rotation stiffness, was verified. The numerical model for the hybrid isolation system in Phase-1 shows high similarity with the actual hysteretic behavior and proved the reliability of the computation.

The amplification of the bushing response in the slider-isolation system observed in Phase-1 test was simulated. The same phenomenon was reproduced by time-history analysis. The relationship of the natural frequency of the bushing to the vertical natural frequency of the system, and the response acceleration of the bushing was studied. It was concluded that the amplification of the bushing was caused by the resonance of the vertical natural frequency of the system and the horizontal bushing frequency. The vertical vibration of the system was linked to the friction force of the sliders, which was in turn transmitted to the bushing.

A case study of an existing system was studied by a time-history analysis. Detailed information of the transformer/bushing system was obtained from the literature, and an isolation system was designed for this study. Artificial waves based on the response spectrum of IEEE-693, 1940 El Centro, and 1995 Kobe (Takatori) were used as ground motions. In the base-isolated system with segmented high-damping rubber bearings (SHRB), the peak response acceleration at the top of bushing was 60% of PGA, whereas in the fixed-base system it was more than 5 times PGA.

However, as predicted in the sliding bearing system, the acceleration at the bushing top was amplified and the peak acceleration was about 2 times PGA. The sliding systems with different friction coefficients, 0.04 and 0.16, were subjected to simulation. The results show that the lower friction coefficient will keep the amplification of the acceleration at the bushing low with some increase in displacement. The low friction system may be an optimized solution of the sliding system for protection of the transformer/bushing system. Finally, the applicability of a rubber ring, developed in Phase-2 testing, was evaluated. The acceleration of the bushing was reduced 20 to 40%, and the rotation angle of the rubber ring was 1.7 to 2.4 degrees--quite acceptable for the design of this flexible joint.

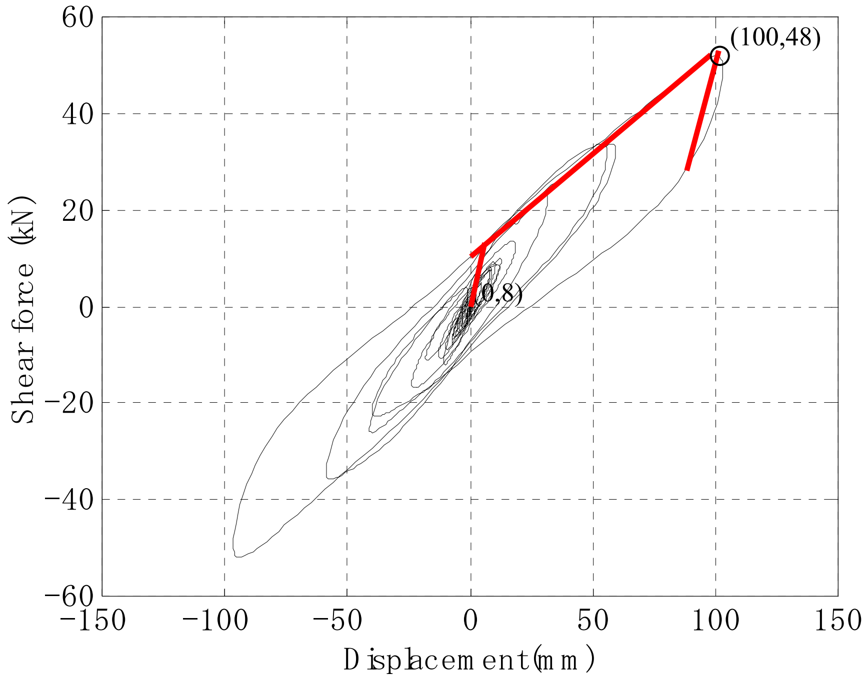

Post-yield stiffness $K_2 = 0.4$ (kN/mm), Characteristic strength $Q_d = 8.0$ (kN),
Initial stiffness $K_1 = 4.0K_2 = 1.6$ (kN/mm)

Figure 5-22 Numerical Model (Bi-linear Model) of SHRB defined from Test Results: FB/Kobe/x375

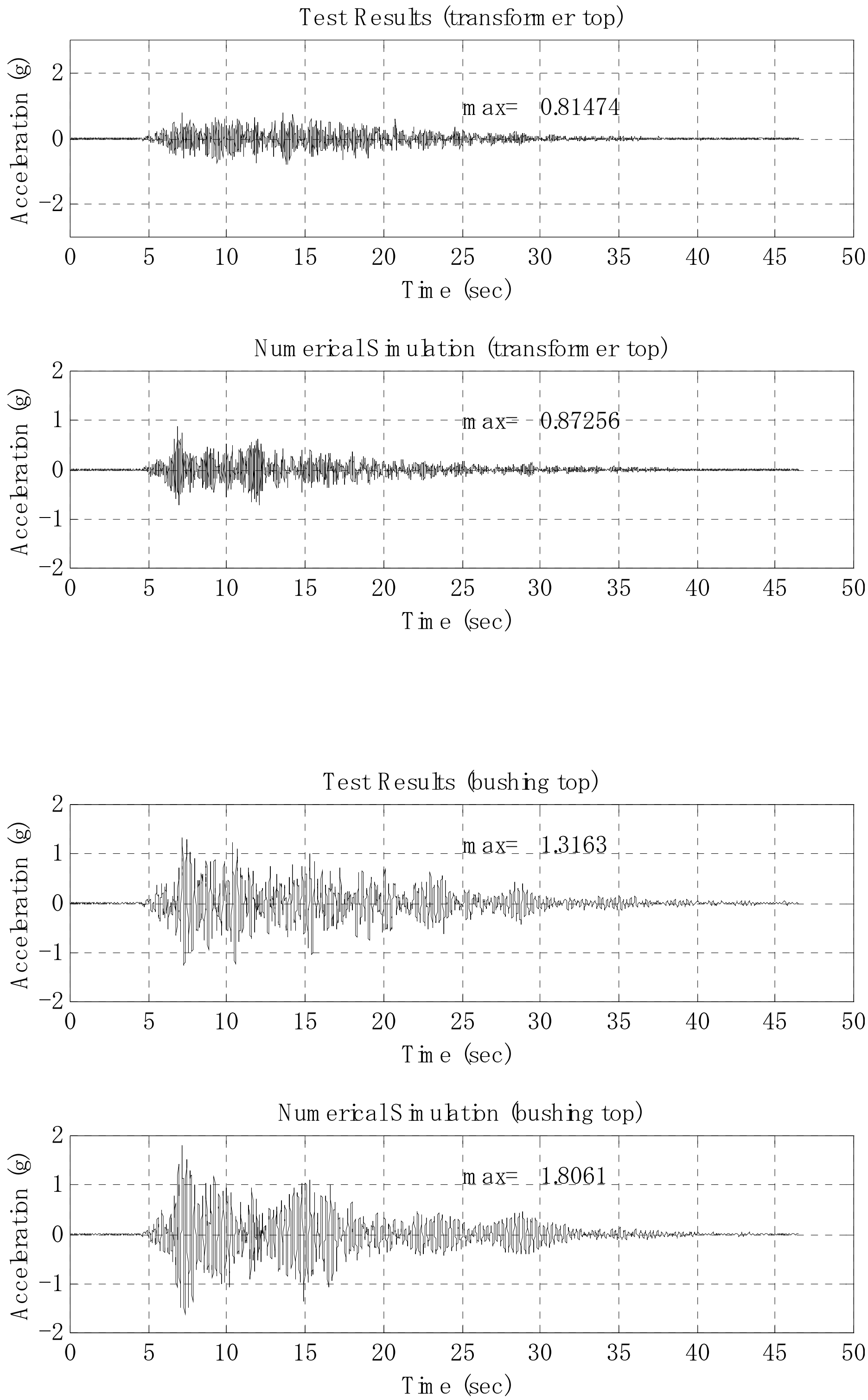

Figure 5-23 Comparison of Test Results and Numerical Simulation: RF/Art-693/x375

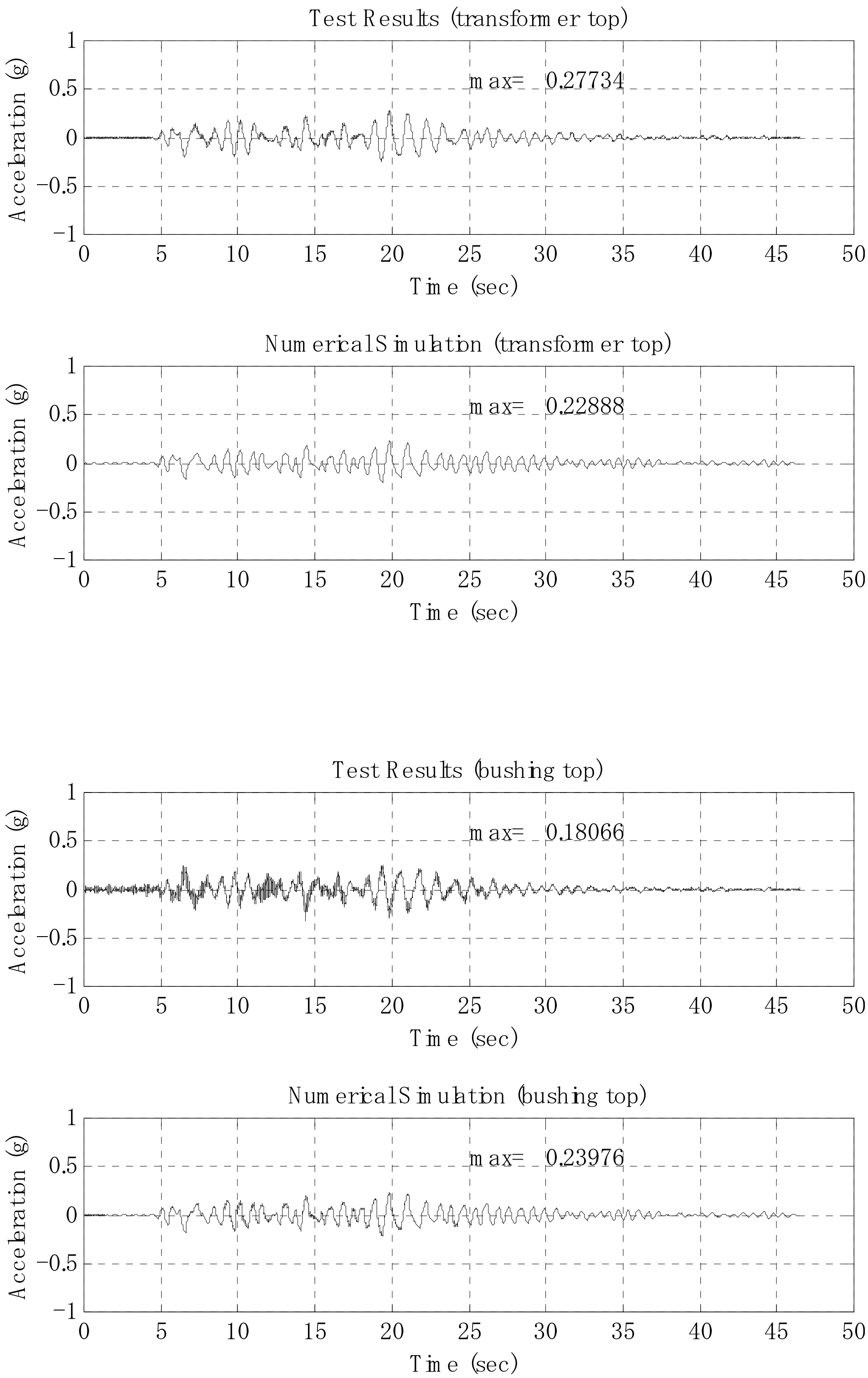

Figure 5-24 Comparison of Test Results and Numerical Simulation: FB/Art 693/x375

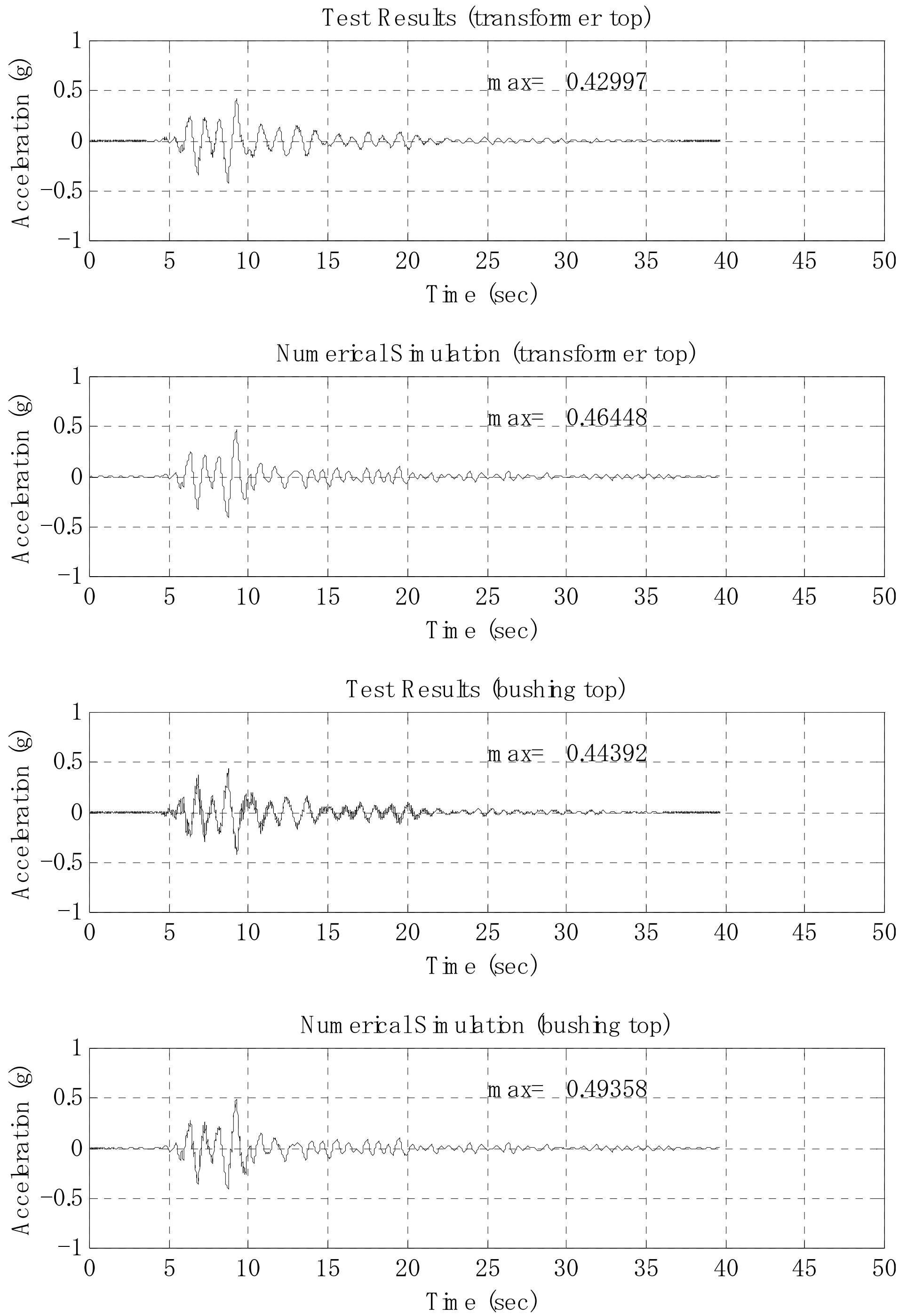

Figure 5-25 Comparison of Test Results and Numerical Simulation: FB/Kobe/x375

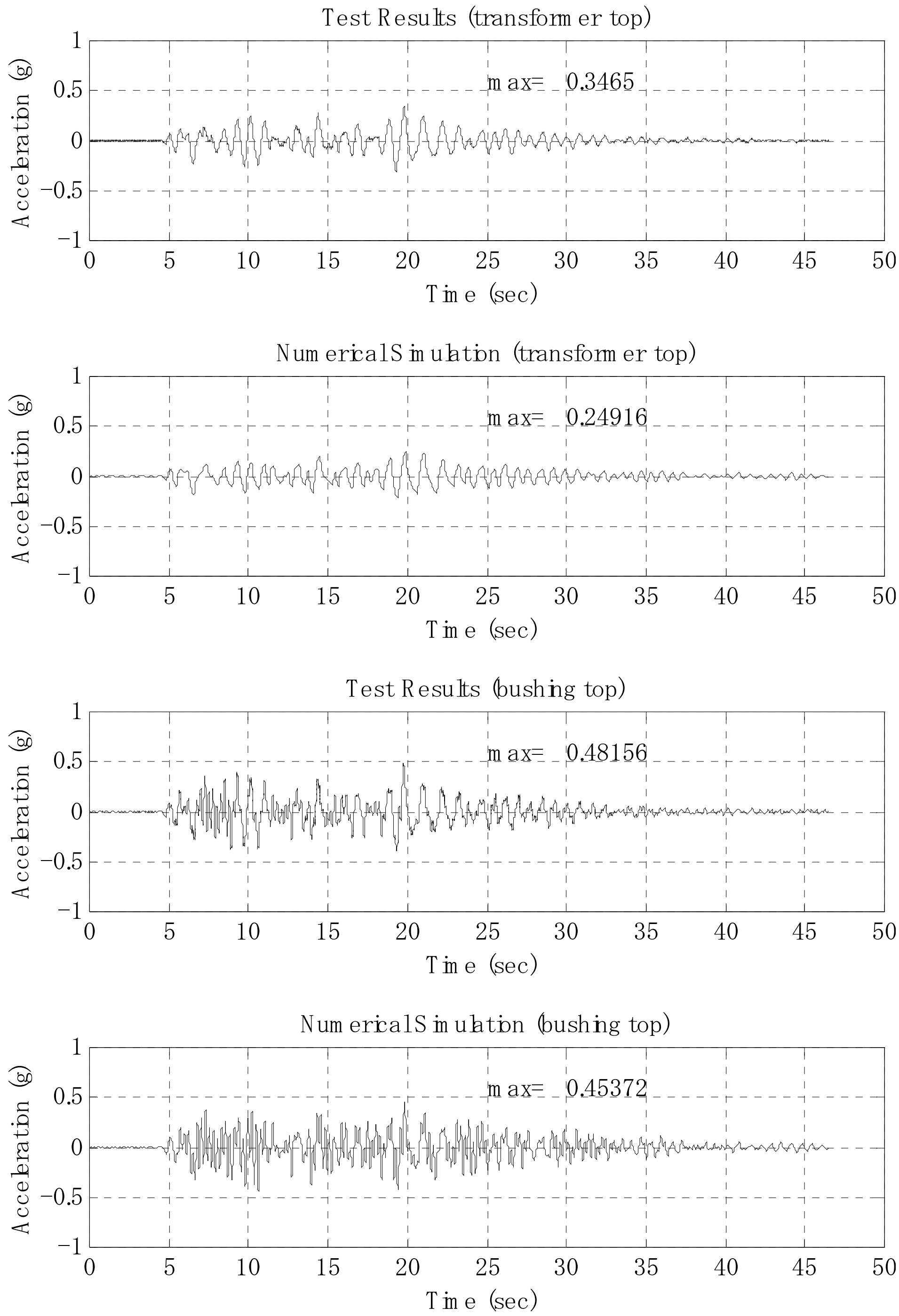

Figure 5-26 Comparison of Test Results and Numerical Simulation: RB/Art-693/x375

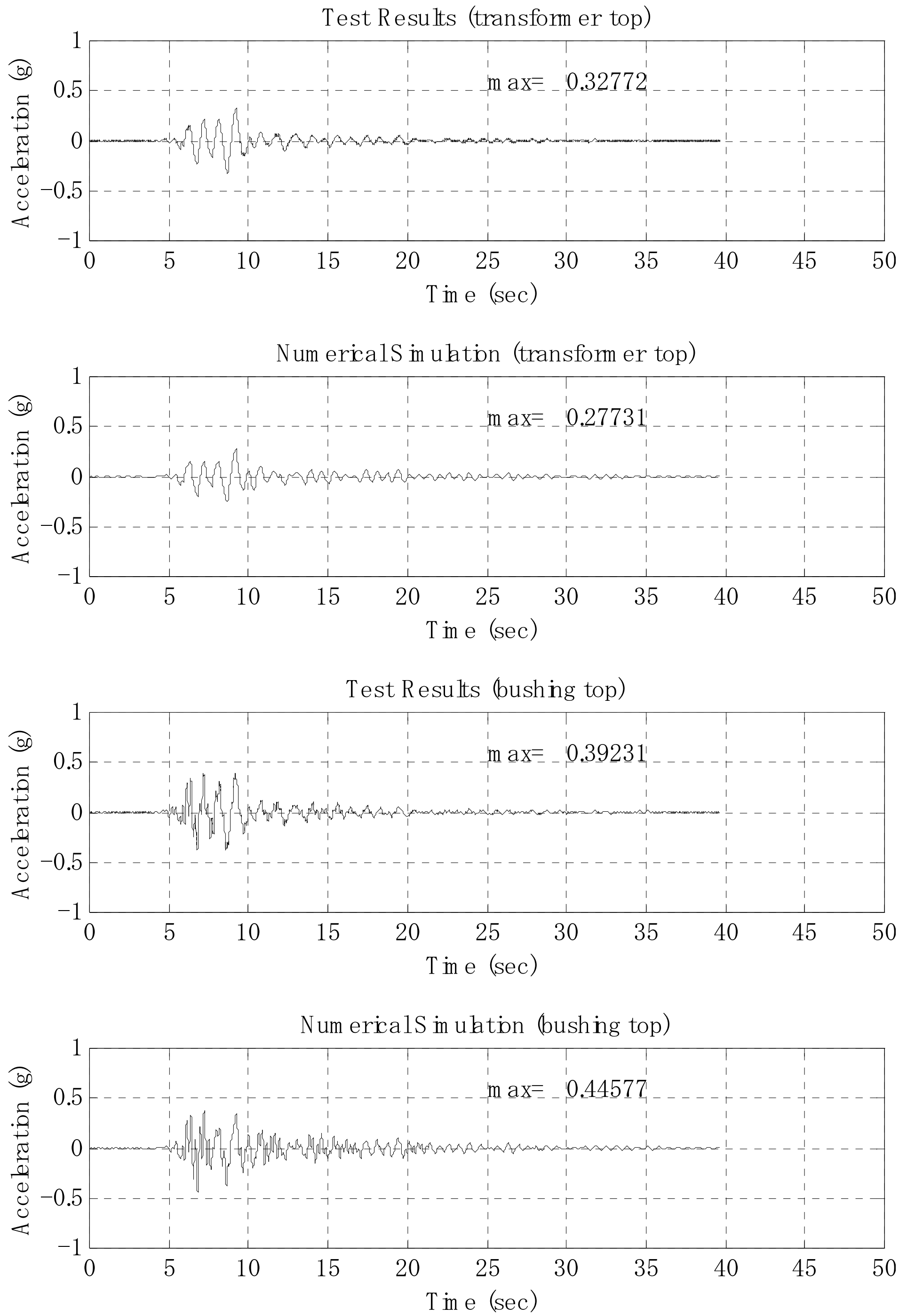

Figure 5-27 Comparison of Test Results and Numerical Simulation: RB/Kobe/x375

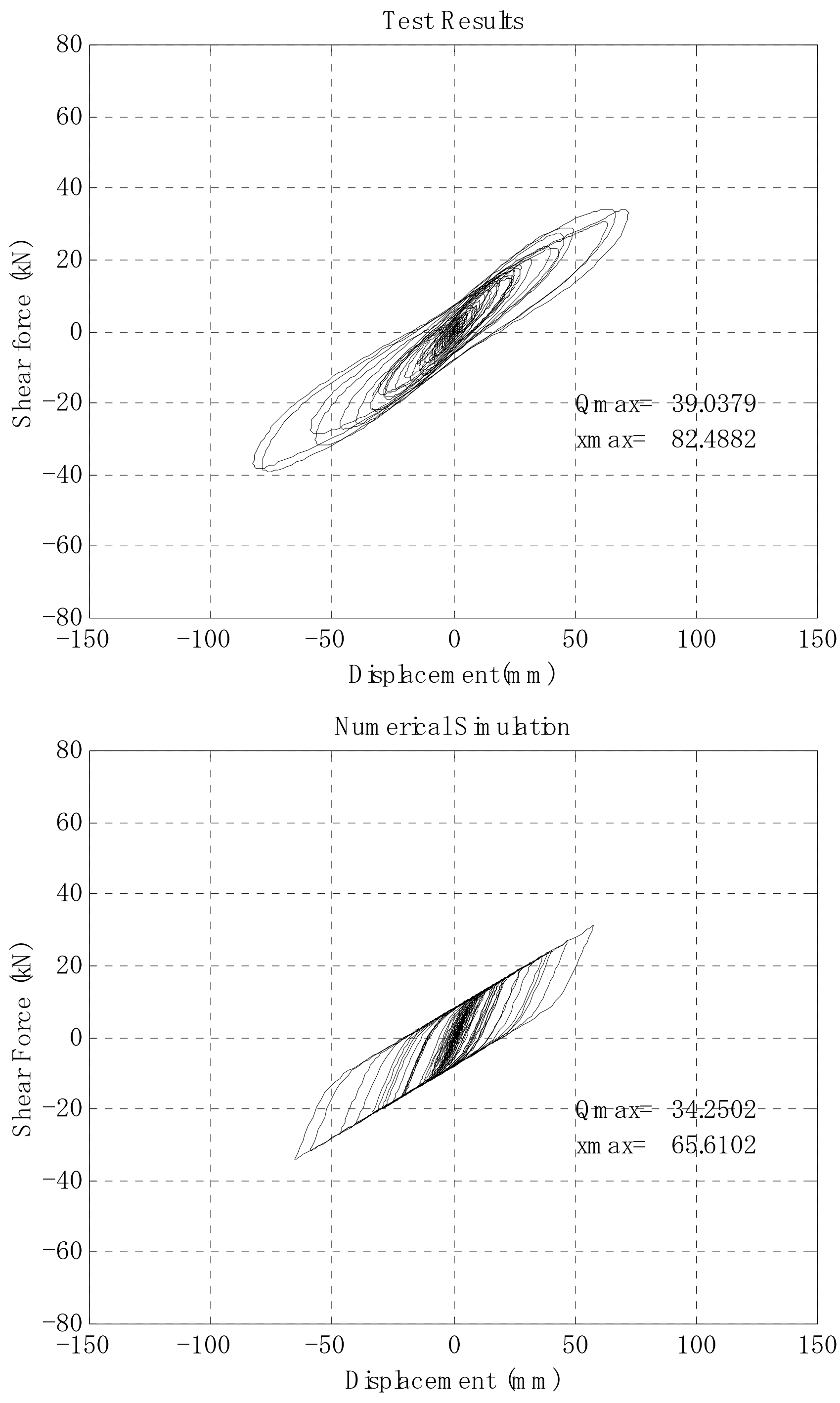

Figure 5-28 Comparison of Force-Displacement Curves in Test Results and Numerical Simulation: FB/Art-693/x375

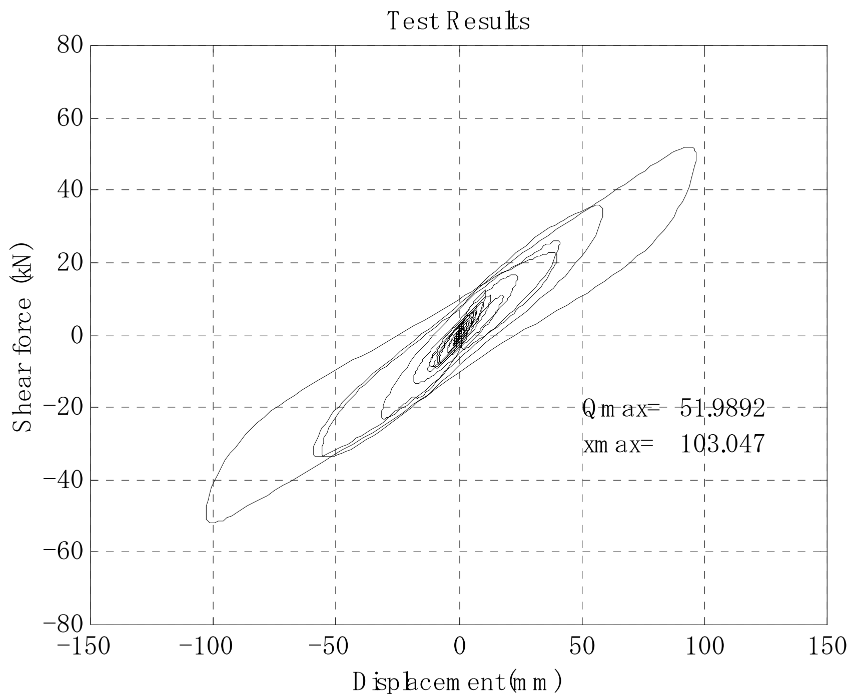

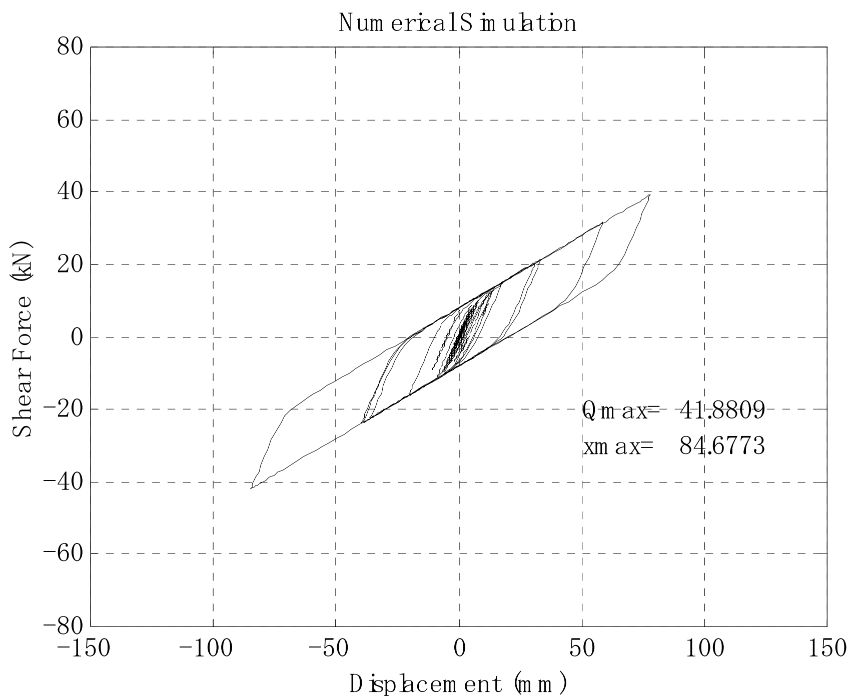

Figure 5-29 Comparison of Force-Displacement Curves in Test Results and Numerical Simulation: RB/Kobe/x375

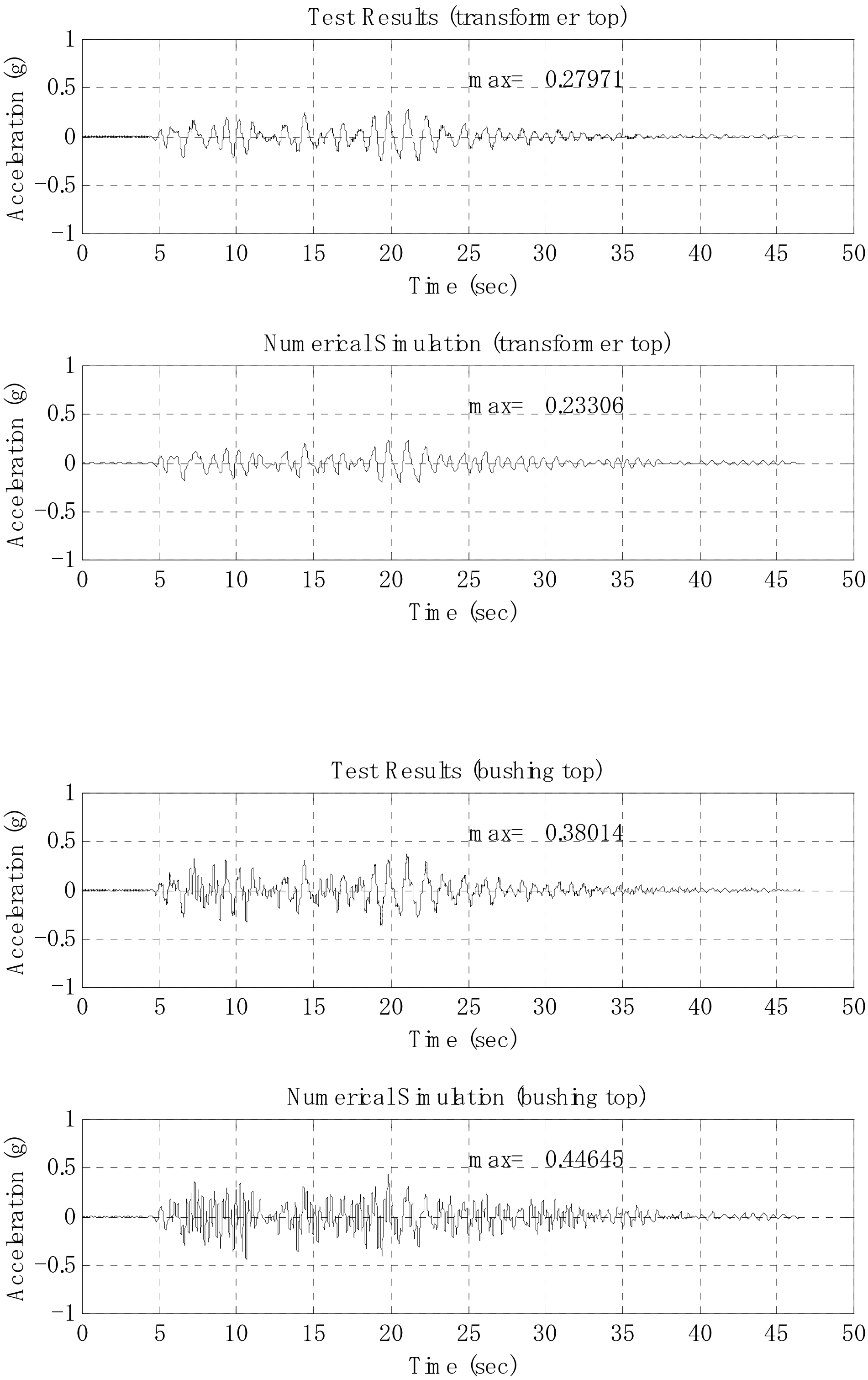

Figure 5-30 Comparison of Test Results and Numerical Simulation in RB/Art-693/xy375, x-dir.

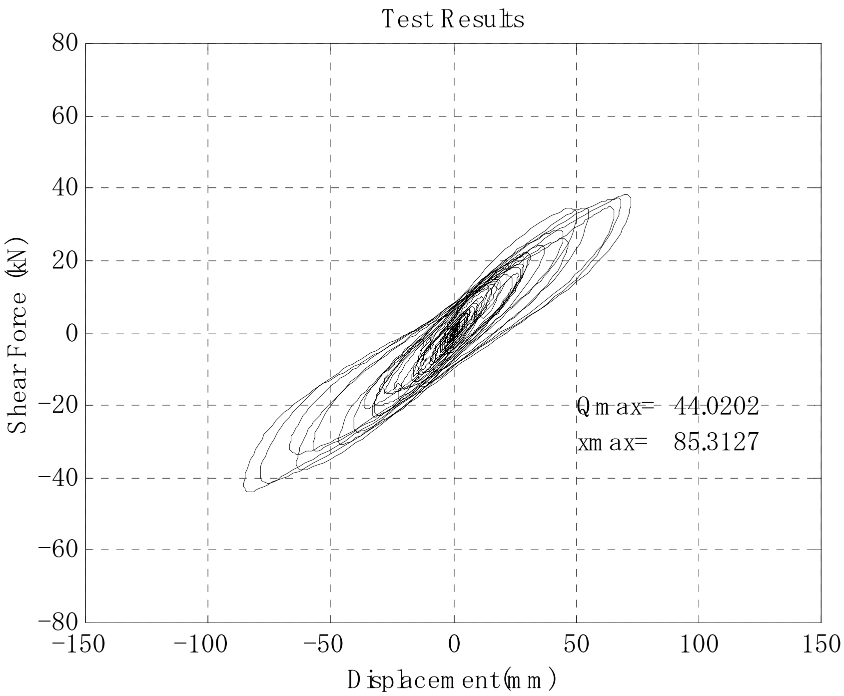

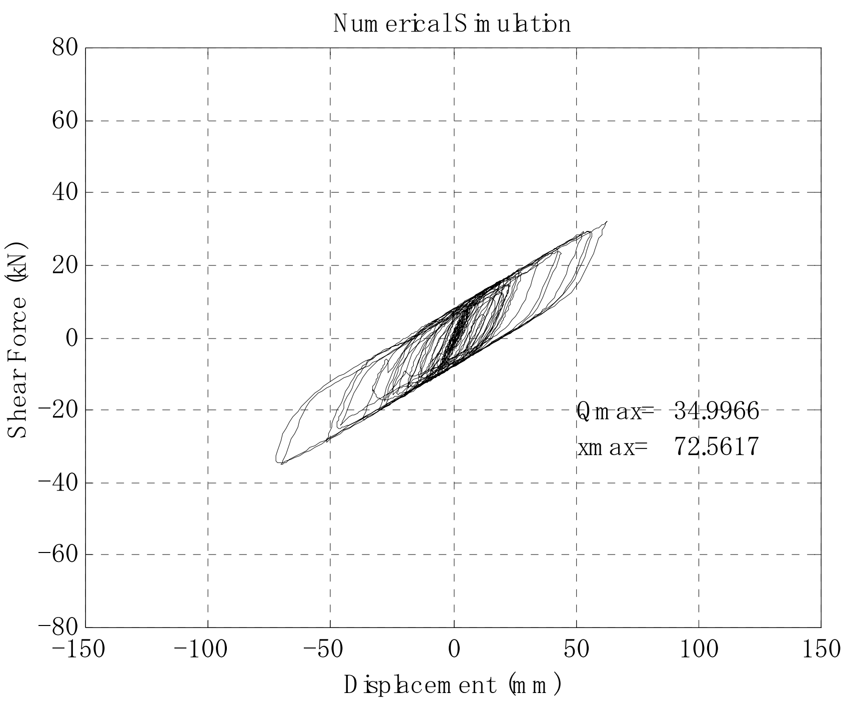

Figure 5-31 Comparison of Force-Displacement Curves in Test Results and Numerical Simulation: RB/Art-693/xy375, x-dir.

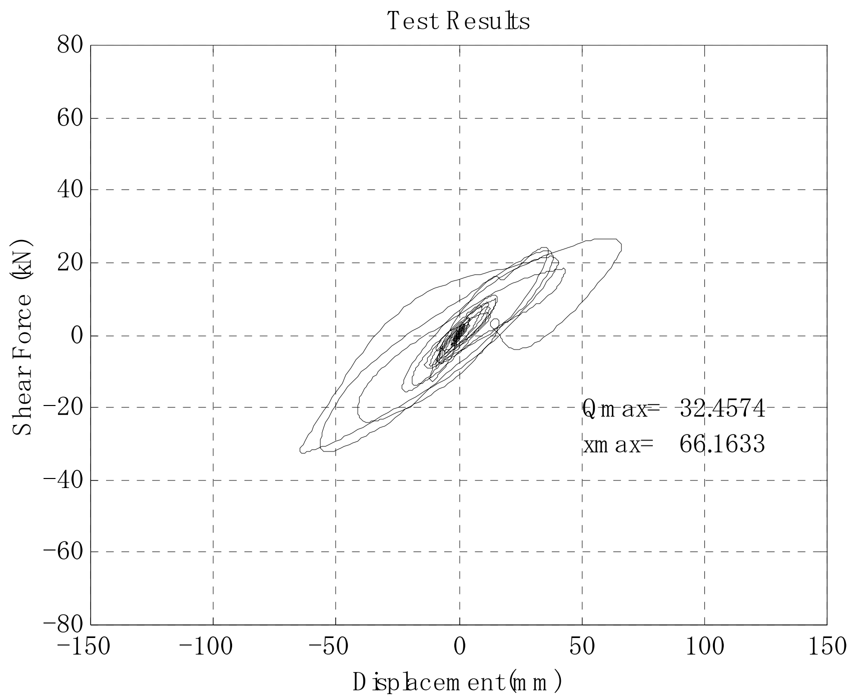

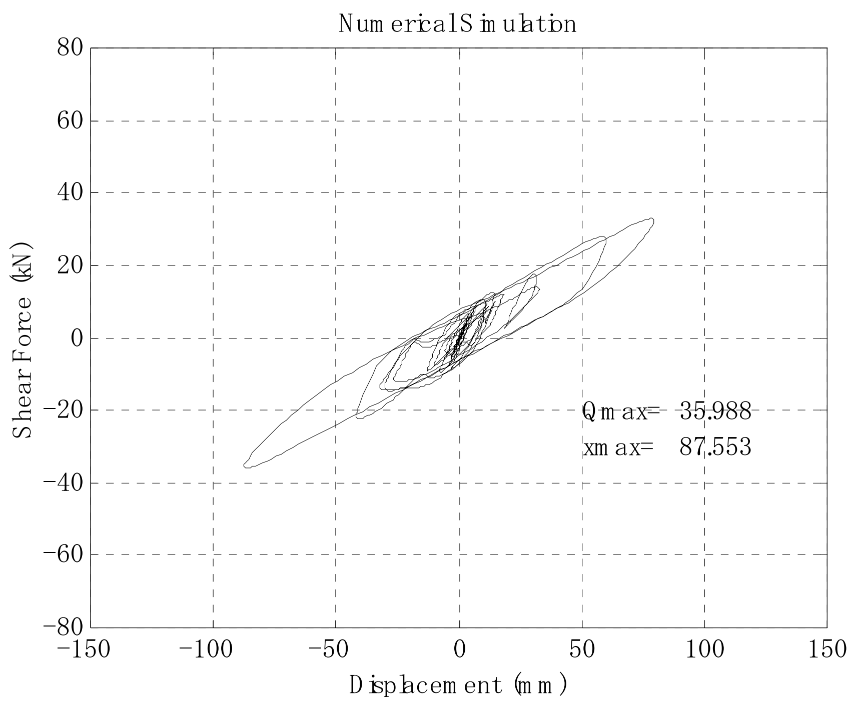

Figure 5-32 Comparison of Force-Displacement Curves in Test Results and Numerical Simulation: RB/Kobe/xy250, x-dir.

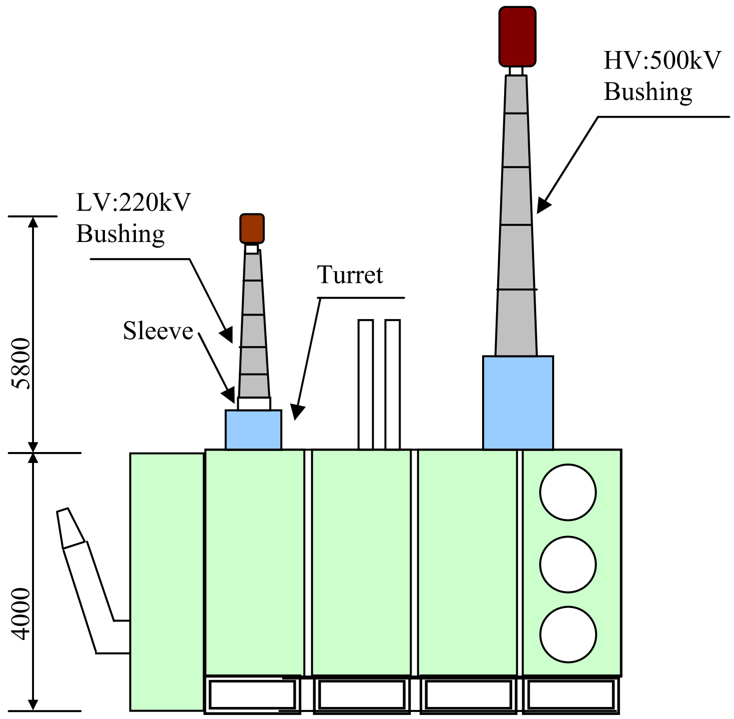

Transformer body weight: 1785(kN)
Bushing weight (220kV) : 29.6(kN), weight (mass) ratio=0.0166

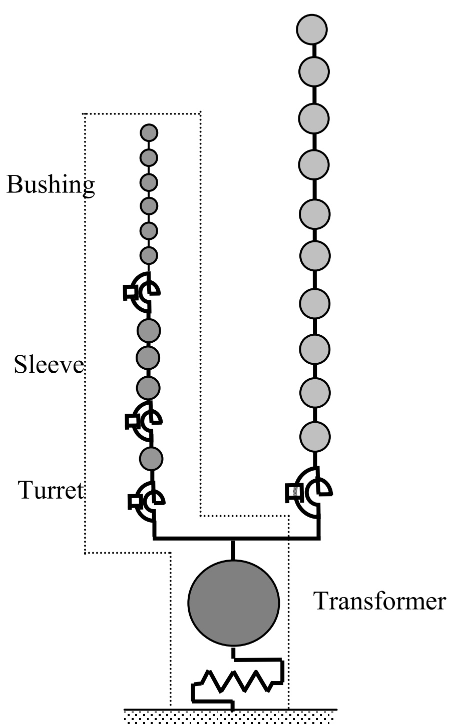

Node	Z-cor.(mm)	Mass (kg)
1	8345	96
2	9808	172
3	9316	55
4	8834	83
5	7852	128
6	6948	9
7	7336	155
8	7040	0
9	7048	9
10	6848	0
11	5434	2100
12	5349	0
14	6840	0
17	4020	182000
18	2200	0
19	0	0

Figure 5-33 Case Study: 220kV/500kV Transformer and Numerical Model

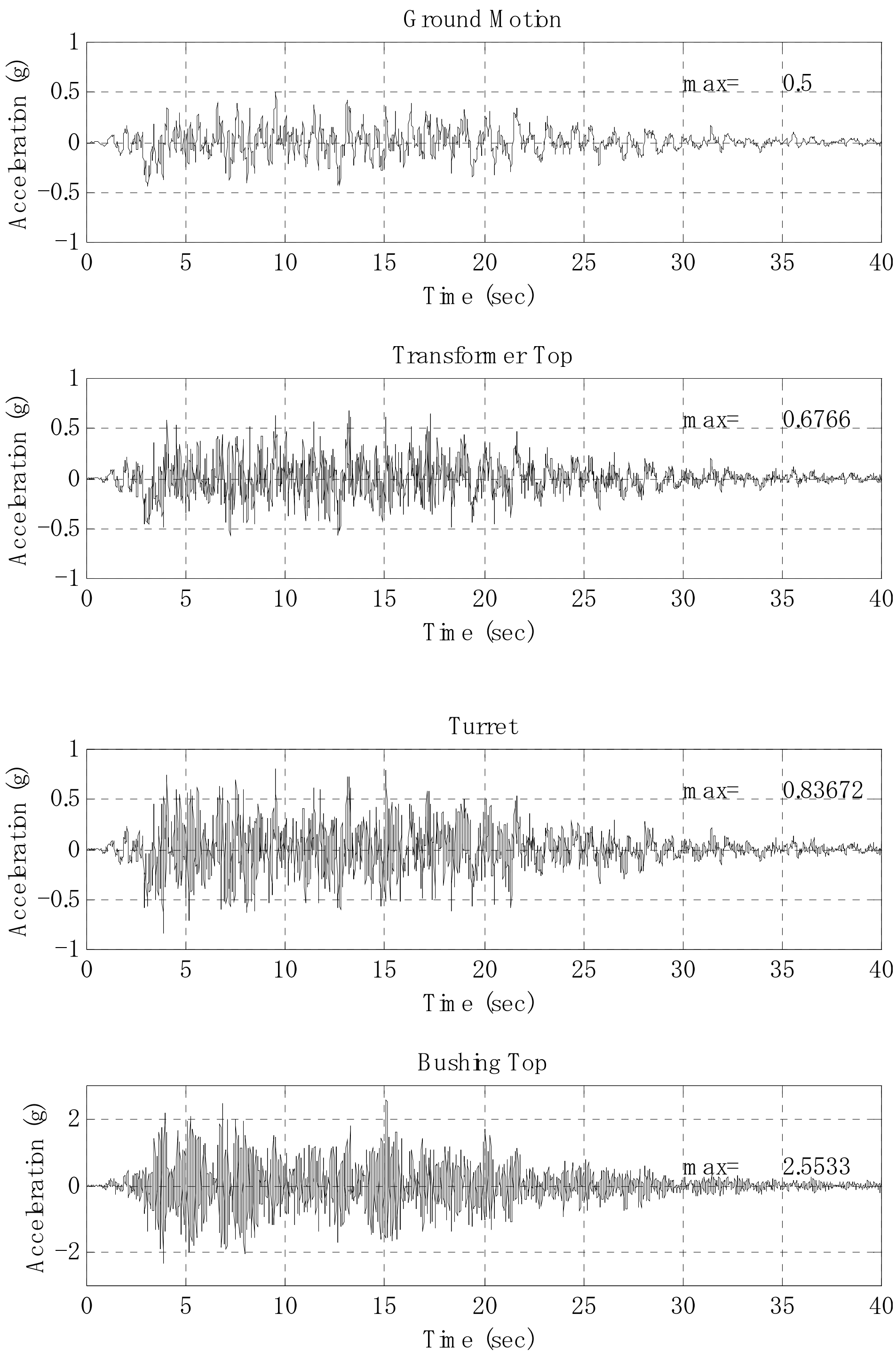

Figure 5-34 Time Histories of Fixed-Base System: Art-693 x0.5gz0.4g

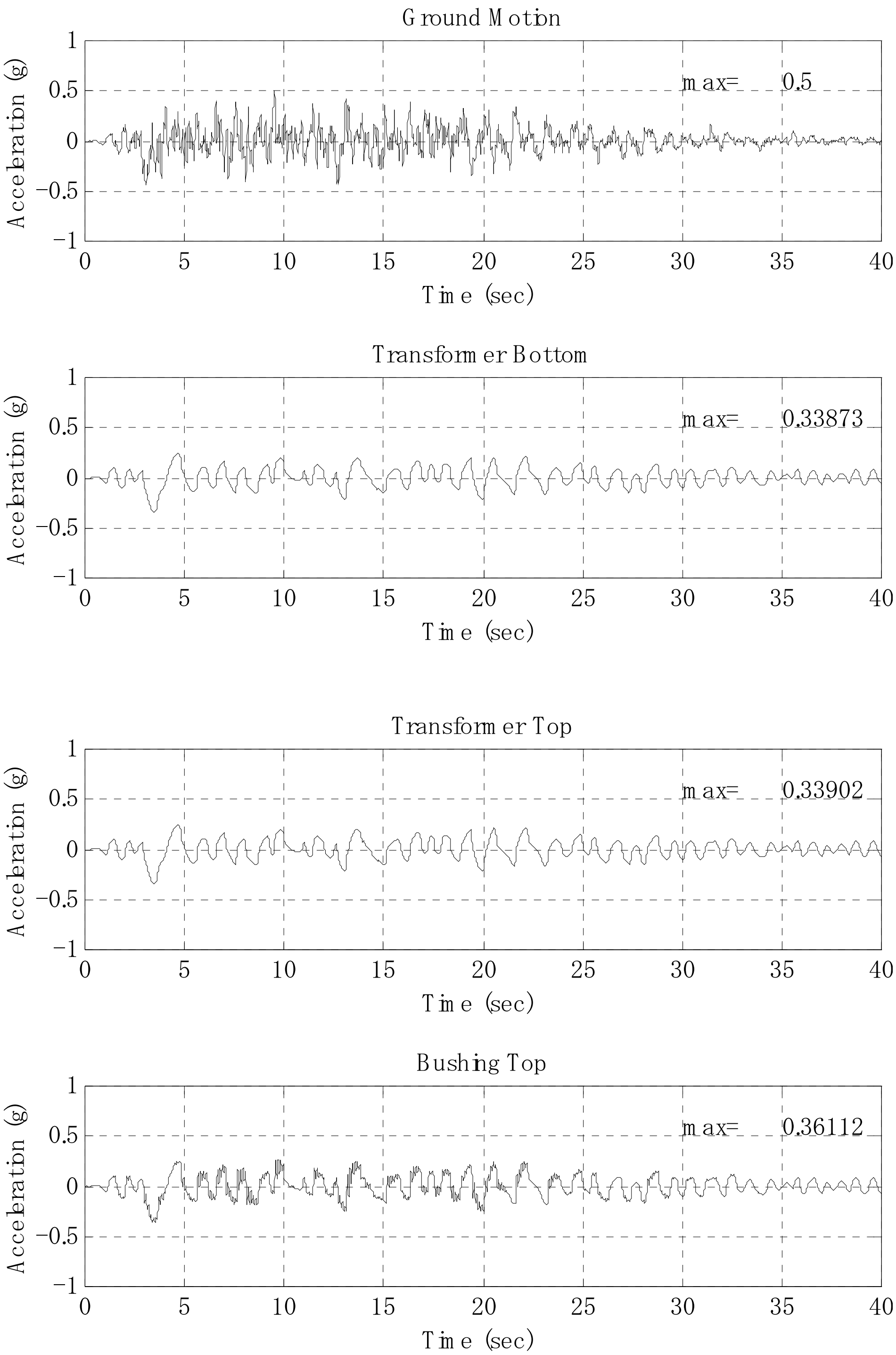

Figure 5-35 Time Histories of Base-Isolated System/SHRB: Art-693 x0.5gz0.4g

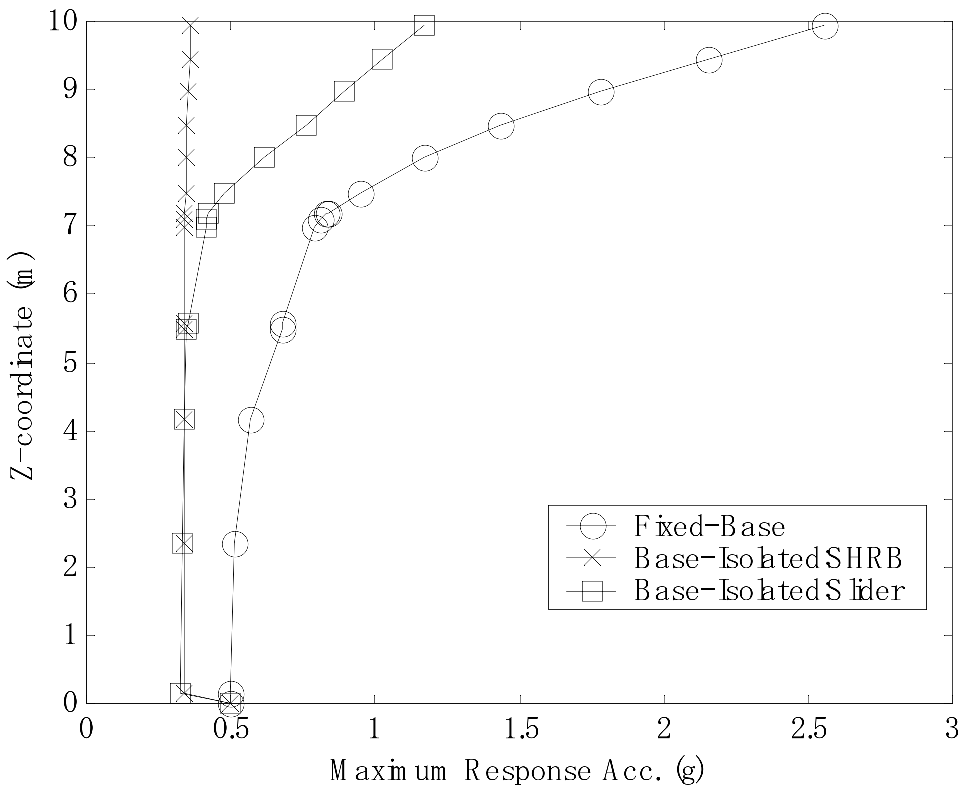

Figure 5-36 Maximum Response Acceleration at each Node in Fixed-Base, Base-Isolated-SHRB, and Base-Isolated-Slider System : Art-693 x0.5g z0.4g

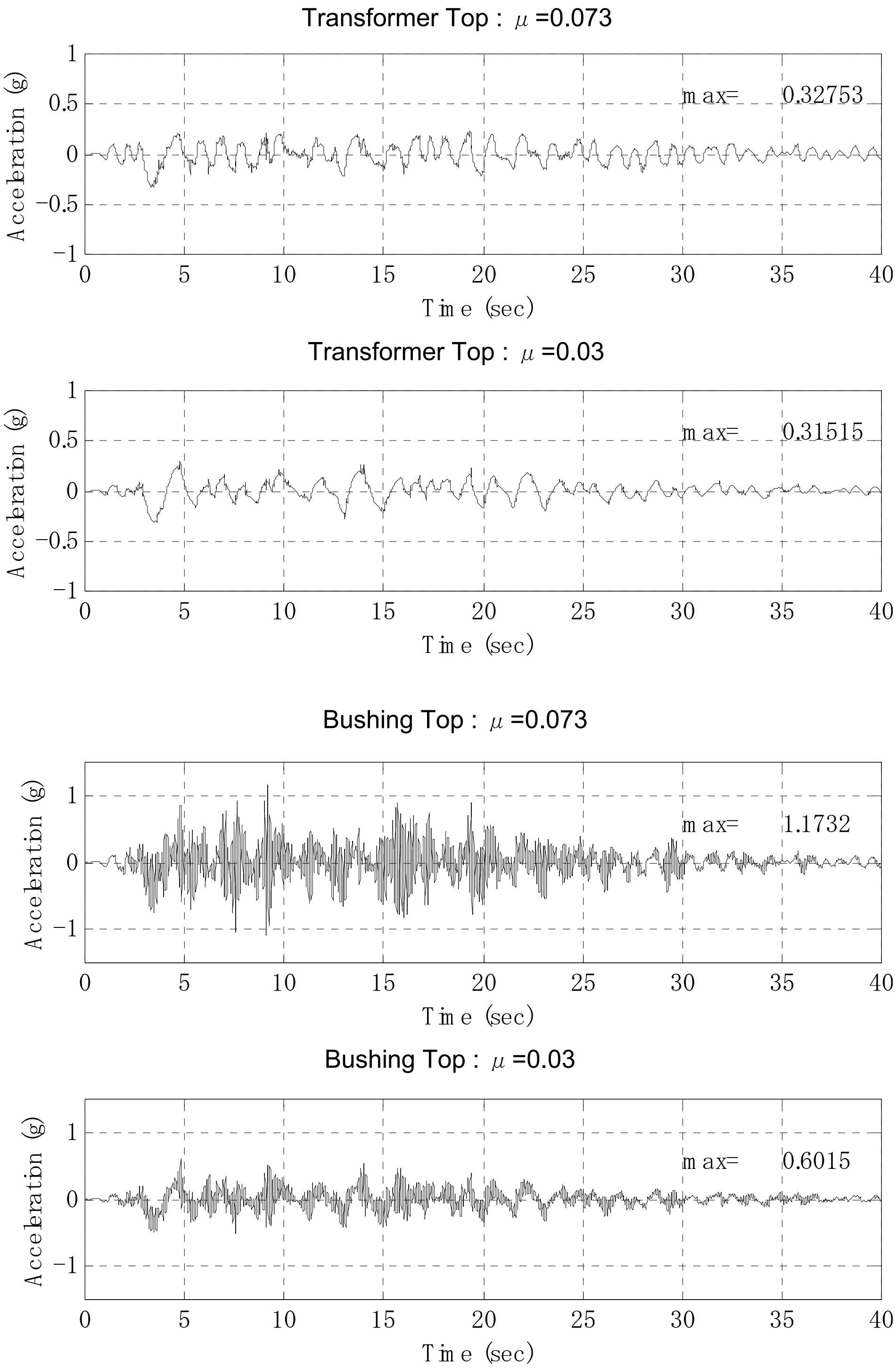

Figure 5-37 Comparison of Response Acceleration in Sliding System with Friction Coef.=0.073 and 0.03: Art-693 x0.5gz0.4g

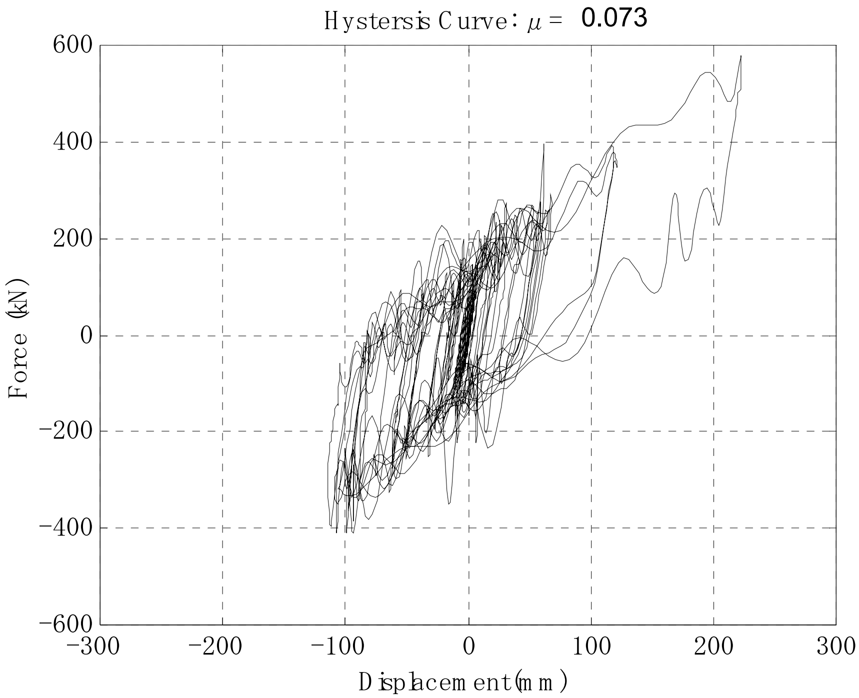

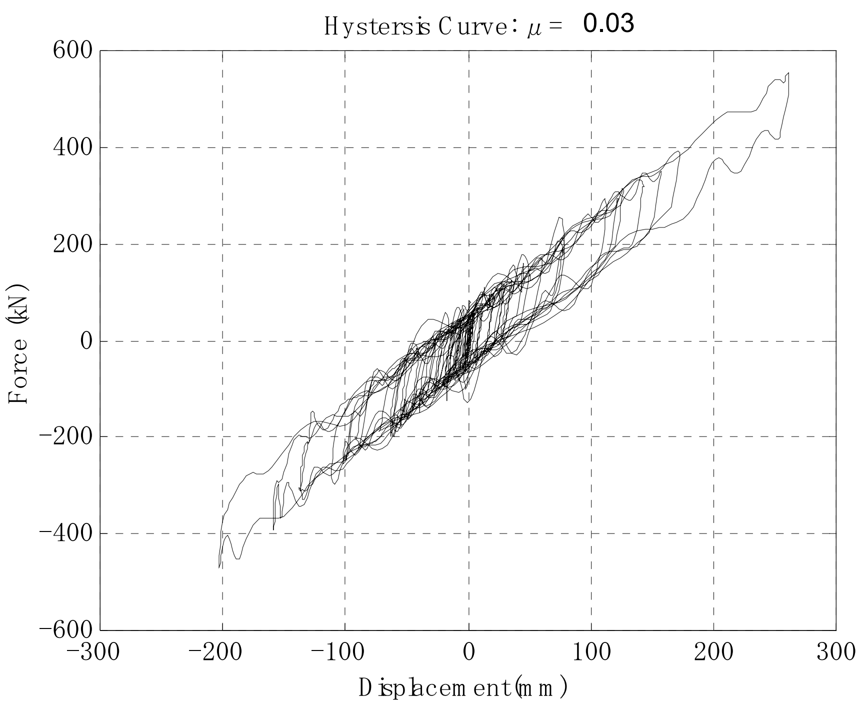

Figure 5-38 Comparison of Force-Displacement Curves in Sliding System with Friction Coef. =0.073 and 0.03: Art-693 x0.5gz0.4g

SECTION 6
CONCLUSIONS

6.1 Background

This report presents a comprehensive study using a tri-axial earthquake simulator to analyze applicability of base isolation technology for seismic protection of transformers. The testing was carried out with a large-scale transformer model with a real porcelain bushing in two phases. In Phase-1, the combination of sliding bearings and low-damping bearings for re-centering were developed and applied as an isolation system. In Phase-2 testing, the segmented high-damping rubber bearings were used. Analytical study by non-linear time history analysis was conducted to verify the test results and further study the dynamic response of the base-isolated transformer including the case study. Finally, the case study of a real transformer system was conducted by non-linear time history analysis.

6.2 Conclusions

Many significant conclusions were made through this research. They are listed as follows.

1. This study represents the first effort in testing based-isolated large-scale transformer/bushing systems using an earthquake simulator.
2. A base isolation system using conventional rubber bearings is not suitable for seismic protection of a lightweight structure such as a transformer (most of which are less than 2 MN) because of its limited ability to lengthen the natural period of the entire isolated system. This difficulty was alleviated in this study by: 1) combining sliding bearings with rubber bearings; and 2) using segmented high-damping rubber bearings.
3. The effectiveness of the proposed base isolation system in reducing the response acceleration of the transformer/bushing systems was demonstrated in the uni-axial and bi-axial earthquake simulator tests.
4. The tri-axial earthquake simulator test with the sliding system provided highly valuable information, which was not previously available. The response acceleration of the

bushing in the base-isolated system was sometimes larger than that of the fixed-based system. This is believed to be due to the fact that the friction force of the sliding bearing is affected by the vertical load change of the system involving high-frequency components, stimulating the high-frequency mode of the bushing in the horizontal direction. The vertical frequency characteristics are dependent on the compressive stiffness of the isolators. Therefore, the compressive stiffness of the sliding system should be carefully designed not to induce the high-mode vibration of the bushing.

5. On the other hand, no coupling effect was seen in the system of segmented high-damping rubber bearings.
6. Rubber rings were developed for the purpose of adding flexibility at the fixed end joint between the bushing and the transformer top. The rings worked well and the bushing acceleration was reduced in the testing. The flexible ring absorbed energy by rotational deformation without any failure or instability and reduced the transmission of force to the bushing.
7. The simplified numerical model for the transformer/bushing system was proposed and verified by comparing the results with the testing. The rotational movement around the fixed end is dominant in bushings, whereas shear movement is dominant in transformers.
8. The amplification of the bushing response with a sliding bearing system was verified by numerical simulation.
9. The friction coefficient of sliding bearings has a significant effect on the amplification of the bushing in tri-axial shaking. Lower friction coefficients, such as 0.04, are desired for application in the transformer system considering the bushing amplification.
10. The case study of real power transformer system strongly supported the efficacy of base isolation.

SECTION 7
REFERENCES

Anon., Computers and Structures, Inc. (1996), *SAP2000 Analysis Reference Manual, Version 6.13*, Berkeley, CA

Anon., IEEE 1998. *IEEE Std 693-1997*, “Recommended practices for seismic design of substations”, Piscataway, N.J.: IEEE Standards Department

Anon., International Conference of Building Officials (1997), “Earthquake Regulations for Seismic-Isolated Structures,” *Uniform Building Code*, Appendix Chapter 16, Whittier, CA

Anon., JESC E0001 (1999), Japan Electric Association, *Seismic Design Guideline of Electric Facilities in Substation* (in Japanese)

Anon., “www.ncree.gov.tw” *Tri-Axial Seismic Simulator*, National Center for Research on Earthquake Engineering, web site

Anon., The Power System Seismic Program Management Committee of the City of Los Angeles Department of Water and Power, (1995), “Intermediate Term Plan For Seismically Hardening the Los Angeles Transmission-Level Power Facilities,”

Bonacina, G & Bonetti, P.et al. (1995), “Seismic Base Isolation of Gas Insulated Electrical Substations: Design, Experimental and Numerical Activities, Evaluation of the Applicability,” 10th European Conference on Earthquake Engineering, Duma (ed.)

Buckle, I.G., and Liu, H.(1994).”Stability of Elastomeric Seismic Isolation Systems,” Seminar on Seismic Isolation, Passive Energy Dissipation, and Control, Applied Technology Council, Redwood City, Calif., pp.293-305

Chopra, A. K., *Dynamics of Structures: Theory and Applications to Earthquake Engineering*, PRENCTICE HALL

Clark, P.W., Aiken, I.D., and Kelly, J.M. (1997), “Experimental Studies of The Ultimate Behavior of Seismically-Isolated Structure,” Report No. UCB/EERC-97/18, Earthquake Engineering Research Center, College of Engineering, University of California, Berkeley

Constantinou, M.C., Mokha, A.S, and Reinhorn, A. M. (1990), “Experimental and Analytical

Study of a Combined Sliding Disc Bearing and Helical Steel Spring Isolation System," Technical Report NCEER-90-0019, National Center for Earthquake Engineering Research, State University of New York at Buffalo

Constantinou, M. C., Mokha, A.S, and Reinhorn, A. M. (1990) " Teflon Bearings in Base Isolation II: Modeling", J. Struct. Engrg. ASCE, 116(2), 455-474

Feng, M. Q. and Okamoto, S.(1994), "Shaking Table Tests on Base-Isolated Bridges with Flexible Piers," Proceedings of Third US-Japan Workshop of Protective Systems for Bridges, Berkeley, CA.

Fujita, T., Fujita, S., and Yoshizawa, T. (1984), "Base Isolation Support of Heavy Equipment with Laminated Rubber Bearings –1," *The Japan Society of Mechanical Engineers, 50-454, 1984-6*, (in Japanese)

Fujita, T., Fujita, S., Yoshizawa, T., and Suzuki, S. (1985), "Base Isolation Support of Heavy Equipment with Laminated Rubber Bearings –2," *The Japan Society of Mechanical Engineers, 51-461, 1985-1*, (in Japanese)

Gent, A.N. and Lindley, P.B. (1959), "The Compression of Bonded Rubber Blocks," Proceedings of Institution of Mechanical Engineers, London, Vol.173, No.3, pp.111-122

Gilani, A.S., Chavez, J.W., Fenves, G.L. and Whittaker, A.S. (1998), "Seismic Evaluation of 196kV Porcelain Transformer Bushings", Report No.PEER-98-02, Pacific Earthquake Engineering Research Center, University of California, Berkeley

Gilani, A.S., Chavez, J.W., Fenves, G.L. and Whittaker, A.S. (1999), " Seismic Evaluation of 550kV Porcelain Transformer Bushings," PEER 1999/05 October 1999

Gilani, A.S., Chavez, J.W., Fenves, G.L. and Whittaker, A.S. (1999), "Seismic Evaluation and Retrofit of 230-kV Porcelain Transformer Bushings," PEER 1999/14 Dec.1999

Iizuka M., Takaoka E., Takenaka, Y. and Yoshikawa, K. (1998), "Shaking Table Tests of Base Isolation Systems Consisting of Rubber Bearings and Sliding Bearings," Proceedings of The 10th Earthquake Engineering Symposium, Yokohama, Japan

Ishizuka, H., Murota, N., and Fukumori, T. (1995), "Dynamic and Failure Properties of High Damping Rubber Bearing under High Axial Stress," PVP-Vol.319, Seismic Shock and

Vibration Isolation ASME

Kelly, J.M. (1993), *Earthquake-Resistant Design with Rubber*, 2nd ed., Springer-Verlag, London

Koh, C.G. and Kelly, J.M. (1988), "A Simple Mechanical Model for Elastomeric Bearings Used in Base Isolation," International Journal on Mechanical Science, 30, pp.933-943

Masaki, N. (1999), "Study of Multistage Rubber Bearings for Seismic Isolation and Vibration Control System," Dissertation for Doctor of Engineering from The University of Tokyo

Mullins, L., "Softening of Rubber by Deformation," *Rubber Chemistry and Technology*, 42(1): pp.339-362, 1962

Murota, N., Goda, K., Suzuki, S., Sudo, C., and Suizu, Y., "Recovery Characteristics of Dynamic Properties of High Damping Rubber Bearings," Proceedings of the Third U.S.-Japan Workshop on Protective Systems for Bridges, pp.2-63 – 2-76, Berkeley, California, 1994

Nagarajaiah, S., Reinhorn, A.M., and Constantinou, M.C., "3D-BASIS Nonlinear Dynamic Analysis of Three-Dimensional Base Isolated Structures: Part II," Technical Report NCEER-91-0005, National Center for Earthquake Engineering Research, State University of New York at Buffalo

Pansini, J.A. (1988), *Electrical Transformers and Power Equipment*, by Prentice Hall

Park, Y. J., Wen, Y. K. and Ang, A. H. S., (1986), "Random Vibration of Hysteretic System under Bi-Directional Ground Motions" Earthquake Eng. Struct. Dyn., 14(4), 543-557

Sato, H., Sato, K., Tohma, J., and Higashi, S., (2002) "Estimation of Strong Ground Motion Using KIK-NET Records and Its Application for Investigation of The Cause of Structure Damage – A Case Study of Electrical Substation Structure Damage during the 2000 Tottori-ken-Seibu Earthquake," AIJ J.Technol.Des, No.15, p93-98, Jun.

Serino, G., Bonacina, G. and Bettinali, F. (1995), "Passive Protection Devices for High-Voltage Equipment: Design Procedures and Performance Evaluation," Proceedings of the Fourth U.S.Conference Sponsored by the Technical Council on Lifeline Earthquake Engineering/ASCE

Shinozuka, M., Rose, A., and Eguchi R.T., ed. *Engineering and Socioeconomic Impacts of Earthquakes*, Monograph Series 2, Multidisciplinary Center for Earthquake Engineering Research, State University of New York at Buffalo

Shinozuka, M.,ed. (1995), "The Hanshin-Awaji Earthquake of January 17:1995 Performance of Lifelines," Technical Report NCEER-95-0015, Buffalo, N.Y.: National Center for Earthquake Engineering Research, State University of New York

Skinner I.R., Robinson H.W., and McVerry H.G. (1993), *An Introduction to Seismic Isolation*, *John Wiley & Sons Ltd*

Thomas, A.G. (1982), "The Design of Laminated Bearings I," Proceedings of the International Conference on Natural Rubber for Earthquake Protection of Building and Vibration Isolation, Kuala Lumpur, Malaysia, February, pp.229-246

Villaverde, R., Pardoen, G., (1999), "Ground Motion Amplification at Base of Bushings Mounted on Electric Substation Transformer," A Technical Report of Research Supported by PEER/PG&E Under Award No. PGE-09566, Department of Civil Engineering, University of California, Irvine

Wen, Y. K. (1976) "Method of Random Vibration of Hysteretic Systems" J. of Engrg. Mech. Div. ASCE, 102(EM2), 249-263

Wilcoski, J. (1997), "Demonstration of CERL Equipment Fragility and Protection Procedure by Fragility Testing of a Power Transformer Bushing," ATC-29-1, Seminar Technical Papers, p.349

APPENDIX A

ADDITIONAL TEST RESULTS

Transformers are cable-connected to equipment in substations. The seismic interaction between base-isolated transformers and other equipment is an important factor to be considered in the design of the system. As a preliminary study of the interaction problem, the transformer/bushing system in Phase-2 was cable-connected to a pole, fixed on the platform of the simulator, and then subjected to uni-axial shaking. An aluminum strand cable, which had been previously used in a substation, was connected from the top of the bushing to the pole top.

A.1 Experimental Setup

Figures A-1 and A-2 show the experimental setup. The purpose of the testing was to investigate the influence of the cable-connection to the response of the transformer model and the bushing. The specification of the cable was "954MCM AAC" (code word "Magnolia" in the ASTM B231) and its material was pure aluminum of "E. C. Grade." The diameter was 28.55 mm and the tensile strength was 7420 kg. The stranding was of Class AA and 37×4.079 mm diameter, Figure A-3. As shown in Figure A-2, the length of the cable was 2660 mm and the horizontal distance from the pole to the bushing was 1880 mm. The horizontal displacement of the transformer to where the cable would start to harden and pull the pole was calculated from the geometry of Figure A-2 as 493.9 mm. The maximum displacement of the base-isolated transformer/bushing system was assumed as less than 200 mm according to the results in the Phase-2 testing. Therefore, the cable had enough length to accommodate the movement of the base-isolated transformer model without hardening.

An H-beam measuring 200 mm x 200 mm x 16 mm was used as the pole fixed to the platform of the simulator. The natural frequencies of the pole with a clamped-free condition were calculated as 9.18 Hz in the 1st mode and 57.5 Hz in the 2nd mode.

A.2 Testing Program

The earthquake records and the PGA are summarized in Table A-1. The 161-kV bushing was installed on to the transformer model without the use of a rubber ring. The transformer with and without an SHRB base isolation system was subjected to the uni-axial shaking.

Table A-1 Program of Additional Testing

Earthquake Record	PGA in x-direction
Art-693	0.25 g, 0.375 g
Kobe (Takatori)	0.25 g, 0.375 g
Chi-Chi	0.25 g, 0.375 g

A.3 Test Results

The maximum response acceleration at each measurement point in the fixed-base and base-isolated system is shown in Figure A-4. The effect of base isolation is very obvious. In Figures A-5 and A-6, the results of the response acceleration and displacement in the base-isolated system (with and without cable-connection), are compared. The results of the system without cable-connection were picked up from Phase-2 test results. A significant difference is observed in response acceleration at the top of the bushing for the with/without conditions of cable-connection. The response acceleration of the bushing top with cable-connection was amplified 1.5 to 2.0 times the acceleration at the transformer top.

Figure A-7 shows the normalized Fourier amplitude of response acceleration at the bushing- top and the pole-top. According to the results, the pole has its dominant frequency at around 14.6 Hz. The Fourier amplitude at the bushing top also has a second peak around 14 Hz corresponding to the dominant frequency of the pole. This indicates an interaction between the cable-connected bushing and pole.

A.4 Summary

The base-isolated transformer/bushing system with cable-connection was subjected to a uni-axial shaking test to investigate the interaction between the bushing and the ground-fixed pole.

Although the results show some effectiveness of the base isolation in comparison with fixed-base system, an interaction exists between the bushing and the pole. Enough attention should be paid to the relationship between the transformer and other connected facilities in the design of base isolation systems. The test results prompt further study on this problem.

Figure A-1 Cable-Connected Base-Isolated Transformer Model

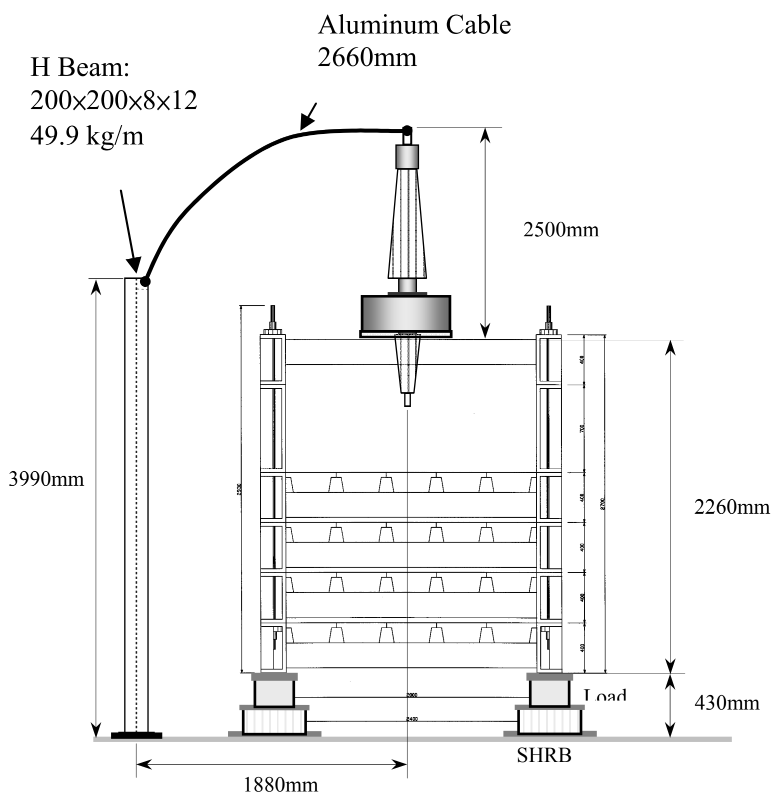

Figure A-2 Geometry of the Test Setup

Figure A-3 An Aluminum Strand Cable: Class AA / 37×4.079 mm dia.

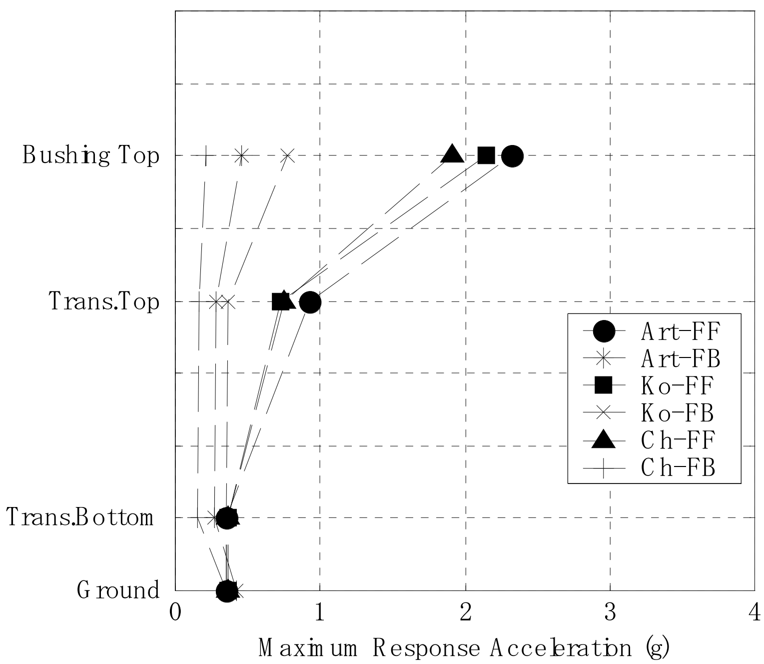

Figure A-4 Maximum Response Acceleration at each Measurement Point in the Fixed-Base and the Base-Isolated System

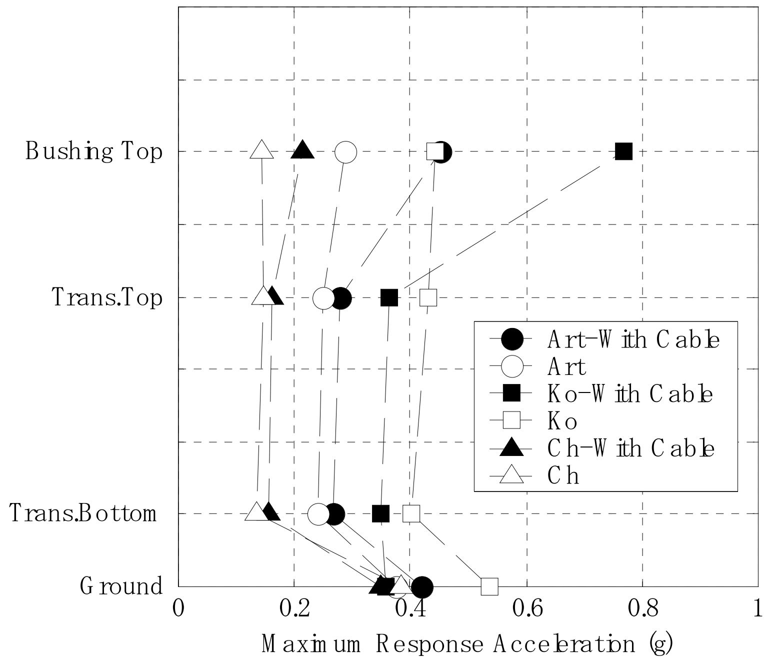

Figure A-5 Maximum Response Acceleration at each Measurement Point in the Base-Isolated System

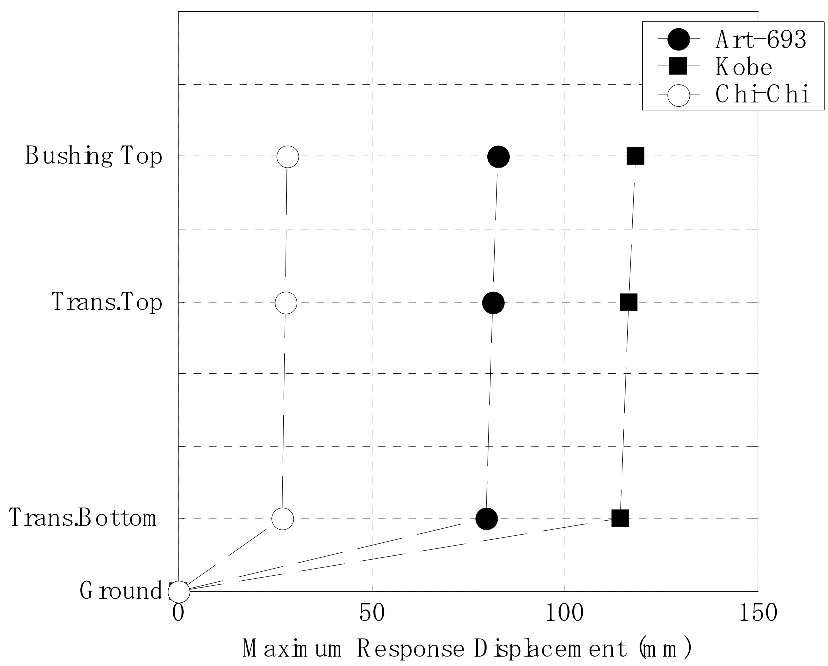

Figure A-6 Maximum Response Displacement at each Measurement Point in the Base-Isolated System

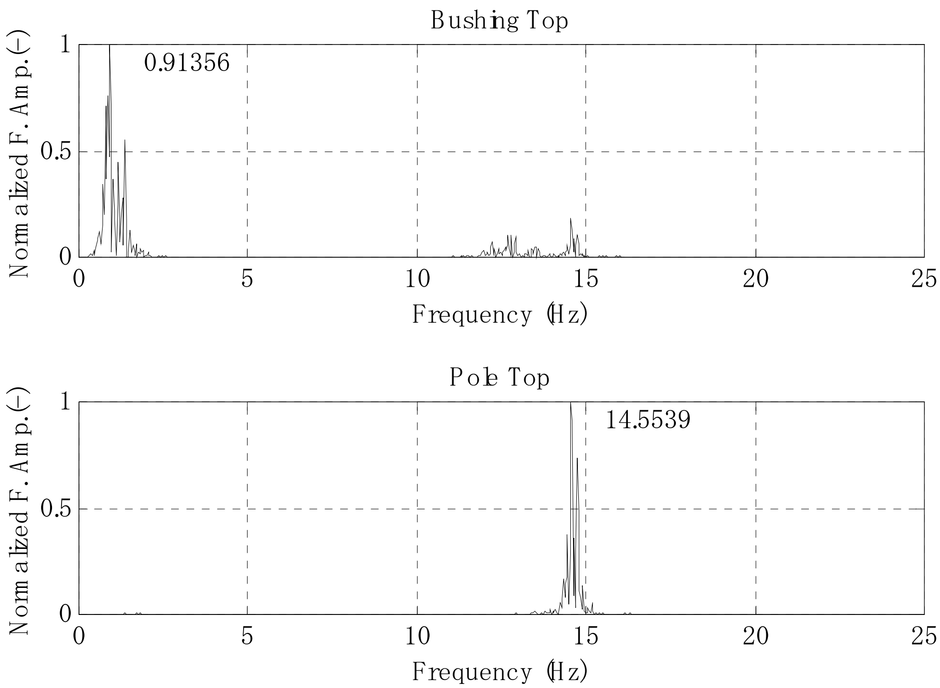

Figure A-7 Normalized Fourier Amplitude at Bushing Top and Pole Top in Base-Isolated System under Art/x375

Multidisciplinary Center for Earthquake Engineering Research
List of Technical Reports

The Multidisciplinary Center for Earthquake Engineering Research (MCEER) publishes technical reports on a variety of subjects related to earthquake engineering written by authors funded through MCEER. These reports are available from both MCEER Publications and the National Technical Information Service (NTIS). Requests for reports should be directed to MCEER Publications, Multidisciplinary Center for Earthquake Engineering Research, State University of New York at Buffalo, Red Jacket Quadrangle, Buffalo, New York 14261. Reports can also be requested through NTIS, 5285 Port Royal Road, Springfield, Virginia 22161. NTIS accession numbers are shown in parenthesis, if available.

NCEER-87-0001 "First-Year Program in Research, Education and Technology Transfer," 3/5/87, (PB88-134275, A04, MF-A01).

NCEER-87-0002 "Experimental Evaluation of Instantaneous Optimal Algorithms for Structural Control," by R.C. Lin, T.T. Soong and A.M. Reinhorn, 4/20/87, (PB88-134341, A04, MF-A01).

NCEER-87-0003 "Experimentation Using the Earthquake Simulation Facilities at University at Buffalo," by A.M. Reinhorn and R.L. Ketter, to be published.

NCEER-87-0004 "The System Characteristics and Performance of a Shaking Table," by J.S. Hwang, K.C. Chang and G.C. Lee, 6/1/87, (PB88-134259, A03, MF-A01). This report is available only through NTIS (see address given above).

NCEER-87-0005 "A Finite Element Formulation for Nonlinear Viscoplastic Material Using a Q Model," by O. Gyebi and G. Dasgupta, 11/2/87, (PB88-213764, A08, MF-A01).

NCEER-87-0006 "Symbolic Manipulation Program (SMP) - Algebraic Codes for Two and Three Dimensional Finite Element Formulations," by X. Lee and G. Dasgupta, 11/9/87, (PB88-218522, A05, MF-A01).

NCEER-87-0007 "Instantaneous Optimal Control Laws for Tall Buildings Under Seismic Excitations," by J.N. Yang, A. Akbarpour and P. Ghaemmaghami, 6/10/87, (PB88-134333, A06, MF-A01). This report is only available through NTIS (see address given above).

NCEER-87-0008 "IDARC: Inelastic Damage Analysis of Reinforced Concrete Frame - Shear-Wall Structures," by Y.J. Park, A.M. Reinhorn and S.K. Kunnath, 7/20/87, (PB88-134325, A09, MF-A01). This report is only available through NTIS (see address given above).

NCEER-87-0009 "Liquefaction Potential for New York State: A Preliminary Report on Sites in Manhattan and Buffalo," by M. Budhu, V. Vijayakumar, R.F. Giese and L. Baumgras, 8/31/87, (PB88-163704, A03, MF-A01). This report is available only through NTIS (see address given above).

NCEER-87-0010 "Vertical and Torsional Vibration of Foundations in Inhomogeneous Media," by A.S. Veletsos and K.W. Dotson, 6/1/87, (PB88-134291, A03, MF-A01). This report is only available through NTIS (see address given above).

NCEER-87-0011 "Seismic Probabilistic Risk Assessment and Seismic Margins Studies for Nuclear Power Plants," by Howard H.M. Hwang, 6/15/87, (PB88-134267, A03, MF-A01). This report is only available through NTIS (see address given above).

NCEER-87-0012 "Parametric Studies of Frequency Response of Secondary Systems Under Ground-Acceleration Excitations," by Y. Yong and Y.K. Lin, 6/10/87, (PB88-134309, A03, MF-A01). This report is only available through NTIS (see address given above).

NCEER-87-0013 "Frequency Response of Secondary Systems Under Seismic Excitation," by J.A. HoLung, J. Cai and Y.K. Lin, 7/31/87, (PB88-134317, A05, MF-A01). This report is only available through NTIS (see address given above).

NCEER-87-0014 "Modelling Earthquake Ground Motions in Seismically Active Regions Using Parametric Time Series Methods," by G.W. Ellis and A.S. Cakmak, 8/25/87, (PB88-134283, A08, MF-A01). This report is only available through NTIS (see address given above).

NCEER-87-0015 "Detection and Assessment of Seismic Structural Damage," by E. DiPasquale and A.S. Cakmak, 8/25/87, (PB88-163712, A05, MF-A01). This report is only available through NTIS (see address given above).

NCEER-87-0016 "Pipeline Experiment at Parkfield, California," by J. Isenberg and E. Richardson, 9/15/87, (PB88-163720, A03, MF-A01). This report is available only through NTIS (see address given above).

NCEER-87-0017 "Digital Simulation of Seismic Ground Motion," by M. Shinozuka, G. Deodatis and T. Harada, 8/31/87, (PB88-155197, A04, MF-A01). This report is available only through NTIS (see address given above).

NCEER-87-0018 "Practical Considerations for Structural Control: System Uncertainty, System Time Delay and Truncation of Small Control Forces," J.N. Yang and A. Akbarpour, 8/10/87, (PB88-163738, A08, MF-A01). This report is only available through NTIS (see address given above).

NCEER-87-0019 "Modal Analysis of Nonclassically Damped Structural Systems Using Canonical Transformation," by J.N. Yang, S. Sarkani and F.X. Long, 9/27/87, (PB88-187851, A04, MF-A01).

NCEER-87-0020 "A Nonstationary Solution in Random Vibration Theory," by J.R. Red-Horse and P.D. Spanos, 11/3/87, (PB88-163746, A03, MF-A01).

NCEER-87-0021 "Horizontal Impedances for Radially Inhomogeneous Viscoelastic Soil Layers," by A.S. Veletsos and K.W. Dotson, 10/15/87, (PB88-150859, A04, MF-A01).

NCEER-87-0022 "Seismic Damage Assessment of Reinforced Concrete Members," by Y.S. Chung, C. Meyer and M. Shinozuka, 10/9/87, (PB88-150867, A05, MF-A01). This report is available only through NTIS (see address given above).

NCEER-87-0023 "Active Structural Control in Civil Engineering," by T.T. Soong, 11/11/87, (PB88-187778, A03, MF-A01).

NCEER-87-0024 "Vertical and Torsional Impedances for Radially Inhomogeneous Viscoelastic Soil Layers," by K.W. Dotson and A.S. Veletsos, 12/87, (PB88-187786, A03, MF-A01).

NCEER-87-0025 "Proceedings from the Symposium on Seismic Hazards, Ground Motions, Soil-Liquefaction and Engineering Practice in Eastern North America," October 20-22, 1987, edited by K.H. Jacob, 12/87, (PB88-188115, A23, MF-A01). This report is available only through NTIS (see address given above).

NCEER-87-0026 "Report on the Whittier-Narrows, California, Earthquake of October 1, 1987," by J. Pantelic and A. Reinhorn, 11/87, (PB88-187752, A03, MF-A01). This report is available only through NTIS (see address given above).

NCEER-87-0027 "Design of a Modular Program for Transient Nonlinear Analysis of Large 3-D Building Structures," by S. Srivastav and J.F. Abel, 12/30/87, (PB88-187950, A05, MF-A01). This report is only available through NTIS (see address given above).

NCEER-87-0028 "Second-Year Program in Research, Education and Technology Transfer," 3/8/88, (PB88-219480, A04, MF-A01).

NCEER-88-0001 "Workshop on Seismic Computer Analysis and Design of Buildings With Interactive Graphics," by W. McGuire, J.F. Abel and C.H. Conley, 1/18/88, (PB88-187760, A03, MF-A01). This report is only available through NTIS (see address given above).

NCEER-88-0002 "Optimal Control of Nonlinear Flexible Structures," by J.N. Yang, F.X. Long and D. Wong, 1/22/88, (PB88-213772, A06, MF-A01).

NCEER-88-0003 "Substructuring Techniques in the Time Domain for Primary-Secondary Structural Systems," by G.D. Manolis and G. Juhn, 2/10/88, (PB88-213780, A04, MF-A01).

NCEER-88-0004 "Iterative Seismic Analysis of Primary-Secondary Systems," by A. Singhal, L.D. Lutes and P.D. Spanos, 2/23/88, (PB88-213798, A04, MF-A01).

NCEER-88-0005 "Stochastic Finite Element Expansion for Random Media," by P.D. Spanos and R. Ghanem, 3/14/88, (PB88-213806, A03, MF-A01).

NCEER-88-0006 "Combining Structural Optimization and Structural Control," by F.Y. Cheng and C.P. Pantelides, 1/10/88, (PB88-213814, A05, MF-A01).

NCEER-88-0007 "Seismic Performance Assessment of Code-Designed Structures," by H.H-M. Hwang, J-W. Jaw and H-J. Shau, 3/20/88, (PB88-219423, A04, MF-A01). This report is only available through NTIS (see address given above).

NCEER-88-0008 "Reliability Analysis of Code-Designed Structures Under Natural Hazards," by H.H-M. Hwang, H. Ushiba and M. Shinozuka, 2/29/88, (PB88-229471, A07, MF-A01). This report is only available through NTIS (see address given above).

NCEER-88-0009 "Seismic Fragility Analysis of Shear Wall Structures," by J-W Jaw and H.H-M. Hwang, 4/30/88, (PB89-102867, A04, MF-A01).

NCEER-88-0010 "Base Isolation of a Multi-Story Building Under a Harmonic Ground Motion - A Comparison of Performances of Various Systems," by F-G Fan, G. Ahmadi and I.G. Tadjbakhsh, 5/18/88, (PB89-122238, A06, MF-A01). This report is only available through NTIS (see address given above).

NCEER-88-0011 "Seismic Floor Response Spectra for a Combined System by Green's Functions," by F.M. Lavelle, L.A. Bergman and P.D. Spanos, 5/1/88, (PB89-102875, A03, MF-A01).

NCEER-88-0012 "A New Solution Technique for Randomly Excited Hysteretic Structures," by G.Q. Cai and Y.K. Lin, 5/16/88, (PB89-102883, A03, MF-A01).

NCEER-88-0013 "A Study of Radiation Damping and Soil-Structure Interaction Effects in the Centrifuge," by K. Weissman, supervised by J.H. Prevost, 5/24/88, (PB89-144703, A06, MF-A01).

NCEER-88-0014 "Parameter Identification and Implementation of a Kinematic Plasticity Model for Frictional Soils," by J.H. Prevost and D.V. Griffiths, to be published.

NCEER-88-0015 "Two- and Three- Dimensional Dynamic Finite Element Analyses of the Long Valley Dam," by D.V. Griffiths and J.H. Prevost, 6/17/88, (PB89-144711, A04, MF-A01).

NCEER-88-0016 "Damage Assessment of Reinforced Concrete Structures in Eastern United States," by A.M. Reinhorn, M.J. Seidel, S.K. Kunnath and Y.J. Park, 6/15/88, (PB89-122220, A04, MF-A01). This report is only available through NTIS (see address given above).

NCEER-88-0017 "Dynamic Compliance of Vertically Loaded Strip Foundations in Multilayered Viscoelastic Soils," by S. Ahmad and A.S.M. Israil, 6/17/88, (PB89-102891, A04, MF-A01).

NCEER-88-0018 "An Experimental Study of Seismic Structural Response With Added Viscoelastic Dampers," by R.C. Lin, Z. Liang, T.T. Soong and R.H. Zhang, 6/30/88, (PB89-122212, A05, MF-A01). This report is available only through NTIS (see address given above).

NCEER-88-0019 "Experimental Investigation of Primary - Secondary System Interaction," by G.D. Manolis, G. Juhn and A.M. Reinhorn, 5/27/88, (PB89-122204, A04, MF-A01).

NCEER-88-0020 "A Response Spectrum Approach For Analysis of Nonclassically Damped Structures," by J.N. Yang, S. Sarkani and F.X. Long, 4/22/88, (PB89-102909, A04, MF-A01).

NCEER-88-0021 "Seismic Interaction of Structures and Soils: Stochastic Approach," by A.S. Veletsos and A.M. Prasad, 7/21/88, (PB89-122196, A04, MF-A01). This report is only available through NTIS (see address given above).

NCEER-88-0022 "Identification of the Serviceability Limit State and Detection of Seismic Structural Damage," by E. DiPasquale and A.S. Cakmak, 6/15/88, (PB89-122188, A05, MF-A01). This report is available only through NTIS (see address given above).

NCEER-88-0023 "Multi-Hazard Risk Analysis: Case of a Simple Offshore Structure," by B.K. Bhartia and E.H. Vanmarcke, 7/21/88, (PB89-145213, A05, MF-A01).

NCEER-88-0024 "Automated Seismic Design of Reinforced Concrete Buildings," by Y.S. Chung, C. Meyer and M. Shinozuka, 7/5/88, (PB89-122170, A06, MF-A01). This report is available only through NTIS (see address given above).

NCEER-88-0025 "Experimental Study of Active Control of MDOF Structures Under Seismic Excitations," by L.L. Chung, R.C. Lin, T.T. Soong and A.M. Reinhorn, 7/10/88, (PB89-122600, A04, MF-A01).

NCEER-88-0026 "Earthquake Simulation Tests of a Low-Rise Metal Structure," by J.S. Hwang, K.C. Chang, G.C. Lee and R.L. Ketter, 8/1/88, (PB89-102917, A04, MF-A01).

NCEER-88-0027 "Systems Study of Urban Response and Reconstruction Due to Catastrophic Earthquakes," by F. Kozin and H.K. Zhou, 9/22/88, (PB90-162348, A04, MF-A01).

NCEER-88-0028 "Seismic Fragility Analysis of Plane Frame Structures," by H.H-M. Hwang and Y.K. Low, 7/31/88, (PB89-131445, A06, MF-A01).

NCEER-88-0029 "Response Analysis of Stochastic Structures," by A. Kardara, C. Bucher and M. Shinozuka, 9/22/88, (PB89-174429, A04, MF-A01).

NCEER-88-0030 "Nonnormal Accelerations Due to Yielding in a Primary Structure," by D.C.K. Chen and L.D. Lutes, 9/19/88, (PB89-131437, A04, MF-A01).

NCEER-88-0031 "Design Approaches for Soil-Structure Interaction," by A.S. Veletsos, A.M. Prasad and Y. Tang, 12/30/88, (PB89-174437, A03, MF-A01). This report is available only through NTIS (see address given above).

NCEER-88-0032 "A Re-evaluation of Design Spectra for Seismic Damage Control," by C.J. Turkstra and A.G. Tallin, 11/7/88, (PB89-145221, A05, MF-A01).

NCEER-88-0033 "The Behavior and Design of Noncontact Lap Splices Subjected to Repeated Inelastic Tensile Loading," by V.E. Sagan, P. Gergely and R.N. White, 12/8/88, (PB89-163737, A08, MF-A01).

NCEER-88-0034 "Seismic Response of Pile Foundations," by S.M. Mamoon, P.K. Banerjee and S. Ahmad, 11/1/88, (PB89-145239, A04, MF-A01).

NCEER-88-0035 "Modeling of R/C Building Structures With Flexible Floor Diaphragms (IDARC2)," by A.M. Reinhorn, S.K. Kunnath and N. Panahshahi, 9/7/88, (PB89-207153, A07, MF-A01).

NCEER-88-0036 "Solution of the Dam-Reservoir Interaction Problem Using a Combination of FEM, BEM with Particular Integrals, Modal Analysis, and Substructuring," by C-S. Tsai, G.C. Lee and R.L. Ketter, 12/31/88, (PB89-207146, A04, MF-A01).

NCEER-88-0037 "Optimal Placement of Actuators for Structural Control," by F.Y. Cheng and C.P. Pantelides, 8/15/88, (PB89-162846, A05, MF-A01).

NCEER-88-0038 "Teflon Bearings in Aseismic Base Isolation: Experimental Studies and Mathematical Modeling," by A. Mokha, M.C. Constantinou and A.M. Reinhorn, 12/5/88, (PB89-218457, A10, MF-A01). This report is available only through NTIS (see address given above).

NCEER-88-0039 "Seismic Behavior of Flat Slab High-Rise Buildings in the New York City Area," by P. Weidlinger and M. Ettouney, 10/15/88, (PB90-145681, A04, MF-A01).

NCEER-88-0040 "Evaluation of the Earthquake Resistance of Existing Buildings in New York City," by P. Weidlinger and M. Ettouney, 10/15/88, to be published.

NCEER-88-0041 "Small-Scale Modeling Techniques for Reinforced Concrete Structures Subjected to Seismic Loads," by W. Kim, A. El-Attar and R.N. White, 11/22/88, (PB89-189625, A05, MF-A01).

NCEER-88-0042 "Modeling Strong Ground Motion from Multiple Event Earthquakes," by G.W. Ellis and A.S. Cakmak, 10/15/88, (PB89-174445, A03, MF-A01).

NCEER-88-0043 "Nonstationary Models of Seismic Ground Acceleration," by M. Grigoriu, S.E. Ruiz and E. Rosenblueth, 7/15/88, (PB89-189617, A04, MF-A01).

NCEER-88-0044 "SARCF User's Guide: Seismic Analysis of Reinforced Concrete Frames," by Y.S. Chung, C. Meyer and M. Shinozuka, 11/9/88, (PB89-174452, A08, MF-A01).

NCEER-88-0045 "First Expert Panel Meeting on Disaster Research and Planning," edited by J. Pantelic and J. Stoyle, 9/15/88, (PB89-174460, A05, MF-A01).

NCEER-88-0046 "Preliminary Studies of the Effect of Degrading Infill Walls on the Nonlinear Seismic Response of Steel Frames," by C.Z. Chrysostomou, P. Gergely and J.F. Abel, 12/19/88, (PB89-208383, A05, MF-A01).

NCEER-88-0047 "Reinforced Concrete Frame Component Testing Facility - Design, Construction, Instrumentation and Operation," by S.P. Pessiki, C. Conley, T. Bond, P. Gergely and R.N. White, 12/16/88, (PB89-174478, A04, MF-A01).

NCEER-89-0001 "Effects of Protective Cushion and Soil Compliancy on the Response of Equipment Within a Seismically Excited Building," by J.A. HoLung, 2/16/89, (PB89-207179, A04, MF-A01).

NCEER-89-0002 "Statistical Evaluation of Response Modification Factors for Reinforced Concrete Structures," by H.H-M. Hwang and J-W. Jaw, 2/17/89, (PB89-207187, A05, MF-A01).

NCEER-89-0003 "Hysteretic Columns Under Random Excitation," by G-Q. Cai and Y.K. Lin, 1/9/89, (PB89-196513, A03, MF-A01).

NCEER-89-0004 "Experimental Study of `Elephant Foot Bulge' Instability of Thin-Walled Metal Tanks," by Z-H. Jia and R.L. Ketter, 2/22/89, (PB89-207195, A03, MF-A01).

NCEER-89-0005 "Experiment on Performance of Buried Pipelines Across San Andreas Fault," by J. Isenberg, E. Richardson and T.D. O'Rourke, 3/10/89, (PB89-218440, A04, MF-A01). This report is available only through NTIS (see address given above).

NCEER-89-0006 "A Knowledge-Based Approach to Structural Design of Earthquake-Resistant Buildings," by M. Subramani, P. Gergely, C.H. Conley, J.F. Abel and A.H. Zaghw, 1/15/89, (PB89-218465, A06, MF-A01).

NCEER-89-0007 "Liquefaction Hazards and Their Effects on Buried Pipelines," by T.D. O'Rourke and P.A. Lane, 2/1/89, (PB89-218481, A09, MF-A01).

NCEER-89-0008 "Fundamentals of System Identification in Structural Dynamics," by H. Imai, C-B. Yun, O. Maruyama and M. Shinozuka, 1/26/89, (PB89-207211, A04, MF-A01).

NCEER-89-0009 "Effects of the 1985 Michoacan Earthquake on Water Systems and Other Buried Lifelines in Mexico," by A.G. Ayala and M.J. O'Rourke, 3/8/89, (PB89-207229, A06, MF-A01).

NCEER-89-R010 "NCEER Bibliography of Earthquake Education Materials," by K.E.K. Ross, Second Revision, 9/1/89, (PB90-125352, A05, MF-A01). This report is replaced by NCEER-92-0018.

NCEER-89-0011 "Inelastic Three-Dimensional Response Analysis of Reinforced Concrete Building Structures (IDARC-3D), Part I - Modeling," by S.K. Kunnath and A.M. Reinhorn, 4/17/89, (PB90-114612, A07, MF-A01). This report is available only through NTIS (see address given above).

NCEER-89-0012 "Recommended Modifications to ATC-14," by C.D. Poland and J.O. Malley, 4/12/89, (PB90-108648, A15, MF-A01).

NCEER-89-0013 "Repair and Strengthening of Beam-to-Column Connections Subjected to Earthquake Loading," by M. Corazao and A.J. Durrani, 2/28/89, (PB90-109885, A06, MF-A01).

NCEER-89-0014 "Program EXKAL2 for Identification of Structural Dynamic Systems," by O. Maruyama, C-B. Yun, M. Hoshiya and M. Shinozuka, 5/19/89, (PB90-109877, A09, MF-A01).

NCEER-89-0015 "Response of Frames With Bolted Semi-Rigid Connections, Part I - Experimental Study and Analytical Predictions," by P.J. DiCorso, A.M. Reinhorn, J.R. Dickerson, J.B. Radziminski and W.L. Harper, 6/1/89, to be published.

NCEER-89-0016 "ARMA Monte Carlo Simulation in Probabilistic Structural Analysis," by P.D. Spanos and M.P. Mignolet, 7/10/89, (PB90-109893, A03, MF-A01).

NCEER-89-P017 "Preliminary Proceedings from the Conference on Disaster Preparedness - The Place of Earthquake Education in Our Schools," Edited by K.E.K. Ross, 6/23/89, (PB90-108606, A03, MF-A01).

NCEER-89-0017 "Proceedings from the Conference on Disaster Preparedness - The Place of Earthquake Education in Our Schools," Edited by K.E.K. Ross, 12/31/89, (PB90-207895, A012, MF-A02). This report is available only through NTIS (see address given above).

NCEER-89-0018 "Multidimensional Models of Hysteretic Material Behavior for Vibration Analysis of Shape Memory Energy Absorbing Devices, by E.J. Graesser and F.A. Cozzarelli, 6/7/89, (PB90-164146, A04, MF-A01).

NCEER-89-0019 "Nonlinear Dynamic Analysis of Three-Dimensional Base Isolated Structures (3D-BASIS)," by S. Nagarajaiah, A.M. Reinhorn and M.C. Constantinou, 8/3/89, (PB90-161936, A06, MF-A01). This report has been replaced by NCEER-93-0011.

NCEER-89-0020 "Structural Control Considering Time-Rate of Control Forces and Control Rate Constraints," by F.Y. Cheng and C.P. Pantelides, 8/3/89, (PB90-120445, A04, MF-A01).

NCEER-89-0021 "Subsurface Conditions of Memphis and Shelby County," by K.W. Ng, T-S. Chang and H-H.M. Hwang, 7/26/89, (PB90-120437, A03, MF-A01).

NCEER-89-0022 "Seismic Wave Propagation Effects on Straight Jointed Buried Pipelines," by K. Elhmadi and M.J. O'Rourke, 8/24/89, (PB90-162322, A10, MF-A02).

NCEER-89-0023 "Workshop on Serviceability Analysis of Water Delivery Systems," edited by M. Grigoriu, 3/6/89, (PB90-127424, A03, MF-A01).

NCEER-89-0024 "Shaking Table Study of a 1/5 Scale Steel Frame Composed of Tapered Members," by K.C. Chang, J.S. Hwang and G.C. Lee, 9/18/89, (PB90-160169, A04, MF-A01).

NCEER-89-0025 "DYNA1D: A Computer Program for Nonlinear Seismic Site Response Analysis - Technical Documentation," by Jean H. Prevost, 9/14/89, (PB90-161944, A07, MF-A01). This report is available only through NTIS (see address given above).

NCEER-89-0026 "1:4 Scale Model Studies of Active Tendon Systems and Active Mass Dampers for Aseismic Protection," by A.M. Reinhorn, T.T. Soong, R.C. Lin, Y.P. Yang, Y. Fukao, H. Abe and M. Nakai, 9/15/89, (PB90-173246, A10, MF-A02). This report is available only through NTIS (see address given above).

NCEER-89-0027 "Scattering of Waves by Inclusions in a Nonhomogeneous Elastic Half Space Solved by Boundary Element Methods," by P.K. Hadley, A. Askar and A.S. Cakmak, 6/15/89, (PB90-145699, A07, MF-A01).

NCEER-89-0028 "Statistical Evaluation of Deflection Amplification Factors for Reinforced Concrete Structures," by H.H.M. Hwang, J-W. Jaw and A.L. Ch'ng, 8/31/89, (PB90-164633, A05, MF-A01).

NCEER-89-0029 "Bedrock Accelerations in Memphis Area Due to Large New Madrid Earthquakes," by H.H.M. Hwang, C.H.S. Chen and G. Yu, 11/7/89, (PB90-162330, A04, MF-A01).

NCEER-89-0030 "Seismic Behavior and Response Sensitivity of Secondary Structural Systems," by Y.Q. Chen and T.T. Soong, 10/23/89, (PB90-164658, A08, MF-A01).

NCEER-89-0031 "Random Vibration and Reliability Analysis of Primary-Secondary Structural Systems," by Y. Ibrahim, M. Grigoriu and T.T. Soong, 11/10/89, (PB90-161951, A04, MF-A01).

NCEER-89-0032 "Proceedings from the Second U.S. - Japan Workshop on Liquefaction, Large Ground Deformation and Their Effects on Lifelines, September 26-29, 1989," Edited by T.D. O'Rourke and M. Hamada, 12/1/89, (PB90-209388, A22, MF-A03).

NCEER-89-0033 "Deterministic Model for Seismic Damage Evaluation of Reinforced Concrete Structures," by J.M. Bracci, A.M. Reinhorn, J.B. Mander and S.K. Kunnath, 9/27/89, (PB91-108803, A06, MF-A01).

NCEER-89-0034 "On the Relation Between Local and Global Damage Indices," by E. DiPasquale and A.S. Cakmak, 8/15/89, (PB90-173865, A05, MF-A01).

NCEER-89-0035 "Cyclic Undrained Behavior of Nonplastic and Low Plasticity Silts," by A.J. Walker and H.E. Stewart, 7/26/89, (PB90-183518, A10, MF-A01).

NCEER-89-0036 "Liquefaction Potential of Surficial Deposits in the City of Buffalo, New York," by M. Budhu, R. Giese and L. Baumgrass, 1/17/89, (PB90-208455, A04, MF-A01).

NCEER-89-0037 "A Deterministic Assessment of Effects of Ground Motion Incoherence," by A.S. Veletsos and Y. Tang, 7/15/89, (PB90-164294, A03, MF-A01).

NCEER-89-0038 "Workshop on Ground Motion Parameters for Seismic Hazard Mapping," July 17-18, 1989, edited by R.V. Whitman, 12/1/89, (PB90-173923, A04, MF-A01).

NCEER-89-0039 "Seismic Effects on Elevated Transit Lines of the New York City Transit Authority," by C.J. Costantino, C.A. Miller and E. Heymsfield, 12/26/89, (PB90-207887, A06, MF-A01).

NCEER-89-0040 "Centrifugal Modeling of Dynamic Soil-Structure Interaction," by K. Weissman, Supervised by J.H. Prevost, 5/10/89, (PB90-207879, A07, MF-A01).

NCEER-89-0041 "Linearized Identification of Buildings With Cores for Seismic Vulnerability Assessment," by I-K. Ho and A.E. Aktan, 11/1/89, (PB90-251943, A07, MF-A01).

NCEER-90-0001 "Geotechnical and Lifeline Aspects of the October 17, 1989 Loma Prieta Earthquake in San Francisco," by T.D. O'Rourke, H.E. Stewart, F.T. Blackburn and T.S. Dickerman, 1/90, (PB90-208596, A05, MF-A01).

NCEER-90-0002 "Nonnormal Secondary Response Due to Yielding in a Primary Structure," by D.C.K. Chen and L.D. Lutes, 2/28/90, (PB90-251976, A07, MF-A01).

NCEER-90-0003 "Earthquake Education Materials for Grades K-12," by K.E.K. Ross, 4/16/90, (PB91-251984, A05, MF-A05). This report has been replaced by NCEER-92-0018.

NCEER-90-0004 "Catalog of Strong Motion Stations in Eastern North America," by R.W. Busby, 4/3/90, (PB90-251984, A05, MF-A01).

NCEER-90-0005 "NCEER Strong-Motion Data Base: A User Manual for the GeoBase Release (Version 1.0 for the Sun3)," by P. Friberg and K. Jacob, 3/31/90 (PB90-258062, A04, MF-A01).

NCEER-90-0006 "Seismic Hazard Along a Crude Oil Pipeline in the Event of an 1811-1812 Type New Madrid Earthquake," by H.H.M. Hwang and C-H.S. Chen, 4/16/90, (PB90-258054, A04, MF-A01).

NCEER-90-0007 "Site-Specific Response Spectra for Memphis Sheahan Pumping Station," by H.H.M. Hwang and C.S. Lee, 5/15/90, (PB91-108811, A05, MF-A01).

NCEER-90-0008 "Pilot Study on Seismic Vulnerability of Crude Oil Transmission Systems," by T. Ariman, R. Dobry, M. Grigoriu, F. Kozin, M. O'Rourke, T. O'Rourke and M. Shinozuka, 5/25/90, (PB91-108837, A06, MF-A01).

NCEER-90-0009 "A Program to Generate Site Dependent Time Histories: EQGEN," by G.W. Ellis, M. Srinivasan and A.S. Cakmak, 1/30/90, (PB91-108829, A04, MF-A01).

NCEER-90-0010 "Active Isolation for Seismic Protection of Operating Rooms," by M.E. Talbott, Supervised by M. Shinozuka, 6/8/9, (PB91-110205, A05, MF-A01).

NCEER-90-0011 "Program LINEARID for Identification of Linear Structural Dynamic Systems," by C-B. Yun and M. Shinozuka, 6/25/90, (PB91-110312, A08, MF-A01).

NCEER-90-0012 "Two-Dimensional Two-Phase Elasto-Plastic Seismic Response of Earth Dams," by A.N. Yiagos, Supervised by J.H. Prevost, 6/20/90, (PB91-110197, A13, MF-A02).

NCEER-90-0013 "Secondary Systems in Base-Isolated Structures: Experimental Investigation, Stochastic Response and Stochastic Sensitivity," by G.D. Manolis, G. Juhn, M.C. Constantinou and A.M. Reinhorn, 7/1/90, (PB91-110320, A08, MF-A01).

NCEER-90-0014 "Seismic Behavior of Lightly-Reinforced Concrete Column and Beam-Column Joint Details," by S.P. Pessiki, C.H. Conley, P. Gergely and R.N. White, 8/22/90, (PB91-108795, A11, MF-A02).

NCEER-90-0015 "Two Hybrid Control Systems for Building Structures Under Strong Earthquakes," by J.N. Yang and A. Danielians, 6/29/90, (PB91-125393, A04, MF-A01).

NCEER-90-0016 "Instantaneous Optimal Control with Acceleration and Velocity Feedback," by J.N. Yang and Z. Li, 6/29/90, (PB91-125401, A03, MF-A01).

NCEER-90-0017 "Reconnaissance Report on the Northern Iran Earthquake of June 21, 1990," by M. Mehrain, 10/4/90, (PB91-125377, A03, MF-A01).

NCEER-90-0018 "Evaluation of Liquefaction Potential in Memphis and Shelby County," by T.S. Chang, P.S. Tang, C.S. Lee and H. Hwang, 8/10/90, (PB91-125427, A09, MF-A01).

NCEER-90-0019 "Experimental and Analytical Study of a Combined Sliding Disc Bearing and Helical Steel Spring Isolation System," by M.C. Constantinou, A.S. Mokha and A.M. Reinhorn, 10/4/90, (PB91-125385, A06, MF-A01). This report is available only through NTIS (see address given above).

NCEER-90-0020 "Experimental Study and Analytical Prediction of Earthquake Response of a Sliding Isolation System with a Spherical Surface," by A.S. Mokha, M.C. Constantinou and A.M. Reinhorn, 10/11/90, (PB91-125419, A05, MF-A01).

NCEER-90-0021 "Dynamic Interaction Factors for Floating Pile Groups," by G. Gazetas, K. Fan, A. Kaynia and E. Kausel, 9/10/90, (PB91-170381, A05, MF-A01).

NCEER-90-0022 "Evaluation of Seismic Damage Indices for Reinforced Concrete Structures," by S. Rodriguez-Gomez and A.S. Cakmak, 9/30/90, PB91-171322, A06, MF-A01).

NCEER-90-0023 "Study of Site Response at a Selected Memphis Site," by H. Desai, S. Ahmad, E.S. Gazetas and M.R. Oh, 10/11/90, (PB91-196857, A03, MF-A01).

NCEER-90-0024 "A User's Guide to Strongmo: Version 1.0 of NCEER's Strong-Motion Data Access Tool for PCs and Terminals," by P.A. Friberg and C.A.T. Susch, 11/15/90, (PB91-171272, A03, MF-A01).

NCEER-90-0025 "A Three-Dimensional Analytical Study of Spatial Variability of Seismic Ground Motions," by L-L. Hong and A.H.-S. Ang, 10/30/90, (PB91-170399, A09, MF-A01).

NCEER-90-0026 "MUMOID User's Guide - A Program for the Identification of Modal Parameters," by S. Rodriguez-Gomez and E. DiPasquale, 9/30/90, (PB91-171298, A04, MF-A01).

NCEER-90-0027 "SARCF-II User's Guide - Seismic Analysis of Reinforced Concrete Frames," by S. Rodriguez-Gomez, Y.S. Chung and C. Meyer, 9/30/90, (PB91-171280, A05, MF-A01).

NCEER-90-0028 "Viscous Dampers: Testing, Modeling and Application in Vibration and Seismic Isolation," by N. Makris and M.C. Constantinou, 12/20/90 (PB91-190561, A06, MF-A01).

NCEER-90-0029 "Soil Effects on Earthquake Ground Motions in the Memphis Area," by H. Hwang, C.S. Lee, K.W. Ng and T.S. Chang, 8/2/90, (PB91-190751, A05, MF-A01).

NCEER-91-0001 "Proceedings from the Third Japan-U.S. Workshop on Earthquake Resistant Design of Lifeline Facilities and Countermeasures for Soil Liquefaction, December 17-19, 1990," edited by T.D. O'Rourke and M. Hamada, 2/1/91, (PB91-179259, A99, MF-A04).

NCEER-91-0002 "Physical Space Solutions of Non-Proportionally Damped Systems," by M. Tong, Z. Liang and G.C. Lee, 1/15/91, (PB91-179242, A04, MF-A01).

NCEER-91-0003 "Seismic Response of Single Piles and Pile Groups," by K. Fan and G. Gazetas, 1/10/91, (PB92-174994, A04, MF-A01).

NCEER-91-0004 "Damping of Structures: Part 1 - Theory of Complex Damping," by Z. Liang and G. Lee, 10/10/91, (PB92-197235, A12, MF-A03).

NCEER-91-0005 "3D-BASIS - Nonlinear Dynamic Analysis of Three Dimensional Base Isolated Structures: Part II," by S. Nagarajaiah, A.M. Reinhorn and M.C. Constantinou, 2/28/91, (PB91-190553, A07, MF-A01). This report has been replaced by NCEER-93-0011.

NCEER-91-0006 "A Multidimensional Hysteretic Model for Plasticity Deforming Metals in Energy Absorbing Devices," by E.J. Graesser and F.A. Cozzarelli, 4/9/91, (PB92-108364, A04, MF-A01).

NCEER-91-0007 "A Framework for Customizable Knowledge-Based Expert Systems with an Application to a KBES for Evaluating the Seismic Resistance of Existing Buildings," by E.G. Ibarra-Anaya and S.J. Fenves, 4/9/91, (PB91-210930, A08, MF-A01).

NCEER-91-0008 "Nonlinear Analysis of Steel Frames with Semi-Rigid Connections Using the Capacity Spectrum Method," by G.G. Deierlein, S-H. Hsieh, Y-J. Shen and J.F. Abel, 7/2/91, (PB92-113828, A05, MF-A01).

NCEER-91-0009 "Earthquake Education Materials for Grades K-12," by K.E.K. Ross, 4/30/91, (PB91-212142, A06, MF-A01). This report has been replaced by NCEER-92-0018.

NCEER-91-0010 "Phase Wave Velocities and Displacement Phase Differences in a Harmonically Oscillating Pile," by N. Makris and G. Gazetas, 7/8/91, (PB92-108356, A04, MF-A01).

NCEER-91-0011 "Dynamic Characteristics of a Full-Size Five-Story Steel Structure and a 2/5 Scale Model," by K.C. Chang, G.C. Yao, G.C. Lee, D.S. Hao and Y.C. Yeh," 7/2/91, (PB93-116648, A06, MF-A02).

NCEER-91-0012 "Seismic Response of a 2/5 Scale Steel Structure with Added Viscoelastic Dampers," by K.C. Chang, T.T. Soong, S-T. Oh and M.L. Lai, 5/17/91, (PB92-110816, A05, MF-A01).

NCEER-91-0013 "Earthquake Response of Retaining Walls; Full-Scale Testing and Computational Modeling," by S. Alampalli and A-W.M. Elgamal, 6/20/91, to be published.

NCEER-91-0014 "3D-BASIS-M: Nonlinear Dynamic Analysis of Multiple Building Base Isolated Structures," by P.C. Tsopelas, S. Nagarajaiah, M.C. Constantinou and A.M. Reinhorn, 5/28/91, (PB92-113885, A09, MF-A02).

NCEER-91-0015 "Evaluation of SEAOC Design Requirements for Sliding Isolated Structures," by D. Theodossiou and M.C. Constantinou, 6/10/91, (PB92-114602, A11, MF-A03).

NCEER-91-0016 "Closed-Loop Modal Testing of a 27-Story Reinforced Concrete Flat Plate-Core Building," by H.R. Somaprasad, T. Toksoy, H. Yoshiyuki and A.E. Aktan, 7/15/91, (PB92-129980, A07, MF-A02).

NCEER-91-0017 "Shake Table Test of a 1/6 Scale Two-Story Lightly Reinforced Concrete Building," by A.G. El-Attar, R.N. White and P. Gergely, 2/28/91, (PB92-222447, A06, MF-A02).

NCEER-91-0018 "Shake Table Test of a 1/8 Scale Three-Story Lightly Reinforced Concrete Building," by A.G. El-Attar, R.N. White and P. Gergely, 2/28/91, (PB93-116630, A08, MF-A02).

NCEER-91-0019 "Transfer Functions for Rigid Rectangular Foundations," by A.S. Veletsos, A.M. Prasad and W.H. Wu, 7/31/91, to be published.

NCEER-91-0020 "Hybrid Control of Seismic-Excited Nonlinear and Inelastic Structural Systems," by J.N. Yang, Z. Li and A. Danielians, 8/1/91, (PB92-143171, A06, MF-A02).

NCEER-91-0021 "The NCEER-91 Earthquake Catalog: Improved Intensity-Based Magnitudes and Recurrence Relations for U.S. Earthquakes East of New Madrid," by L. Seeber and J.G. Armbruster, 8/28/91, (PB92-176742, A06, MF-A02).

NCEER-91-0022 "Proceedings from the Implementation of Earthquake Planning and Education in Schools: The Need for Change - The Roles of the Changemakers," by K.E.K. Ross and F. Winslow, 7/23/91, (PB92-129998, A12, MF-A03).

NCEER-91-0023 "A Study of Reliability-Based Criteria for Seismic Design of Reinforced Concrete Frame Buildings," by H.H.M. Hwang and H-M. Hsu, 8/10/91, (PB92-140235, A09, MF-A02).

NCEER-91-0024 "Experimental Verification of a Number of Structural System Identification Algorithms," by R.G. Ghanem, H. Gavin and M. Shinozuka, 9/18/91, (PB92-176577, A18, MF-A04).

NCEER-91-0025 "Probabilistic Evaluation of Liquefaction Potential," by H.H.M. Hwang and C.S. Lee," 11/25/91, (PB92-143429, A05, MF-A01).

NCEER-91-0026 "Instantaneous Optimal Control for Linear, Nonlinear and Hysteretic Structures - Stable Controllers," by J.N. Yang and Z. Li, 11/15/91, (PB92-163807, A04, MF-A01).

NCEER-91-0027 "Experimental and Theoretical Study of a Sliding Isolation System for Bridges," by M.C. Constantinou, A. Kartoum, A.M. Reinhorn and P. Bradford, 11/15/91, (PB92-176973, A10, MF-A03).

NCEER-92-0001 "Case Studies of Liquefaction and Lifeline Performance During Past Earthquakes, Volume 1: Japanese Case Studies," Edited by M. Hamada and T. O'Rourke, 2/17/92, (PB92-197243, A18, MF-A04).

NCEER-92-0002 "Case Studies of Liquefaction and Lifeline Performance During Past Earthquakes, Volume 2: United States Case Studies," Edited by T. O'Rourke and M. Hamada, 2/17/92, (PB92-197250, A20, MF-A04).

NCEER-92-0003 "Issues in Earthquake Education," Edited by K. Ross, 2/3/92, (PB92-222389, A07, MF-A02).

NCEER-92-0004 "Proceedings from the First U.S. - Japan Workshop on Earthquake Protective Systems for Bridges," Edited by I.G. Buckle, 2/4/92, (PB94-142239, A99, MF-A06).

NCEER-92-0005 "Seismic Ground Motion from a Haskell-Type Source in a Multiple-Layered Half-Space," A.P. Theoharis, G. Deodatis and M. Shinozuka, 1/2/92, to be published.

NCEER-92-0006 "Proceedings from the Site Effects Workshop," Edited by R. Whitman, 2/29/92, (PB92-197201, A04, MF-A01).

NCEER-92-0007 "Engineering Evaluation of Permanent Ground Deformations Due to Seismically-Induced Liquefaction," by M.H. Baziar, R. Dobry and A-W.M. Elgamal, 3/24/92, (PB92-222421, A13, MF-A03).

NCEER-92-0008 "A Procedure for the Seismic Evaluation of Buildings in the Central and Eastern United States," by C.D. Poland and J.O. Malley, 4/2/92, (PB92-222439, A20, MF-A04).

NCEER-92-0009 "Experimental and Analytical Study of a Hybrid Isolation System Using Friction Controllable Sliding Bearings," by M.Q. Feng, S. Fujii and M. Shinozuka, 5/15/92, (PB93-150282, A06, MF-A02).

NCEER-92-0010 "Seismic Resistance of Slab-Column Connections in Existing Non-Ductile Flat-Plate Buildings," by A.J. Durrani and Y. Du, 5/18/92, (PB93-116812, A06, MF-A02).

NCEER-92-0011 "The Hysteretic and Dynamic Behavior of Brick Masonry Walls Upgraded by Ferrocement Coatings Under Cyclic Loading and Strong Simulated Ground Motion," by H. Lee and S.P. Prawel, 5/11/92, to be published.

NCEER-92-0012 "Study of Wire Rope Systems for Seismic Protection of Equipment in Buildings," by G.F. Demetriades, M.C. Constantinou and A.M. Reinhorn, 5/20/92, (PB93-116655, A08, MF-A02).

NCEER-92-0013 "Shape Memory Structural Dampers: Material Properties, Design and Seismic Testing," by P.R. Witting and F.A. Cozzarelli, 5/26/92, (PB93-116663, A05, MF-A01).

NCEER-92-0014 "Longitudinal Permanent Ground Deformation Effects on Buried Continuous Pipelines," by M.J. O'Rourke, and C. Nordberg, 6/15/92, (PB93-116671, A08, MF-A02).

NCEER-92-0015 "A Simulation Method for Stationary Gaussian Random Functions Based on the Sampling Theorem," by M. Grigoriu and S. Balopoulou, 6/11/92, (PB93-127496, A05, MF-A01).

NCEER-92-0016 "Gravity-Load-Designed Reinforced Concrete Buildings: Seismic Evaluation of Existing Construction and Detailing Strategies for Improved Seismic Resistance," by G.W. Hoffmann, S.K. Kunnath, A.M. Reinhorn and J.B. Mander, 7/15/92, (PB94-142007, A08, MF-A02).

NCEER-92-0017 "Observations on Water System and Pipeline Performance in the Limón Area of Costa Rica Due to the April 22, 1991 Earthquake," by M. O'Rourke and D. Ballantyne, 6/30/92, (PB93-126811, A06, MF-A02).

NCEER-92-0018 "Fourth Edition of Earthquake Education Materials for Grades K-12," Edited by K.E.K. Ross, 8/10/92, (PB93-114023, A07, MF-A02).

NCEER-92-0019 "Proceedings from the Fourth Japan-U.S. Workshop on Earthquake Resistant Design of Lifeline Facilities and Countermeasures for Soil Liquefaction," Edited by M. Hamada and T.D. O'Rourke, 8/12/92, (PB93-163939, A99, MF-E11).

NCEER-92-0020 "Active Bracing System: A Full Scale Implementation of Active Control," by A.M. Reinhorn, T.T. Soong, R.C. Lin, M.A. Riley, Y.P. Wang, S. Aizawa and M. Higashino, 8/14/92, (PB93-127512, A06, MF-A02).

NCEER-92-0021 "Empirical Analysis of Horizontal Ground Displacement Generated by Liquefaction-Induced Lateral Spreads," by S.F. Bartlett and T.L. Youd, 8/17/92, (PB93-188241, A06, MF-A02).

NCEER-92-0022 "IDARC Version 3.0: Inelastic Damage Analysis of Reinforced Concrete Structures," by S.K. Kunnath, A.M. Reinhorn and R.F. Lobo, 8/31/92, (PB93-227502, A07, MF-A02).

NCEER-92-0023 "A Semi-Empirical Analysis of Strong-Motion Peaks in Terms of Seismic Source, Propagation Path and Local Site Conditions, by M. Kamiyama, M.J. O'Rourke and R. Flores-Berrones, 9/9/92, (PB93-150266, A08, MF-A02).

NCEER-92-0024 "Seismic Behavior of Reinforced Concrete Frame Structures with Nonductile Details, Part I: Summary of Experimental Findings of Full Scale Beam-Column Joint Tests," by A. Beres, R.N. White and P. Gergely, 9/30/92, (PB93-227783, A05, MF-A01).

NCEER-92-0025 "Experimental Results of Repaired and Retrofitted Beam-Column Joint Tests in Lightly Reinforced Concrete Frame Buildings," by A. Beres, S. El-Borgi, R.N. White and P. Gergely, 10/29/92, (PB93-227791, A05, MF-A01).

NCEER-92-0026 "A Generalization of Optimal Control Theory: Linear and Nonlinear Structures," by J.N. Yang, Z. Li and S. Vongchavalitkul, 11/2/92, (PB93-188621, A05, MF-A01).

NCEER-92-0027 "Seismic Resistance of Reinforced Concrete Frame Structures Designed Only for Gravity Loads: Part I - Design and Properties of a One-Third Scale Model Structure," by J.M. Bracci, A.M. Reinhorn and J.B. Mander, 12/1/92, (PB94-104502, A08, MF-A02).

NCEER-92-0028 "Seismic Resistance of Reinforced Concrete Frame Structures Designed Only for Gravity Loads: Part II - Experimental Performance of Subassemblages," by L.E. Aycardi, J.B. Mander and A.M. Reinhorn, 12/1/92, (PB94-104510, A08, MF-A02).

NCEER-92-0029 "Seismic Resistance of Reinforced Concrete Frame Structures Designed Only for Gravity Loads: Part III - Experimental Performance and Analytical Study of a Structural Model," by J.M. Bracci, A.M. Reinhorn and J.B. Mander, 12/1/92, (PB93-227528, A09, MF-A01).

NCEER-92-0030 "Evaluation of Seismic Retrofit of Reinforced Concrete Frame Structures: Part I - Experimental Performance of Retrofitted Subassemblages," by D. Choudhuri, J.B. Mander and A.M. Reinhorn, 12/8/92, (PB93-198307, A07, MF-A02).

NCEER-92-0031 "Evaluation of Seismic Retrofit of Reinforced Concrete Frame Structures: Part II - Experimental Performance and Analytical Study of a Retrofitted Structural Model," by J.M. Bracci, A.M. Reinhorn and J.B. Mander, 12/8/92, (PB93-198315, A09, MF-A03).

NCEER-92-0032 "Experimental and Analytical Investigation of Seismic Response of Structures with Supplemental Fluid Viscous Dampers," by M.C. Constantinou and M.D. Symans, 12/21/92, (PB93-191435, A10, MF-A03). This report is available only through NTIS (see address given above).

NCEER-92-0033 "Reconnaissance Report on the Cairo, Egypt Earthquake of October 12, 1992," by M. Khater, 12/23/92, (PB93-188621, A03, MF-A01).

NCEER-92-0034 "Low-Level Dynamic Characteristics of Four Tall Flat-Plate Buildings in New York City," by H. Gavin, S. Yuan, J. Grossman, E. Pekelis and K. Jacob, 12/28/92, (PB93-188217, A07, MF-A02).

NCEER-93-0001 "An Experimental Study on the Seismic Performance of Brick-Infilled Steel Frames With and Without Retrofit," by J.B. Mander, B. Nair, K. Wojtkowski and J. Ma, 1/29/93, (PB93-227510, A07, MF-A02).

NCEER-93-0002 "Social Accounting for Disaster Preparedness and Recovery Planning," by S. Cole, E. Pantoja and V. Razak, 2/22/93, (PB94-142114, A12, MF-A03).

NCEER-93-0003 "Assessment of 1991 NEHRP Provisions for Nonstructural Components and Recommended Revisions," by T.T. Soong, G. Chen, Z. Wu, R-H. Zhang and M. Grigoriu, 3/1/93, (PB93-188639, A06, MF-A02).

NCEER-93-0004 "Evaluation of Static and Response Spectrum Analysis Procedures of SEAOC/UBC for Seismic Isolated Structures," by C.W. Winters and M.C. Constantinou, 3/23/93, (PB93-198299, A10, MF-A03).

NCEER-93-0005 "Earthquakes in the Northeast - Are We Ignoring the Hazard? A Workshop on Earthquake Science and Safety for Educators," edited by K.E.K. Ross, 4/2/93, (PB94-103066, A09, MF-A02).

NCEER-93-0006 "Inelastic Response of Reinforced Concrete Structures with Viscoelastic Braces," by R.F. Lobo, J.M. Bracci, K.L. Shen, A.M. Reinhorn and T.T. Soong, 4/5/93, (PB93-227486, A05, MF-A02).

NCEER-93-0007 "Seismic Testing of Installation Methods for Computers and Data Processing Equipment," by K. Kosar, T.T. Soong, K.L. Shen, J.A. HoLung and Y.K. Lin, 4/12/93, (PB93-198299, A07, MF-A02).

NCEER-93-0008 "Retrofit of Reinforced Concrete Frames Using Added Dampers," by A. Reinhorn, M. Constantinou and C. Li, to be published.

NCEER-93-0009 "Seismic Behavior and Design Guidelines for Steel Frame Structures with Added Viscoelastic Dampers," by K.C. Chang, M.L. Lai, T.T. Soong, D.S. Hao and Y.C. Yeh, 5/1/93, (PB94-141959, A07, MF-A02).

NCEER-93-0010 "Seismic Performance of Shear-Critical Reinforced Concrete Bridge Piers," by J.B. Mander, S.M. Waheed, M.T.A. Chaudhary and S.S. Chen, 5/12/93, (PB93-227494, A08, MF-A02).

NCEER-93-0011 "3D-BASIS-TABS: Computer Program for Nonlinear Dynamic Analysis of Three Dimensional Base Isolated Structures," by S. Nagarajaiah, C. Li, A.M. Reinhorn and M.C. Constantinou, 8/2/93, (PB94-141819, A09, MF-A02).

NCEER-93-0012 "Effects of Hydrocarbon Spills from an Oil Pipeline Break on Ground Water," by O.J. Helweg and H.H.M. Hwang, 8/3/93, (PB94-141942, A06, MF-A02).

NCEER-93-0013 "Simplified Procedures for Seismic Design of Nonstructural Components and Assessment of Current Code Provisions," by M.P. Singh, L.E. Suarez, E.E. Matheu and G.O. Maldonado, 8/4/93, (PB94-141827, A09, MF-A02).

NCEER-93-0014 "An Energy Approach to Seismic Analysis and Design of Secondary Systems," by G. Chen and T.T. Soong, 8/6/93, (PB94-142767, A11, MF-A03).

NCEER-93-0015 "Proceedings from School Sites: Becoming Prepared for Earthquakes - Commemorating the Third Anniversary of the Loma Prieta Earthquake," Edited by F.E. Winslow and K.E.K. Ross, 8/16/93, (PB94-154275, A16, MF-A02).

NCEER-93-0016 "Reconnaissance Report of Damage to Historic Monuments in Cairo, Egypt Following the October 12, 1992 Dahshur Earthquake," by D. Sykora, D. Look, G. Croci, E. Karaesmen and E. Karaesmen, 8/19/93, (PB94-142221, A08, MF-A02).

NCEER-93-0017 "The Island of Guam Earthquake of August 8, 1993," by S.W. Swan and S.K. Harris, 9/30/93, (PB94-141843, A04, MF-A01).

NCEER-93-0018 "Engineering Aspects of the October 12, 1992 Egyptian Earthquake," by A.W. Elgamal, M. Amer, K. Adalier and A. Abul-Fadl, 10/7/93, (PB94-141983, A05, MF-A01).

NCEER-93-0019 "Development of an Earthquake Motion Simulator and its Application in Dynamic Centrifuge Testing," by I. Krstelj, Supervised by J.H. Prevost, 10/23/93, (PB94-181773, A-10, MF-A03).

NCEER-93-0020 "NCEER-Taisei Corporation Research Program on Sliding Seismic Isolation Systems for Bridges: Experimental and Analytical Study of a Friction Pendulum System (FPS)," by M.C. Constantinou, P. Tsopelas, Y-S. Kim and S. Okamoto, 11/1/93, (PB94-142775, A08, MF-A02).

NCEER-93-0021 "Finite Element Modeling of Elastomeric Seismic Isolation Bearings," by L.J. Billings, Supervised by R. Shepherd, 11/8/93, to be published.

NCEER-93-0022 "Seismic Vulnerability of Equipment in Critical Facilities: Life-Safety and Operational Consequences," by K. Porter, G.S. Johnson, M.M. Zadeh, C. Scawthorn and S. Eder, 11/24/93, (PB94-181765, A16, MF-A03).

NCEER-93-0023 "Hokkaido Nansei-oki, Japan Earthquake of July 12, 1993, by P.I. Yanev and C.R. Scawthorn, 12/23/93, (PB94-181500, A07, MF-A01).

NCEER-94-0001 "An Evaluation of Seismic Serviceability of Water Supply Networks with Application to the San Francisco Auxiliary Water Supply System," by I. Markov, Supervised by M. Grigoriu and T. O'Rourke, 1/21/94, (PB94-204013, A07, MF-A02).

NCEER-94-0002 "NCEER-Taisei Corporation Research Program on Sliding Seismic Isolation Systems for Bridges: Experimental and Analytical Study of Systems Consisting of Sliding Bearings, Rubber Restoring Force Devices and Fluid Dampers," Volumes I and II, by P. Tsopelas, S. Okamoto, M.C. Constantinou, D. Ozaki and S. Fujii, 2/4/94, (PB94-181740, A09, MF-A02 and PB94-181757, A12, MF-A03).

NCEER-94-0003 "A Markov Model for Local and Global Damage Indices in Seismic Analysis," by S. Rahman and M. Grigoriu, 2/18/94, (PB94-206000, A12, MF-A03).

NCEER-94-0004 "Proceedings from the NCEER Workshop on Seismic Response of Masonry Infills," edited by D.P. Abrams, 3/1/94, (PB94-180783, A07, MF-A02).

NCEER-94-0005 "The Northridge, California Earthquake of January 17, 1994: General Reconnaissance Report," edited by J.D. Goltz, 3/11/94, (PB94-193943, A10, MF-A03).

NCEER-94-0006 "Seismic Energy Based Fatigue Damage Analysis of Bridge Columns: Part I - Evaluation of Seismic Capacity," by G.A. Chang and J.B. Mander, 3/14/94, (PB94-219185, A11, MF-A03).

NCEER-94-0007 "Seismic Isolation of Multi-Story Frame Structures Using Spherical Sliding Isolation Systems," by T.M. Al-Hussaini, V.A. Zayas and M.C. Constantinou, 3/17/94, (PB94-193745, A09, MF-A02).

NCEER-94-0008 "The Northridge, California Earthquake of January 17, 1994: Performance of Highway Bridges," edited by I.G. Buckle, 3/24/94, (PB94-193851, A06, MF-A02).

NCEER-94-0009 "Proceedings of the Third U.S.-Japan Workshop on Earthquake Protective Systems for Bridges," edited by I.G. Buckle and I. Friedland, 3/31/94, (PB94-195815, A99, MF-A06).

NCEER-94-0010 "3D-BASIS-ME: Computer Program for Nonlinear Dynamic Analysis of Seismically Isolated Single and Multiple Structures and Liquid Storage Tanks," by P.C. Tsopelas, M.C. Constantinou and A.M. Reinhorn, 4/12/94, (PB94-204922, A09, MF-A02).

NCEER-94-0011 "The Northridge, California Earthquake of January 17, 1994: Performance of Gas Transmission Pipelines," by T.D. O'Rourke and M.C. Palmer, 5/16/94, (PB94-204989, A05, MF-A01).

NCEER-94-0012 "Feasibility Study of Replacement Procedures and Earthquake Performance Related to Gas Transmission Pipelines," by T.D. O'Rourke and M.C. Palmer, 5/25/94, (PB94-206638, A09, MF-A02).

NCEER-94-0013 "Seismic Energy Based Fatigue Damage Analysis of Bridge Columns: Part II - Evaluation of Seismic Demand," by G.A. Chang and J.B. Mander, 6/1/94, (PB95-18106, A08, MF-A02).

NCEER-94-0014 "NCEER-Taisei Corporation Research Program on Sliding Seismic Isolation Systems for Bridges: Experimental and Analytical Study of a System Consisting of Sliding Bearings and Fluid Restoring Force/Damping Devices," by P. Tsopelas and M.C. Constantinou, 6/13/94, (PB94-219144, A10, MF-A03).

NCEER-94-0015 "Generation of Hazard-Consistent Fragility Curves for Seismic Loss Estimation Studies," by H. Hwang and J-R. Huo, 6/14/94, (PB95-181996, A09, MF-A02).

NCEER-94-0016 "Seismic Study of Building Frames with Added Energy-Absorbing Devices," by W.S. Pong, C.S. Tsai and G.C. Lee, 6/20/94, (PB94-219136, A10, A03).

NCEER-94-0017 "Sliding Mode Control for Seismic-Excited Linear and Nonlinear Civil Engineering Structures," by J. Yang, J. Wu, A. Agrawal and Z. Li, 6/21/94, (PB95-138483, A06, MF-A02).

NCEER-94-0018 "3D-BASIS-TABS Version 2.0: Computer Program for Nonlinear Dynamic Analysis of Three Dimensional Base Isolated Structures," by A.M. Reinhorn, S. Nagarajaiah, M.C. Constantinou, P. Tsopelas and R. Li, 6/22/94, (PB95-182176, A08, MF-A02).

NCEER-94-0019 "Proceedings of the International Workshop on Civil Infrastructure Systems: Application of Intelligent Systems and Advanced Materials on Bridge Systems," Edited by G.C. Lee and K.C. Chang, 7/18/94, (PB95-252474, A20, MF-A04).

NCEER-94-0020 "Study of Seismic Isolation Systems for Computer Floors," by V. Lambrou and M.C. Constantinou, 7/19/94, (PB95-138533, A10, MF-A03).

NCEER-94-0021 "Proceedings of the U.S.-Italian Workshop on Guidelines for Seismic Evaluation and Rehabilitation of Unreinforced Masonry Buildings," Edited by D.P. Abrams and G.M. Calvi, 7/20/94, (PB95-138749, A13, MF-A03).

NCEER-94-0022 "NCEER-Taisei Corporation Research Program on Sliding Seismic Isolation Systems for Bridges: Experimental and Analytical Study of a System Consisting of Lubricated PTFE Sliding Bearings and Mild Steel Dampers," by P. Tsopelas and M.C. Constantinou, 7/22/94, (PB95-182184, A08, MF-A02).

NCEER-94-0023 “Development of Reliability-Based Design Criteria for Buildings Under Seismic Load,” by Y.K. Wen, H. Hwang and M. Shinozuka, 8/1/94, (PB95-211934, A08, MF-A02).

NCEER-94-0024 “Experimental Verification of Acceleration Feedback Control Strategies for an Active Tendon System,” by S.J. Dyke, B.F. Spencer, Jr., P. Quast, M.K. Sain, D.C. Kaspari, Jr. and T.T. Soong, 8/29/94, (PB95-212320, A05, MF-A01).

NCEER-94-0025 “Seismic Retrofitting Manual for Highway Bridges,” Edited by I.G. Buckle and I.F. Friedland, published by the Federal Highway Administration (PB95-212676, A15, MF-A03).

NCEER-94-0026 “Proceedings from the Fifth U.S.-Japan Workshop on Earthquake Resistant Design of Lifeline Facilities and Countermeasures Against Soil Liquefaction,” Edited by T.D. O’Rourke and M. Hamada, 11/7/94, (PB95-220802, A99, MF-E08).

NCEER-95-0001 "Experimental and Analytical Investigation of Seismic Retrofit of Structures with Supplemental Damping: Part 1 - Fluid Viscous Damping Devices," by A.M. Reinhorn, C. Li and M.C. Constantinou, 1/3/95, (PB95-266599, A09, MF-A02).

NCEER-95-0002 "Experimental and Analytical Study of Low-Cycle Fatigue Behavior of Semi-Rigid Top-And-Seat Angle Connections," by G. Pekcan, J.B. Mander and S.S. Chen, 1/5/95, (PB95-220042, A07, MF-A02).

NCEER-95-0003 "NCEER-ATC Joint Study on Fragility of Buildings," by T. Anagnos, C. Rojahn and A.S. Kiremidjian, 1/20/95, (PB95-220026, A06, MF-A02).

NCEER-95-0004 "Nonlinear Control Algorithms for Peak Response Reduction," by Z. Wu, T.T. Soong, V. Gattulli and R.C. Lin, 2/16/95, (PB95-220349, A05, MF-A01).

NCEER-95-0005 "Pipeline Replacement Feasibility Study: A Methodology for Minimizing Seismic and Corrosion Risks to Underground Natural Gas Pipelines," by R.T. Eguchi, H.A. Seligson and D.G. Honegger, 3/2/95, (PB95-252326, A06, MF-A02).

NCEER-95-0006 "Evaluation of Seismic Performance of an 11-Story Frame Building During the 1994 Northridge Earthquake," by F. Naeim, R. DiSulio, K. Benuska, A. Reinhorn and C. Li, to be published.

NCEER-95-0007 "Prioritization of Bridges for Seismic Retrofitting," by N. Basöz and A.S. Kiremidjian, 4/24/95, (PB95-252300, A08, MF-A02).

NCEER-95-0008 "Method for Developing Motion Damage Relationships for Reinforced Concrete Frames," by A. Singhal and A.S. Kiremidjian, 5/11/95, (PB95-266607, A06, MF-A02).

NCEER-95-0009 "Experimental and Analytical Investigation of Seismic Retrofit of Structures with Supplemental Damping: Part II - Friction Devices," by C. Li and A.M. Reinhorn, 7/6/95, (PB96-128087, A11, MF-A03).

NCEER-95-0010 "Experimental Performance and Analytical Study of a Non-Ductile Reinforced Concrete Frame Structure Retrofitted with Elastomeric Spring Dampers," by G. Pekcan, J.B. Mander and S.S. Chen, 7/14/95, (PB96-137161, A08, MF-A02).

NCEER-95-0011 "Development and Experimental Study of Semi-Active Fluid Damping Devices for Seismic Protection of Structures," by M.D. Symans and M.C. Constantinou, 8/3/95, (PB96-136940, A23, MF-A04).

NCEER-95-0012 "Real-Time Structural Parameter Modification (RSPM): Development of Innervated Structures," by Z. Liang, M. Tong and G.C. Lee, 4/11/95, (PB96-137153, A06, MF-A01).

NCEER-95-0013 "Experimental and Analytical Investigation of Seismic Retrofit of Structures with Supplemental Damping: Part III - Viscous Damping Walls," by A.M. Reinhorn and C. Li, 10/1/95, (PB96-176409, A11, MF-A03).

NCEER-95-0014 "Seismic Fragility Analysis of Equipment and Structures in a Memphis Electric Substation," by J-R. Huo and H.H.M. Hwang, 8/10/95, (PB96-128087, A09, MF-A02).

NCEER-95-0015 "The Hanshin-Awaji Earthquake of January 17, 1995: Performance of Lifelines," Edited by M. Shinozuka, 11/3/95, (PB96-176383, A15, MF-A03).

NCEER-95-0016 "Highway Culvert Performance During Earthquakes," by T.L. Youd and C.J. Beckman, available as NCEER-96-0015.

NCEER-95-0017 "The Hanshin-Awaji Earthquake of January 17, 1995: Performance of Highway Bridges," Edited by I.G. Buckle, 12/1/95, to be published.

NCEER-95-0018 "Modeling of Masonry Infill Panels for Structural Analysis," by A.M. Reinhorn, A. Madan, R.E. Valles, Y. Reichmann and J.B. Mander, 12/8/95, (PB97-110886, MF-A01, A06).

NCEER-95-0019 "Optimal Polynomial Control for Linear and Nonlinear Structures," by A.K. Agrawal and J.N. Yang, 12/11/95, (PB96-168737, A07, MF-A02).

NCEER-95-0020 "Retrofit of Non-Ductile Reinforced Concrete Frames Using Friction Dampers," by R.S. Rao, P. Gergely and R.N. White, 12/22/95, (PB97-133508, A10, MF-A02).

NCEER-95-0021 "Parametric Results for Seismic Response of Pile-Supported Bridge Bents," by G. Mylonakis, A. Nikolaou and G. Gazetas, 12/22/95, (PB97-100242, A12, MF-A03).

NCEER-95-0022 "Kinematic Bending Moments in Seismically Stressed Piles," by A. Nikolaou, G. Mylonakis and G. Gazetas, 12/23/95, (PB97-113914, MF-A03, A13).

NCEER-96-0001 "Dynamic Response of Unreinforced Masonry Buildings with Flexible Diaphragms," by A.C. Costley and D.P. Abrams," 10/10/96, (PB97-133573, MF-A03, A15).

NCEER-96-0002 "State of the Art Review: Foundations and Retaining Structures," by I. Po Lam, to be published.

NCEER-96-0003 "Ductility of Rectangular Reinforced Concrete Bridge Columns with Moderate Confinement," by N. Wehbe, M. Saiidi, D. Sanders and B. Douglas, 11/7/96, (PB97-133557, A06, MF-A02).

NCEER-96-0004 "Proceedings of the Long-Span Bridge Seismic Research Workshop," edited by I.G. Buckle and I.M. Friedland, to be published.

NCEER-96-0005 "Establish Representative Pier Types for Comprehensive Study: Eastern United States," by J. Kulicki and Z. Prucz, 5/28/96, (PB98-119217, A07, MF-A02).

NCEER-96-0006 "Establish Representative Pier Types for Comprehensive Study: Western United States," by R. Imbsen, R.A. Schamber and T.A. Osterkamp, 5/28/96, (PB98-118607, A07, MF-A02).

NCEER-96-0007 "Nonlinear Control Techniques for Dynamical Systems with Uncertain Parameters," by R.G. Ghanem and M.I. Bujakov, 5/27/96, (PB97-100259, A17, MF-A03).

NCEER-96-0008 "Seismic Evaluation of a 30-Year Old Non-Ductile Highway Bridge Pier and Its Retrofit," by J.B. Mander, B. Mahmoodzadegan, S. Bhadra and S.S. Chen, 5/31/96, (PB97-110902, MF-A03, A10).

NCEER-96-0009 "Seismic Performance of a Model Reinforced Concrete Bridge Pier Before and After Retrofit," by J.B. Mander, J.H. Kim and C.A. Ligozio, 5/31/96, (PB97-110910, MF-A02, A10).

NCEER-96-0010 "IDARC2D Version 4.0: A Computer Program for the Inelastic Damage Analysis of Buildings," by R.E. Valles, A.M. Reinhorn, S.K. Kunnath, C. Li and A. Madan, 6/3/96, (PB97-100234, A17, MF-A03).

NCEER-96-0011 "Estimation of the Economic Impact of Multiple Lifeline Disruption: Memphis Light, Gas and Water Division Case Study," by S.E. Chang, H.A. Seligson and R.T. Eguchi, 8/16/96, (PB97-133490, A11, MF-A03).

NCEER-96-0012 "Proceedings from the Sixth Japan-U.S. Workshop on Earthquake Resistant Design of Lifeline Facilities and Countermeasures Against Soil Liquefaction, Edited by M. Hamada and T. O'Rourke, 9/11/96, (PB97-133581, A99, MF-A06).

NCEER-96-0013 "Chemical Hazards, Mitigation and Preparedness in Areas of High Seismic Risk: A Methodology for Estimating the Risk of Post-Earthquake Hazardous Materials Release," by H.A. Seligson, R.T. Eguchi, K.J. Tierney and K. Richmond, 11/7/96, (PB97-133565, MF-A02, A08).

NCEER-96-0014 "Response of Steel Bridge Bearings to Reversed Cyclic Loading," by J.B. Mander, D-K. Kim, S.S. Chen and G.J. Premus, 11/13/96, (PB97-140735, A12, MF-A03).

NCEER-96-0015 "Highway Culvert Performance During Past Earthquakes," by T.L. Youd and C.J. Beckman, 11/25/96, (PB97-133532, A06, MF-A01).

NCEER-97-0001 "Evaluation, Prevention and Mitigation of Pounding Effects in Building Structures," by R.E. Valles and A.M. Reinhorn, 2/20/97, (PB97-159552, A14, MF-A03).

NCEER-97-0002 "Seismic Design Criteria for Bridges and Other Highway Structures," by C. Rojahn, R. Mayes, D.G. Anderson, J. Clark, J.H. Hom, R.V. Nutt and M.J. O'Rourke, 4/30/97, (PB97-194658, A06, MF-A03).

NCEER-97-0003 “Proceedings of the U.S.-Italian Workshop on Seismic Evaluation and Retrofit,” Edited by D.P. Abrams and G.M. Calvi, 3/19/97, (PB97-194666, A13, MF-A03).

NCEER-97-0004 "Investigation of Seismic Response of Buildings with Linear and Nonlinear Fluid Viscous Dampers," by A.A. Seleemah and M.C. Constantinou, 5/21/97, (PB98-109002, A15, MF-A03).

NCEER-97-0005 "Proceedings of the Workshop on Earthquake Engineering Frontiers in Transportation Facilities," edited by G.C. Lee and I.M. Friedland, 8/29/97, (PB98-128911, A25, MR-A04).

NCEER-97-0006 "Cumulative Seismic Damage of Reinforced Concrete Bridge Piers," by S.K. Kunnath, A. El-Bahy, A. Taylor and W. Stone, 9/2/97, (PB98-108814, A11, MF-A03).

NCEER-97-0007 "Structural Details to Accommodate Seismic Movements of Highway Bridges and Retaining Walls," by R.A. Imbsen, R.A. Schamber, E. Thorkildsen, A. Kartoum, B.T. Martin, T.N. Rosser and J.M. Kulicki, 9/3/97, (PB98-108996, A09, MF-A02).

NCEER-97-0008 "A Method for Earthquake Motion-Damage Relationships with Application to Reinforced Concrete Frames," by A. Singhal and A.S. Kiremidjian, 9/10/97, (PB98-108988, A13, MF-A03).

NCEER-97-0009 "Seismic Analysis and Design of Bridge Abutments Considering Sliding and Rotation," by K. Fishman and R. Richards, Jr., 9/15/97, (PB98-108897, A06, MF-A02).

NCEER-97-0010 "Proceedings of the FHWA/NCEER Workshop on the National Representation of Seismic Ground Motion for New and Existing Highway Facilities," edited by I.M. Friedland, M.S. Power and R.L. Mayes, 9/22/97, (PB98-128903, A21, MF-A04).

NCEER-97-0011 "Seismic Analysis for Design or Retrofit of Gravity Bridge Abutments," by K.L. Fishman, R. Richards, Jr. and R.C. Divito, 10/2/97, (PB98-128937, A08, MF-A02).

NCEER-97-0012 "Evaluation of Simplified Methods of Analysis for Yielding Structures," by P. Tsopelas, M.C. Constantinou, C.A. Kircher and A.S. Whittaker, 10/31/97, (PB98-128929, A10, MF-A03).

NCEER-97-0013 "Seismic Design of Bridge Columns Based on Control and Repairability of Damage," by C-T. Cheng and J.B. Mander, 12/8/97, (PB98-144249, A11, MF-A03).

NCEER-97-0014 "Seismic Resistance of Bridge Piers Based on Damage Avoidance Design," by J.B. Mander and C-T. Cheng, 12/10/97, (PB98-144223, A09, MF-A02).

NCEER-97-0015 “Seismic Response of Nominally Symmetric Systems with Strength Uncertainty,” by S. Balopoulou and M. Grigoriu, 12/23/97, (PB98-153422, A11, MF-A03).

NCEER-97-0016 “Evaluation of Seismic Retrofit Methods for Reinforced Concrete Bridge Columns,” by T.J. Wipf, F.W. Klaiber and F.M. Russo, 12/28/97, (PB98-144215, A12, MF-A03).

NCEER-97-0017 “Seismic Fragility of Existing Conventional Reinforced Concrete Highway Bridges,” by C.L. Mullen and A.S. Cakmak, 12/30/97, (PB98-153406, A08, MF-A02).

NCEER-97-0018 “Loss Asssessment of Memphis Buildings,” edited by D.P. Abrams and M. Shinozuka, 12/31/97, (PB98-144231, A13, MF-A03).

NCEER-97-0019 “Seismic Evaluation of Frames with Infill Walls Using Quasi-static Experiments,” by K.M. Mosalam, R.N. White and P. Gergely, 12/31/97, (PB98-153455, A07, MF-A02).

NCEER-97-0020 “Seismic Evaluation of Frames with Infill Walls Using Pseudo-dynamic Experiments,” by K.M. Mosalam, R.N. White and P. Gergely, 12/31/97, (PB98-153430, A07, MF-A02).

NCEER-97-0021 “Computational Strategies for Frames with Infill Walls: Discrete and Smeared Crack Analyses and Seismic Fragility,” by K.M. Mosalam, R.N. White and P. Gergely, 12/31/97, (PB98-153414, A10, MF-A02).

NCEER-97-0022 "Proceedings of the NCEER Workshop on Evaluation of Liquefaction Resistance of Soils," edited by T.L. Youd and I.M. Idriss, 12/31/97, (PB98-155617, A15, MF-A03).

MCEER-98-0001 "Extraction of Nonlinear Hysteretic Properties of Seismically Isolated Bridges from Quick-Release Field Tests," by Q. Chen, B.M. Douglas, E.M. Maragakis and I.G. Buckle, 5/26/98, (PB99-118838, A06, MF-A01).

MCEER-98-0002 "Methodologies for Evaluating the Importance of Highway Bridges," by A. Thomas, S. Eshenaur and J. Kulicki, 5/29/98, (PB99-118846, A10, MF-A02).

MCEER-98-0003 "Capacity Design of Bridge Piers and the Analysis of Overstrength," by J.B. Mander, A. Dutta and P. Goel, 6/1/98, (PB99-118853, A09, MF-A02).

MCEER-98-0004 "Evaluation of Bridge Damage Data from the Loma Prieta and Northridge, California Earthquakes," by N. Basoz and A. Kiremidjian, 6/2/98, (PB99-118861, A15, MF-A03).

MCEER-98-0005 "Screening Guide for Rapid Assessment of Liquefaction Hazard at Highway Bridge Sites," by T. L. Youd, 6/16/98, (PB99-118879, A06, not available on microfiche).

MCEER-98-0006 "Structural Steel and Steel/Concrete Interface Details for Bridges," by P. Ritchie, N. Kauhl and J. Kulicki, 7/13/98, (PB99-118945, A06, MF-A01).

MCEER-98-0007 "Capacity Design and Fatigue Analysis of Confined Concrete Columns," by A. Dutta and J.B. Mander, 7/14/98, (PB99-118960, A14, MF-A03).

MCEER-98-0008 "Proceedings of the Workshop on Performance Criteria for Telecommunication Services Under Earthquake Conditions," edited by A.J. Schiff, 7/15/98, (PB99-118952, A08, MF-A02).

MCEER-98-0009 "Fatigue Analysis of Unconfined Concrete Columns," by J.B. Mander, A. Dutta and J.H. Kim, 9/12/98, (PB99-123655, A10, MF-A02).

MCEER-98-0010 "Centrifuge Modeling of Cyclic Lateral Response of Pile-Cap Systems and Seat-Type Abutments in Dry Sands," by A.D. Gadre and R. Dobry, 10/2/98, (PB99-123606, A13, MF-A03).

MCEER-98-0011 "IDARC-BRIDGE: A Computational Platform for Seismic Damage Assessment of Bridge Structures," by A.M. Reinhorn, V. Simeonov, G. Mylonakis and Y. Reichman, 10/2/98, (PB99-162919, A15, MF-A03).

MCEER-98-0012 "Experimental Investigation of the Dynamic Response of Two Bridges Before and After Retrofitting with Elastomeric Bearings," by D.A. Wendichansky, S.S. Chen and J.B. Mander, 10/2/98, (PB99-162927, A15, MF-A03).

MCEER-98-0013 "Design Procedures for Hinge Restrainers and Hinge Sear Width for Multiple-Frame Bridges," by R. Des Roches and G.L. Fenves, 11/3/98, (PB99-140477, A13, MF-A03).

MCEER-98-0014 "Response Modification Factors for Seismically Isolated Bridges," by M.C. Constantinou and J.K. Quarshie, 11/3/98, (PB99-140485, A14, MF-A03).

MCEER-98-0015 "Proceedings of the U.S.-Italy Workshop on Seismic Protective Systems for Bridges," edited by I.M. Friedland and M.C. Constantinou, 11/3/98, (PB2000-101711, A22, MF-A04).

MCEER-98-0016 "Appropriate Seismic Reliability for Critical Equipment Systems: Recommendations Based on Regional Analysis of Financial and Life Loss," by K. Porter, C. Scawthorn, C. Taylor and N. Blais, 11/10/98, (PB99-157265, A08, MF-A02).

MCEER-98-0017 "Proceedings of the U.S. Japan Joint Seminar on Civil Infrastructure Systems Research," edited by M. Shinozuka and A. Rose, 11/12/98, (PB99-156713, A16, MF-A03).

MCEER-98-0018 "Modeling of Pile Footings and Drilled Shafts for Seismic Design," by I. PoLam, M. Kapuskar and D. Chaudhuri, 12/21/98, (PB99-157257, A09, MF-A02).

MCEER-99-0001 "Seismic Evaluation of a Masonry Infilled Reinforced Concrete Frame by Pseudodynamic Testing," by S.G. Buonopane and R.N. White, 2/16/99, (PB99-162851, A09, MF-A02).

MCEER-99-0002 "Response History Analysis of Structures with Seismic Isolation and Energy Dissipation Systems: Verification Examples for Program SAP2000," by J. Scheller and M.C. Constantinou, 2/22/99, (PB99-162869, A08, MF-A02).

MCEER-99-0003 "Experimental Study on the Seismic Design and Retrofit of Bridge Columns Including Axial Load Effects," by A. Dutta, T. Kokorina and J.B. Mander, 2/22/99, (PB99-162877, A09, MF-A02).

MCEER-99-0004 "Experimental Study of Bridge Elastomeric and Other Isolation and Energy Dissipation Systems with Emphasis on Uplift Prevention and High Velocity Near-source Seismic Excitation," by A. Kasalanati and M. C. Constantinou, 2/26/99, (PB99-162885, A12, MF-A03).

MCEER-99-0005 "Truss Modeling of Reinforced Concrete Shear-flexure Behavior," by J.H. Kim and J.B. Mander, 3/8/99, (PB99-163693, A12, MF-A03).

MCEER-99-0006 "Experimental Investigation and Computational Modeling of Seismic Response of a 1:4 Scale Model Steel Structure with a Load Balancing Supplemental Damping System," by G. Pekcan, J.B. Mander and S.S. Chen, 4/2/99, (PB99-162893, A11, MF-A03).

MCEER-99-0007 "Effect of Vertical Ground Motions on the Structural Response of Highway Bridges," by M.R. Button, C.J. Cronin and R.L. Mayes, 4/10/99, (PB2000-101411, A10, MF-A03).

MCEER-99-0008 "Seismic Reliability Assessment of Critical Facilities: A Handbook, Supporting Documentation, and Model Code Provisions," by G.S. Johnson, R.E. Sheppard, M.D. Quilici, S.J. Eder and C.R. Scawthorn, 4/12/99, (PB2000-101701, A18, MF-A04).

MCEER-99-0009 "Impact Assessment of Selected MCEER Highway Project Research on the Seismic Design of Highway Structures," by C. Rojahn, R. Mayes, D.G. Anderson, J.H. Clark, D'Appolonia Engineering, S. Gloyd and R.V. Nutt, 4/14/99, (PB99-162901, A10, MF-A02).

MCEER-99-0010 "Site Factors and Site Categories in Seismic Codes," by R. Dobry, R. Ramos and M.S. Power, 7/19/99, (PB2000-101705, A08, MF-A02).

MCEER-99-0011 "Restrainer Design Procedures for Multi-Span Simply-Supported Bridges," by M.J. Randall, M. Saiidi, E. Maragakis and T. Isakovic, 7/20/99, (PB2000-101702, A10, MF-A02).

MCEER-99-0012 "Property Modification Factors for Seismic Isolation Bearings," by M.C. Constantinou, P. Tsopelas, A. Kasalanati and E. Wolff, 7/20/99, (PB2000-103387, A11, MF-A03).

MCEER-99-0013 "Critical Seismic Issues for Existing Steel Bridges," by P. Ritchie, N. Kauhl and J. Kulicki, 7/20/99, (PB2000-101697, A09, MF-A02).

MCEER-99-0014 "Nonstructural Damage Database," by A. Kao, T.T. Soong and A. Vender, 7/24/99, (PB2000-101407, A06, MF-A01).

MCEER-99-0015 "Guide to Remedial Measures for Liquefaction Mitigation at Existing Highway Bridge Sites," by H.G. Cooke and J. K. Mitchell, 7/26/99, (PB2000-101703, A11, MF-A03).

MCEER-99-0016 "Proceedings of the MCEER Workshop on Ground Motion Methodologies for the Eastern United States," edited by N. Abrahamson and A. Becker, 8/11/99, (PB2000-103385, A07, MF-A02).

MCEER-99-0017 "Quindío, Colombia Earthquake of January 25, 1999: Reconnaissance Report," by A.P. Asfura and P.J. Flores, 10/4/99, (PB2000-106893, A06, MF-A01).

MCEER-99-0018 "Hysteretic Models for Cyclic Behavior of Deteriorating Inelastic Structures," by M.V. Sivaselvan and A.M. Reinhorn, 11/5/99, (PB2000-103386, A08, MF-A02).

MCEER-99-0019 "Proceedings of the 7th U.S.- Japan Workshop on Earthquake Resistant Design of Lifeline Facilities and Countermeasures Against Soil Liquefaction," edited by T.D. O'Rourke, J.P. Bardet and M. Hamada, 11/19/99, (PB2000-103354, A99, MF-A06).

MCEER-99-0020 "Development of Measurement Capability for Micro-Vibration Evaluations with Application to Chip Fabrication Facilities," by G.C. Lee, Z. Liang, J.W. Song, J.D. Shen and W.C. Liu, 12/1/99, (PB2000-105993, A08, MF-A02).

MCEER-99-0021 "Design and Retrofit Methodology for Building Structures with Supplemental Energy Dissipating Systems," by G. Pekcan, J.B. Mander and S.S. Chen, 12/31/99, (PB2000-105994, A11, MF-A03).

MCEER-00-0001 "The Marmara, Turkey Earthquake of August 17, 1999: Reconnaissance Report," edited by C. Scawthorn; with major contributions by M. Bruneau, R. Eguchi, T. Holzer, G. Johnson, J. Mander, J. Mitchell, W. Mitchell, A. Papageorgiou, C. Scaethorn, and G. Webb, 3/23/00, (PB2000-106200, A11, MF-A03).

MCEER-00-0002 "Proceedings of the MCEER Workshop for Seismic Hazard Mitigation of Health Care Facilities," edited by G.C. Lee, M. Ettouney, M. Grigoriu, J. Hauer and J. Nigg, 3/29/00, (PB2000-106892, A08, MF-A02).

MCEER-00-0003 "The Chi-Chi, Taiwan Earthquake of September 21, 1999: Reconnaissance Report," edited by G.C. Lee and C.H. Loh, with major contributions by G.C. Lee, M. Bruneau, I.G. Buckle, S.E. Chang, P.J. Flores, T.D. O'Rourke, M. Shinozuka, T.T. Soong, C-H. Loh, K-C. Chang, Z-J. Chen, J-S. Hwang, M-L. Lin, G-Y. Liu, K-C. Tsai, G.C. Yao and C-L. Yen, 4/30/00, (PB2001-100980, A10, MF-A02).

MCEER-00-0004 "Seismic Retrofit of End-Sway Frames of Steel Deck-Truss Bridges with a Supplemental Tendon System: Experimental and Analytical Investigation," by G. Pekcan, J.B. Mander and S.S. Chen, 7/1/00, (PB2001-100982, A10, MF-A02).

MCEER-00-0005 "Sliding Fragility of Unrestrained Equipment in Critical Facilities," by W.H. Chong and T.T. Soong, 7/5/00, (PB2001-100983, A08, MF-A02).

MCEER-00-0006 "Seismic Response of Reinforced Concrete Bridge Pier Walls in the Weak Direction," by N. Abo-Shadi, M. Saiidi and D. Sanders, 7/17/00, (PB2001-100981, A17, MF-A03).

MCEER-00-0007 "Low-Cycle Fatigue Behavior of Longitudinal Reinforcement in Reinforced Concrete Bridge Columns," by J. Brown and S.K. Kunnath, 7/23/00, (PB2001-104392, A08, MF-A02).

MCEER-00-0008 "Soil Structure Interaction of Bridges for Seismic Analysis," I. PoLam and H. Law, 9/25/00, (PB2001-105397, A08, MF-A02).

MCEER-00-0009 "Proceedings of the First MCEER Workshop on Mitigation of Earthquake Disaster by Advanced Technologies (MEDAT-1), edited by M. Shinozuka, D.J. Inman and T.D. O'Rourke, 11/10/00, (PB2001-105399, A14, MF-A03).

MCEER-00-0010 "Development and Evaluation of Simplified Procedures for Analysis and Design of Buildings with Passive Energy Dissipation Systems," by O.M. Ramirez, M.C. Constantinou, C.A. Kircher, A.S. Whittaker, M.W. Johnson, J.D. Gomez and C. Chrysostomou, 11/16/01, (PB2001-105523, A23, MF-A04).

MCEER-00-0011 "Dynamic Soil-Foundation-Structure Interaction Analyses of Large Caissons," by C-Y. Chang, C-M. Mok, Z-L. Wang, R. Settgast, F. Waggoner, M.A. Ketchum, H.M. Gonnermann and C-C. Chin, 12/30/00, (PB2001-104373, A07, MF-A02).

MCEER-00-0012 "Experimental Evaluation of Seismic Performance of Bridge Restrainers," by A.G. Vlassis, E.M. Maragakis and M. Saiid Saiidi, 12/30/00, (PB2001-104354, A09, MF-A02).

MCEER-00-0013 "Effect of Spatial Variation of Ground Motion on Highway Structures," by M. Shinozuka, V. Saxena and G. Deodatis, 12/31/00, (PB2001-108755, A13, MF-A03).

MCEER-00-0014 "A Risk-Based Methodology for Assessing the Seismic Performance of Highway Systems," by S.D. Werner, C.E. Taylor, J.E. Moore, II, J.S. Walton and S. Cho, 12/31/00, (PB2001-108756, A14, MF-A03).

MCEER-01-0001 "Experimental Investigation of P-Delta Effects to Collapse During Earthquakes," by D. Vian and M. Bruneau, 6/25/01, (PB2002-100534, A17, MF-A03).

MCEER-01-0002 "Proceedings of the Second MCEER Workshop on Mitigation of Earthquake Disaster by Advanced Technologies (MEDAT-2)," edited by M. Bruneau and D.J. Inman, 7/23/01, (PB2002-100434, A16, MF-A03).

MCEER-01-0003 "Sensitivity Analysis of Dynamic Systems Subjected to Seismic Loads," by C. Roth and M. Grigoriu, 9/18/01, (PB2003-100884, A12, MF-A03).

MCEER-01-0004 "Overcoming Obstacles to Implementing Earthquake Hazard Mitigation Policies: Stage 1 Report," by D.J. Alesch and W.J. Petak, 12/17/01, (PB2002-107949, A07, MF-A02).

MCEER-01-0005 "Updating Real-Time Earthquake Loss Estimates: Methods, Problems and Insights," by C.E. Taylor, S.E. Chang and R.T. Eguchi, 12/17/01, (PB2002-107948, A05, MF-A01).

MCEER-01-0006 "Experimental Investigation and Retrofit of Steel Pile Foundations and Pile Bents Under Cyclic Lateral Loadings," by A. Shama, J. Mander, B. Blabac and S. Chen, 12/31/01, (PB2002-107950, A13, MF-A03).

MCEER-02-0001 "Assessment of Performance of Bolu Viaduct in the 1999 Duzce Earthquake in Turkey" by P.C. Roussis, M.C. Constantinou, M. Erdik, E. Durukal and M. Dicleli, 5/8/02, (PB2003-100883, A08, MF-A02).

MCEER-02-0002 "Seismic Behavior of Rail Counterweight Systems of Elevators in Buildings," by M.P. Singh, Rildova and L.E. Suarez, 5/27/02. (PB2003-100882, A11, MF-A03).

MCEER-02-0003 "Development of Analysis and Design Procedures for Spread Footings," by G. Mylonakis, G. Gazetas, S. Nikolaou and A. Chauncey, 10/02/02, (PB2004-101636, A13, MF-A03, CD-A13).

MCEER-02-0004 "Bare-Earth Algorithms for Use with SAR and LIDAR Digital Elevation Models," by C.K. Huyck, R.T. Eguchi and B. Houshmand, 10/16/02, (PB2004-101637, A07, CD-A07).

MCEER-02-0005 "Review of Energy Dissipation of Compression Members in Concentrically Braced Frames," by K.Lee and M. Bruneau, 10/18/02, (PB2004-101638, A10, CD-A10).

MCEER-03-0001 "Experimental Investigation of Light-Gauge Steel Plate Shear Walls for the Seismic Retrofit of Buildings" by J. Berman and M. Bruneau, 5/2/03, (PB2004-101622, A10, MF-A03, CD-A10).

MCEER-03-0002 "Statistical Analysis of Fragility Curves," by M. Shinozuka, M.Q. Feng, H. Kim, T. Uzawa and T. Ueda, 6/16/03, (PB2004-101849, A09, CD-A09).

MCEER-03-0003 "Proceedings of the Eighth U.S.-Japan Workshop on Earthquake Resistant Design f Lifeline Facilities and Countermeasures Against Liquefaction," edited by M. Hamada, J.P. Bardet and T.D. O'Rourke, 6/30/03, (PB2004-104386, A99, CD-A99).

MCEER-03-0004 "Proceedings of the PRC-US Workshop on Seismic Analysis and Design of Special Bridges," edited by L.C. Fan and G.C. Lee, 7/15/03, (PB2004-104387, A14, CD-A14).

MCEER-03-0005 "Urban Disaster Recovery: A Framework and Simulation Model," by S.B. Miles and S.E. Chang, 7/25/03, (PB2004-104388, A07, CD-A07).

MCEER-03-0006 "Behavior of Underground Piping Joints Due to Static and Dynamic Loading," by R.D. Meis, M. Maragakis and R. Siddharthan, 11/17/03, (PB2005-102194, A13, MF-A03, CD-A00).

MCEER-03-0007 "Seismic Vulnerability of Timber Bridges and Timber Substructures," by A.A. Shama, J.B. Mander, I.M. Friedland and D.R. Allicock, 12/15/03.

MCEER-04-0001 "Experimental Study of Seismic Isolation Systems with Emphasis on Secondary System Response and Verification of Accuracy of Dynamic Response History Analysis Methods," by E. Wolff and M. Constantinou, 1/16/04 (PB2005-102195, A99, MF-E08, CD-A00).

MCEER-04-0002 "Tension, Compression and Cyclic Testing of Engineered Cementitious Composite Materials," by K. Kesner and S.L. Billington, 3/1/04, (PB2005-102196, A08, CD-A08).

MCEER-04-0003 "Cyclic Testing of Braces Laterally Restrained by Steel Studs to Enhance Performance During Earthquakes," by O.C. Celik, J.W. Berman and M. Bruneau, 3/16/04, (PB2005-102197, A13, MF-A03, CD-A00).

MCEER-04-0004 "Methodologies for Post Earthquake Building Damage Detection Using SAR and Optical Remote Sensing: Application to the August 17, 1999 Marmara, Turkey Earthquake," by C.K. Huyck, B.J. Adams, S. Cho, R.T. Eguchi, B. Mansouri and B. Houshmand, 6/15/04, (PB2005-104888, A10, CD-A00).

MCEER-04-0005 "Nonlinear Structural Analysis Towards Collapse Simulation: A Dynamical Systems Approach," by M.V. Sivaselvan and A.M. Reinhorn, 6/16/04, (PB2005-104889, A11, MF-A03, CD-A00).

MCEER-04-0006 "Proceedings of the Second PRC-US Workshop on Seismic Analysis and Design of Special Bridges," edited by G.C. Lee and L.C. Fan, 6/25/04, (PB2005-104890, A16, CD-A00).

MCEER-04-0007 "Seismic Vulnerability Evaluation of Axially Loaded Steel Built-up Laced Members," by K. Lee and M. Bruneau, 6/30/04, (PB2005-104891, A16, CD-A00).

MCEER-04-0008 "Evaluation of Accuracy of Simplified Methods of Analysis and Design of Buildings with Damping Systems for Near-Fault and for Soft-Soil Seismic Motions," by E.A. Pavlou and M.C. Constantinou, 8/16/04, (PB2005-104892, A08, MF-A02, CD-A00).

MCEER-04-0009 "Assessment of Geotechnical Issues in Acute Care Facilities in California," by M. Lew, T.D. O'Rourke, R. Dobry and M. Koch, 9/15/04, (PB2005-104893, A08, CD-A00).

MCEER-04-0010 "Scissor-Jack-Damper Energy Dissipation System," by A.N. Sigaher-Boyle and M.C. Constantinou, 12/1/04.

MCEER-04-0011 "Seismic Retrofit of Bridge Steel Truss Piers Using a Controlled Rocking Approach," by M. Pollino and M. Bruneau, 12/20/04.

MCEER-05-0001 "Experimental and Analytical Studies of Structures Seismically Isolated with an Uplift-Restraint Isolation System," by P.C. Roussis and M.C. Constantinou, 1/10/05.

MCEER-05-0002 "A Versatile Experimentation Model for Study of Structures Near Collapse Applied to Seismic Evaluation of Irregular Structures," by D. Kusumastuti, A.M. Reinhorn and A. Rutenberg, 3/31/05.

MCEER-05-0003 "Proceedings of the Third PRC-US Workshop on Seismic Analysis and Design of Special Bridges," edited by L.C. Fan and G.C. Lee, 4/20/05.

MCEER-05-0004 "Approaches for the Seismic Retrofit of Braced Steel Bridge Piers and Proof-of-Concept Testing of an Eccentrically Braced Frame with Tubular Link," by J.W. Berman and M. Bruneau, 4/21/05.

MCEER-05-0005 "Simulation of Strong Ground Motions for Seismic Fragility Evaluation of Nonstructural Components in Hospitals," by A. Wanitkorkul and A. Filiatrault, 5/26/05.

MCEER-05-0006 "Seismic Safety in California Hospitals: Assessing an Attempt to Accelerate the Replacement or Seismic Retrofit of Older Hospital Facilities," by D.J. Alesch, L.A. Arendt and W.J. Petak, 6/6/05.

MCEER-05-0007 "Development of Seismic Strengthening and Retrofit Strategies for Critical Facilities Using Engineered Cementitious Composite Materials," by K. Kesner and S.L. Billington, 8/29/05.

MCEER-05-0008 "Experimental and Analytical Studies of Base Isolation Systems for Seismic Protection of Power Transformers," by N. Murota, M.Q. Feng and G-Y. Liu, 9/30/05.

MCEER
MULTIDISCIPLINARY CENTER FOR EARTHQUAKE ENGINEERING RESEARCH
A National Center of Excellence in Advanced Technology Applications
University at Buffalo, State University of New York
Red Jacket Quadrangle ■ Buffalo, New York 14261
Phone: (716) 645-3391 ■ Fax: (716) 645-3399
E-mail: *mceer@mceermail.buffalo.edu* ■ WWW Site *http://mceer.buffalo.edu*
University at Buffalo *The State University of New York*

ISSN 1520-295X